Analysis of sensorimotor rhythms based on lower-limbs motor imagery for brain-computer interface

A thesis submitted in fulfilment of the requirements for the degree of Doctor of Philosophy

Madiha Tariq

MS Mechatronics Engineering, Air University, Islamabad, Pakistan

B.Eng. Mechatronics Engineering, Air University, Islamabad, Pakistan

School of Engineering

College of Science, Engineering and Health

RMIT University

November, 2019

Declaration

I certify that except where due acknowledgment has been made, the work is that of the author alone; the work has not been submitted previously, in whole or in part, to qualify for any other academic award; the content of the thesis is the result of work which has been carried out since the official commencement date of the approved research program; any editorial work, paid or unpaid, carried out by a third party is acknowledged; and, ethics procedures and guidelines have been followed.

I acknowledge the support I have received for my research through the provision of Australian Government Research Training Program Scholarship.

Madiha Tariq
Dated: 07-11-2019

The important thing is not to stop questioning. Curiosity has its own reason for existing.

ALBERT EINSTEIN (1879-1955)

This page is left intentionally blank

Dedication

To

my most precious Ami Abu,

dear husband, and

my world, Maheen & Zeenya.

Abstract

Over recent years significant advancements in the field of assistive technologies have been observed. One of the paramount needs for the development and advancement that urged researchers to contribute in the field other than congenital or diagnosed chronic disorders, is the rising number of affectees from accidents, natural calamity (due to climate change), or warfare, worldwide resulting in spinal cord injuries (SCI), neural disorder, or amputation (interception) of limbs, that impede a human to live a normal life. In addition to this, more than ten million people in the world are living with some form of handicap due to the central nervous system (CNS) disorder, which is precarious. Biomedical devices for rehabilitation are the center of research focus for many years. For people with lost motor control, or amputation, but unscathed sensory control, instigation of control signals from the source, i.e. electrophysiological signals, is vital for seamless control of assistive biomedical devices. Control signals, i.e. motion intentions, arouse in the sensorimotor cortex of the brain that can be detected using invasive or non-invasive modality. With non-invasive modality, the electroencephalography (EEG) is used to record these motion intentions encoded in electrical activity of the cortex, and are deciphered to recognize user intent for locomotion. They are further transferred to the actuator, or end effector of the assistive device for control purposes. This can be executed via the brain-computer interface (BCI) technology.

BCI is an emerging research field that establishes a real-time bidirectional connection between the human brain and a computer/output device. Amongst its diverse applications, neurorehabilitation to deliver sensory feedback and brain controlled biomedical devices for rehabilitation are most popular. While substantial literature on control of upper-limb assistive technologies controlled via BCI is there, less is known about the lower-limb (LL) control of biomedical devices for navigation or gait assistance via BCI. The types of EEG signals compatible with an independent BCI are the oscillatory/sensorimotor rhythms (SMR) and event-related potential (ERP). These signals have successfully been used in BCIs for navigation control of assistive devices. However, ERP paradigm accounts for a voluminous setup for stimulus presentation to the user during operation of BCI assistive device. Contrary to this, the SMR does not require large setup for activation of cortical activity; it instead depends on the motor imagery (MI) that is produced

synchronously or asynchronously by the user. MI is a covert cognitive process also termed kinaesthetic motor imagery (KMI) and elicits clearly after rigorous training trials, in form of event-related desynchronization (ERD) or synchronization (ERS), depending on imagery activity or resting period. It usually comprises of limb movement tasks, but is not limited to it in a BCI paradigm. In order to produce detectable features that correlate to the user's intent, selection of cognitive task is an important aspect to improve the performance of a BCI. MI used in BCI predominantly remains associated with the upper-limbs, particularly hands, due to the somatotopic organization of the motor cortex. The hand representation area is substantially large, in contrast to the anatomical location of the LL representation areas in the human sensorimotor cortex. The LL area is located within the interhemispheric fissure, i.e. between the mesial walls of both hemispheres of the cortex. This makes it arduous to detect EEG features prompted upon imagination of LL. Detailed investigation of the ERD/ERS in the *mu* and *beta* oscillatory rhythms during left and right LL KMI tasks is required, as the user's intent to walk is of paramount importance associated to everyday activity. This is an important area of research, followed by the improvisation of the already existing rehabilitation system that serves the LL affectees. Though challenging, solution to these issues is also imperative for the development of robust controllers that follow the asynchronous BCI paradigms to operate LL assistive devices seamlessly.

This thesis focusses on the investigation of cortical lateralization of ERD/ERS in the SMR, based on foot dorsiflexion KMI and knee extension KMI separately. This research infers the possibility to deploy these features in real-time BCI by finding maximum possible classification accuracy from the machine learning (ML) models. EEG signal is non-stationary, as it is characterized by individual-to-individual and trial-to-trial variability, and a low signal-to-noise ratio (SNR), which is challenging. They are high in dimension with relatively low number of samples available for fitting ML models to the data. These factors account for ML methods that were developed into the tool of choice to analyse single-trial EEG data. Hence, the selection of appropriate ML model for true detection of class label with no tradeoff of overfitting is crucial. The feature extraction part of the thesis constituted of testing the band-power (BP) and the common spatial pattern (CSP) methods individually. The study focused on the synchronous BCI paradigm. This was to ensure the exhibition of SMR for the possibility of a practically viable control system in a BCI. For the left vs. right foot KMI, the objective was to

distinguish the bilateral tasks, in order to use them as unilateral commands in a 2-class BCI for controlling/navigating a robotic/prosthetic LL for rehabilitation. Similar was the approach for left-right knee KMI. The research was based on four main experimental studies. In addition to the four studies, the research is also inclusive of the comparison of intra-cognitive tasks within the same limb, i.e. left foot vs. left knee and right foot vs. right knee tasks, respectively **(Chapter 4)**. This added to another novel contribution towards the findings based on comparison of different tasks within the same LL. It provides basis to increase the dimensionality of control signals within one BCI paradigm, such as a BCI-controlled LL assistive device with multiple degrees of freedom (DOF) for restoration of locomotion function. This study was based on analysis of statistically significant *mu* ERD feature using BP feature extraction method.

The first stage of this research comprised of the left vs. right foot KMI tasks, wherein the ERD/ERS that elicited in the *mu-beta* rhythms were analysed using BP feature extraction method **(Chapter 5)**. Three individual features, i.e. *mu* ERD, *beta* ERD, and *beta* ERS were investigated on EEG topography and time-frequency (TF) maps, and average time course of power percentage, using the common average reference and bipolar reference methods. A comparative study was drawn for both references to infer the optimal method. This was followed by ML, i.e. classification of the three feature vectors (*mu* ERD, *beta* ERD, and *beta* ERS), using linear discriminant analysis (LDA), support vector machine (SVM), and k-nearest neighbour (KNN) algorithms, separately. Finally, the multiple correction statistical tests were done, in order to predict maximum possible classification accuracy amongst all paradigms for the most significant feature. All classifier models were supported with the statistical techniques of *k*-fold cross validation and evaluation of area under receiver-operator characteristic curves (AUC-ROC) for prediction of the true class label. The highest classification accuracy of 83.4% ± 6.72 was obtained with KNN model for *beta* ERS feature. The next study was based on enhancing the classification accuracy obtained from previous study. It was based on using similar cognitive tasks as study in Chapter 5, however deploying different methodology for feature extraction and classification procedure. In the second study, ERD/ERS from *mu* and *beta* rhythms were extracted using CSP and filter bank common spatial pattern (FBCSP) algorithms, to optimize the individual spatial patterns **(Chapter 6)**. This was followed by ML process, for which the supervised logistic regression (Logreg) and LDA were deployed separately. Maximum classification accuracy resulted in 77.5% ± 4.23 with FBCSP feature vector

and LDA model, with a maximum kappa coefficient of 0.55 that is in the moderate range of agreement between the two classes. The left vs. right foot discrimination results were nearly same, however the BP feature vector performed better than CSP.

The third stage was based on the deployment of novel cognitive task of left vs. right knee extension KMI. Analysis of the ERD/ERS in the *mu-beta* rhythms was done for verification of cortical lateralization via BP feature vector **(Chapter 7)**. Similar to Chapter 5, in this study the analysis of ERD/ERS features was done on the EEG topography and TF maps, followed by the determination of average time course and peak latency of feature occurrence. However, for this study, only *mu* ERD and *beta* ERS features were taken into consideration and the EEG recording method only comprised of common average reference. This was due to the established results from the foot study earlier, in Chapter 5, where beta ERD features showed less average amplitude. The LDA and KNN classification algorithms were employed. Unexpectedly, the left vs. right knee KMI reflected the highest accuracy of 81.04% ± 7.5 and an AUC-ROC = 0.84, strong enough to be used in a real-time BCI as two independent control features. This was using KNN model for *beta* ERS feature. The final study of this research followed the same paradigm as used in Chapter 6, but for left vs. right knee KMI cognitive task **(Chapter 8)**. Primarily this study aimed at enhancing the resulting accuracy from Chapter 7, using CSP and FBCSP methods with Logreg and LDA models respectively. Results were in accordance with those of the already established foot KMI study, i.e. BP feature vector performed better than the CSP. Highest classification accuracy of 70.00% ± 2.85 with kappa score of 0.40 was obtained with Logreg using FBCSP feature vector. Results stipulated the utilization of ERD/ERS in *mu* and *beta* bands, as independent control features for discrimination of bilateral foot or the novel bilateral knee KMI tasks. Resulting classification accuracies implicate that any 2-class BCI, employing unilateral foot, or knee KMI, is suitable for real-time implementation.

In conclusion, this thesis demonstrates the possible EEG pre-processing, feature extraction and classification methods to instigate a real-time BCI from the conducted studies. Following this, the critical aspects of latency in information transfer rate, SNR, and tradeoff between dimensionality and overfitting needs to be taken care of, during design of real-time BCI controller. It also highlights that there is a need for consensus over the development of standardized methods of cognitive tasks for MI based BCI.

Finally, the application of wireless EEG for portable assistance is essential as it will contribute to lay the foundations of the development of independent asynchronous BCI based on SMR.

This page is left intentionally blank.

Acknowledgements

First and foremost my heartiest gratitude goes to Almighty, who gave me the strength, confidence to work on this research idea, and good health to complete this thesis within the allocated timeframe. Further, I would like to acknowledge the assistance and support provided by the following people in the completion of this thesis.

Professor Pavel Trivailo (Principal Supervisor) for his continuous support, guidance, constructive feedbacks and valuable insights on this thesis. I acknowledge his perseverance for conducting high-level research and patience in reading my research articles and this thesis. Despite his busy schedule and lot of responsibilities, he has always been available for discussing different research ideas and has always encouraged me to transform those ideas into constructive work. I practically learnt from him the meaning of 'never give up'. I would confidently say that Professor Trivailo is one of the best leading supervisors at RMIT University and I feel honoured to be under his research supervision.

Dr. Milan Simic (Associate-Supervisor) for his technical discussions, assistance and support throughout my candidature. He is a great source of motivation and has always encouraged me to bring some innovative ideas in my research. With a sincere commitment towards his profession he was always readily available for discussions on research ideas. I am truly privileged to have worked closely with him that helped me to improve my practical skills in conducting research work.

Dr. Yutaka Shoji from RMIT (Biomedical Engineering) for technical discussions and suggestions on different software that embedded the time stamps on recorded EEG signals involved in this work, and installation of unstable versions of EEGLAB and BCILAB.

I am really grateful to my PhD research sponsors RMIT University for awarding me the RMIT PhD International Scholarship (RPIS). I also wish to thank my master student, Lena Uhlenberg for her assistance in establishing the experimental protocol for synchronous BCI in this project.

I would like to express my deepest gratitude to Dr. Greg Oswald and his team at RMIT Bundoora east campus for showing trust in me and giving me after-hours access to the Mechatronics Lab (253.01.028). I would also like to thank Mr Sebastian Naselli for providing me with storage space, tools and access in the Mechatronics Lab.

I am thankful to all my family members: My father and mother for their endless physical and moral support, countless prayers, and ever encouraging words, I always look up to them for they have been the torchbearers in my life, my sisters (Jaweria Tariq and Bushra Komal Tariq) for never letting me lose hope and never letting the cheerful side of mine go away, my dear husband (Dr. Khurram S. Munir) without whom it was impossible to pull this degree off, he is my confidant, inspiration and support system, my precious and prettiest daughters (Maheen Khurram and Zeenya Khurram) who mean the world to me, they make me a proud mother, I hope one day they will read this thesis. Finally, I thank my in-laws for their unconditional encouragement, love and support that instilled in me a belief to complete this research, and make my and our family's dream come true. I can proudly say that I will be the first woman from my generation in my immediate family (the Qureshi clan), after my grandfather's brother Dr. Imtinan Elahi Qureshi, to confer on the title of Doctor of Philosophy.

This page is left intentionally blank.

Contribution to jointly authored papers

The candidate would like to acknowledge the help of all-co-authors who assisted and contributed to the papers included in this thesis. All co-authors have given approval for the relevant papers to be included as part of this dissertation. As reflected by the candidate's position as first author on all included papers, the candidate confirms that she has made the major contribution to all papers forming this dissertation. All papers were primarily written by the candidate. The author indication forms are provided in the appendices.

This page is left intentionally blank

Table of contents

List of figures

Figures in Chapter 4

Figures in Chapter 5

Figures in Chapter 6

Figures in Chapter 7

Figures in Chapter 8

List of tables

Tables in Chapter 2

Tables in Chapter 3

Tables in Chapter 4

Tables in Chapter 5

Tables in Chapter 6

Tables in Chapter 7

Tables in Chapter 8

This page is left intentionally blank

List of author's published papers incorporated into this thesis

M. Tariq, P. M. Trivailo, and M. Simic. *EEG-Based BCI Control Schemes for Lower-Limb Assistive-Robots*. Frontiers in Human Neuroscience, 12, 312, 2018

M. Tariq, P. M. Trivailo, Yutaka Shoji, and M. Simic. *Comparison of event-related changes in oscillatory activity during different cognitive imaginary movements within same lower-limb*. Acta Polytechnica Hungarica, 16 (2) 77-92, 2019.

M. Tariq, P. M. Trivailo, M. Simic. *Mu-beta event-related (de)synchronization and EEG classification of left-right foot dorsiflexion kinaesthetic motor imagery for BCI*. PLOS One (Under Review).

M. Tariq, P. M. Trivailo, and M. Simic. *Classification of left and right foot kinaesthetic motor imagery using common spatial pattern*. Biomedical Physics and Engineering Express (Accepted).

M. Tariq, P. M. Trivailo, M. Simic. *Classification of left and right knee extension motor imagery using common spatial pattern for BCI applications.* International Journal of Knowledge-Based and Intelligent Engineering Systems: Procedia Computer Science, 159, 2598-2606, 2019.

List of author's published papers incorporated into appendices

M. Tariq, Pavel M. Trivailo, and Milan Simic. *Event-related changes detection in sensorimotor rhythm*. International Robotics & Automation Journal, 4(2) 119-120, 2018.

M. Tariq, P.M. Trivailo, and M. Simic. *Motor imagery based EEG features visualization for BCI applications*. International Journal of Knowledge-Based and Intelligent Engineering Systems: Procedia Computer Science 126, 1936-1944, 2018.

M. Tariq, L. Uhlenberg, P.M. Trivailo, K.S. Munir, and M. Simic. *Mu-Beta Rhythm ERD/ERS Quantification for Foot Motor Execution and Imagery Tasks in BCI Applications*. 8th IEEE International Conference on Cognitive Infocommunications (CogInfoCom), 2017, pp. 091-096. IEEE, 2017, Debrecen, Hungary.

M. Tariq, P.M. Trivailo, and M. Simic. *Detection of Knee Motor Imagery by Mu ERD/ERS Quantification for BCI Based Neurorehabilitation Applications.* 11th Asian Control Conference (ASCC), 2017, pp. 2215-2219. IEEE, 2017, Gold Coast, Australia.

List of author's published papers not incorporated into thesis

M. Tariq, Z.U. Koreshi, and P.M. Trivailo. *Optimal Control of an Active Prosthetic Ankle*. 3rd International Conference on Mechatronics and Robotics Engineering (ICMRE), 2017, pp.113-118. ACM, 2017, Paris, France.

List of conference papers and conference abstracts

M. Tariq, L. Uhlenberg, P.M. Trivailo, K.S. Munir, and M. Simic. *Mu-Beta Rhythm ERD/ERS Quantification for Foot Motor Execution and Imagery Tasks in BCI Applications*. 8th IEEE International Conference on Cognitive Infocommunications (CogInfoCom), 2017, pp. 091-096. IEEE, 2017, Debrecen, Hungary.

M. Tariq, P.M. Trivailo, and M. Simic. *Detection of Knee Motor Imagery by Mu ERD/ERS Quantification for BCI Based Neurorehabilitation Applications*. 11th Asian Control Conference (ASCC), 2017, pp. 2215-2219. IEEE, 2017, Gold Coast, Australia.

M. Tariq, Z.U. Koreshi, and P.M. Trivailo. *Optimal Control of an Active Prosthetic Ankle*. 3rd International Conference on Mechatronics and Robotics Engineering (ICMRE), 2017, pp.113-118. ACM, 2017, Paris, France.

List of technical and research presentations

M. Tariq, P.M. Trivailo, and M. Simic. *Brain actuated bionic foot*. Pitch for US-AUS Robotics & Autonomy Workshop, organized by Defence Science Institute, Adelaide Australia, 2017.

List of abbrevations

ACC	Accuracy
ALS	Amyotrophic lateral sclerosis
ANN	Artificial neural network
ANOVA	Analysis of variance
AUC	Area under curve
AUX1	Auxiliary channel-1
AUX2	Auxiliary channel-2
BCI	Brain-computer interface
BP	Band-power
BSS	Blind source separation
CAN	Controller area network
CHEAN	College human ethics advisory network
CMC	Corticomuscular coherence
CNN	Convolutional neural network
CNS	Central nervous system
CPCA	Class-wise principal component analysis
CPG	Central-pattern-generators
CSP	Common spatial pattern
CVA	Canonical variate analysis
DFT	Discrete Fourier Transform
DOF	Degrees of freedom
DRNN	Dynamic recurrent neural network

EEG	Electroencephalography
EMG	Electromyography
ERD	Event-related desynchronization
ERDS	Event-related desynchronization-synchronization
ERP	Event-related potential
ERS	Event-related synchronization
ERSP	Event-related spectral perturbation
FBCSP	Filter bank common spatial pattern
FDR	False discovery rate
FES	Functional electrical stimulation
FIR	Finite impulse response
FP	False positive
FPR	False positive rate
GMM	Gaussian mixture model
ICA	Independent component analysis
ICT	Information and communication technology
IP	Internet protocol
ITC	Inter-trial coherence
ITV	Inter-trial variance
KMI	Kinaesthetic motor imagery
KNN	K-nearest neighbors
LDA	Linear discrimination analysis
LF	Left foot

LK	Left knee
LL	Lower-limb
Logreg	Logistic regression
LSL	Lab streaming layer
MAFO	Motorized ankle-foot orthoses
mcr	misclassification rate
ME	Motor execution
MI	Motor imagery
ML	Machine learning
MLP	Multi-layer perceptron
MRCP	Movement-related cortical potential
PCA	Principal Component analysis
PSD	Power spectral density
RF	Right foot
RK	Right knee
ROC	Receiver-operator characteristic curve
RoGO	Robotic gait orthosis
SCI	Spinal cord injury
SCP	Slow cortical potential
SGRM	Sparse group representation model
SMA	Supplementary motor area
SMR	Sensorimotor rhythm
SNR	Signal-to-noise ratio

SSVEP	Steady-state visually evoked potential
SVM	Support vector machine
TCP	Transmission control protocol
TF	Time-frequency
TMS	Transcranial magnetic stimulation
TP	True positive
TPR	True positive rate
TSGSP	Temporally constrained sparse group spatial pattern
VEP	Visual evoked potential
VRE	Virtual reality environment
VRPN	Virtual reality peripheral network
WMRA	Wheelchair-mounted robotic arm

Chapter 1

Introduction

Chapter Overview

The objective of this chapter is to highlight the significance of various factors involved in the development of brain-computer interface (BCI) controlled actuators/output devices. In this framework, the chapter discusses key issues and challenges involved in the feature selection and classification of sensorimotor-based EEG signals. The motivation and significance of the present study are highlighted, followed by a detailed discussion of the scope of this particular study. In the last section, the structure of the thesis is presented, including a brief summary of each chapter.

1.1 Overview of brain-computer interface controlled actuators/output devices

From a recent survey it is observed that due to central nervous system (CNS) disorder, more than 10 million people in the world live with various forms [1] of disability. Existing assistive lower-limb (LL) devices based on sensors and smart control algorithms are known to be suitable for rehabilitation of lost mobility compared to passive devices that account for high metabolic cost of transport [2]. In order to account for such critical aspects, research has been carried out to develop algorithms matching user's motion intention that could generate correct walking trajectories with wearable robots. However, the control features offered by these devices solely rely on actuation of the system derived from artificial sensors along finite state controller that attempts to implicate biomechanical gait mechanism [3, 4], resulting in a restricted seamless control. This lead to the development of controllers based on actuation signals directly driven by cortical activity in correlation with the user intent for volitional movements [5]. The state of the art brain-computer interface (BCI) provides an augmentative communication source by creating a muscle-free channel between the brain and the output device. It accentuates real-time bidirectional connection between the brain and actuator/output device. With these superior control properties, BCI is considered to be a novel engineering tool for neurorobotics, neuroprosthesis and assistive rehabilitation device applications for patients with neural disorders, spinal cord injury (SCI), or amputation. Successful design with seamless control and development of brain actuated assistive devices with improved classification accuracy, information transfer rate, and signal-to-noise-ratio, remains a significant research area through which it would be possible to minimize occurrence of non-volitional control and enhance the reliability of these devices under severe operating conditions of users.

Since the first successful experiment on creating a direct link between a patient's motor cortex and the external device (a projector), by Grey Walter in 1963 and later by NIH laboratory, to control artificial actuators via cortical neuron recordings [6], significant research has been carried out to monitor and decipher cortical neuron activity using cortical implants. However, the modality employed was invasive. It has significant properties as high spatial resolution (tenths of millimeters), broader bandwidth (0 to 500 Hz), high characteristic amplitude (50 to 100 μV), less vulnerability to artifacts and less user-BCI system adaptability (training); followed by higher cost with an inflated risk of scar tissue formation [7]. The non-

invasive modalities offer better solutions. Electroencephalography (EEG) is one such viable tool that offers effective specifications as, lower in cost, ease of use, safest method to record brain activity and high time resolution (millisecond scale temporal resolution)[8]; however there is a tradeoff between performance and features as, lower spatial resolution (centimeters), lower bandwidth (0 to 50 Hz), lower characteristic amplitude (10 to 20 μV), high susceptibility to artifacts, and several hours of training for user-BCI adaptability [7]. Nevertheless, EEG account for the safest technology therefore remains popular choice for BCI modality.

While BCIs may not require any voluntary muscle control, they are certainly dependent on normal brain function to some degree therefore the choice of BCI type depends on user's condition [9]. Research on EEG based BCIs for assistive device applications have been carried out since 2000 [9]. Majority of the electrophysiological input signals employed by researchers included event-related potentials (ERPs), steady-state visually evoked potentials (SSVEPs), slow cortical potentials (SCPs) and oscillatory/sensorimotor rhythms (mu and beta oscillatory activity also termed SMRs). The most challenging signals discerned, arose in the motor cortex against the execution or imagery of a motor task, i.e. SMRs. This is because of the proprioceptive feedback involved during execution of the task and the varying level of user concentration. Active research contributions were from Graz BCI and Wadsworth BCI research centers that focused on ERPs and SMRs [10, 11]. Their applications addressed amyotrophic lateral sclerosis (ALS)/totally locked-in patients to restore basic communication needs including, 1D-2D cursor control on a computer, answering spoken Yes/No commands, basic word processing speller, first point development of prototype systems integrating submenu for everyday use in people’s homes, and control of orthotic device for opening and closing paralyzed limb (hand grasp) [12]. However, less emphasis reflected LL movement restoration for patients with spinal cord injury (SCI), disarticulated leg muscles, inactive residual LL or amputees, until recently. Concept was made that the central-pattern-generators with less supraspinal control are involved in the control of bipedal locomotion [5, 13]. EEG-based activity mode recognition for assistive portable devices has been deployed recently such as wheelchairs, assistive/guiding robots, orthosis and exoskeletons, [5]. However, challenges still remain in the field.

For BCI systems that employ SMR-based EEG as input signals, the long training process of users to adapt to the BCI system is challenging [14]. Same cortical areas should activate during the actual performance of a limb movement and imagination of the same movement [15]. Although supervised classification methods are employed to learn how to recognize

specific patterns of EEG activities, i.e. to learn the mapping between the EEG data and classes corresponding to mental tasks, such as movement of the left or right hand. However, the learning task is challenging as various governing factors impact the output result, such as the varying physical and mental state (degree of attention and concentration), eye blinks and muscle artifacts that contaminate the EEG signal.

Based on the somatotopic arrangement of sensory and motor cortices, the upper limbs particularly hand representation is on the mantle of the human cortex. It is lateralized, the reason why left and right hand movement's ERD patterns can be spatially distinguished. In contrast, the LL e.g. the foot and knee's motor area representation on the homunculus is located deep inside the interhemispheric fissure with low spatial resolution, which makes it very difficult for the detection of these patterns through the EEG signal [16], hence more exploration needs to be done in this area. There is a need to investigate the probability of using band-power and common spatial pattern features as input control signals to a BCI system.

Before 2009, BCIs to control prosthetic devices were limited to upper limb prosthetics e.g. the DARPA modular prosthetic limb [17]. This was attributable to lack of analysis tools for analyzing cortical dynamics with EEG due to excessive proprioceptive feedback during walking. Until recently, the concept was made that the central-pattern-generators with less supraspinal control is involved in the control of bipedal locomotion [5]. Though scientific contribution has been made in the field of rehabilitative robotics controlled via BCI, yet no contribution has been made to the direct user intent control of active prosthetic LL device via BCI employing SMR-based EEG only.

1.2 Research aims and objectives

The rationale for this research project is to prove the possibility to deploy *mu* and *beta* sensorimotor rhythms, elicited upon LL kinesthetic motor imageries, as input control signals for development of an augmentative communication channel in order to restore lost motor control in subjects with LL amputation, SCI, disarticulated leg muscles, or inactive residual LL. In a BCI paradigm, output device is controlled via input commands extracted from cortical activity but these commands surpass the brain's usual output pathways of peripheral muscles and nerves, and are encoded in an electroencephalographic activity (in case of non-invasive EEG). Henceforth, providing an alternate source of basic communication and control paradigm to the completely or partially paralyzed subjects, in order to express their needs to caregivers, or independently operate program and control neuroprostheses

seamlessly in real-time. Present-day BCIs that determine the intent of the user employ SMR electrophysiological signals. SMR-based BCI are either synchronous or asynchronous. Unlike the P300 (ERP) and SSVEP-based BCIs that require minimum/no training to adapt BCI system and vice versa, SMR-based BCIs typically require much longer training periods to attain high levels of performance. The training process is deployed, both to familiarize the user to system, and to provide calibration data for the system's classifier(s).

Despite advancements in BCI expansion in the recent decade, less literature is available on the employment of SMR based on LL tasks, in particular there is no evidence on the knee kinesthetic motor imagery. Therefore challenges still exist in the development of non-invasive SMR based-BCIs in regards to assistive (wearable) LL devices with a minimal probability of non-volitional output commands. The feature extraction and classification of feature vector for reduced error rate, effective information transfer rate and improved signal-to-noise ratio (SNR) remain an open research problem in BCI systems.

Gaps in the Research Field

1. Less known facts and investigations are observed on the LL kinaesthetic motor imagery (KMI) tasks based band-power and common spatial pattern features, that are deployed as control signals, in any BCI protocol.
2. Selection of optimal frequency-band that consists of the maximum useful features and reliable feature vectors to be used as input control signals to a BCI system is still an open research problem.
3. Cognitive states used in BCI system i.e. the types of mental states/motor actions for motor imagery is still an area open for research [9]. For instance, there is no comprehensive approach to the detection of signals associated to knee imagery.
4. Similarly most efficient algorithms for translating LL SMR signals into device commands are not conclusively defined.
5. No explicit development of ankle-foot prosthesis actuated by LL KMI is available.

The important research questions addressed in this project include:

- What is the interaction platform between human brain signals and output device or outer world?
- How we can quantitatively predict which precise cortical activity is associated to specific tasks?

- How can a BCI system prove to be reliable?
- How BCI can effectively contribute to the use of prosthetic or assistive robotic devices for rehabilitation?

The ultimate objective is to analyze and classify the sensorimotor rhythms i.e. *mu* and *beta* band-power (BP) and common spatial pattern (CSP) features elicited upon user's intent of locomotion, i.e. LL KMI tasks including foot dorsiflexion and knee extension, for BCI applications.

The research objectives include:

i. Development of a clear understanding on human brain anatomy and ankle-foot biomechanics followed by the control mechanism between neurons, LL (motor tasks) and central pattern generators for walking gait. Analysis of the non-invasive modalities to detect and monitor brain activity. Review of conventional and existing BCI systems (based on EEG modality) that have been incorporated in different LL wearable robotic applications.

ii. Establish the experimental set up from scratch and satisfy criteria for synchronous BCI protocol (cue-paced) streaming data and timestamps/event markers to describe the time course of the experiment.

iii. Recruitment of participants in the experiments, train them in LL motor execution and kinesthetic imagery tasks and ensure progressive output in performance.

iv. Observe significant changes in oscillatory activities, in relation to an internally, or externally paced events that are time-locked, but not phase-locked (induced) associated to event-related desynchronization (ERD) or event-related synchronization (ERS). Following this, test statistics for evaluation of significant feature vectors. Consequently, to analyze the ERD-ERS and significant BP changes of most reactive *mu* and *beta* components and CSP for LL tasks, to comply with the already built notion and results from literature referring to the cortical lateralization of ERD/ERS during left-right foot and knee tasks in sensory motor cortex. Establish correlation between the motor execution and motor imagery tasks for the same limb.

v. Employ classification techniques for the 2-class BCI i.e. discrimination between left and right tasks, by comparing results from linear discriminant analysis (LDA), linear support vector machine (SVM), k-nearest neighbors (KNN), and logistic regression (Logreg) (algorithm) models. This includes

data standardization, and training of the classifier to improve the classification accuracy, signal-to-noise ratio, reduce error rate and prove its statistical significance. Consequently conducting the test statistics i.e. multiple comparison corrections for each classifier model outcome.

1.3 Thesis structure

This thesis is assembled as a combination of publications and submitted manuscripts resulting in 9 chapters as follows:

Chapter 1 gives an introduction to the field of research employed and an overall structure of the thesis.

Chapter 2 presents an overview of the related literature on control schemes employed by LL motor imagery based BCIs for controlling LL assistive robots. Particular emphasis is put on the output of different methodologies adopted for the EEG signal pre-processing, feature extraction and training of the classifiers. The assistive LL robotic systems that employ sensorimotor rhythms and event-related potentials as input signals in a BCI for rehabilitation, such as BCI wheelchair, BCI controlled humanoid and guidance robots, BCI orthotic and exoskeleton devices are reviewed here. The role of the shared control paradigms for wearable assistive devices is highlighted. A general framework for BCI controlled LL portable and assistive-robot devices for rehabilitation is represented in the novel form of a three-level hierarchical operational structure coupled to the shared controller and together connected to the portable output device and its surrounding environment. Latest developments in field of EEG-based BCIs are included. The findings of this work were published in the journal of *Frontiers in Human Neuroscience.*

Chapter 3 provides a methodological description of the materials and methods for the EEG data acquisition. The pre-processing methods employed to de-noise and filter the EEG signal are demonstrated. Techniques employed for ERD/ERS percentage power change BP features and CSP feature extraction is shown. Following this, in order to characterize the features belonging to the two classes i.e. left vs. right motor imagery, the classification models are presented. In order to evaluate the performance of each classifier, test statistical analysis methods are discussed and the multiple comparison correction procedures adopted in each chapter.

In **Chapter 4**, the study aimed at highlighting any observed differences in the *mu* oscillatory rhythm derived BP changes during different LL KMI tasks i.e. left vs. right foot dorsiflexion and left vs. right knee extension tasks for the same limb. Despite a small LL sensorimotor area representation in the homunculus, the foot and knee movement imagery elicited ERD patterns. An increase in the mid-central ERD was observed overall with all the participants. The kinaesthetic knee imagery triggered *mu* ERD, mainly in the cortical foot area representation. No contralateral dominance of cortical areas was present in the case of left-right knee imagery tasks, unlike with foot tasks. Results indicate the possibility of discriminating different movements within the same LL. This could increase the dimensionality of control signals in a BCI system. The findings of this work are published in the journal of *Acta Polytechnica Hungarica.*

Chapter 5 presents the experimental outcomes from analysis and classification of ERD/ERS that elicit in the band-power feature vector, for *mu* and *beta* rhythms. This was based on cognitive tasks of left vs. right foot KMI. The analysis was carried out for two EEG montages, common average reference and bipolar reference to draw a comparison of resulting features that are significant enough to confirm the cortical lateralization. Analysis of *mu* and *beta* features was done using time-frequency (TF) maps, scalp topographies, and average time course for ERD/ERS. Consequently machine learning (ML) models were deployed for classifying left vs. right foot KMI. The study comprised of three different models to conclude the best one with maximum classification accuracy and AUC. All test statistics including multiple comparisons correction was included for evaluation of statistically significant model outcomes. The cortical lateralization was confirmed, which proved that *mu* ERD, *beta* ERD, and *beta* ERS can be deployed as independent control features in a BCI. The findings from this study are under review in the journal of *PLOS One.*

Chapter 6 reflects the findings from analysis of ERD/ERS patterns exhibited in the oscillatory rhythm from CSP and filter bank CSP (FBCSP) feature vectors respectively. Experimental protocol was based on left vs. right foot KMI for synchronous BCI. This was followed by deployment of ML models including linear LDA and Logreg. The study was carried out to improve the classification accuracy earlier established by literature. Results proved a successful improvement in the accuracy outcomes from the suggested FBCSP-LDA model. All test statistics including multiple comparisons correction was conducted for statistical evaluation of models. Classification results contribute to the possibility of

exploiting *mu* and *beta* ERD/ERS features as control commands in a BCI. The findings from this work are accepted in the journal of *Biomedical Physics and Engineering Express*.

Chapter 7 highlights the classification accuracies of *mu* ERD and *beta* ERS features based on left and right knee extension KMI. This cognitive task involved full knee extension while in sitting posture. The spatial proximity of left and right knee in the mesial wall of the sensorimotor cortex hinders the discrimination between the left and right tasks. Consequently ERD/ERS patterns were only reflected in the foot area of somatosensory cortex. However, this research's results established the possibility to deploy knee KMI as cognitive input signals and use *mu* and *beta* as independent features for operating a 2 degrees of freedom BCI-controlled prosthetic or robotic knee.

Chapter 8 reflects the results from classification of oscillatory *mu* and *beta* ERD/ERS from CSP and FBCSP feature vectors respectively, following the synchronous BCI protocol of left vs. right knee extension KMI. In order to confirm the cortical lateralization of ERD/ERS, ML models, LDA and Logreg were used for an enhancement in the classification accuracy established from the previous chapter. FBCSP-Logreg model showed maximum classification accuracy amongst other models. Classification results provide the basis for the possibility of exploiting *mu* and *beta* ERD/ERS features as control commands in a BCI. The results from this research are published in the *International Journal of Knowledge-Based and Intelligent Engineering System (Procedia Computer Science)*.

In the end, **Chapter 9** outlines all the significant findings of this thesis and suggests some recommendations for further studies.

1.4 References

1. Chéron, G., et al., *From spinal central pattern generators to cortical network: integrated BCI for walking rehabilitation.* Neural plasticity, 2012. **2012**.
2. Au, S.K., J. Weber, and H. Herr, *Powered Ankle--Foot Prosthesis Improves Walking Metabolic Economy.* IEEE Transactions on Robotics, 2009. **25**(1): p. 51-66.
3. Au, S.K., et al. *Powered ankle-foot prosthesis for the improvement of amputee ambulation*. in *Engineering in Medicine and Biology Society, 2007. EMBS 2007. 29th Annual International Conference of the IEEE*. 2007. IEEE.
4. Jimenez-Fabian, R. and O. Verlinden, *Review of control algorithms for robotic ankle systems in lower-limb orthoses, prostheses, and exoskeletons.* Medical engineering & physics, 2012. **34**(4): p. 397-408.
5. Tucker, M.R., et al., *Control strategies for active lower extremity prosthetics and orthotics: a review.* Journal of neuroengineering and rehabilitation, 2015. **12**(1): p. 1.

6. Lebedev, M.A. and M.A. Nicolelis, *Brain-Machine Interfaces: From Basic Science to Neuroprostheses and Neurorehabilitation.* Physiological Reviews, 2017. **97**(2): p. 767-837.
7. Schalk, G. and J. Mellinger, *A practical guide to brain–computer interfacing with BCI2000: General-purpose software for brain-computer interface research, data acquisition, stimulus presentation, and brain monitoring*. 2010: Springer Science & Business Media.
8. Repovs, G. *Dealing with noise in EEG recording and data analysis*. in *Informatica Medica Slovenica*. 2010.
9. Wolpaw, J.R., et al., *Brain–computer interfaces for communication and control.* Clinical neurophysiology, 2002. **113**(6): p. 767-791.
10. Pfurtscheller, G., et al., *15 years of BCI research at Graz University of Technology: current projects.* IEEE Transactions on Neural Systems and Rehabilitation Engineering, 2006. **14**(2): p. 205-210.
11. Vaughan, T.M., et al., *The wadsworth BCI research and development program: at home with BCI.* IEEE transactions on neural systems and rehabilitation engineering, 2006. **14**(2): p. 229-233.
12. Daly, J.J. and J.R. Wolpaw, *Brain–computer interfaces in neurological rehabilitation.* The Lancet Neurology, 2008. **7**(11): p. 1032-1043.
13. Presacco, A., et al., *Neural decoding of treadmill walking from noninvasive electroencephalographic signals.* Journal of neurophysiology, 2011. **106**(4): p. 1875-1887.
14. He, B., et al., *Noninvasive brain-computer interfaces based on sensorimotor rhythms.* Proceedings of the IEEE, 2015. **103**(6): p. 907-925.
15. Pfurtscheller, G., et al., *Graz-BCI: state of the art and clinical applications.* IEEE Transactions on neural systems and rehabilitation engineering, 2003. **11**(2): p. 1-4.
16. Hashimoto, Y. and J. Ushiba, *EEG-based classification of imaginary left and right foot movements using beta rebound.* Clinical neurophysiology, 2013. **124**(11): p. 2153-2160.
17. Presacco, A., L. Forrester, and J.L. Contreras-Vidal. *Towards a non-invasive brain-machine interface system to restore gait function in humans*. in *Engineering in Medicine and Biology Society, EMBC, 2011 Annual International Conference of the IEEE*. 2011. IEEE.

Chapter 2

Literature Review

Chapter Overview

A brief introduction of BCI systems for controlling LL assistive robots, their potentials, challenges, and the objectives of the research were drawn in Chapter 1. This chapter reviews the existing literature on control schemes, i.e. preprocessing, feature extraction techniques and classification algorithms deployed by EEG-BCIs LL assistive robots for rehabilitation. BCIs employing SMR (*mu* and *beta* rhythms) and ERP as control commands have critically been reviewed. A general control framework is novelly presented for BCI controlled LL portable and assistive-robot devices. Practical challenges associated to the field have also been highlighted.

This work is published in ***Frontiers in Human Neuroscience.***

M. Tariq, P. M. Trivailo, and M. Simic. *EEG-Based BCI Control Schemes for Lower-Limb Assistive-Robots*. Frontiers in Human Neuroscience, 12, 312, 2018.

frontiers in Human Neuroscience

REVIEW
published: 06 August 2018
doi: 10.3389/fnhum.2018.00312

EEG-Based BCI Control Schemes for Lower-Limb Assistive-Robots

*Madiha Tariq, Pavel M. Trivailo and Milan Simic**

School of Engineering, RMIT University Melbourne, Melbourne, VIC, Australia

Over recent years, brain-computer interface (BCI) has emerged as an alternative communication system between the human brain and an output device. Deciphered intents, after detecting electrical signals from the human scalp, are translated into control commands used to operate external devices, computer displays and virtual objects in the real-time. BCI provides an augmentative communication by creating a muscle-free channel between the brain and the output devices, primarily for subjects having neuromotor disorders, or trauma to nervous system, notably spinal cord injuries (SCI), and subjects with unaffected sensorimotor functions but disarticulated or amputated residual limbs. This review identifies the potentials of electroencephalography (EEG) based BCI applications for locomotion and mobility rehabilitation. Patients could benefit from its advancements such as wearable lower-limb (LL) exoskeletons, orthosis, prosthesis, wheelchairs, and assistive-robot devices. The EEG communication signals employed by the aforementioned applications that also provide feasibility for future development in the field are sensorimotor rhythms (SMR), event-related potentials (ERP) and visual evoked potentials (VEP). The review is an effort to progress the development of user's mental task related to LL for BCI reliability and confidence measures. As a novel contribution, the reviewed BCI control paradigms for wearable LL and assistive-robots are presented by a general control framework fitting in hierarchical layers. It reflects informatic interactions, between the user, the BCI operator, the shared controller, the robotic device and the environment. Each sub layer of the BCI operator is discussed in detail, highlighting the feature extraction, classification and execution methods employed by the various systems. All applications' key features and their interaction with the environment are reviewed for the EEG-based activity mode recognition, and presented in form of a table. It is suggested to structure EEG-BCI controlled LL assistive devices within the presented framework, for future generation of intent-based multifunctional controllers. Despite the development of controllers, for BCI-based wearable or assistive devices that can seamlessly integrate user intent, practical challenges associated with such systems exist and have been discerned, which can be constructive for future developments in the field.

Keywords: brain-computer interface (BCI), electroencephalography (EEG), spinal cord injury (SCI), exoskeletons, orthosis, assistive-robot devices

OPEN ACCESS

Edited by:
Mikhail Lebedev,
Duke University, United States

Reviewed by:
Vera Talis,
Institute for Information Transmission Problems (RAS), Russia
Yuri Levik,
Institute for Information Transmission Problems (RAS), Russia

****Correspondence:***
Milan Simic
milan.simic@rmit.edu.au

Received: *03 May 2018*
Accepted: *16 July 2018*
Published: *06 August 2018*

Citation:
Tariq M, Trivailo PM and Simic M (2018) EEG-Based BCI Control Schemes for Lower-Limb Assistive-Robots. Front. Hum. Neurosci. 12:312. doi: 10.3389/fnhum.2018.00312

INTRODUCTION

The field of assistive technologies, for mobility rehabilitation, is ameliorating by the introduction of electrophysiological signals to control these devices. The system runs independent of physical, or muscular interventions, using brain signals that reflect user's intent to control devices/limbs (Millán et al., 2010; Lebedev and Nicolelis, 2017), called brain-computer interface (BCI). Commonly used non-invasive modality to record brain signals is electroencephalography (EEG). EEG signals are deciphered to control commands in order to restore communication between the brain and the output device when the natural communication channel i.e., neuronal activity is disrupted. Recent reviews on EEG-BCI for communication and rehabilitation of lower-limbs (LL) could be found in (Cervera et al., 2018; Deng et al., 2018; He et al., 2018a; Lazarou et al., 2018; Semprini et al., 2018; Slutzky, 2018).

About five decades ago, EEG-BCIs used computer cursor movements to communicate user intents for patient-assistance in various applications (Vidal, 1973; Wolpaw et al., 2002; Lebedev and Nicolelis, 2017). The applications are now widespread, as machine learning has become one essential component of BCI, functional in different fields of neurorobotics and neuroprosthesis. For lower extremity, applications include human locomotion assistance, gait rehabilitation, and enhancement of physical abilities of able-bodied humans (Deng et al., 2018). Devices for locomotion, or mobility assistance, vary from wearable to (non-wearable) assistive-robot devices. Wearable devices such as exoskeletons, orthosis, prosthesis, and assistive-robot devices including wheelchairs, guiding humanoids, telepresence and mobile robots for navigation are the focus of our investigation.

Control schemes, offered by these systems, rely on the inputs derived from electrophysiological signals, electromechanical sensors from the device, and the deployment of finite state controller that attempts to implicate user's motion intention, to generate correct walking trajectories with wearable robots (Duvinage et al., 2012; Jimenez-Fabian and Verlinden, 2012; Herr et al., 2013; Contreras-Vidal et al., 2016). Input signals are typically extracted from the residual limb/muscles i.e., amputated or disarticulated lower-limbs (LL), via electromyography (EMG), from users with no cortical lesion or intact cognitive functions. Such solutions consequently preclude patient groups whose injuries necessitate direct cortical input to the BCI controller, for instance users with neuromotor disorders such as spinal cord injury (SCI) and stroke, or inactive efferent nerves/synergistic muscle groups. In this case direct cortical inputs from EEG could be the central-pattern-generators (CPG) that generate basic motor patterns at the supraspinal or cortical level (premotor and motor cortex); or the LL kinesthetic motor imagery (KMI) signals (Malouin and Richards, 2010). The realization of BCI controllers solely driven by EEG signals, for controlling LL wearable/assistive devices, is therefore possible (Lee et al., 2017). Several investigations reinstate that CPG with less supraspinal control is involved in the control of bipedal locomotion (Dimitrijevic et al., 1998; Beloozerova et al., 2003; Tucker et al., 2015). This provides the basis for the development of controllers, directly driven from cortical activity in correlation to the user intent for volitional movements (Nicolas-Alonso and Gomez-Gil, 2012; Angeli et al., 2014; Tucker et al., 2015; Lebedev and Nicolelis, 2017) instead of EMG signals. Consequently, controllers with EEG-based activity mode recognition for portable assistive devices, have become an alternative to get seamless results (Presacco et al., 2011b). However, when employing EEG signals as input to the BCI controller, there necessitates a validation about the notion that EEG signals from the cortex can be useful for the locomotion control.

Though cortical sites encode movement intents, the kinetic and kinematic changes necessary to execute the intended movement, are essential factors to be considered. Studies indicate that the selective recruitment of embedded "muscle synergies" provide an efficient means of intent-driven, selective movement, i.e., these synergies, stored as CPGs, specify spatial organization of muscle activation and characterize different biomechanical subtasks (Chvatal et al., 2011; Chvatal and Ting, 2013). According to Maguire et al. (2018), during human walking, Chvatal and Ting (2012) identified different muscle synergies for the control of muscle activity and coordination. According to Petersen et al. (2012), the swing-phase was more influenced by the central cortical control, i.e., dorsiflexion in early stance at heel strike, and during pre-swing and swing phases for energy transfer from trunk to leg. They also emphasized the importance of cortical activity during steady unperturbed gait for the support of CPG activity. Descending cortical signals communicate with spinal networks to ensure that accurate changes in limb movement have appropriately integrated into the gait pattern (Armstrong, 1988). The subpopulations of motor-cortical neurons activate sequentially amid the step cycle particularly during the initiation of pre-swing and swing (Drew et al., 2008). The importance of cortical activation upon motor imagery (MI) of locomotor tasks has been reported in Malouin et al. (2003) and Pfurtscheller et al. (2006b). Similarly, the confirmation of electrocortical activity coupled to gait cycle, during treadmill walking or LL control, for applications as EEG-BCI exoskeletons and orthotic devices, has been discerned by (He et al., 2018b, Gwin et al. (2010, 2011), Wieser et al. (2010), Presacco et al. (2011a), Presacco et al. (2011b), Chéron et al. (2012), Bulea et al. (2013), Bulea et al. (2015), Jain et al. (2013), Petrofsky and Khowailed (2014), Kumar et al. (2015), and Liu et al. (2015). This provides the rationale for BCI controllers that incorporate cortical signals for high-level commands, based on user intent to walk/bipedal locomotion or kinesthetic motor imagery of LL.

While BCIs may not require any voluntary muscle control, they are certainly dependent on brain response functions therefore the choice of BCI depends on the user's sensorimotor lesion and adaptability. Non-invasive types of BCI depend on EEG signals used for communication, which elicit under specific experimental protocols. Deployed electrophysiological signals that we investigate, include oscillatory/sensorimotor rhythms (SMR), elicited upon walking intent, MI or motor execution (ME) of a task, and evoked potentials as event-related potentials (ERP/P300) and visual evoked potentials (VEP). Such BCI functions as a bridge to bring sensory input into the brain, bypassing damages sight, listening or sensing abilities. **Figure 1**

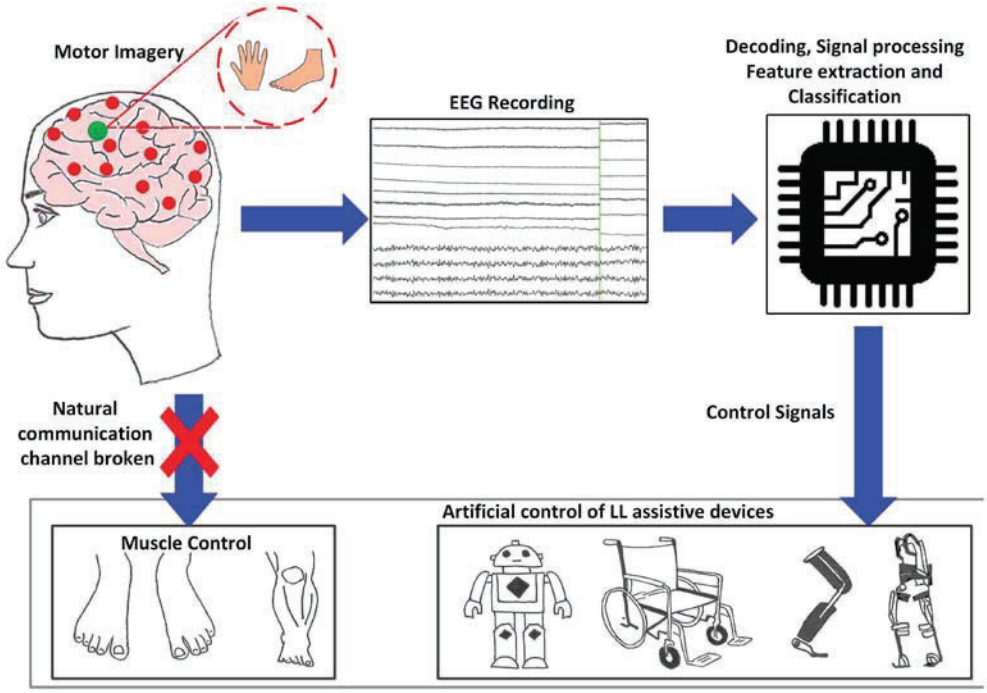

FIGURE 1 | Generic concept/function diagram of BCI controlled assistive LL devices based on motor imagery.

shows a schematic description of a BCI system based on MI, adapted from He et al. (2015). The user performs MI of limb(s), which is encoded in EEG reading; features representing the task are deciphered, processed and translated to commands in order to control assistive-robot device.

Reviewed control schemes deployed by wearable LL and assistive-robots are presented in a novel way, i.e., in form of a general control framework fitting in hierarchical layers. It shows the informatic interactions, between the user, the BCI operator, the shared controller, and the robot device with environment. The BCI operator is discussed in detail in the light of the feature extraction, classification and execution methods employed by all reviewed systems. Key features of present state-of-the-art EEG-based BCI applications and its interaction with the environment are presented and summarized in the form of a table. Proposed BCI control framework can cater similar systems based on fundamentally different classes. We expect a progress in the incorporation of the novel framework for the improvement of user-machine adaptation algorithms in a BCI.

The reviewed control schemes indicated that the MI/ME of LL tasks, as aspects of SMR-based BCI have not been extensively used compared to upper limbs (Tariq et al., 2017a,b, 2018). This is due to the small representation area of LL, in contrast to upper limbs, located inside the interhemispheric fissure of the sensorimotor cortex (Penfield and Boldrey, 1937). The review is an effort to progress the development of user's mental task related to LL for BCI reliability and confidence measures.

Challenges presently faced by EEG-BCI controlled wearable and assistive technology, for seamless control in real-time, to regain natural gait cycle followed by a minimal probability of non-volitional commands, and possible future developments in these applications, are discussed in the last section.

GENERAL CONTROL FRAMEWORK FOR BCI WEARABLE LOWER-LIMB AND ASSISTIVE-ROBOT DEVICES

In order to structure the control architecture adopted by various BCI wearable LL and assistive robot-devices, a general framework is presented in **Figure 2**. This framework was extended from Tucker et al. (2015) applicable to a range of EEG-BCI controlled devices for LL assistance, including portable exoskeletons, orthosis, prosthesis, and assistive-robots (wheelchairs, humanoids, and navigation/telepresence robots).

Figure 2 reflects the generalized control framework, where electrophysiological and transduced signal interactions, along the feedforward and feedback loops, are shown for motion intent recognition, during activity mode. Integral parts of the framework include a user of the assistive robot-device, the assistive-robot device itself, a BCI operator structure with sub-level controls, shared control, communication protocol and the interaction with environment. The BCI operator structure constitutes of three sub-layers which are the feature extraction, translation and execution layer, respectively. As a precaution to ensure human-robot interaction safety, safety layers are used

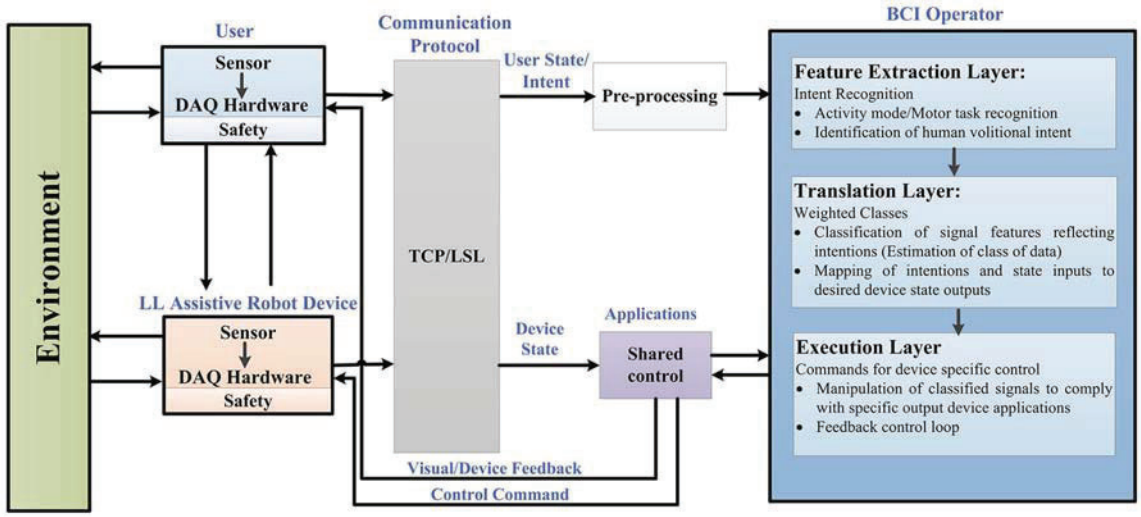

FIGURE 2 | Generalized framework in BCI controlled wearable LL and assistive devices for rehabilitation.

with the user and the robotic device parts of the framework. The control framework is in a generalized form applicable to all brain-controlled assistive robots.

BCI control is driven from the recognition of user's motion intentions; therefore we begin from the point of origin where motion intentions arise (cortical levels). The first step involves how to perceive and interpret the user's physiological state (i.e., MI/ME or ERP) acquired via EEG. Following this, the status of physical interaction between the user and the environment (and vice versa), and the robotic device and the environment (and vice versa) are checked. The assistive-robot's state is determined via electromechanical sensors. The user and assistive-robot status inputs to the BCI operator and shared controller, respectively.

Raw signals from the user and assistive LL device pass through the communication protocol which directs them to the connected client i.e., BCI operator via pre-processing and shared control module. Real-time signal acquisition and operating software could be used to assign event markers to the recorded data e.g., OpenViBE, BioSig, BCI++, BCI2000 etc. (Schalk et al., 2004; Mellinger and Schalk, 2007; Renard et al., 2010). The streaming connection can be made using TCP (when the time synchronization requirements do not need accuracy <100 ms) or LSL which incorporates built-in network and synchronization capabilities (with accuracy of 1 ms) recommended for applications based on ERPs.

Under the control framework components, BCI operator is the core part comprising of three sub layers, described in detail in section BCI Operator.

At feature extraction layer (intent recognition), user's intent of activities related to LL movements are perceived, discerned and interpreted. Signal features associated to user's kinesthetic intent/execution of motor task (in case of SMR) are encoded in form of feature vector (Lotte, 2014). The activity-mode recognition for ERP, against displayed oddball menu for specific location, uses frequency, or time domain features. It is the user's direct volitional control that lets voluntarily manipulate the state of the device (e.g., joint position, speed, velocity and torque).

Translation layer (weighted class) takes account of the translation of extracted signal features to manipulate the robotic device, via machine understandable commands, which carry the user's intent. This is done by supervised, or unsupervised learning (classification algorithm) which essentially estimates the weighted class, represented by the feature vector, and identifies the cognitive patterns for mapping to the desired state (unique command).

The desired state of user intent is carried to the execution layer (commands for device-specific control) where an error approximation is done with reference to current state. The state of the device is also sent to the execution layer via shared controller, as a feedforward control, in order to comply with the execution layer. The execution layer sends control commands to the actuator(s) of the device and visual feedback to the user via shared control unit in order to minimize the possible error. The feedback control plays a vital role in achieving the required output (usually accounts for the kinematic or kinetic properties of the robot-device).

This closes the overall control loop and the robotic device actuates to perform the required task(s). As the wearable assistive-robot is physically placed in close contact with the user, and that the powered device is likely to generate output force, safety mechanisms are kept into consideration with the user and hardware in the control framework. Inter-networking between subsystems of the generalized control architecture relies on the exchange of information sent at signal-level as well as physical-level.

USER ADAPTABILITY AND EEG SIGNAL ACQUISITION

The type of BCI is directed based on the user's lesion level and extent of adaptability to adhere with the specific BCI protocol.

User Adaptability

In order for the portable LL wearable-BCI controllers to be compliant with residual neuromusculoskeletal structures, the sensorimotor control loop of human locomotion is taken into account, since the volitional and reflex-dependent modulation of these locomotion patterns emerges at the cortical levels (Armstrong, 1988; Kautz and Patten, 2005; Bakker et al., 2007; Zelenin et al., 2011; Pons et al., 2013; Angeli et al., 2014; Marlinski and Beloozerova, 2014; Capogrosso et al., 2016). This may essentially preclude the direct control of LL via neural activity alone, while keeping a balance and orientation during dynamic tasks. However, the sole employment of cortical activity is still useful for providing high-level commands to the controller of the device to execute volitional movements (Carlson and Millan, 2013; Contreras-Vidal and Grossman, 2013; Kilicarslan et al., 2013), for patients whose injuries necessitate a direct input from cortex to the robotic device controller. Therefore, the critical aspect for a functional portable LL device is the lesion measure and the physiological constraints based on which the user can adapt to the BCI protocol. The physiological constraints in such cases can be compensated through assistance, like shared control.

EEG Signal Acquisition

The neuronal activity can be divided into spikes and field potentials. Spikes show action potentials of neurons individually and are detected via invasive microelectrodes. Field potentials on the other hand can be measured by EEG and they reflect the combined synaptic, axonal and neuronal activity of the neuron groups (Yang et al., 2014; He, 2016).

The communication components in EEG activity useful for BCI include, the oscillatory activity comprising of delta, theta, alpha/mu, beta and gamma rhythms; the ERP (P300), the VEP, and slow cortical potentials (SCP). Oscillatory rhythms fluctuate according to the states of brain activity; some rhythms are distinguished depending on these states (Semmlow and Griffel, 2014). The *Mu* and *beta* rhythms are also termed SMR. The SMR elicit event-related desynchronization (ERD) or event-related synchronization (ERS) which are directly related to proportional power decrease upon ME/MI of limb(s) movement or power increase in the signal upon rest, respectively; they are non-phase locked signals (Kalcher and Pfurtscheller, 1995). Evoked potentials on the other hand are phase-locked. A BCI system employs evoked potentials when requiring less or no training from the user i.e., a system based on stimulus-evoked EEG signals that provides task-relevant information (Baykara et al., 2016), useful for locked-in or multiple sclerosis patients. This involves the presentation of an odd-ball paradigm in case of P300 or multiple visual stimuli flashing, e.g., letters, digits on screen in case of VEP. The P300 is derived from user response that evokes approximately 300 ms after stimulus triggering and corresponds to positive voltage peak (Lazarou et al., 2018). VEP measures the time for the visual stimulus to travel from the eye to occipital cortex.

Users can generally be grouped based on their physical and mental state, for instance locked-in patients with intact eye muscles, can communicate via ERP signals, whereas patients with motor complete but sensory incomplete SCI can utilize SMR signals based on MI. **Figure 3** shows the electrophysiological signals that are extensively employed by BCI system for communication; however EEG signals employed by the wearable LL and assistive devices are highlighted for this study.

Deployed Oscillatory Rhythms

For assistive devices, the two commonly used SMR acquired from the motor cortex are *mu* (8–11 Hz) and *beta* (12–30 Hz) rhythms, which elicit upon ME/MI tasks. The ME task is based on the physical motion of the user's limbs that activate the motor cortex; this includes the development of muscular tension, contraction or flexion. The MI is a covert cognitive process based on the kinesthetic imagination of the user's own limb movement with no muscular activity also termed "kinesthetic motor imagery" (KMI) (Mokienko et al., 2013). Motor tasks can generally be upper or lower limb related (Malouin et al., 2008). The upper limb motor tasks activate hand area (Vasilyev et al., 2017) and LL motor tasks activate foot representation area of the cortex respectively (Wolpaw and Wolpaw, 2012). The advantage with MI signals is that they are free of proprioceptive feedback unlike ME tasks.

It was suggested by Wolpaw and Mcfarland (2004), that the use of *mu* and *beta* rhythms could give similar results as those presented by invasive methods for motor substitution. A non-invasive BCI could clinically support medical device applications (as discussed in section Lower-Limb Assistive-Robot Applications in Different Environments). The BCIs for control of medical device applications are reported in Allison et al. (2007); Daly and Wolpaw (2008), and Frolov et al. (2017). It was observed that BCI employed by assistive-robot devices for control purposes was focused on upper limb MI (Belda-Lois et al.,

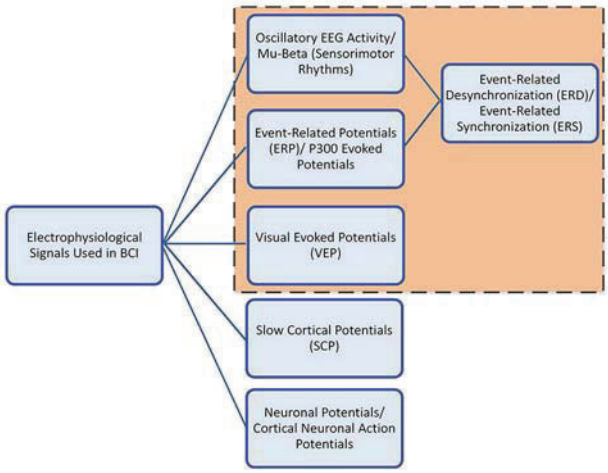

FIGURE 3 | Electrophysiological signals used in BCI controlled wearable LL and assistive-robot devices.

2011) such as hand and fingers, for applications including BCI hand orthotics and exoskeleton (Schwartz et al., 2006; Soekadar et al., 2015). This is because the foot representation area is near the mantelkante, which is situated deep within interhemispheric fissure of the human sensorimotor cortex (Penfield and Boldrey, 1937). However, it never withheld progress into this direction. Research on LL, precisely the foot MI/ME for controlling assistive robots, is in progress (Pfurtscheller et al., 2006a; Hashimoto and Ushiba, 2013; Tariq et al., 2017b, 2018). It was proved that the induction of *beta* ERS in addition to *mu-beta* ERD, improved the discrimination between left and right foot imagery and stepping tasks, as accurate as hand MI (Pfurtscheller et al., 2005, 2006a; Pfurtscheller and Solis-Escalante, 2009; Hashimoto and Ushiba, 2013; Liu et al., 2018) which provides a basis for research in BCI controlled foot neuroprosthesis. To our knowledge no literature on explicit employment of knee or hip KMI tasks in any BCI experimental protocol is available except for (Tariq et al., 2017a).

Besides the KMI of LL, cortical signals arising from the sensorimotor control loop of human locomotion intent is taken into account, for the portable LL wearable-BCI controllers to be compliant with the residual neuromusculoskeletal structures (La Fougere et al., 2010) suggested that brain areas underlying walking MI overlie the supplementary motor area and pre-frontal cortex. The idea of walking from thought based on foot imagery has also been presented in Pfurtscheller et al. (2006b). A novel way of therapy that earlier provided limited grade of motor-function recovery for chronic gait function impaired subjects due to foot-drop was described (Do et al., 2011, 2012). They integrated EEG-based BCI with non-invasive functional electrical stimulation (FES) system. It resulted in enabling the brain-control of foot dorsiflexion directly in healthy individuals. Takahashi et al. (2009, 2012) validated the feasibility of short-term training by employing ERD and FES based on dorsiflexion of paralyzed ankle experiments. Beta corticomuscular coherence (CMC) gave a measure of communication amid sensorimotor cortex and muscles. García-Cossio et al. (2015) demonstrated the possibility to decode walking intentions from cortical patterns. Raethjen et al. (2008) found coherence in EEG at stepping frequency and electromyography (EMG) anterior tibial muscles pattern for rhythmic foot movements.

Work on analyzing EEG signals for detection of unexpected obstacles during walking was presented recently (Salazar-Varas et al., 2015). Observation of electrocortical activity related to walking gait-cycle and balancing experiments has been reported in Presacco et al. (2011b). Electrocortical activity resulting from gait-like movements and balancing with treadmill, Erigo R tilt table, and customized stationary bicycle with rigid reclined backboard (as pedaling device) have been discussed in Wieser et al. (2010), Gwin et al. (2011), Presacco et al. (2011a), Jain et al. (2013), Petrofsky and Khowailed (2014), Bulea et al. (2015), Kumar et al. (2015), and Liu et al. (2015).

Deployed Event-Related and Evoked Potentials

ERPs have successfully been deployed in ambulatory and motor conditions without affecting the recorded EEG data. P300 showed to improve the performance of an EEG-based BCI system during ambulatory conditions or foot dorsiflexion/plantar-flexion condition (Lotte et al., 2009; Castermans et al., 2011b; Duvinage et al., 2012). They used similar experimental protocol i.e., oddball paradigm while subjects were physically walking or moving feet in dorsiflexion or plantar-flexion direction. In addition to this, the somatosensory evoked potentials (SEP) were deployed in assistive technologies. These potentials commonly elicit by bipolar transcutaneous electrical stimulation applied on the skin over the trajectory of peripheral nerves of the upper limb (the median nerve) or LL (the posterior tibial nerve), and then recorded from the scalp (Sczesny-Kaiser et al., 2015). In addition to the wearable devices, assistive technologies as EEG-BCI controlled wheelchairs and humanoid robots have successfully deployed the P300 (Rebsamen et al., 2007, 2010; Pires et al., 2008; Iturrate et al., 2009b; Palankar et al., 2009; Lopes et al., 2011; Kaufmann et al., 2014) and VEP signals (Bell et al., 2008). However, the only drawback, with employment of ERP and VEP signals in a BCI for the control of assistive devices precisely wearables, is the presence of visual stimulus set-up within the device that makes it less convenient for portable applications.

COMMUNICATION PROTOCOL

Like a basic communication system, the BCI for control of assistive devices has an input, an output, translation components for converting input to output, and a protocol responsible for the real-time operation onset, offset and timing.

Acquired EEG signals are transferred to the BCI operator via a communication protocol. Similarly sensor output from the robot device is directed to the shared control unit via communication protocol, **Figure 2**. Communication protocol could be a transmission control/internet protocol (TCP/IP), a suite of communication protocols used to interconnect network devices on the internet or a private network. For instance, in EEG-BCI controlled humanoids, the data (visual feedback images from the humanoid monocular camera and motion commands from the BCI system) were transmitted using wireless TCP/IP communication between the humanoid and other systems (Chae et al., 2011a,b, 2012).

An alternate approach is the lab streaming layer (LSL), which allows synchronization of the streaming data across devices. Information can be streamed over the network from "Presentation to the LSL" (Iturrate et al., 2009b; Renard et al., 2010; Kothe and Makeig, 2013; Gramann et al., 2014). Recent assistive applications (Galán et al., 2008; Millán et al., 2009) such as wheelchairs, and mobile robots, use controller area network (CAN) bus which is a robust vehicle bus standard. It is designed to allow microcontrollers and devices to communicate in applications without a host computer and follows a message-based protocol. It is a low cost, fault tolerant communication system, with the data transfer rates in the range of 40 Kbit/s to 1 Mbit/s.

BCI OPERATOR

After passing through the communication protocol, acquired EEG signals are directed to connected

client, i.e., the BCI operator, but are pre-processed first.

Preprocessing

The acquired raw EEG signals are pre-processed, as they are susceptible to noise and artifacts. It could be hardware/environmental noise, experimental error or physiological artifact. As hardware and environmental noise are not brain-related, it is best to remove them before converting raw EEG to signal features.

Removal of Noise

Hardware noise in the EEG signal usually occurs due to instrument degradation, electrode wear, mains interference (AC power lines), electromagnetic wave sources as computers, mobile phones, notebooks, wireless routers or other electronic equipment. High noise frequencies in the signal can be removed by notch filters (50 or 60 Hz for power lines). To block electromagnetic waves, electromagnetic shields could be used.

Removal of Artifacts

EEG artifacts arise due to physiological activities such as skin impedance fluctuations, electrooculography activity, eye blinks, electrocardiographic activity, facial/body muscle EMG activity and respiration. As the frequency ranges, for the aforementioned physiological signals are typically known, the bandpass filter can be an effective preprocessing tool. Most EEG-based BCI systems for assistive technologies have shown the successful implementation of simple low-pass, high-pass, or bandpass filters to remove physiological artifacts. Other methods for artifact removal include temporal filtering, spatial filtering, independent component analysis (ICA) (Viola et al., 2009), principal component analysis (PCA), linear regression, blind source separation (BSS) (Ferdousy et al., 2010), wavelet transform, autoregressive moving average, nonlinear adaptive filtering, source dipole analysis (Fatourechi et al., 2007) or thresholding of meaningful parameters (e.g., channel variance) based on a prior statistical analysis (Nolan et al., 2010).

Feature Extraction Layer

After preprocessing of data, different brain activities are classified based on their selected features.

Band Power Features

The band power features, usually used, are the time-frequency components of ERD/ERS. After bandpass filtering, resulting signal is squared to obtain its power $p[t] = x^2[t]$, where x is the filtered single band EEG signal amplitudes and p is the resulting band-power values. To smooth-out (average) the signal, a w-sized smoothing window operation is used. This is followed by a logarithm of the processed signal sample, using Equation 1:

$$\bar{p}[n] = \ln\left(\frac{1}{w}\sum_{k=0}^{w} p[n-k]\right) \quad (1)$$

where $\bar{p}[n]$ are the smoothed band-power values, and w is the smoothing window size. In their work (Presacco et al., 2011b; Contreras-Vidal and Grossman, 2013), the feature extraction method employed by EEG-BCI lower exoskeleton, for neural decoding of walking pattern, included power spectral density (PSD) analysis of the kinematic data and adaptive Thompson's multitaper for each channel of EEG recorded, during rest and walking tasks. Decoding method employed a time-embedded linear Wiener filter, independently designed and cross-validated for each extracted gait pattern. Parameters of the model were calculated with Gaussian distribution method. This ensured the feasibility of successfully decoding human gait patterns with EEG-BCI LL exoskeleton. Similarly, the results tested a on paraplegic subject for BCI controlled lower exoskeleton (Kilicarslan et al., 2013) reflect the method of decoding closed loop implementation structure of user intent with evaluation accuracy of 98%. Data was filtered in *delta* band (0.1–2 Hz) using 2nd order Butterworth filter. The filtered data was standardized and separate channels were used, to create feature matrix to extract *delta* band features.

In 2012 (Noda et al., 2012) proposed an exoskeleton robot that could assist user stand-up movements. For online decoding they used 9th order Butterworth filter for 7–30 Hz band. After down-sampling, Laplace filter and common average subtraction were applied for voltage bias removal. The covariance matrix of the processed data was used as input variable for the two-class classifier; the results were productive. Other EEG-BCI lower exoskeletons (Gancet et al., 2011, 2012) considered employing steady-state VEP (SSVEP) for motion intention recognition. Proprioceptive artifacts removal (during walk) is aimed to be removed using ICA. Other recent work on LL exoskeleton controlled via SSVEP includes (Kwak et al., 2015). In the SEP-controlled LL exoskeleton (Sczesny-Kaiser et al., 2015), SEP signals were sampled at 5 kHz and bandpass filtered between 2 and 1,000 Hz. In total 800 evoked potentials were recorded in epochs from 30 before to 150 ms after the stimulus, and then averaged. Paired-pulse suppression was expressed as a ratio of the amplitudes of second and first peaks, which was the primary outcome parameter. For correlation analysis, they calculated the difference of mean amplitude ratios.

For a BCI controlled robotic gait orthosis (Do et al., 2011, 2013) an EEG prediction model was generated to exclude EEG channels with excessive artifacts. The EEG epochs corresponding to idling and walking states were then transformed into frequency domain, their PSD were integrated over 2 Hz bins, followed by dimensionality reduction using class-wise principal component analysis (CPCA). The results established feasibility of the application.

BCI and shared control wheelchairs, based on MI signals to ensure interference free navigation protocol, was presented in Millán et al. (2009) and Carlson and Millan (2013). They estimated PSD in the 4–48 Hz band with a 2 Hz resolution. ERD was observed in the *mu* band power 8–13 Hz. These changes were detected by estimating the PSD features every 16 times/s using Welch method with five overlapped (25%) Hanning windows of 500 ms. In order to select subject-specific features, that maximize the separability between different tasks (based on training data cross validation) the canonical variate analysis (CVA) was used. In a similar work presented by Galán et al. (2008) for BCI controlled wheelchair, feature selection

was done by picking stable frequency components. The stability of frequency components was assessed using CVA one per frequency component on the training set.

Time-Domain Parameters

The time-domain parameters compute time-varying power of the first k derivatives of the signal; $p_i(t) = \frac{d^i x(t)}{dt^i}$ where $i = 0, 1, \ldots, k$ and x is the initial EEG signal. Resulting derivatives are smoothed using exponential moving average and logarithm, used in feature vector generation, as given in Equation 2:

$$\overline{p_i}[n] = \ln\left(u\, p_i[n] - (1-u)\, p_i[n-1]\right) \tag{2}$$

where $\overline{p}$ is the smoothed signal derivatives, u is the moving average parameter, $u \in [0; 1]$.

EEG-BCI for control of LL orthosis (Taylor et al., 2001; Duvinage et al., 2012) combined a human gait model based on a CPG and a classic but virtual P300 to decipher user's intent for four different speeds. P300 was used to control the CPG model and the orthosis device by sending high-level commands. The frequency band for P300 were high-pass filtered (temporal) at 1 Hz cut off frequency using 4th order Butterworth filter. This was followed by designing of an xDAWN-based spatial filter, by linearly combining EEG channels. When EEG signals were projected into this subspace, P300 detection was enhanced. The resulting signal was epoched using time window that started after stimulus, averaged and sent to the classifier. In another related work (Lotte et al., 2009), the epoching of P300 signal was done by selection of related time window, followed by bandpass filtering in 1–12 Hz range using 4th order Butterworth filter. Post this; winsorizing for each channel was done by replacing values within 5% most extreme values by most extreme values from remaining 95% samples from that window. A subset of the features was selected using the sequential forward floating (SFFS) feature selection algorithm that ensured the maximization of performance of the BCI system.

The EEG-BCI for foot orthosis reported in Xu et al. (2014), employed bandpass filtering (0–3 Hz). The system was based on the detection of movement-related cortical potentials (MRCP). The data between 0.5 and before 1.5 s, after the movements, were extracted as the "signal intervals" while others were extracted as the "noise intervals." The measure analysis of variance, ANOVA, was used for statistical analysis.

The P300-BCI wheelchair incorporated bandpass filtering between 0.5 and 30 Hz and characterized the P300 signal in the time domain. For each EEG channel, 1-s sample recordings were extracted after each stimulus onset and filtered using the moving average technique. The resulting data segments for each channel selected were concatenated, creating a single-feature vector (Iturrate et al., 2009a,b).

Common Spatial Patterns

The common spatial pattern (CSP) features are sourced from a preprocessing technique (filter) used to separate a multivariate signal into subcomponents that have maximum differences in variance (Müller-Gerking et al., 1999). The difference allows simple signal classification. Generally, the filter can be described as a spatial coefficient matrix W, as shown in Equation 3:

$$S = W^T E \tag{3}$$

where S is the filtered signal matrix, E is the original EEG signal vector. Columns of W denote spatial filters, while W^{T} are the spatial patterns of EEG signal. In their work (Choi and Cichocki, 2008) used SMR to control wheelchair. For pre-processing they employed the second order BSS algorithm using a modified and improved real-time AMUSE algorithm that enabled a rapid and reliable estimation of independent components with automatic ranking (sorting) according to their increasing frequency contents and/or decreased linear predictability. The AMUSE algorithm worked as 2 consecutive PCAs; one applied to the input data and the second applied to the time-delayed covariance matrix of the output from the previous stage. For feature extraction, CSP filter was used that distinguish each data group optimally from the multichannel EEG signals.

SMR-based humanoid robots used the KMI of left hand, right hand, and foot as control signals (Chae et al., 2011b, 2012). Sampled EEG signals were spatially filtered with large Laplacian filter. During the overall BCI protocols, Laplacian waveforms were subjected to an autoregressive spectral analysis. For amplitude features extraction, every 250 ms observation segment was analyzed by the autoregressive algorithm, and the square root of power in 1 Hz wide frequency bands within 4–36 Hz was calculated.

Translation Layer

After passing through the feature extraction layer, the feature vector is directed to the translation layer to identify user intent brain signals, and manipulate the robotic device via machine understandable commands for interfacing. Different classification techniques for distinct features are used. Classification algorithms, calibrated via supervised or unsupervised learning, during training phase, are able to detect brain-signal patterns during the testing stage. This essentially estimates the weighted class, represented by the feature vector for mapping to the desired state (unique command). A recent review on most commonly used classification algorithms for EEG-BCIs has been reported by (Lotte et al., 2018). Some of the commonly used classification methods in EEG-BCI controllers for LL assistance are LDA, SVM, GMM, and ANN (Delorme et al., 2010, 2011).

Linear Discriminant Analysis

One of the most extensive and successfully deployed classification algorithms, in EEG-BCI for assistive technologies is the linear discriminant analysis (LDA). The method employs discriminant hyper-plane(s) in order to separate data representing two or more classes. Since it has low computational requirements, it is most suitable for online BCI systems. A feature a can be projected onto a direction defined by a unit vector $\hat{\omega}$, resulting in a scalar projection b, given by Equation 4:

$$b = \vec{a} \cdot \hat{\omega}^2 \tag{4}$$

The aim of LDA classification is to find a direction $\hat{\omega}$, such that, when projecting the data onto $\hat{\omega}$ it maximizes the distance between the means and minimizes the variance of the two classes (dimensionality reduction). It assumes a normal data distribution along with an equal covariance matrix for both classes (Lotte et al., 2007). LDA minimizes the expression given by Equation 5:

$$\frac{(m_\phi - m_\Psi)^2}{s_\phi^2 + s_\Psi^2} \tag{5}$$

where m_ϕ and m_Ψ are the means and s_ϕ and s_Ψ are the standard deviations of the two respective classes, after projecting the features onto $\hat{\omega}$. EEG-BCI lower exoskeletons used LDA for the reduction of data dimensionality (Kilicarslan et al., 2013). EEG-BCI lower orthosis employed a 12-fold LDA using voting rule for decision making in selection of speed (Lotte et al., 2009; Duvinage et al., 2012). Dimensionality reduction, using CPCA and approximate information discriminant analysis (AIDA), were used in the robotic gait orthosis system (Do et al., 2011, 2013). The BCI-driven orthosis (Xu et al., 2014) used the manifold based non-linear dimensionality reduction method, called locality preserving projection (LPP), along with LDA, to detect MRCPs. EEG-BCI wheelchairs successfully deployed LDA (Galán et al., 2008; Iturrate et al., 2009a,b). LDA was successfully used for translation of EEG signal into movement commands in humanoids (Chae et al., 2011a,b, 2012).

Support Vector Machine

The goal of SVM classifier is to maximize the distance between the separating hyper plane and the nearest training point(s) also termed support vectors. The separating hyper plane in the 2D feature space is given by the Equation 6:

$$y = \omega^T x + b \tag{6}$$

where ω, $x \in R^2$ and $b \in R^1$. The hyper plane (also called the decision border) divides the feature space into two parts. Classified results depend on which side of the hyper plane the example is located. In SVM, the distances between a hyper plane and the nearest examples are called margins.

Though SVM is a linear classifier, it can be made with non-linear decision boundaries using non-linear kernel functions, such as Gaussian or radial basis functions (known as RBF). The non-linear SVM offers a more flexible decision boundary, resulting in an increase in classification accuracy. The kernel functions, however, could be computationally more demanding. EEG-BCI wheelchairs have successfully used linear SVM for dynamic feature classification (Bell et al., 2008; Choi and Cichocki, 2008; Ferreira et al., 2008; Rebsamen et al., 2010; Belluomo et al., 2011). It was also successfully implemented in EEG-BCI humanoid (Bell et al., 2008) and mobile robots (Ferreira et al., 2008; Belluomo et al., 2011).

Gaussian Mixture Model

The GMM is an unsupervised classifier. This implies that the training samples of a classifier are not labeled to show their class. More precisely, what makes GMM unsupervised is that during the training of the classifier, estimation is done for the underlying probability density functions of the observations (Scherrer, 2007). Several EEG-BCI applications utilized the GMM as a feature classifier, such as lower exoskeletons, wheelchairs and mobile robots (Galán et al., 2008; Millán et al., 2009; Carlson and Millan, 2013; Kilicarslan et al., 2013).

Artificial Neural Network

The ANNs are non-linear classifiers inspired by human's nervous system ability to adaptively react to changes in surroundings. They are commonly used in pattern recognition problems, due to their post-training capability to recognize sets of training-data-related patterns. ANNs comprise of assemblies of artificial neurons that allow the drawing of non-linear decision boundaries. They can be used in different algorithms including multilayer perception, Gaussian classifier, learning vector quantization, RBF neural networks, etc. (Anthony and Bartlett, 2009). In their proposed model for lower exoskeleton (Gancet et al., 2011, 2012), they aim at adopting processing method as dynamic recurrent neural network (DRNN).

Execution Layer

Once classified, the desired state of user intent is carried to the execution layer for an error approximation. The approximation in reference to the present state of the device is used to drive the actuator for reducing any error. The execution layer of control is highly device-specific. It could rely on feedforward or feedback loops (Tucker et al., 2015).

Feedforward control needs some model to predict the system's future state, based on the past and present set of inputs and the device state. Aforementioned control inputs can be effective for reducing the undesired interaction forces, that could occur due to the added mass, inertia and friction of the device (Murray and Goldfarb, 2012). On the contrary feedback controllers do not require a model of the system, but require an estimate of the current state. The controller compares current state with the desired state of the device and modulates the power input to the device accordingly (Millán et al., 2009; Duvinage et al., 2012; Noda et al., 2012; Contreras-Vidal and Grossman, 2013; Do et al., 2013; Kilicarslan et al., 2013; Xu et al., 2014; Contreras-Vidal et al., 2016).

SHARED CONTROL

Shared control is used to couple the user's intelligence, i.e., cognitive signals with precise capabilities of the robotic device given the context of surroundings, resulting in reduced workload for the user to continuously deliver commands to drive the robotic device. Inputs to the shared control module are sensory readings of the robotic device and output of the BCI operator (classified signal). The classified signal is combined with the robot's precise parameter e.g., velocity to generate smoother driving output. Several assistive technologies for motor impairment have successfully employed shared controllers for navigational assistance to maneuver the assistive devices in different directions, independently and safely (Galán et al., 2008;

Millán et al., 2009; Tonin et al., 2010, 2011; Carlson and Millan, 2013).

This refers to the idea of switching between operators, i.e., if the user needs no navigational assistance he will be granted full control over the robotic device; otherwise, sole mental commands will be used and modified by the system. One key aspect of shared control is the two-way communication between the human and the robot. The shared control is beneficial primarily for navigational directions. In the case of robots with only three possible steering mental commands such as forward, left, and right, there is a need of assistance by the device for fine maneuvering. Secondly, the cognitive commands might not always be perfect, i.e., could be vague. In the case of errors, an extra navigational safety is required by the system to interpret the meaning of the command. In this way the system would be able to perceive any new environment.

LOWER-LIMB ASSISTIVE-ROBOT APPLICATIONS IN DIFFERENT ENVIRONMENTS

The last integral part, of the control framework, is the robotic device, as observed in **Figure 2**. In this section, the current state-of-the-art EEG-based activity mode recognition in a BCI for control of LL assistive devices is summarized in **Table 1**.

BCI Exoskeletons

In order to control a LL robotic exoskeleton (NeuroRex), Contreras-Vidal and Grossman (2013) and Kilicarslan et al. (2013) decoded neural data for human walking from Presacco et al. (2011b). They evaluated the degree of cognitive-motor-body adaptations while using portable robot. Their results proved that NeuroRex can be regarded as an augmented system of locomotor therapy (LT) by reviewing its initial validation in a paraplegic patient having SCI. They also performed comprehensive clinic assessments for user safety protection.

The MINDWALKER (Gancet et al., 2011, 2012) is another project where researchers proposed a novel idea of presenting the SCI patients with intact brain capabilities. The facility of crutch-less assistive LL exoskeleton is based on brain neural-computer interface (BNCI) control for balanced walking patterns. It also evaluated the potential effects of Virtual Reality (VR) based technology that could support patient/user training for reaching a high confidence level for controlling the exoskeleton virtually before the real transition. Other brain controlled exoskeletons are reported in Noda et al. (2012), Kwak et al. (2015), Sczesny-Kaiser et al. (2015), and Lee et al. (2017).

BCI Orthosis

EEG-based activity mode recognition for orthotic devices has been investigated by Duvinage et al. (2012). They proved the concept of considering user's intent by combining CPG-based human gait model and classic P300-BCI for five different states; three speed variations, a stop state and a non-control state. Using unnatural P300 command by augmented reality eyewear (from Vuzix, Rchester, USA) decision was sent to the Virtual Reality Peripheral Network (VRPN) server to be exploited while wearing LL orthosis. This was based on the pilot study carried by Lotte et al. (2009), where a solution to the constraints, such as deterioration of signals (during ambulation), was avoided by using slow P300 for control during sitting, walking and standing. Authors of Castermans et al. (2011a) used an experimental protocol to limit movement artifacts present in EEG signals compared to real walk on treadmill. They suggested that rhythmic EEG activity could be exploited for driving a user intent-based foot-ankle orthosis built on PCPG algorithm. Similar investigation was conducted by Raethjen et al. (2008).

In their work, Do et al. (2013) proposed a novel approach of BCI controlled lower extremity orthotics to restore LL ambulation for partially and complete SCI subjects suffering from cardiovascular disease, osteoporosis, metabolic derangements and pressure ulcers. They developed an EEG prediction model to operate the BCI online and tested the commercial robotic gait orthosis system (RoGO) for two states, idling and walking KMI. Similarly, testing for intuitive and self-paced control of ambulation was also done with an avatar in a virtual reality environment (VRE) (Wang et al., 2012; King et al., 2013). Other similar investigations are reported in Wang et al. (2010) and Do et al. (2011).

The BCI driven motorized ankle-foot orthoses, known as (BCI-MAFO), intended for stroke rehabilitation was presented in Xu et al. (2014). Their system was able to detect imaginary dorsiflexion movements (for walking gait) within a short latency, by analyzing MRCPs. Upon each detection, the MAFO was triggered to elicit passive dorsiflexion, hence, providing the user a binary control of robotic orthosis. The MEP was elicited by transcranial magnetic stimulation (TMS); the results reflected an effective way to induce cortical plasticity for motor function rehabilitation.

BCI Wheelchairs, Humanoids, and Mobile Robots

Assistive technologies such as wheelchairs controlled via EEG-BCI have extensively been researched. In their work, Carlson and Millan (2013) proposed the idea of combining a commercial wheelchair and BCI with a shared control protocol. The paradigm was based on KMI of left/right hand, both feet, or in idle state; each against three distinct tasks as move left/right or forward by avoiding obstacles. Modifications in the commercial mid-wheel drive model (by Invacare Corporation) were directly controlled by a laptop. An interface module, based on remote joystick, was used between the laptop and wheelchair's CANBUS-based control network. Wheel-encoders were added for motion feedback alongside sonar sensors and webcams for environment feedback to the controller using cheap sensors compared to other systems. Previous solution required continuous commands from the user, in order to drive the wheelchair, that ended up in high user workload (Millán et al., 2009). Other similar systems were proposed by Vanacker et al. (2007) and Galán et al. (2008).

Research on the challenges faced during fully control automated wheelchairs with BCI was done by Rebsamen et al. (2007, 2010). Their results proved that if synchronous evoked

TABLE 1 | Key features of EEG-based activity mode recognition exoskeletons, orthosis, wheelchairs and assistive robots for rehabilitation.

Devices	Brain activity	Pre-processing and feature extraction	Classifier	Classifi-cation accuracy (%)	Key findings	Type of support and applications	References
NeuroRex	Oscillatory rhythms	Bandpass filter, PSD analysis	GMM, LDA	-, >90 (GMM), -	For standing-up, self-balancing, walking and backing, turning, ascending and descending stairs applications. An augmented form of Locomotor Therapy (LT)	Lower body exoskeleton based on user intent control for walking independently for subjects with paraparesis, complete paraplegia, stroke and SCI	Noda et al., 2012; Contreras-Vidal and Grossman, 2013; Kilicarslan et al., 2013
MIND-WALK-ER	SSVEP*	ICA	DRNN Chéron et al., 2011, KNN	-, -, 92.6% (online)	Exploitation of motor cortex EEG signals for generating online legs kinematics angles corresponding to walking pattern and pace as imagined by user deploying VR	Crutch-less assistive LL exoskeleton for walk empowering (dynamic balance) for SCI patients with intact brain capabilities	Gancet et al., 2011, 2012; Kwak et al., 2015
HAL® Exo-skeleton	SEP	Bandpass filter	-		Significant improvement in paired-pulse SEP in SCI patients compared to the controls at baseline following training. The robotic-assisted BWSTT in SCI patients is capable of inducing cortical plasticity following highly repetitive, active locomotive use of paretic legs.	HAL® exoskeleton-assisted bodyweight supported treadmill training (BWSTT) for improving walking function in SCI patients	Sczesny-Kaiser et al., 2015
Five-State Foot Lifter	P300*	Temporal high-pass filter, xDAWN-based spatial filter Rivet et al., 2009, epoch averaging, SFFS	LDA (using voting rule for decision making)	83 ± 15.5% (walking) 75% (walking)	Proof of the concept of combining a human gait model based on CPG widely used in robotics and P300 based BCI to consider user's intent. This CPG allowed to automatically generate a periodic gait pattern/behavior of the patient and his desired speed. No required training by the user to manage the P300 paradigm provided by augmented reality eyewear for external stimulus presentation.	A five-state foot lifter orthosis for sitting, standing and walking at four speeds & a non-control state for stroke patients unable to lift their feet or foot drop problems Pilot study for ambulatory BCI	Lotte et al., 2009; Duvinage et al., 2012

(Continued)

TABLE 1 | Continued

Devices	Brain activity	Pre-processing and feature extraction	Classifier	Classifi-cation accuracy (%)	Key findings	Type of support and applications	References
BCI-RoGO	Oscillatory rhythms**	FFT, PSD, CPCA	AIDA, linear Bayesian classifier	>85%, -, -	Development of EEG prediction model based on idling and KMI states. Preliminary evidence from results reflect the feasibility of restoring brain-controlled walking after SCI.	BCI Robotic gait orthosis for SCI, tetraplegia, and paraplegia patients to improve neurological outcomes beyond those of standard therapy to improve ambulation	Wang et al., 2010; Do et al., 2011, 2013
BCI-MAFO	MRCP***	Bandpass filter, large Laplacian filter, ANOVA	LPP and LDA	73 ± 10.3%.	Efficient induction of cortical neuroplasticity in healthy subjects with a short intervention procedure to use self-paced BCI for binary control of the robotic orthosis.	BCI-driven motorized ankle-foot orthosis (MAFO). An ambulatory rehabilitation-tool for stroke patients	Xu et al., 2014
BCI Wheel-chair	Oscillatory rhythms	Spatial filter (CAR), Laplacian filter, PSD (Welch method), CVA, Bandpass filter, FFT	Gaussian model, LDA	≥90%, -, ≥80%, 80%	Reduced cognitive workload due to BCI protocol coupled with shared control, compared to previous systems. Spontaneous control given to user to move left, right or forward and avoid obstacles automatically by perceiving surrounding environment, no waiting for external cues compared to synchronous P300 protocol. Based on combination of cheaper sensors for providing controller with environmental feedback.	Brain-actuated wheelchair for users with severe mobility impairment. Suitable for experienced/inexperienced users to continuously and safely operate with even complex navigation independently	Vanacker et al., 2007; Galán et al., 2008; Millán et al., 2009; Carlson and Millan, 2013
P300 BCI Wheel-chair	P300, ERP	Bandpass filter, moving average filter	SVM, Gaussian model, LDA	≈100%, ≈100%, ≥94%, ≥94%, 100%, 100%, ≥95%, ≥85.8%	Successfully targeted people suffering from a very low information transfer rate using the P300 paradigm, using virtual guiding paths and predictable trajectories. Incorporation of *mu/beta* (a faster BCI) to stop wheelchair. Provision of destination selection from predefined localities in the menu.	BCI wheelchair for locked-in or ALS patients. Intelligent and safe BCI wheelchair where known surroundings as, toilet, kitchen, bedroom and living room in house is highlighted by standard oddball paradigm.	Rebsamen et al., 2007, 2010; Pires et al., 2008; Iturrate et al., 2009a,b; Palankar et al., 2009; Lopes et al., 2011; Kaufmann et al., 2014

(Continued)

TABLE 1 | Continued

Devices	Brain activity	Pre-processing and feature extraction	Classifier	Classifi-cation accuracy (%)	Key findings	Type of support and applications	References
BMI wheel-chair	Oscillatory rhythms*	2nd order BSS with AMUSE algorithm, CSP filter, Bandpass filter	SVM	-	Effective feedback training method resulting in multi DOFs/freely controlling wheelchair parallel to controlling with a joystick	BCI wheelchair based on MI protocol for motor impaired patients.	Choi and Cichocki, 2008
BCI mobile robot/humanoid	Oscillatory rhythms	Bandpass filter, Laplacian filter, PSD (Welch method)	Statistical Gaussian model	74%, ≥75.6%, 81%, ≥75.6%, -, -	Allow subjects to complete complex tasks in same time and with same number of commands as required by manual control	BCI based telepresence robot for left/right steering via imagination of left/ right hand or feet movement of physically impaired people. Control navigation of humanoid robot via MI.	Millan et al., 2004; Tonin et al., 2010, 2011; Chae et al., 2011a,b, 2012
BCI mobile robot/humanoid	SMR, ERP, P300*	Spatial filter, temporal filter, Bandpass filter	SVM	95%, -, 95%, ≥93%, 80.5%	Development of an interactive BCI system to control twin coordinated mobile robot movements via two EEG signals (imagery left-right arm). The concentration and relaxation states of visual cortex, was used to allow operator to successfully control a robot without using hands. Successful control of BCI humanoid for sophisticated interaction with the environment, involving not only navigation but also manipulation and transport of objects.	BCI controlled mobile and telepresence robots for navigation in required direction for motor disability assistance. BCI controlled humanoid for navigation assistance as well as transportation of objects.	Bell et al., 2008; Ferreira et al., 2008; Belluomo et al., 2011; Escolano et al., 2012; De Venuto et al., 2017

They used combined EEG and EMG modalities in their system.

***They used combined EEG, FES, and EMG modalities in their BCI orthosis.*

****They used combined EEG and TMS modalities for brain signal acquisition and for classification purposes, they used additional features from EMG in their BCI orthosis.*

P300 signals are used for mobile commands, and oscillatory rhythms are used for stop command, the system is efficient and safe enough to drive the real-time wheelchair in possible directions. They used Yamaha JW-I power wheelchair with two optical rotary encoders attached to glide-wheels for odometry, a bar code scanner for global positioning and a proximity sensor mounted in front of the wheelchair for collision avoidance. User could reach the destination, by selecting amongst a list of pre-defined locations. This was primarily for patients with lost voluntary muscle control, but intact cognitive behavior who could use a BCI, such as LL amputees.

Other P300-BCI wheelchairs' research include work done by Iturrate et al. (2009a,b) where the system relied on synchronous stimulus-driven protocol. The work done by Palankar et al. (2009) focused on, completely and partially locked-in patients, and provided them with an effective model of a 9-DOF wheelchair-mounted robotic arm (WMRA) system. Pires et al. (2008) and Lopes et al. (2011) contributed in visual P300 based BCI for steering wheelchair assisted by shared-control. Kaufmann et al. (2014) validated the feasibility of a BCI based on tactually-evoked ERP for wheelchair control. Other wheelchairs controlled via EEG-based BCI include (Choi and Cichocki, 2008; Tsui et al., 2011; Huang et al., 2012; De Venuto et al., 2017).

In their report (Tonin et al., 2010, 2011) presented a BMI-controlled telepresence robot for people with motor impairment that could allow them completion of complex tasks, in similar time as that consumed by healthy subjects. They were able to steer Robotino^{TM} (by FESTO), via asynchronous KMI of left/right hand and feet. The system incorporated shared control for obstacle avoidance, safety measures and for interpreting user intentions to reach goal autonomously. A similar project was earlier presented by Millan et al. (2004) for mobile robot control in indoor environment via EEG. In order to recognize environment situations, a multilayer perception was implemented. Sensory readings were mapped to 6 classes of environmental states: forward movement, turn left, follow left wall, right turn, follow right wall and stop. These environmental states were generated against mental tasks as relax, KMI of left/right hand, cube rotation imagery, subtraction and word association. Research for control of two coordinated mobile robots, via SMR and ERP, that could be useful for motor impaired people, is done by Belluomo et al. (2011). Similarly mobile robot (Pioneer 2-DX) control based on *mu* ERD/ERS was done by Ferreira et al. (2008).

As per our knowledge, reflected from the literature, there is no viable active prosthetic ankle-foot, or prosthetic LL device, controlled via EEG-BCI for amputees.

PRACTICAL CHALLENGES

In order to design a controller for an assistive-robot device there is a need of a seamless integration between the BCI operator, and the execution of required tasks from the output device with minimal cognitive disruption. However, there are challenges associated to the real-time implementation of the system, when dealt with motor impaired population. Some open problems and challenges associated to wearable systems have recently been summarized in (Deng et al., 2018; Lazarou et al., 2018; Semprini et al., 2018). The following sections discuss in detail practical challenges associated to EEG-BCI wearable and assistive technologies.

Wearable Lower-Limb Device Challenges

A critical need for reliable EEG-BCI is required that could interpret user intent and make context-based decisions from the user's present internal state. This would allow a direct and voluntary operation of the wearable LL devices beyond the user's affected physical, cognitive or sensory capabilities. With wearable LL devices it is observed that they did not embed shared controllers. The system should involve the development of reliable discrete classifiers, combined with continuous (model-based) neural interfaces, to predict the subject's intent without needing continuous supervisory control, but an *"assist-as-needed"* control from the BCI. Wearable LL technologies should embed features such as, self-calibration, self-analysis (with backward-forward failure attribution analysis) and error-correction. This is followed by adopting appropriate behavioral testing methods for performance evaluations of the system.

Clinical evaluation of wearables needs standardized safety and tolerability assessment of important factors such as cardiometabolic, musculoskeletal, skin, and biomechanical risks, followed by the assessment of cognitive-behavioral discrepancies that define the user profile. Cardiorespiratory safety is of principal importance as individuals with stroke and SCI may have autonomic instability that can alter the pressure of blood-flow. Their heart rates may not respond correctly to increased cardiorespiratory demands, depending on the lesion intensity. The cardiorespiratory demands of supported BCI-exoskeleton/orthosis usage must primarily be assessed and carefully monitored also for reasons as: (1) the mean peak heart fitness levels after SCI vary considerably depending on the lesion characteristics, but are generally much lower than normal; and (2) the skeletal muscle after SCI (or any central-nervous system injury) shifts in a shortfall severity from slow to a fast jerk molecular composition. Patients with abnormal gait biomechanics and fitness levels must show adequate cardiorespiratory tolerance based on subject perceived exertion scales, and objective monitoring of metabolic profiles. This metabolic surveillance, along with careful clinical measures, to assess muscle injury, is inevitable for validating the cardiorespiratory, metabolic, and muscle safety during exoskeleton/orthosis use.

During rehabilitation, the wearable robotics may impose unusual joint kinetics and kinematics that could potentially injure bone or skin, particularly in stroke or SCI patients that usually have osteoporosis, unusual spasticity patterns, or contractures. For safe utilization a standard screening for assessment of bone health using dual X-ray absorptiometry and identification of abnormal torque or impulses ahead of time, could retain from injury. There should be a careful consideration between engineers, clinicians, and subjects with neurological disability to rightly apply this new technology.

Substantial research and understanding of the cortical representations, for the perception of bipedal locomotion, is vital for evaluating changes in cortical dynamics when wearing closed-loop BCI portable devices, and gauging on how these changes are correlated with gait adaptation. As the BCI wearable devices are designed to be stable, they have to finish one complete cycle of gait before stopping, resulting in a slow time-response compared to the model's output. This is why in some systems the subject has to keep standing, as long as he can, after stopping the robot for continuously recording the model's output state.

With P300-wearable LL devices, the decision time is relatively slow for real-time applications such as walking. The solution could involve implementation of more complex pipelines that include artifact removal techniques specific to gait-artifacts, followed by a better management of stimulus presentation duration. The P300 pipeline does not allow working asynchronously, which is an important aspect for the patient's comfort (can be tiring). Following this, the poor experimental paradigm that usually includes a screen on a treadmill is not applicable for street walking; accordingly, an augmented reality eyewear seems to be indispensable.

Assistive-Robot Challenges

Clinical evaluations revealed that subjects with poor BCI performance require an extra need for assistance while maneuvering assistive-robots during complex path plans such as narrow corridors, despite the arduous BCI training.

The use of adaptive assistance with BCI wheelchairs increases the task performance of the user; however, the fixed activation levels of the system do not integrate the user's performance. This is due to the varying fatigue and hormone levels of the user, due to which the shared controller may not offer constant level of assistance. Consequently, similar system behavior is always activated when the activation threshold is reached, even though an experienced user might still be able to recover from the disorientation on its own. System performance could be increased, if a user model is built at runtime, and the level of experience to determine the thresholds is estimated when the system behavior is activated.

Various customized filtering approaches have been deployed by researchers during different states of wheelchair use, for instance, the regular on and off switching of filter in between sessions of start and stop. Given in Kwak et al. (2015), when the filter was switched on or off, the subject was required to use another mental mode (or at least adapt its existing one) as the driving system was different when the filtering was applied. This resulted in a confusion mode which is a common problem in shared control systems. When the subject's acquired strategies are built up using one driving system (i.e., without filtering) and applied to the other situation (i.e., with filtering), it ends up in a weak performance, leading to a situation where the environmental filter is actually working against the user's intention. With present BCI-wheelchairs that incorporate shared controllers, if the activation levels of the system do not integrate the user's performance, it could lead to degradation or loss of function.

Reportedly P300-wheelchairs were too slow to stop in real-time, after the selection of a sub-goal from menu, the user has to focus on a validation option, due to which the wheelchair stops and waits for the next command (followed by validation) from the user. Consequently this ends up in more stationary positions than actually moving to specific destinations.

CONCLUSIONS

In this paper, we have presented a comprehensive review of the state-of-the-art EEG-BCI controlled wearable and assistive technologies for users having neuromotor disorder, SCI, stroke, disarticulation or amputation of residual LL. All reviewed applications are presented in the form of a generalized BCI control framework. The control framework is inclusive of the user, the BCI operator, the shared controller, and the robot device with the environment. Each element of the control framework was discussed in detail. The BCI operator is based on sub-layers, each of which is highlighting the feature extraction, classification and execution methods respectively, employed by each application. The reviewed applications comprised of oscillatory rhythms, event-related and evoked potentials as input signals. The EEG-BCI based portable and assistive device applications included exoskeletons, orthosis, wheelchairs, mobile/navigation robots and humanoids. Key features from each application were discussed and presented in the **Table 1**.

Based on the review we concluded that LL tasks, such as knee, or hip joint movements, have never been explicitly employed as MI or ME tasks in any BCI experimental protocol. Only foot or upper limb kinesthetic tasks are deployed. Additionally, it is observed that the EEG-based activity mode recognition, used to control wearable LL devices, only comprise of exoskeletons and orthosis. No viable prosthetic ankle-foot, or prosthetic LL device, employing EEG signals, for activity mode recognition, is currently available.

In most applications based on P300, strong output signals were observed that resulted in accurate command functions. It was followed by a slow performance pace and a loss in the user concentration due to stimulus presentation. On the contrary, applications employing SMR, where no stimulus protocol is involved, reflected a faster performance speed, followed by a weaker output signal during asynchronous mode.

Performance of EEG-based BCI, deployed by assistive technologies, is constrained due to the design of non-invasive modalities, compared to invasive ones and due to the limited size of features employed. In the case of complex movements more sets of parameters are required to execute a seamless output. This is still one of the challenging problems that require expertise to develop efficient and robust algorithms to apprehend user's motion intention.

In the most of the reviewed applications, there is a lack of quantitative performance indicators for the algorithms' evaluations. There is no explicit signal classification, percentage given. Error measurements between expected and real system trajectories are missing. There is no indication about the

measurements of the user-energy consumption, the walking endurance and the system costs. Finally, an important issue of carrying tests under realistic conditions, with patients having LL pathologies, needs special attention, provided the observations make the comparison of the dynamic behavior of each application difficult.

AUTHOR CONTRIBUTIONS

MT devised, drafted, structured, analyzed, and coordinated reading and writing of this review. She contributed text throughout, generated the figures and developed the structure of the generalized control framework and provided final approval of the manuscript. PT contributed to analysis, critical revision, provided feedback and final approval on the manuscript. MS contributed to the **Figure 1**, analyzed, critically revised, provided feedback and final approval on the manuscript. All authors read and approved the final version of the manuscript. All authors agree to be accountable for all aspects of the work in ensuring that questions related to the accuracy or integrity of any part of the work are appropriately investigated and resolved.

ACKNOWLEDGMENTS

Authors acknowledge the financial support received for this research provided by RMIT University Ph.D. International Scholarship (RPIS).

REFERENCES

Allison, B. Z., Wolpaw, E. W., and Wolpaw, J. R. (2007). Brain–computer interface systems: progress and prospects. *Expert Rev. Med. Devices* 4, 463–474. doi: 10.1586/17434440.4.4.463

Angeli, C. A., Edgerton, V. R., Gerasimenko, Y. P., and Harkema, S. J. (2014). Altering spinal cord excitability enables voluntary movements after chronic complete paralysis in humans. *Brain* 137, 1394–1409. doi: 10.1093/brain/awu038

Anthony, M., and Bartlett, P. L. (2009). *Neural Network Learning*: *Theoretical Foundations*. London: Cambridge University Press.

Armstrong, D. M. (1988). The supraspinal control of mammalian locomotion. *J. Physiol.* 405, 1–37. doi: 10.1113/jphysiol.1988.sp017319

Bakker, M., Verstappen, C., Bloem, B., and Toni, I. (2007). Recent advances in functional neuroimaging of gait. *J. Neural Transm.* 114, 1323–1331. doi: 10.1007/s00702-007-0783-8

Baykara, E., Ruf, C. A., Fioravanti, C., Käthner, I., Simon, N., Kleih, S. C., et al. (2016). Effects of training and motivation on auditory P300 brain-computer interface performance. *Clin. Neurophysiol.* 127, 379–387. doi: 10.1016/j.clinph.2015.04.054

Belda-Lois, J.-M., Mena-Del Horno, S., Bermejo-Bosch, I., Moreno, J. C., Pons, J. L., Farina, D., et al. (2011). Rehabilitation of gait after stroke: a review towards a top-down approach. *J. Neuroeng. Rehabil.* 8, 66. doi: 10.1186/1743-0003-8-66

Bell, C. J., Shenoy, P., Chalodhorn, R., and Rao, R. P. (2008). Control of a humanoid robot by a noninvasive brain–computer interface in humans. *J. Neural Eng.* 5, 214. doi: 10.1088/1741-2560/5/2/012

Belluomo, P., Bucolo, M., Fortuna, L., and Frasca, M. (2011). "Robot control through brain computer interface for patterns generation," in *AIP Conference Proceedings* (Halkidiki), 1031–1034.

Beloozerova, I. N., Sirota, M. G., and Swadlow, H. A. (2003). Activity of different classes of neurons of the motor cortex during locomotion. *J. Neurosci.* 23, 1087–1097. doi: 10.1523/JNEUROSCI.23-03-01087.2003

Bulea, T. C., Kilicarslan, A., Ozdemir, R., Paloski, W. H., and Contreras-Vidal, J. L. (2013). Simultaneous scalp electroencephalography (EEG), electromyography (EMG), and whole-body segmental inertial recording for multi-modal neural decoding. *J. Vis. Exp.* 77:e50602. doi: 10.3791/50602

Bulea, T. C., Kim, J., Damiano, D. L., Stanley, C. J., and Park, H.-S. (2015). Prefrontal, Posterior parietal and sensorimotor network activity underlying speed control during walking. *Front. Hum. Neurosci.* 9:247. doi: 10.3389/fnhum.2015.00247

Capogrosso, M., Milekovic, T., Borton, D., Wagner, F., Moraud, E. M., Mignardot, J.-B., et al. (2016). A brain–spine interface alleviating gait deficits after spinal cord injury in primates. *Nature* 539, 284–288. doi: 10.1038/nature20118

Carlson, T., and Millan, J. D. R. (2013). Brain-controlled wheelchairs: a robotic architecture. *IEEE Rob. Autom. Mag.* 20, 65–73. doi: 10.1109/MRA.2012.2229936

Castermans, T., Duvinage, M., Hoellinger, T., Petieau, M., Dutoit, T., and Cheron, G. (2011a). "An analysis of EEG signals during voluntary rhythmic foot movements," in *2011 5th International IEEE/EMBS Conference on the Neural Engineering (NER)* (Cancún), 584–588.

Castermans, T., Duvinage, M., Petieau, M., Hoellinger, T., De Saedeleer, C., Seetharaman, K., et al. (2011b). "Optimizing the performances of a P300-based brain–computer interface in ambulatory conditions," in *IEEE Journal on Emerging and Selected Topics in Circuits and Systems,* Vol. 1 (New York, NY), 566–577.

Cervera, M. A., Soekadar, S. R., Ushiba, J., Millán, J. D. R., Liu, M., Birbraumer, N., et al. (2018). Brain-computer interfaces for post-stroke motor rehabilitation: a meta-analysis. *Ann. Clin. Transl. Neurol.* 5, 651–663. doi: 10.1002/acn3.544

Chae, Y., Jeong, J., and Jo, S. (2011a). "Noninvasive brain-computer interface-based control of humanoid navigation," in *2011 IEEE/RSJ International Conference on the Intelligent Robots and Systems (IROS)* (San Francisco, CA), 685–691.

Chae, Y., Jeong, J., and Jo, S. (2012). Toward brain-actuated humanoid robots: asynchronous direct control using an EEG-based BCI. *IEEE Trans. Rob.* 28, 1131–1144. doi: 10.1109/TRO.2012.2201310

Chae, Y., Jo, S., and Jeong, J. (2011b). "Brain-actuated humanoid robot navigation control using asynchronous brain-computer interface," in *2011 5th International IEEE/EMBS Conference on the Neural Engineering (NER)* (Cancún), 519–524.

Chéron, G., Duvinage, M., Castermans, T., Leurs, F., Cebolla, A., Bengoetxea, A., et al. (2011). "Toward an integrative dynamic recurrent neural network for sensorimotor coordination dynamics," in *Recurrent Neural Networks for Temporal Data Processing,* Vol. 5, ed H. Cardot (Rijeka: InTech), 67–80.

Chéron, G., Duvinage, M., De Saedeleer, C., Castermans, T., Bengoetxea, A., Petieau, M., et al. (2012). From spinal central pattern generators to cortical network: integrated BCI for walking rehabilitation. *Neural Plast.* 2012:375148. doi: 10.1155/2012/375148

Choi, K., and Cichocki, A. (2008). Control of a wheelchair by motor imagery in real time. *Intell. Data Eng. Autom. Learn.* 2008, 330–337. doi: 10.1007/978-3-540-88906-9_42

Chvatal, S. A., and Ting, L. H. (2012). Voluntary and reactive recruitment of locomotor muscle synergies during perturbed walking. *J. Neurosci.* 32, 12237–12250. doi: 10.1523/JNEUROSCI.6344-11.2012

Chvatal, S. A., and Ting, L. H. (2013). Common muscle synergies for balance and walking. *Front. Comput. Neurosci.* 7:48. doi: 10.3389/fncom.2013.00048

Chvatal, S. A., Torres-Oviedo, G., Safavynia, S. A., and Ting, L. H. (2011). Common muscle synergies for control of center of mass and force in nonstepping and stepping postural behaviors. *J. Neurophysiol.* 106, 999–1015. doi: 10.1152/jn.00549.2010

Contreras-Vidal, J. L., Bhagat, N. A., Brantley, J., Cruz-Garza, J. G., He, Y., Manley, Q., et al. (2016). Powered exoskeletons for bipedal locomotion after spinal cord injury. *J. Neural Eng.* 13:031001. doi: 10.1088/1741-2560/13/3/031001

Contreras-Vidal, J. L., and Grossman, R. G. (2013). "NeuroRex: A clinical neural interface roadmap for EEG-based brain machine interfaces to a lower body

robotic exoskeleton," in *2013 35th Annual International Conference of the IEEE Engineering in Medicine and Biology Society (EMBC)* (Osaka), 1579–1582.

Daly, J. J., and Wolpaw, J. R. (2008). Brain–computer interfaces in neurological rehabilitation. *Lancet Neurol.* 7, 1032–1043. doi: 10.1016/S1474-4422(08)70223-0

Delorme, A., Kothe, C., Vankov, A., Bigdely-Shamlo, N., Oostenveld, R., Zander, T. O., et al. (2010). *MATLAB-Based Tools for BCI Research*. London: Springer, Brain-computer interfaces.

Delorme, A., Mullen, T., Kothe, C., Acar, Z. A., Bigdely-Shamlo, N., Vankov, A., et al. (2011). EEGLAB, SIFT, NFT, BCILAB, and ERICA: new tools for advanced EEG processing. *Comput. Intell. Neurosci.* 2011:10. doi: 10.1155/2011/130714

Deng, W., Papavasileiou, I., Qiao, Z., Zhang, W., Lam, K.-Y., and Han, S. (2018). Advances in automation technologies for lower-extremity neurorehabilitation: a review and future challenges. *IEEE Rev. Biomed. Eng.* 11, 289–305. doi: 10.1109/RBME.2018.2830805

De Venuto, D., Annese, V. F., and Mezzina, G. (2017). "An embedded system remotely driving mechanical devices by P300 brain activity," in *Proceedings of the Conference on Design, Automation & Test in Europe, European Design and Automation Association* (Lausanne), 1014–1019.

Dimitrijevic, M. R., Gerasimenko, Y., and Pinter, M. M. (1998). Evidence for a spinal central pattern generator in humans. *Ann. N. Y. Acad. Sci.* 860, 360–376. doi: 10.1111/j.1749-6632.1998.tb09062.x

Do, A. H., Wang, P. T., King, C. E., Abiri, A., and Nenadic, Z. (2011). Brain-computer interface controlled functional electrical stimulation system for ankle movement. *J. Neuroeng. Rehabil.* 8:49. doi: 10.1186/1743-0003-8-49

Do, A. H., Wang, P. T., King, C. E., Chun, S. N., and Nenadic, Z. (2013). Brain-computer interface controlled robotic gait orthosis. *J. Neuroeng. Rehabil.* 10:111. doi: 10.1186/1743-0003-10-111

Do, A. H., Wang, P. T., King, C. E., Schombs, A., Cramer, S. C., and Nenadic, Z. (2012). "Brain-computer interface controlled functional electrical stimulation device for foot drop due to stroke," in *2012 Annual International Conference of the IEEE Engineering in Medicine and Biology Society (EMBC)* (San Diego, CA), 6414–6417.

Drew, T., Kalaska, J., and Krouchev, N. (2008). Muscle synergies during locomotion in the cat: a model for motor cortex control. *J. Physiol.* 586, 1239–1245. doi: 10.1113/jphysiol.2007.146605

Duvinage, M., Castermans, T., Jiménez-Fabián, R., Hoellinger, T., De Saedeleer, C., Petieau, M., et al. (2012). "A five-state P300-based foot lifter orthosis: Proof of concept," in *Biosignals and Biorobotics Conference (BRC)*, *2012 ISSNIP* (Manaus: IEEE), 1–6.

Escolano, C., Antelis, J. M., and Minguez, J. (2012). A telepresence mobile robot controlled with a noninvasive brain–computer interface. *IEEE Trans. Syst. Man Cybern. B Cybern.* 42, 793–804. doi: 10.1109/TSMCB.2011.2177968

Fatourechi, M., Bashashati, A., Ward, R. K., and Birch, G. E. (2007). EMG and EOG artifacts in brain computer interface systems: a survey. *Clin. Neurophysiol.* 118, 480–494. doi: 10.1016/j.clinph.2006.10.019

Ferdousy, R., Choudhory, A. I., Islam, M. S., Rab, M. A., and Chowdhory, M. E. H. (2010). "Electrooculographic and electromyographic artifacts removal from EEG," in *2010 2nd International Conference on the Chemical, Biological and Environmental Engineering (ICBEE)* (Cairo), 163–167.

Ferreira, A., Celeste, W. C., Cheein, F. A., Bastos-Filho, T. F., Sarcinelli-Filho, M., and Carelli, R. (2008). Human-machine interfaces based on EMG and EEG applied to robotic systems. *J. Neuroeng. Rehabil.* 5:10. doi: 10.1186/1743-0003-5-10

Frolov, A. A., Mokienko, O., Lyukmanov, R., Biryukova, E., Kotov, S., Turbina, L., et al. (2017). Post-stroke rehabilitation training with a motor-imagery-based brain-computer interface (BCI)-controlled hand exoskeleton: a randomized controlled multicenter trial. *Front. Neurosci.* 11:400. doi: 10.3389/fnins.2017.00400

Galán, F., Nuttin, M., Lew, E., Ferrez, P. W., Vanacker, G., Philips, J., et al. (2008). A brain-actuated wheelchair: asynchronous and non-invasive brain–computer interfaces for continuous control of robots. *Clin. Neurophysiol.* 119, 2159–2169. doi: 10.1016/j.clinph.2008.06.001

Gancet, J., Ilzkovitz, M., Cheron, G., Ivanenko, Y., Van Der Kooij, H., Van Der Helm, F., et al. (2011). "MINDWALKER: a brain controlled lower limbs exoskeleton for rehabilitation. Potential applications to space," in *11th Symposium on Advanced Space Technologies in Robotics and Automation* (Noordwijk), 12–14.

Gancet, J., Ilzkovitz, M., Motard, E., Nevatia, Y., Letier, P., De Weerdt, D., et al. (2012). "MINDWALKER: going one step further with assistive lower limbs exoskeleton for SCI condition subjects," in *2012 4th IEEE RAS & EMBS International Conference on the Biomedical Robotics and Biomechatronics (BioRob)* (Rome), 1794–1800.

García-Cossio, E., Severens, M., Nienhuis, B., Duysens, J., Desain, P., Keijsers, N., et al. (2015). Decoding sensorimotor rhythms during robotic-assisted treadmill walking for brain computer interface (BCI) applications. *PLoS ONE* 10:e0137910. doi: 10.1371/journal.pone.0137910

Gramann, K., Ferris, D. P., Gwin, J., and Makeig, S. (2014). Imaging natural cognition in action. *Int. J. Psychophysiol.* 91, 22–29. doi: 10.1016/j.ijpsycho.2013.09.003

Gwin, J. T., Gramann, K., Makeig, S., and Ferris, D. P. (2010). Removal of movement artifact from high-density EEG recorded during walking and running. *J. Neurophysiol.* 103, 3526–3534. doi: 10.1152/jn.00105.2010

Gwin, J. T., Gramann, K., Makeig, S., and Ferris, D. P. (2011). Electrocortical activity is coupled to gait cycle phase during treadmill walking. *Neuroimage* 54, 1289–1296. doi: 10.1016/j.neuroimage.2010.08.066

Hashimoto, Y., and Ushiba, J. (2013). EEG-based classification of imaginary left and right foot movements using beta rebound. *Clin. Neurophysiol.* 124, 2153–2160. doi: 10.1016/j.clinph.2013.05.006

He, B. (2016). *Neural Engineering*. New York, NY: Springer, U. S.

He, B., Baxter, B., Edelman, B. J., Cline, C. C., and Wenjing, W. Y. (2015). Noninvasive brain-computer interfaces based on sensorimotor rhythms. *Proc. IEEE* 103, 907–925. doi: 10.1109/JPROC.2015.2407272

He, Y., Eguren, D., Azorín, J. M., Grossman, R. G., Luu, T. P., and Contreras-Vidal, J. L. (2018a). Brain-machine interfaces for controlling lower-limb powered robotic systems. *J. Neural Eng.* 15:021004. doi: 10.1088/1741-2552/aaa8c0

He, Y., Luu, T. P., Nathan, K., Nakagome, S., and Contreras-Vidal, J. L. (2018b). A mobile brain-body imaging dataset recorded during treadmill walking with a brain-computer interface. *Sci. Data* 5:180074. doi: 10.1038/sdata.2018.74

Herr, H. M., Weber, J. A., Au, S. K., Deffenbaugh, B. W., Magnusson, L. H., Hofmann, A. G., et al. (2013). *Powered Ankle-Foot Prothesis*. Google Patents No. 60/934,223. Cambridge, MA: Massachusetts Institute of Technology.

Huang, D., Qian, K., Fei, D.-Y., Jia, W., Chen, X., and Bai, O. (2012). Electroencephalography (EEG)-based brain–computer interface (BCI): a 2-D virtual wheelchair control based on event-related desynchronization/synchronization and state control. *IEEE Trans. Neural Syst. Rehabil. Eng.* 20, 379–388. doi: 10.1109/TNSRE.2012.2190299

Iturrate, I., Antelis, J., and Minguez, J. (2009a). "Synchronous EEG brain-actuated wheelchair with automated navigation," in *IEEE International Conference on the Robotics and Automation ICRA'09* (Kobe), 2318–2325.

Iturrate, I., Antelis, J. M., Kubler, A., and Minguez, J. (2009b). A noninvasive brain-actuated wheelchair based on a P300 neurophysiological protocol and automated navigation. *IEEE Trans. Rob.* 25, 614–627. doi: 10.1109/TRO.2009.2020347

Jain, S., Gourab, K., Schindler-Ivens, S., and Schmit, B. D. (2013). EEG during pedaling: evidence for cortical control of locomotor tasks. *Clin. Neurophysiol.* 124, 379–390. doi: 10.1016/j.clinph.2012.08.021

Jimenez-Fabian, R., and Verlinden, O. (2012). Review of control algorithms for robotic ankle systems in lower-limb orthoses, prostheses, and exoskeletons. *Med. Eng. Phys.* 34, 397–408. doi: 10.1016/j.medengphy.2011.11.018

Kalcher, J., and Pfurtscheller, G. (1995). Discrimination between phase-locked and non-phase-locked event-related EEG activity. *Electroencephalogr. Clin. Neurophysiol.* 94, 381–384. doi: 10.1016/0013-4694(95)00040-6

Kaufmann, T., Herweg, A., and Kübler, A. (2014). Toward brain-computer interface based wheelchair control utilizing tactually-evoked event-related potentials. *J. Neuroeng. Rehabil.* 11:7. doi: 10.1186/1743-0003-11-7

Kautz, S. A., and Patten, C. (2005). Interlimb influences on paretic leg function in poststroke hemiparesis. *J. Neurophysiol.* 93, 2460–2473. doi: 10.1152/jn.00963.2004

Kilicarslan, A., Prasad, S., Grossman, R. G., and Contreras-Vidal, J. L. (2013). "High accuracy decoding of user intentions using EEG to control a

lower-body exoskeleton," in *2013 35th Annual International Conference of the IEEE Engineering in Medicine and Biology Society (EMBC)* (Osaka), 5606–5609.

King, C. E., Wang, P. T., Chui, L. A., Do, A. H., and Nenadic, Z. (2013). Operation of a brain-computer interface walking simulator for individuals with spinal cord injury. *J. Neuroeng. Rehabil.* 10:77. doi: 10.1186/1743-0003-10-77

Kothe, C. A., and Makeig, S. (2013). BCILAB: a platform for brain–computer interface development. *J. Neural Eng.* 10:056014. doi: 10.1088/1741-2560/10/5/056014

Kumar, D., Aggarwal, G., Sehgal, R., Das, A., Lahiri, U., and Dutta, A. (2015). "Engagement-sensitive interactive neuromuscular electrical therapy system for post-stroke balance rehabilitation-a concept study," in *2015 7th International IEEE/EMBS Conference on the Neural Engineering (NER)* (Montpellier), 190–193.

Kwak, N.-S., Müller, K.-R., and Lee, S.-W. (2015). A lower limb exoskeleton control system based on steady state visual evoked potentials. *J. Neural Eng.* 12:056009. doi: 10.1088/1741-2560/12/5/056009

La Fougere, C., Zwergal, A., Rominger, A., Förster, S., Fesl, G., Dieterich, M., et al. (2010). Real versus imagined locomotion: a [18 F]-FDG PET-fMRI comparison. *Neuroimage* 50, 1589–1598. doi: 10.1016/j.neuroimage.2009.12.060

Lazarou, I., Nikolopoulos, S., Petrantonakis, P. C., Kompatsiaris, I., and Tsolaki, M. (2018). EEG-based brain-computer interfaces for communication and rehabilitation of people with motor impairment: a novel approach of the 21st century. *Front. Hum. Neurosci.* 12:14. doi: 10.3389/fnhum.2018.00014

Lebedev, M. A., and Nicolelis, M. A. (2017). Brain-machine interfaces: from basic science to neuroprostheses and neurorehabilitation. *Physiol. Rev.* 97, 767–837. doi: 10.1152/physrev.00027.2016

Lee, K., Liu, D., Perroud, L., Chavarriaga, R., and Millán, J. D. R. (2017). *Endogenous Control of Powered Lower-Limb Exoskeleton*. Basel: Springer: Wearable Robotics: Challenges and Trends.

Liu, Y.-H., Lin, L.-F., Chou, C.-W., Chang, Y., Hsiao, Y.-T., and Hsu, W.-C. (2018). Analysis of electroencephalography event-related desynchronisation and synchronisation induced by lower-limb stepping motor imagery. *J. Med. Biol. Eng.* 4, 1–16. doi: 10.1007/s40846-018-0379-9

Liu, Y.-H., Zhang, B., Liu, Q., Hsu, W.-C., Hsiao, Y.-T., Su, J.-Y., et al. (2015). "A robotic gait training system integrating split-belt treadmill, footprint sensing and synchronous EEG recording for neuro-motor recovery," in *2015 37th Annual International Conference of the IEEE Engineering in Medicine and Biology Society (EMBC)* (Milan), 3573–3577.

Lopes, A. C., Pires, G., Vaz, L., and Nunes, U. (2011). "Wheelchair navigation assisted by human-machine shared-control and a P300-based brain computer interface," in *2011 IEEE/RSJ International Conference on the IEEE Intelligent Robots and Systems (IROS)* (San Francisco, CA), 2438–2444.

Lotte, F. (2014). *A Tutorial on EEG Signal-Processing Techniques for Mental-State Recognition in Brain–Computer Interfaces*. London: Springer, Guide to Brain-Computer Music Interfacing.

Lotte, F., Bougrain, L., Cichocki, A., Clerc, M., Congedo, M., Rakotomamonjy, A., et al. (2018). A review of classification algorithms for EEG-based brain-computer interfaces: a 10 year update. *J. Neural Eng.* 15:031005. doi: 10.1088/1741-2552/aab2f2

Lotte, F., Congedo, M., Lécuyer, A., Lamarche, F., and Arnaldi, B. (2007). A review of classification algorithms for EEG-based brain–computer interfaces. *J. Neural Eng.* 4:R1. doi: 10.1088/1741-2560/4/2/R01

Lotte, F., Fujisawa, J., Touyama, H., Ito, R., Hirose, M., and Lécuyer, A. (2009). "Towards ambulatory brain-computer interfaces: A pilot study with P300 signals," in *Proceedings of the International Conference on Advances in Computer Enterntainment Technology,* (Athens: ACM), 336–339.

Maguire, C. C., Sieben, J. M., and De Bie, R. A. (2018). Movement goals encoded within the cortex and muscle synergies to reduce redundancy pre and post-stroke. The relevance for gait rehabilitation and the prescription of walking-aids. A literature review and scholarly discussion. *Physiother. Theory Pract.* 5, 1–14. doi: 10.1080/09593985.2018.1434579

Malouin, F., and Richards, C. L. (2010). Mental practice for relearning locomotor skills. *Phys. Ther.* 90, 240–251. doi: 10.2522/ptj.20090029

Malouin, F., Richards, C. L., Durand, A., and Doyon, J. (2008). Clinical assessment of motor imagery after stroke. *Neurorehabil. Neural Repair.* 22, 330–340. doi: 10.1177/1545968307313499

Malouin, F., Richards, C. L., Jackson, P. L., Dumas, F., and Doyon, J. (2003). Brain activations during motor imagery of locomotor-related tasks: a PET study. *Hum. Brain Mapp.* 19, 47–62. doi: 10.1002/hbm.10103

Marlinski, V., and Beloozerova, I. N. (2014). Burst firing of neurons in the thalamic reticular nucleus during locomotion. *J. Neurophysiol.* 112, 181–192. doi: 10.1152/jn.00366.2013

Mellinger, J., and Schalk, G. (2007). *BCI2000: A General-Purpose Software Platform for BCI Research*. Cambridge, MA: Towards Brain-Computer Interfacing.

Millán, J. D. R., Galán, F., Vanhooydonck, D., Lew, E., Philips, J., and Nuttin, M. (2009). "Asynchronous non-invasive brain-actuated control of an intelligent wheelchair," in *Annual International Conference of the IEEE Engineering in Medicine and Biology Society (EMBC)* (Minneapolis, MN), 3361–3364.

Millán, J. D. R., Rupp, R., Müller-Putz, G. R., Murray-Smith, R., Giugliemma, C., Tangermann, M., et al. (2010). Combining brain–computer interfaces and assistive technologies: state-of-the-art and challenges. *Front. Neurosci.* 4:161. doi: 10.3389/fnins.2010.00161

Millan, J. R., Renkens, F., Mourino, J., and Gerstner, W. (2004). Noninvasive brain-actuated control of a mobile robot by human EEG. *IEEE Trans. Biomed. Eng.* 51, 1026–1033. doi: 10.1109/TBME.2004.827086

Mokienko, O., Chervyakov, A., Kulikova, S., Bobrov, P., Chernikova, L., Frolov, A., et al. (2013). Increased motor cortex excitability during motor imagery in brain-computer interface trained subjects. *Front. Comput. Neurosci.* 7:168. doi: 10.3389/fncom.2013.00168

Müller-Gerking, J., Pfurtscheller, G., and Flyvbjerg, H. (1999). Designing optimal spatial filters for single-trial EEG classification in a movement task. *Clin. Neurophysiol.* 110, 787–798. doi: 10.1016/S1388-2457(98)00038-8

Murray, S., and Goldfarb, M. (2012). "Towards the use of a lower limb exoskeleton for locomotion assistance in individuals with neuromuscular locomotor deficits," in *2012 Annual International Conference of the IEEE Engineering in Medicine and Biology Society (EMBC)*, (San Diego, CA: IEEE), 1912–1915.

Nicolas-Alonso, L. F., and Gomez-Gil, J. (2012). Brain computer interfaces, a review. *Sensors* 12, 1211–1279. doi: 10.3390/s120201211

Noda, T., Sugimoto, N., Furukawa, J., Sato, M.-A., Hyon, S.-H., and Morimoto, J. (2012). "Brain-controlled exoskeleton robot for BMI rehabilitation," in *2012 12th IEEE-RAS International Conference on Humanoid Robots (Humanoids)* (Osaka: IEEE), 21–27.

Nolan, H., Whelan, R., and Reilly, R. (2010). FASTER: fully automated statistical thresholding for EEG artifact rejection. *J. Neurosci. Methods* 192, 152–162. doi: 10.1016/j.jneumeth.2010.07.015

Palankar, M., De Laurentis, K. J., Alqasemi, R., Veras, E., Dubey, R., Arbel, Y., et al. (2009). "Control of a 9-DoF wheelchair-mounted robotic arm system using a P300 brain computer interface: Initial experiments," in *2008 IEEE International Conference on Robotics and Biomimetics, ROBIO* (Bangkok: IEEE), 348–353. doi: 10.1109/ROBIO.2009.4913028

Penfield, W., and Boldrey, E. (1937). Somatic motor and sensory representation in the cerebral cortex of man as studied by electrical stimulation. *Brain* 60, 389–443. doi: 10.1093/brain/60.4.389

Petersen, T. H., Willerslev-Olsen, M., Conway, B. A., and Nielsen, J. B. (2012). The motor cortex drives the muscles during walking in human subjects. *J. Physiol.* 590, 2443–2452. doi: 10.1113/jphysiol.2012.227397

Petrofsky, J. S., and Khowailed, I. A. (2014). Postural sway and motor control in trans-tibial amputees as assessed by electroencephalography during eight balance training tasks. *Med. Sci. Monit.* 20: 2695–2704. doi: 10.12659/MSM.891361

Pfurtscheller, G., Brunner, C., Schlögl, A., and Da Silva, F. L. (2006a). Mu rhythm (de) synchronization and EEG single-trial classification of different motor imagery tasks. *Neuroimage* 31, 153–159. doi: 10.1016/j.neuroimage.2005.12.003

Pfurtscheller, G., Leeb, R., Keinrath, C., Friedman, D., Neuper, C., Guger, C., et al. (2006b). Walking from thought. *Brain Res.* 1071, 145–152. doi: 10.1016/j.brainres.2005.11.083

Pfurtscheller, G., Neuper, C., Brunner, C., and Da Silva, F. L. (2005). Beta rebound after different types of motor imagery in man. *Neurosci. Lett.* 378, 156–159. doi: 10.1016/j.neulet.2004.12.034

Pfurtscheller, G., and Solis-Escalante, T. (2009). Could the beta rebound in the EEG be suitable to realize a "brain switch"? *Clin. Neurophysiol.* 120, 24–29. doi: 10.1016/j.clinph.2008.09.027

Pires, G., Castelo-Branco, M., and Nunes, U. (2008). "Visual P300-based BCI to steer a wheelchair: a Bayesian approach," in *2008 30th Annual International Conference of the IEEE Engineering in Medicine and Biology Society EMBS* (Vancouver, BC: IEEE), 658–661.

Pons, J., Moreno, J., Torricelli, D., and Taylor, J. (2013). "Principles of human locomotion: a review," in *2013 35th Annual International Conference of the IEEE Engineering in Medicine and Biology Society (EMBC)* (Osaka: IEEE), 6941–6944.

Presacco, A., Forrester, L., and Contreras-Vidal, J. L. (2011a). "Towards a non-invasive brain-machine interface system to restore gait function in humans," in *2011 Annual International Conference of the IEEE Engineering in Medicine and Biology Society, EMBC* (Boston, MA: IEEE), 4588–4591.

Presacco, A., Goodman, R., Forrester, L., and Contreras-Vidal, J. L. (2011b). Neural decoding of treadmill walking from noninvasive electroencephalographic signals. *J. Neurophysiol.* 106, 1875–1887. doi: 10.1152/jn.00104.2011

Raethjen, J., Govindan, R., Binder, S., Zeuner, K. E., Deuschl, G., and Stolze, H. (2008). Cortical representation of rhythmic foot movements. *Brain Res.* 1236, 79–84. doi: 10.1016/j.brainres.2008.07.046

Rebsamen, B., Burdet, E., Guan, C., Zhang, H., Teo, C. L., Zeng, Q., et al. (2007). Controlling a wheelchair indoors using thought. *IEEE Intell. Syst.* 22, 18–24. doi: 10.1109/MIS.2007.26

Rebsamen, B., Guan, C., Zhang, H., Wang, C., Teo, C., Ang, M. H., et al. (2010). A brain controlled wheelchair to navigate in familiar environments. *IEEE Trans. Neural Syst. Rehabil. Eng.* 18, 590–598. doi: 10.1109/TNSRE.2010.2049862

Renard, Y., Lotte, F., Gibert, G., Congedo, M., Maby, E., Delannoy, V., et al. (2010). Openvibe: an open-source software platform to design, test, and use brain–computer interfaces in real and virtual environments. *Presence* 19, 35–53. doi: 10.1162/pres.19.1.35

Rivet, B., Souloumiac, A., Attina, V., and Gibert, G. (2009). xDAWN algorithm to enhance evoked potentials: application to brain–computer interface. *IEEE Trans. Biomed. Eng.* 56, 2035–2043. doi: 10.1109/TBME.2009.2012869

Salazar-Varas, R., Costa, Á., Iáñez, E., Úbeda, A., Hortal, E., and Azorín, J. (2015). Analyzing EEG signals to detect unexpected obstacles during walking. *J. Neuroeng. Rehabil.* 12, 101. doi: 10.1186/s12984-015-0095-4

Schalk, G., Mcfarland, D. J., Hinterberger, T., Birbaumer, N., and Wolpaw, J. R. (2004). BCI2000: a general-purpose brain-computer interface (BCI) system. *IEEE Trans. Biomed. Eng.* 51, 1034–1043. doi: 10.1109/TBME.2004.827072

Scherrer, B. (2007). *Gaussian Mixture Model Classifiers*. Lecture Notes, February.

Schwartz, A. B., Cui, X. T., Weber, D. J., and Moran, D. W. (2006). Brain-controlled interfaces: movement restoration with neural prosthetics. *Neuron* 52, 205–220. doi: 10.1016/j.neuron.2006.09.019

Sczesny-Kaiser, M., Höffken, O., Aach, M., Cruciger, O., Grasmücke, D., Meindl, R., et al. (2015). HAL® exoskeleton training improves walking parameters and normalizes cortical excitability in primary somatosensory cortex in spinal cord injury patients. *J. Neuroeng. Rehabil.* 12, 68. doi: 10.1186/s12984-015-0058-9

Semprini, M., Laffranchi, M., Sanguineti, V., Avanzino, L., De Icco, R., De Michieli, L., et al. (2018). Technological approaches for neurorehabilitation: from robotic devices to brain stimulation and beyond. *Fronti. Neurol.* 9:212. doi: 10.3389/fneur.2018.00212

Semmlow, J. L., and Griffel, B. (2014). *Biosignal and Medical Image Processing*. Cambridge, MA: CRC press.

Slutzky, M. W. (2018). Brain-machine interfaces: powerful tools for clinical treatment and neuroscientific investigations. *Neuroscientist*. doi: 10.1177/1073858418775355. [Epub ahead of print].

Soekadar, S. R., Witkowski, M., Vitiello, N., and Birbaumer, N. (2015). An EEG/EOG-based hybrid brain-neural computer interaction (BNCI) system to control an exoskeleton for the paralyzed hand. *Biomed. Tech. (Berl)* 60, 199–205. doi: 10.1515/bmt-2014-0126

Takahashi, M., Gouko, M., and Ito, K. (2009). "Fundamental research about electroencephalogram (EEG)-functional electrical stimulation (FES) rehabilitation system," in 2009 *IEEE International Conference on, IEEE Rehabilitation Robotics, (2009) ICORR* (Kyoto), 316–321.

Takahashi, M., Takeda, K., Otaka, Y., Osu, R., Hanakawa, T., Gouko, M., et al. (2012). Event related desynchronization-modulated functional electrical stimulation system for stroke rehabilitation: a feasibility study. *J. Neuroeng. Rehabil.* 9, 56. doi: 10.1186/1743-0003-9-56

Tariq, M., Trivailo, P. M., and Simic, M. (2017a). "Detection of knee motor imagery by Mu ERD/ERS quantification for BCI based neurorehabilitation applications," in *2017 11th Asian Control Conference (ASCC)*, (Gold Coast, QLD), 2215–2219.

Tariq, M., Trivailo, P. M., and Simic, M. (2018). Event-related changes detection in sensorimotor rhythm. *Int. Rob. Autom. J.* 4, 119–120. doi: 10.15406/iratj.2018.04.00105

Tariq, M., Uhlenberg, L., Trivailo, P., Munir, K. S., and Simic, M. (2017b). "Mu-beta rhythm ERD/ERS quantification for foot motor execution and imagery tasks in BCI applications," in *2017 8th IEEE International Conference on Cognitive Infocommunications (CogInfoCom)* (Debrecen), 000091–000096.

Taylor II, R. M., Hudson, T. C., Seeger, A., Weber, H., Juliano, J., and Helser, A. T. (2001). "VRPN: a device-independent, network-transparent VR peripheral system," in *Proceedings of the ACM Symposium on Virtual Reality Software and Technology*, (Baniff, AB: ACM), 55–61.

Tonin, L., Carlson, T., Leeb, R., and Millán, J. D. R. (2011). "Brain-controlled telepresence robot by motor-disabled people," in *2011 Annual International Conference of the IEEE Engineering in Medicine and Biology Society, EMBC* (Boston, MA: IEEE), 4227–4230.

Tonin, L., Leeb, R., Tavella, M., Perdikis, S., and Millán, J. D. R. (2010). "The role of shared-control in BCI-based telepresence," in *2010 IEEE International Conference on Systems Man and Cybernetics*, (Istanbul: IEEE), 1462–1466.

Tsui, C. S. L., Gan, J. Q., and Hu, H. (2011). A self-paced motor imagery based brain-computer interface for robotic wheelchair control. *Clin. EEG Neurosci.* 42, 225–229. doi: 10.1177/155005941104200407

Tucker, M. R., Olivier, J., Pagel, A., Bleuler, H., Bouri, M., Lambercy, O., et al. (2015). Control strategies for active lower extremity prosthetics and orthotics: a review. *J. Neuroeng. Rehabil.* 12, 1. doi: 10.1186/1743-0003-12-1

Vanacker, G., Del R Millán, J., Lew, E., Ferrez, P. W., Moles, F. G., Philips, J., et al. (2007). Context-based filtering for assisted brain-actuated wheelchair driving. *Comput. Intell. Neurosci.* 2007, 3–3. doi: 10.1155/2007/25130

Vasilyev, A., Liburkina, S., Yakovlev, L., Perepelkina, O., and Kaplan, A. (2017). Assessing motor imagery in brain-computer interface training: psychological and neurophysiological correlates. *Neuropsychologia* 97, 56–65. doi: 10.1016/j.neuropsychologia.2017.02.005

Vidal, J. J. (1973). Toward direct brain-computer communication. *Annu. Rev. Biophys. Bioeng.* 2, 157–180. doi: 10.1146/annurev.bb.02.060173.001105

Viola, F. C., Thorne, J., Edmonds, B., Schneider, T., Eichele, T., and Debener, S. (2009). Semi-automatic identification of independent components representing EEG artifact. *Clin. Neurophysiol.* 120, 868–877. doi: 10.1016/j.clinph.2009.01.015

Wang, P. T., King, C., Chui, L. A., Nenadic, Z., and Do, A. (2010). "BCI controlled walking simulator for a BCI driven FES device," in *Proceedings of RESNA Annual Conference*, (Arlington: VA: RESNA).

Wang, P. T., King, C. E., Chui, L. A., Do, A. H., and Nenadic, Z. (2012). Self-paced brain–computer interface control of ambulation in a virtual reality environment. *J. Neural Eng.* 9:056016. doi: 10.1088/1741-2560/9/5/056016

Wieser, M., Haefeli, J., Bütler, L., Jäncke, L., Riener, R., and Koeneke, S. (2010). Temporal and spatial patterns of cortical activation during assisted lower limb movement. *Exp. Brain Res.* 203, 181–191. doi: 10.1007/s00221-010-2223-5

Wolpaw, J., and Wolpaw, E. W. (2012). Brain-*Computer Interfaces*: *Principles* and *Practice*, New York, NY: Oxford University Press.

Wolpaw, J. R., Birbaumer, N., McFarland, D. J., Pfurtscheller, G., and Vaughan, T. M. (2002). Brain-computer interfaces for communication and control. *Clin. Neurophysiol.* 113, 767–791. doi: 10.1016/S1388-2457(02)00057-3

Wolpaw, J. R., and Mcfarland, D. J. (2004). Control of a two-dimensional movement signal by a noninvasive brain-computer interface in humans. *Proc. Natl. Acad. Sci. U.S.A.* 101, 17849–17854. doi: 10.1073/pnas.0403504101

Xu, R., Jiang, N., Mrachacz-Kersting, N., Lin, C., Prieto, G. A., Moreno, J. C., et al. (2014). A closed-loop brain–computer interface triggering an active ankle–foot orthosis for inducing cortical neural plasticity.

IEEE Trans. Biomed. Eng. 61, 2092–2101. doi: 10.1109/TBME.2014.2313867

Yang, Z., Wang, Y., and Ouyang, G. (2014). Adaptive neuro-fuzzy inference system for classification of background EEG signals from ESES patients and controls. *ScientificWorldJournal* 2014:140863. doi: 10.1155/2014/140863

Zelenin, P. V., Deliagina, T. G., Orlovsky, G. N., Karayannidou, A., Dasgupta, N. M., Sirota, M. G., et al. (2011). Contribution of different limb controllers to modulation of motor cortex neurons during locomotion. *J. Neurosci.* 31, 4636–4649. doi: 10.1523/JNEUROSCI.6511-10.2011

Conflict of Interest Statement: The authors declare that the research was conducted in the absence of any commercial or financial relationships that could be construed as a potential conflict of interest.

Chapter 3

Materials and Methods

Chapter Overview

This chapter describes the experimental protocol adopted for synchronous BCI, and the recruitment of participants alongside the establishment of hardware-software interface setup for acquisition of EEG data. Techniques which are used to pre-process raw EEG data in order to reduce noise from the signal are presented, followed by EEG feature extraction methods, for band-power (BP) and common spatial patterns (CSP). Machine learning (ML) models used to estimate the class of feature vectors are discussed in detail. Consequently, criteria used to evaluate the performance of the BCI system offline are described. The advantages associated to individual classification algorithms for improving classification accuracy and signal to noise ratio (SNR) during various LL KMI tasks are highlighted. Finally multiple comparison corrections for ML models are discussed.

3.1 Introduction

This chapter describes the established paradigm to acquire EEG signals elicited by following Graz BCI protocol. The signal processing techniques employed for extraction and classification of ERD/ERS from BP and CSP features that elicit upon distinct left-right LL KMI tasks have been discerned. This chapter is divided into five key sections: Section 3.2 discussed the experimental setup and data acquisition method used in the research, section 3.3 discusses pre-processing techniques used to denoise and filter *mu* and *beta* frequency bands from the EEG signal, section 3.4 discusses the methods used for BP and CSP feature extraction, section 3.5 describes the ML models i.e. classification techniques for mapping task to the desired state, and section 3.6 discusses the evaluation criteria of the offline BCI performance.

3.2 Experimental paradigm and data acquisition

3.2.1 Subjects and experimental design

This research recruited nine healthy participants as shown in Table 3-1, with no history of neurological disorder, or any impairment, aged between 21-28 years, who voluntarily participated in the experiments. The participants had no BCI experience either. Ethics approval for the research was granted by the College Human Ethics Advisory Network (CHEAN) of RMIT University, Melbourne, Australia.

Table 3-1 Characteristics of participants volunteering in BCI experiments

Participants	Gender	Age	Neuromuscular Disorder	BCI Experience (prior biosignal feedback training)
1	Female	25	Nil	No
2	Female	25	Nil	No
3	Male	23	Nil	No
4	Male	27	Nil	No
5	Male	22	Nil	No
6	Female	28	Nil	No
7	Female	24	Nil	No
8	Male	21	Nil	No
9	Male	23	Nil	No

Participants were directed to sit on a comfortable seat in front of a monitor screen (17''), keeping a distance of about 1.5 m, as shown in figure 3.1 and figure 3.2. Experimental paradigm was based on the standard Graz BCI protocol for synchronous BCI. To avoid the probability of any proprioceptive signals induced because of muscle movement, a flat wooden plate was put underneath the feet of participants. This was to loosely fix both legs and allow the knees to flex at 60^0 from full extension position, and keep the ankles at neutral position. During the foot KMI experiment, participants were asked to dorsiflex their foot approximately 25^0 for 1-2 seconds, in accordance with the nominal walking gait measurements [1]. Similarly during knee KMI experiment, participants fully extended their knee following the respective visual cue, for the same duration.

Figure 3.3 shows schematic overview of protocol timing for the experiment. Each run was initiated with a blank screen, called 'baseline' that lasted for 30 seconds. During baseline period, the participant was asked to relax and get ready for the experiment. Baseline was followed by the initiation of each trial. The trial began with the presentation of a fixation cross on screen for 3 seconds (used as reference period for processing of epochs). One second long audio beep stimulus, right before the visual cue display, was incorporated in the first trial only, to alert the participant about the beginning of the experiment. This was followed by 2 seconds of visual cue display and 5 seconds long blank screen to perform related task (kinaesthetic motor imagery or execution), making 10 seconds in total for one trial. The visual cues in each trial reflected the left or right lower-limb movement directions. In foot KMI experiments, participants were instructed to dorsiflex their foot only once (for 1-2 seconds) during each task performance period. Similarly, for knee KMI experiments participants were asked to extend their knee once, i.e. for 1-2 seconds. To ensure no adaptation is taking place the visual cues in each of the LL experiment were displayed in a random order. Each trial was followed by a random pause interval of 1.5 to 3.5 seconds during which participants were asked to relax. Figure 3.4 represents the experimental plan for each run. Each run/session consisted of 40 trials, with a total of 20 trials for left and 20 for right KMI task. The experiment consisted of four runs/sessions for processing and analysis of data during each LL study.

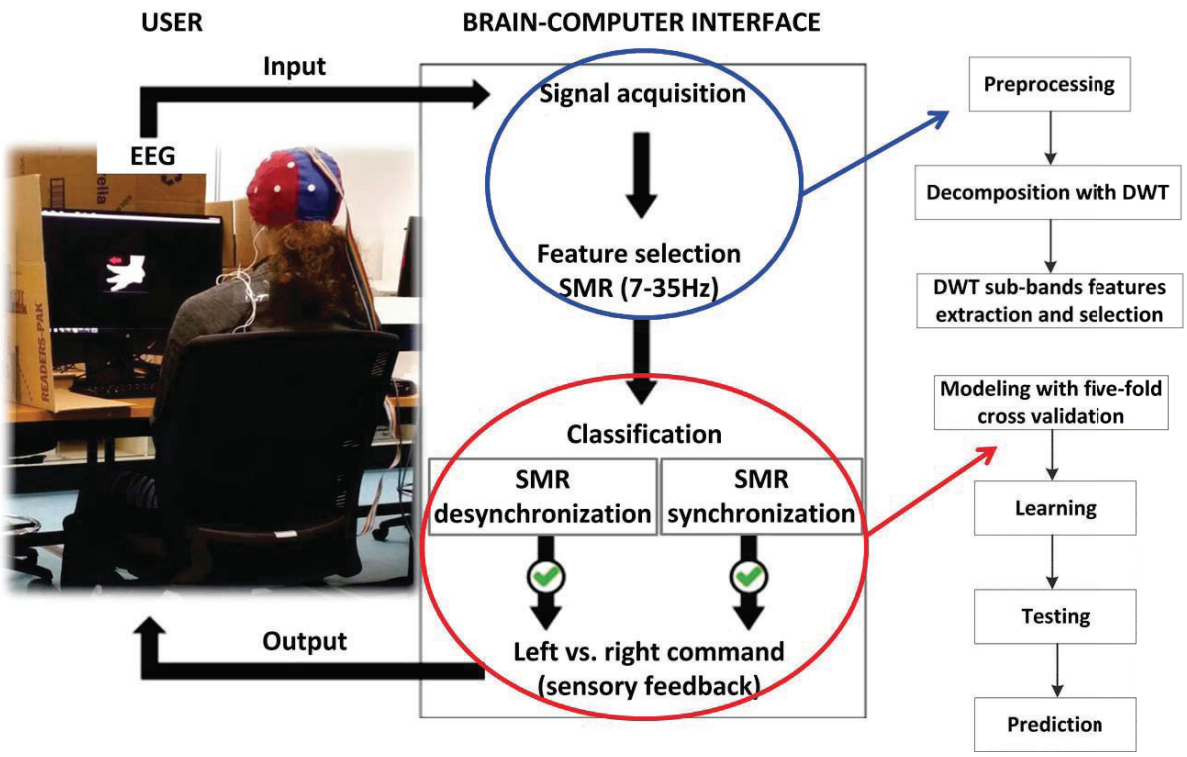

Figure 3.1 Systematic overview of the established experimental setup for ERD/ERS band-power feature extraction and classification using machine learning.

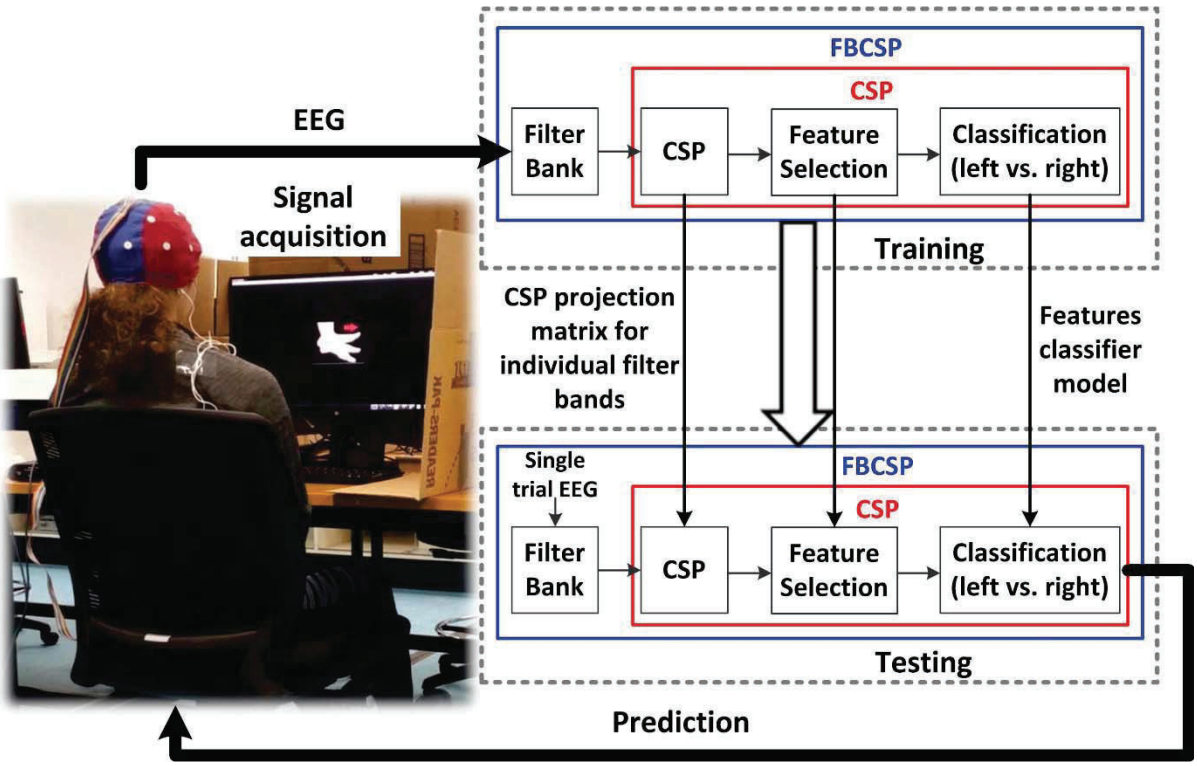

Figure 3.2 Overview of experimental setup for feature extraction using common spatial pattern (CSP) and filter-bank CSP (FBCSP), and classification using machine learning.

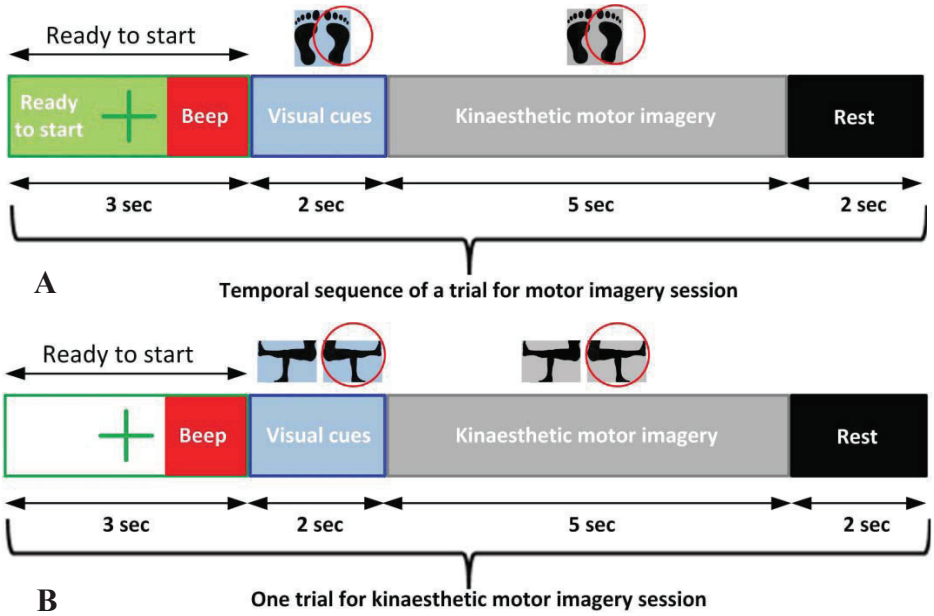

Figure 3.3 Experimental Protocol for each trial reflecting timing of visual cues, with audio beep for first trial only, for (A) foot KMI and (B) knee KMI.

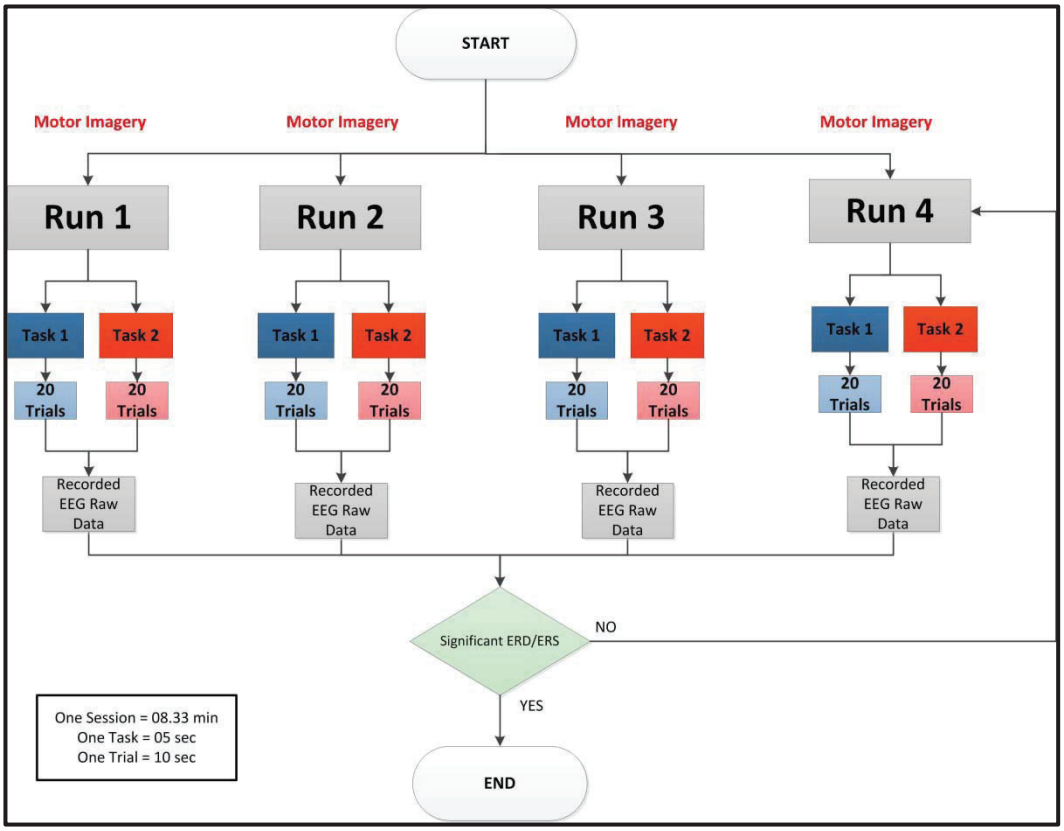

Figure 3.4 Experimental plan reflecting details of each run (session).

3.2.2 **Measuring brain activity**

The neural activity measurement techniques are important tools for investigation of the spatial and temporal arrangement of the supra-spinal neurons involved in motor control such as locomotion and other limb movements. The electrophysiological activity of human brain is produced both by the electro-chemical transmitters exchanging information between the neurons and by the ionic currents generated within the neurons. This allows for direct characterization of the neuronal activity. Electrophysiological activity can be measured by various modalities. This research explicitly involved the electroencephalography (EEG) modality for being the safest technology (highly non-invasive) and portable. It provides a high time resolution (millisecond scale temporal resolution) [2], with a spatial resolution in centimetres, frequency bandwidth between 0 to 50 Hz, and characteristic amplitude of 10 to 20 μV [3].

3.2.3 **10-20 System used in EEG**

To measure the small electrical potentials reflecting the activity of neuron in the brain, metal electrodes are placed on the head/scalp, usually by means of a conducting electrode gel (not in case of dry electrodes). Basically a bio-signal amplifier measures the potential difference between two electrodes. Measurement from each electrode is referred to a common electrode called `reference'. I used the BrainMaster Discovery 24E amplifier (BrainMaster Technologies Inc., Bedford, USA) with 10-20 eletrocap embedding Tin electrodes. Electrodes were mounted in the cap based on the 10-20 system. The international 10-20 system is a standard scheme standardized by the American Electroencephalographic Society, for naming and positioning scalp electrodes for EEG [4]. Wherein ‘10’ and ‘20’ refer that the actual distance between adjacent electrodes are either 10% or 20% of total right-left (ear to ear) or front-back (nasion to inion) distance of the skull, as shown in figure 3.5.

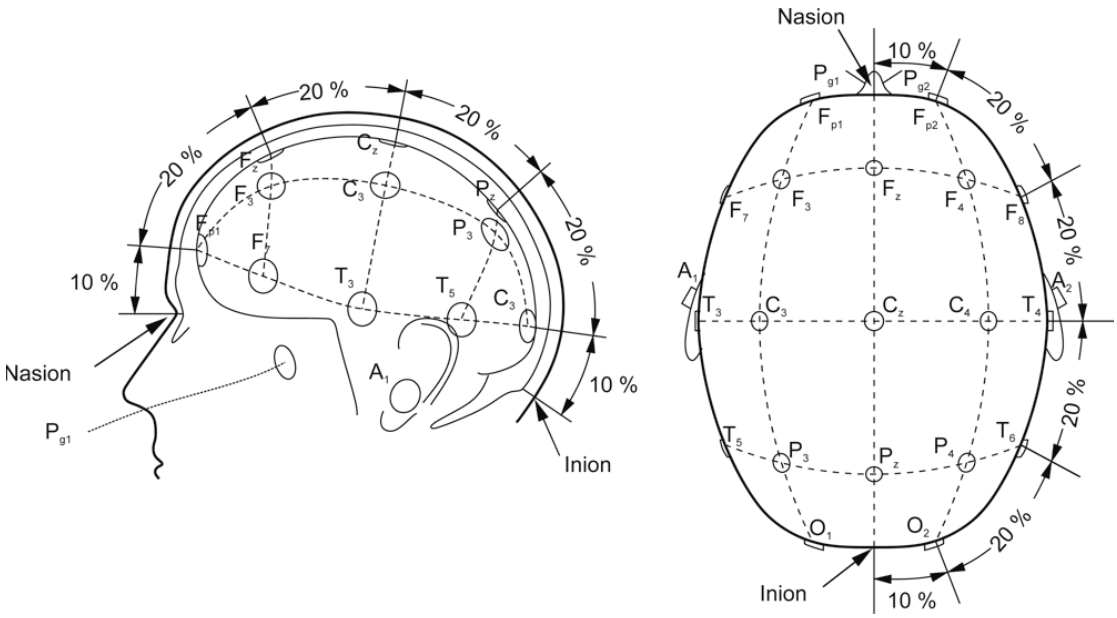

Figure 3.5 The standard 10-20 system for electrode placement over scalp used in EEG cap [5].

Figure 3.6 Setting up the EEG electrocap on a participant in mechatronics lab at Bundoora east campus RMIT.

3.2.4 **Data acquisition**

In order to record EEG signals from each participant, the EEG neurofeedback BrainMaster Discovery 24E amplifier (BrainMaster Technologies Inc., Bedford, USA) was used in the experiment as shown in figure 3.6. It was interfaced with the acquisition server of OpenViBE software http://openvibe.inria.fr/downloads/. The standard 10-20 Electro-cap was used to acquire brain signals from the motor cortex [6]. System's 19 channels were referenced to linked earlobes (LE) derived from the electrodes A1, A2 and a ground electrode. Remaining channels provided for monitoring other electrophysiological signals were not used. All

channels were sampled using 256 Hz sampling frequency, with a 24-bit resolution. Amplifier bandwidth was from 0 to 100 Hz and EEG channel bandwidth was from 0.43 to 80 Hz.

In order to set the experimental protocol, the OpenViBE designer tool that comes along integrated feature boxes was used. Inside OpenViBE designer window the *.lua* script and the default settings were customized for using the Graz-Stimulator box to allow for the onset of different visual cue timings. The BrainMaster Discovery and OpenViBE software were interfaced by setting the acquisition server properties of OpenViBE and connecting the required modules as presented in figure 3.7. The recordings were made using the *edf* and *gdf* writer boxes of OpenViBE that lead to the storage of both signals and the corresponding stimulations, respectively [7].

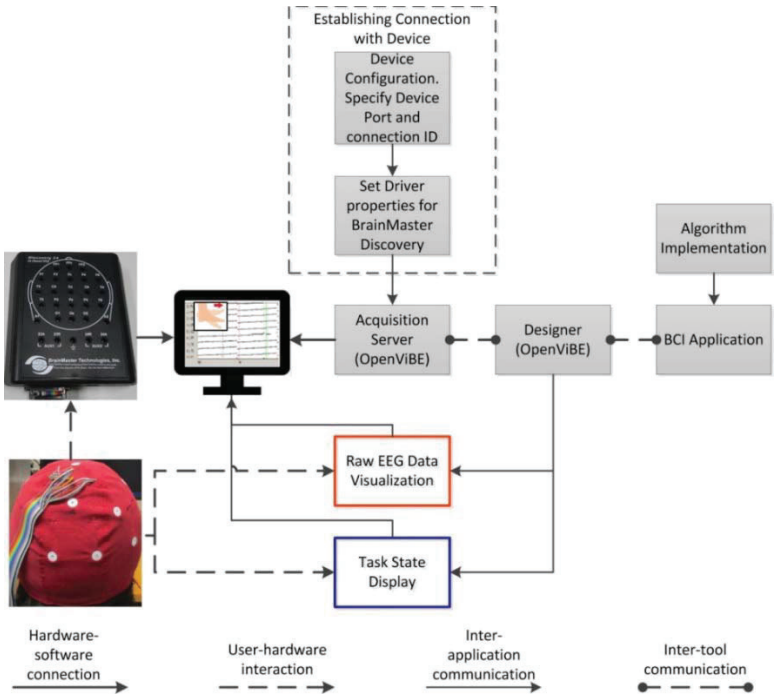

Figure 3.7 As part of experimental setup, the established hardware-software connection between Discovery 24E amplifier and OpenViBE acquisition software.

3.3 Pre-processing techniques to reduce noise and artifacts from EEG

For pre-processing of acquired EEG signal, the statistical EEGLAB package (a plugin of MATLAB) was used [8]. During offline mode, the EEG data was converted to reference-free form by using the common average reference method. Data was pre-processed using finite impulse response (FIR) bandpass filter (implemented in EEGLAB [8]) with a low-cut frequency of 7 Hz and high-cut frequency of 12 Hz for *mu* rhythm and 13 Hz low-cut with 30

Hz as high-cut frequency for *beta* rhythm as shown in figure 3.8. These frequency bands contain most informative features about the limb movements for classification of feature vectors [9]. In order to filter out the 50 Hz (electrical) line noise and continuous component from biological drift, the notch filter was already incorporated in the amplifier (Discovery 24E) recording settings. Next, for tasks belonging to each class, epochs, i.e. trial of 10 seconds length were extracted for left task first and then for right task, with respect to the visual cues presented to the participants. Each epoch starts 3 seconds prior to the cue onset, to be used as reference period during analysis, and ends 5 seconds after the offset, making a total of 10 seconds. The time window of cue for task performance was kept 5 seconds since dominant ERS occurs following movement offset. The processing of recorded data was based on single-trial EEG signals.

3.3.1 Spatial filtering (ICA and CSP)

Based on literature [10] it has been demonstrated that for improving the signal-to-noise ratio, spatial filters overall are useful in single-trial analyses. For this reason, this study includes both the independent component analysis (ICA) and common spatial patterns (CSP) filters. For the band-power (BP) features classification, ICA was employed whereas for CSP features the CSP filter was used.

In the first case, i.e. for BP features, the source signal (epoched data) was filtered using the ICA spatial filter. Observed EEG signal is given as:

$$\mathbf{S_j} = \mathbf{W}\mathbf{E_j}, \qquad 1$$

where $\mathbf{E_j}$ is the observed single-trial EEG signal, $j = 1 \ldots n$, where n is the number of training trials. $\mathbf{W}$ is the un-mixing matrix and $\mathbf{S_j}$ is the single-trial signal. This method was used for time-frequency analysis of ERD/ERS band-power features. The ICA finds a linear transformation $\mathbf{W}$ of non-Gaussian data $\mathbf{E}$, to get the resulting components $\mathbf{S}$ as statistically independent as possible [11]. EEG signal is therefore separated into independent components to account for different neural activities, this also includes artifacts such as eye movements (saccades), blinks and muscle activities [8]. In this thesis, the logistic infomax ICA algorithm, executed in the EEGLAB function 'bin' [8], is used for the preprocessing of training set. It yielded an un-mixing matrix $\mathbf{W} \in \mathbb{R}^{s \times c}$ and source signals i.e. independent components $\mathbf{S_j} \in \mathbb{R}^{s \times t}$, where s is the number of independent components, c is the number of channels, t the

number of time samples and $j = 1 \ldots n$, is the number of training trials. This procedure resulted in the elimination of eye artefacts and muscle movements.

In second part of our research, the other spatial filters were used i.e. the CSP and filter bank CSP (FBCSP) for CSP features classification. FBCSP method computes the un-mixing matrix **W** in order to yield features that have optimal variances for discriminating the classes of measured EEG signal [12, 13] (in this case 2 classes). This is achieved by resolving the eigenvalue decomposition problem.

$$\sum_1 W = (\Sigma_1 + \Sigma_2)WD, \qquad 2$$

where Σ_1 and Σ_2 are the estimates of the covariance matrices of EEG signal based on two tasks i.e. left and right movement, the diagonal matrix D consists of the eigenvalues of Σ_1, and the column vectors of W^{-1} are the filters for CSP projections. For best results, most suitable contrast is provided by filters with the highest and lowest eigenvalues. It is therefore common to retain e eigenvectors from both ends of the eigenvalue spectrum [13].

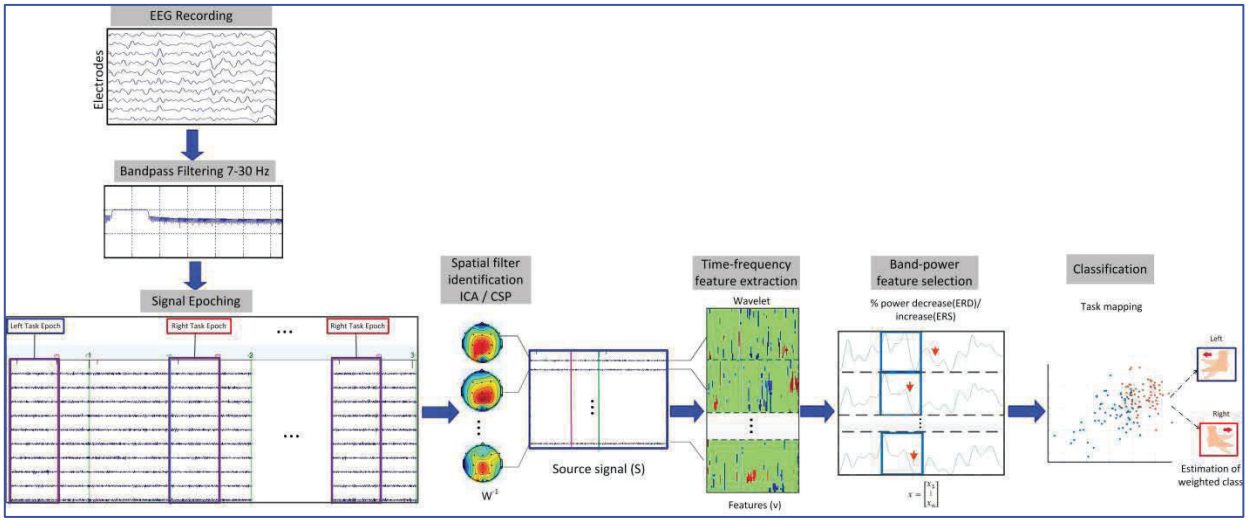

Figure 3.8 Band-power/Common spatial pattern feature decoder and classifier training in one fold of the cross-validation.

3.4 Feature extraction techniques

3.4.1 Time-frequency analysis: the wavelet transform

In order to analyse the difference between left and right foot (dorsiflexion) and left and right knee (extension) movements in the spectral and temporal domains, for BP features, the EEG

power spectrum for left and right movement KMI was taken into account. The time-frequency features represent the subject-specific ERD/ERS patterns, from the single-trial signals $\mathbf{S}$ as shown in figure 3.8. For every trial, a wavelet coefficient matrix is computed with 100 time samples and 3 separate frequency bins (7-12 Hz for *mu*, 13-24 Hz for low *beta* and 25-35 Hz for high *beta*) for the *i*-th source signal. In order to get spectral power, the resulting coefficients are squared and the $10log_{10}$ transformation is computed to get resulting time-frequency representation c_i. The feature vector of the *j*-th trial v_j is obtained by the concatenation of the time-frequency coefficients c_i that is computed from the *i*-th independent component signal inside $\boldsymbol{S}_j$ [9]:

$$\boldsymbol{v}_j = \begin{bmatrix} \boldsymbol{c_1} \\ \boldsymbol{c_i} \\ . \\ . \\ . \\ \boldsymbol{c_s} \end{bmatrix}, \boldsymbol{c_i} = \left[c_{11}, \ldots, c_{f1}, c_{12}, \ldots, c_{f2}, \ldots, c_{1t}, \ldots, c_{ft}\right]^T \qquad 3$$

In equation 3, $\boldsymbol{v}_j$ is the *j*-th feature vector, where $j = 1 \ldots n$, here n is the number of training trials, $\boldsymbol{c_i}$ is the time-frequency coefficient vector of the *i*-th source, $i = 1 \ldots s$, here s is the number of independent components in $\boldsymbol{S}_j$, the number of time samples is t and f is the number of frequency bins.

In EEGLAB, the event-related spectral (amplitude, phase and coherence) perturbation function 'ERSP' (i.e. the epoch-mean power spectrum) was used to extract and assess the ERD/ERS patterns. This function was applied to the ICA components (data recorded from single electrodes). I evaluated the event-related time/frequency measure using ERSP, i.e. calculating the mean event-related changes in the power spectrum at a data channel or component over time in the broad frequency range for oscillatory rhythms (*mu-beta*) [14]. ERSP plots generalize the narrow-band ERD and ERS. ERSP Calculation requires computing the power spectrum over a sliding latency window then averaging across data trials. The colour at each image pixel indicates power (in dB) at a given frequency and latency relative to the time locking event. For n trials, if $F_k(f,t)$ is the spectral estimate of trial k at frequency f and time t

$$ERSP(f,t) = \frac{1}{n}\sum_{k=1}^{n}|F_k(f,t)|^2 \qquad 4$$

In equation 4, the sinusoidal wavelet (short-time Discrete Fourier Transform) transform (DWT) was used to compute $F_k(f,t)$ i.e. for calculating the power spectrum density of each

EEG epoch. In DWT the number of cycles is increased slowly with frequency. This feature provides better frequency resolution at higher frequencies than conventional wavelet approaches which use constant cycle length [8]. This method is also better matched to the linear scale for frequencies visualization. For visualization of power changes across the frequency range, the mean baseline log power spectrum is subtracted from each spectral estimate, producing the baseline-normalized ERSP. The significance of deviations from baseline power was evaluated using the bootstrap-*t* statistical method, with confidence interval of 95% ($p<0.05$). In this method, a substitution for data distribution is created by selecting spectral estimates for each trial from the randomly selected latency windows in the assigned epoch baseline i.e. prior to the stimulus onset, followed by their averaging. After repeating this process many times (default: N=200) a substitute 'baseline' amplitude distribution is generated whose specified percentiles are then taken as significant thresholds i.e. significant ERD and ERS features. This was implemented by developing a MATLAB script based on following equations 5 to 8.

$$y_{ij} = (x_{ij} - \bar{x}_j)^2 \qquad 5$$

$$P_j = \frac{1}{N-1}\sum_{i=1}^{N} y_{ij} \qquad 6$$

$$R = \frac{1}{k+1}\sum_{r_0}^{r_0+k} P_j \qquad 7$$

$$ERDS_j = \frac{P_j - R}{R} * 100\% \qquad 8$$

The sample differences were squared, labelled as y_{ij} after subtracting the mean of the bandpass filtered data for each sample to overcome masking of induced activities caused by the evoked potentials. Samples were subsequently averaged over trials and over sample points. Here N is the total number of trials, x_{ij} is the *j*-th sample of the *i*-th trial of the bandpass filtered data, and $\bar{x}_j$ is the mean of the *j*-th sample averaged over all bandpass filtered trials. Whereas P_j is the power or inter-trial variance of the *j*-th sample and R is the average power in the reference interval $[r_0, r_0 + k]$ [15-18].

3.4.2 Band power (percentage power change in ERD/ERS) features

The channels associated to the sensorimotor cortex i.e. features elicited by the central electrode sites C3, Cz, and C4 were analysed with the most significant BP decrease, or increase, during each of the left and right KMI task. It is a well-established fact that the oscillatory brain activity lie in the 0 to 50 Hz frequency band, however the frequency window for analysis of ERD and ERS associated to KMI was kept to 7-12 Hz and 13-30 Hz because they occur within only this narrow frequency sub-band. As mentioned earlier, the power spectrum density of each EEG signal epoch was calculated using DWT. For band-power calculations, let $x(t_0, t_f)$ be a single-trial EEG signal epoch within the time interval $t_0 - t_f$, where t_0 and t_f are the time points in seconds satisfying the condition for task performance duration i.e. $2 \leq t_0 < t_f \leq 7$. Here the single-trial EEG signal refers to the EEG signals recorded during the KMI task (left vs. right) of one single trial, that is, one-time KMI. For a specific frequency band i.e. *mu* first then *beta*, the percentage power change y for left or right KMI EEG epoch $x(t_0, t_f)$ is given as:

$$y(t_0, t_f) = \frac{BP_{MI}(t_0,t_f) - \overline{BP}_{baseline}(t_0,t_f)}{\overline{BP}_{baseline}(t_0,t_f)} \qquad 9$$

In equation 9, $BP_{MI}(t_0, t_f)$ is the band-power of $x(t_0, t_f)$; and $\overline{BP}_{baseline}(t_0, t_f)$ is the mean band-power of the baseline prior to cue onset EEG epochs within the same time interval, given as:

$$\overline{BP}_{baseline}(t_0, t_f) = \frac{1}{N}\sum_{i=1}^{N} BP_{baseline}\,(t_0, t_f) \qquad 10$$

In equation 10, $N = 20$, since 20 baseline EEG signals were taken as reference for each participant [19]. The left vs. right KMI task-based ERD/ERS amplitude for foot dorsiflexion and knee extension were tested statistically for two EEG montages, i.e. common average and bipolar reference respectively. We followed figure 3.9, where multiple comparisons were drawn between common average reference and bipolar reference extracted BP features at each channel. This was conducted by applying the family-wise error rate, using Bonferroni correction. Finally, the performance of the three ML models and their comparison was done using false discovery rate (FDR) correction.

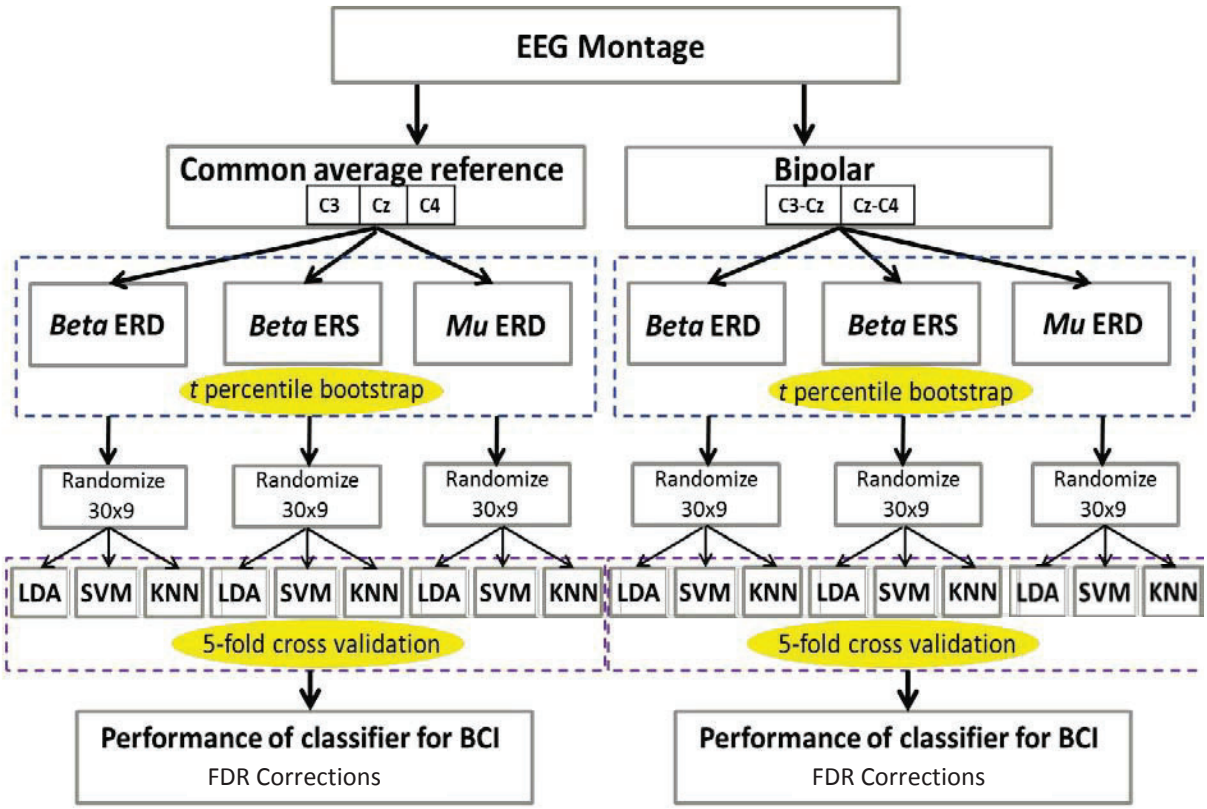

Figure 3.9 Layout of study carried out for band-power features

$$\mathrm{ERSP_j} = 10(\log_{10})\frac{\mathrm{P_j}}{\mathrm{R}}$$

3.4.3 Common spatial pattern (CSP) features

In the case of the CSP feature extraction, the FBCSP filter was applied for a left vs. baseline and right vs. baseline, for three different frequency bands 7–12 Hz (*mu*), 13–30 Hz (*beta*), 7–30 Hz (*mu* and *beta*), in the time segment starting after the cue i.e. task performance duration of 5 seconds. Furthermore e = 2 eigenvectors from the top and from the bottom of the eigenvalue spectrum were retained. This method was implemented on the pre-processed training dataset, that yielded the un-mixing matrix $\mathbf{W} \in \mathbb{R}^{s\times c}$ and source signals $\mathbf{S_j} \in \mathbb{R}^{s\times t}$, where $s = 2 \times e \times 3\ (frequency\ bands) \times 2(classes)$ is the number of sources i.e. the CSP projections, c is the number of channels, the number of time samples is t and $j = 1 \ldots n$, here n is the number of trials of training sets.

When the spatial filtered signal $\mathbf{S_j}$ from (1) uses $\mathbf{W}$ from (2), it maximizes the difference in variance of the two classes of bandpass filtered EEG signal. The m pairs of CSP features of j-th trial for band-pass filtered EEG signal are given by:

$$v_j = \log \frac{\mathrm{diag}\left(\overline{W}^T E_j E_j^T \overline{W}\right)}{\mathrm{tr}\left[\overline{W}^T E_j E_j^T \overline{W}\right]} \quad 11$$

where $v_j \in \mathbb{R}^{2m}$; $\overline{W}$ signifies the first m and the last m columns of W; $\mathrm{diag}(.)$ returns the diagonal elements of the square matrix; $\mathrm{tr}[.]$ returns the sum of diagonal elements in the square matrix [20].

Consequently, the FBCSP feature vector for the *j*-th trial is formulated as:

$$v_j = \left[v_{1,j}, v_{2,j}, v_{3,j}\right] \quad 12$$

where $v_j \in \mathbb{R}^{1\times(3*2m)}$, $j = 1,2,\ldots,n$; n represents the total number of trials in data.

The training data, that comprised extracted feature data, is given as equation 13 and the true class labels is denoted as equation 14, in order to make a difference from the testing and prediction data,

$$\overline{V} = \begin{bmatrix} \overline{v}_1 \\ \overline{v}_2 \\ . \\ . \\ . \\ \overline{v}_{n_t} \end{bmatrix} \quad 13$$

$$\overline{y} = \begin{bmatrix} \overline{y}_1 \\ \overline{y}_2 \\ . \\ . \\ . \\ \overline{y}_{n_t} \end{bmatrix} \quad 14$$

where $\overline{V} \in \mathbb{R}^{n_t\times(3*2m)}$; $\overline{y} \in \mathbb{R}^{n_t\times 1}$; and $\overline{v}_j$; and $\overline{y}_j$ are the feature vector and true class label respectively, from the *j*-th training trial, $j = 1,2,\ldots,n_t$; where n_t represents the total number of trials in training data [20].

3.5 Classification techniques

3.5.1 Linear discriminant analysis (LDA)

This method is explained for a 2 class BCI; consider a set of n features $\overrightarrow{a_1}, \overrightarrow{a_2}, \ldots, \overrightarrow{a_n}$ defined in a two dimensional feature space. A feature $\vec{a}$ can be projected onto a direction defined by a unit vector $\widehat{\omega}$ using the following equation 15:

$$b = \vec{a} \, . \, \widehat{\omega}^2 \qquad 15$$

This is a scalar projection of a vector $\vec{a}$ onto a unit vector ω. Resulting equation above is a scalar and therefore the projection results in a dimensionality reduction from two to one dimension. The figure 3.9 reflects two projections of the given features onto two different vectors $\widehat{\omega}$. Let us take the two classes as ϕ (reflected as red circles) and Ψ (reflected as green circles). Upon first projection, data from different classes is separable via simple thresholding of the scalar b. If instead of the first projection the second projection is performed, the data becomes inseparable. LDA classification aim is to find such a direction $\widehat{\omega}$ that when projecting the data onto $\widehat{\omega}$ it maximizes the distance between the means and minimizes the variance of the two classes. In short, LDA minimizes the following equation 16:

$$\frac{(m_\phi - m_\Psi)^2}{s_\phi^2 + s_\Psi^2} \qquad 16$$

where m_ϕ and m_Ψ are the means and s_ϕ and s_Ψ are the standard deviations of the two respective classes after projecting the features onto $\widehat{\omega}$ [21].

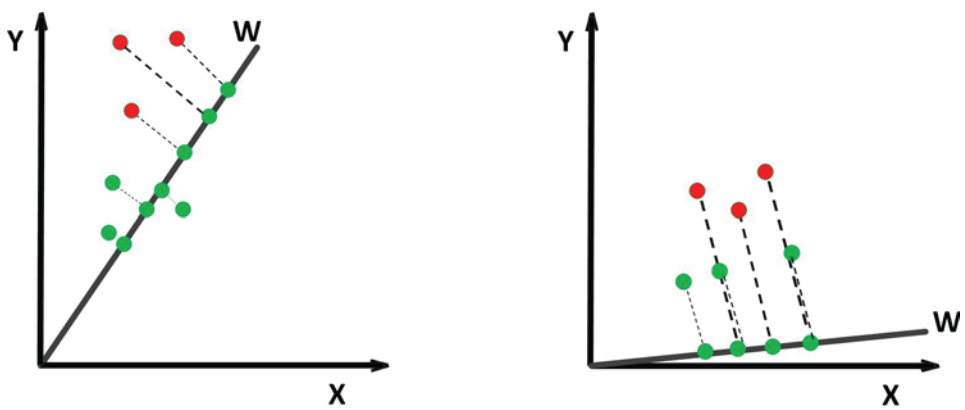

Figure 3.10 Two projections of population from the same class onto different vectors $\widehat{\boldsymbol{\omega}}$. The left projection makes the classification of data simple, the right projection makes the data inseparable.

3.5.2 Support vector machine (SVM)

Support vector machine (SVM) uses a hyperplane i.e. a decision border to divide the feature space into two classes. The hyperplane is defined by the following equation 17:

$$y = \omega^T x + b \qquad 17$$

where $\omega, x \in R^2$and $b \in R^1$. The classified results depend on which side of the hyper plane the feature is located. In SVM, the distances between a hyper plane and the nearest features are called margins. The goal of SVM is to find such a hyperplane for which the distances between the hyperplane and the closest examples are maximized. Figure 3.10 shows an example of two possible hyperplanes in a two-dimensional space. We can see that for the first plot the margins are larger than for the second plot. In that case, the former hyperplane is preferred to the latter by the support vector machines algorithm.

Though SVM is a linear classifier, it can be made with nonlinear decision boundaries using non-linear kernel functions, such as Gaussian or radial basis functions (known as RBF). The non-linear SVM offers a more flexible decision boundary, resulting in an increase in classification accuracy. The kernel functions, however, could be computationally more demanding therefore we kept the classifier with linear boundaries. The high computational time could induce delays in the information transfer rate between the classified feature vector and the mapping to output commands in a BCI.

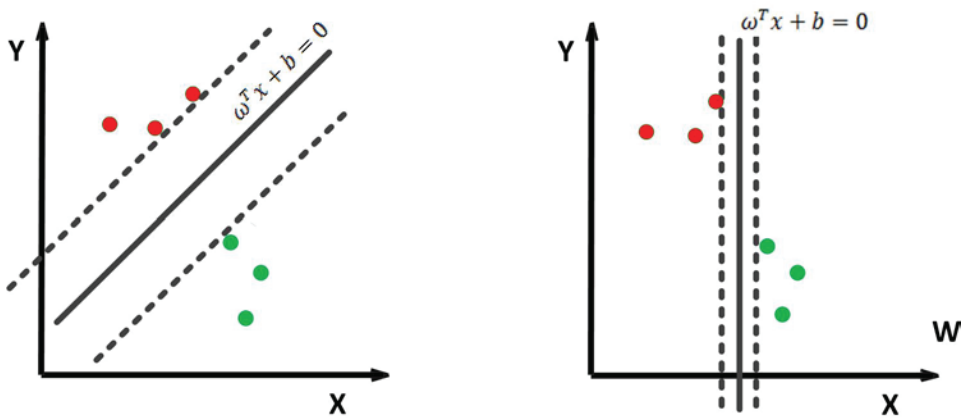

Figure 3.11 Two possible linear decision boundaries, the left decision boundary with a larger margin is preferred over the small margin (on the right) by the SVM.

3.5.3 *k* nearest neighbour (KNN)

The nearest neighbour algorithm aims at assigning a feature vector to a class according to its nearest neighbour(s). In the case of *k* nearest neighbour (KNN), this neighbour can be a feature vector from the training set, or a class prototype. It is a discriminative nonlinear classifier [22].

The aim of this technique is to assign the dominant class to an unseen point among its k nearest neighbours within the training set [23]. These nearest neighbours are typically obtained using a metric distance in BCI studies. KNN can approximate any function with a sufficiently high value of k and enough training samples, this enables it to produce nonlinear decision boundaries. However this algorithm is very sensitive to the curse-of-dimensionality [24]. When used in BCI systems with low dimensional feature vectors, KNN might prove to be efficient [25].

3.5.4 Logistic regression (Logreg)

Logistic regression is a machine learning (ML) algorithm used for classification problems; it is based on the predictive analysis algorithm and the concept of probability. For 2-class BCI, Logreg assigns observations to a discrete set of two classes. It transforms its output by the logistic sigmoid function and returns a probability value. In order to map the predicted values to probabilities, the sigmoid function is used, that maps any real value into another value between 0 and 1 as given:

$$0 \leq h_\theta(x) \leq 1 \qquad 18$$

$$f(x) = \frac{1}{1+e^{-(x)}} \qquad 19$$

where $h_\theta(x)$ is the Logreg hypothesis expectation, and $f(x)$ is the sigmoid function. The classifier is expected to return a set of classified outputs based on probability after passing the inputs through a prediction function with a probability score between 0 and 1.

3.6 Evaluation criteria for BCI performance

3.6.1 Bootstrap statistic

In order to statistically assess the ERD/ERS values, an efficient approach is the bootstrap. It calculates the confidence and significant ERD/ERS values [15]. This method estimates the distribution of a test statistic by resampling the data, i.e. by replacing the unknown population distribution with known empirical distribution [17]. The estimator properties i.e. confidence intervals are determined based on the empirical distribution [26]. This technique does not require any Gaussian or other parametric distribution assumption on the data. The confidence interval $100(1-\alpha)\%$ is determined by equation 20:

$$\left[\bar{e}_j - s_j\hat{\mu}_{j(k_2)} - s_j\hat{\mu}_{j(k_1)}\right] \quad 20$$

where $k_1 = B\,\frac{x}{2}$ and $k_2 = B - k_1 + 1$, here $\bar{e}_j$ is the sample mean and ${s_j}^2$ is the sample variance of the j-th sample of N number of trials, B is the bootstrap that should be larger than 500, $\hat{\mu}_j$ is the mean of the bootstrap estimates. After calculation of the confidence interval, the assessment of whether a value is significant, or not, is determined by checking if both confidence values of this sample show the same sign. This means an ERS is significant with, for instance, 95% confidence, when both 95% confidence limits of this value are positive, similarly for an ERD value to be significant both its confidence limits should be negative.

3.6.2 Cross-validation

Cross-validation is used in the training process of the classifier. During cross-validation, the model is repeatedly tested on different subsets of the training dataset and parameters are optimized. This is done using k-fold cross-validation, meaning the training set is divided into k sets of equal size. The classifier is then trained $k - 1$ times with a different set held out each time to validate the model on the remaining k set. For each fold, a misclassification rate is computed. From this, the average of the k errors can be calculated as a training misclassification rate [23]. Standardization of data is done prior to cross-validation procedure.

3.6.3 Misclassification rate

The misclassification rate (mcr) is directly related to the prediction accuracy as prediction accuracy equals 100 − mcr. This is one of the most common and straightforward performance measures in classification problems. The predicted output is compared to ground truth and the number of misclassified samples is expressed as a loss function. The loss function, or estimate of the misfit between prediction and ground truth, is given by equation 21:

$$L_{mcr}(p,t) = \frac{1}{N}\sum_k \begin{cases} 1, p_k \neq t_k \\ 0, p_k = t_k \end{cases} \quad 21$$

L_{mcr} is the loss estimate of the k-th sample with p being the vector of predictions and t the vector of targets containing the ground truth of the k-th sample, and N the total number of

samples in p [27]. Multiplying L by 100, we obtain the loss expressed as percentage of misclassified samples of the total amount of samples, the misclassification rate (mcr).

3.6.4 Kappa coefficient

The kappa coefficient κ is commonly used as a performance measure for classification algorithms [22, 28]. The Cohen's Kappa is a measure of the agreement between two outputs, here between the ground truth and the prediction. A perfect agreement between prediction and expected value (or ground truth) is indicated by a kappa value of 1. Thus, κ is always less than 1 or equal to 1.

For the kappa computation, the prediction accuracy or the 'observed level of agreement' can be obtained from a confusion matrix; such a sample confusion matrix is seen in table 3-2, or using mcr, as seen in equation 22.

$$p_o = 1 - mcr \tag{22}$$

Table 3-2 Sample confusion matrix for a binary classification problem. It displays probabilities for each occurrence; P11 and P22 representing correctly classified samples.

		Ground Truth		
		Left	**Right**	**Total**
Prediction	**Left**	P11	P12	P1a
	Right	P21	P22	P2a
	Total	P1b	P2b	P_{Total}

To compute kappa score from the confusion matrix, the observed level of agreement p_o is obtained by:

$$p_o = \frac{(P11+P22)}{P_{Total}} \tag{23}$$

Next, the chance agreement p_e is calculated as:

$$p_e = \left(\frac{P1a}{P_{Total}} \times \frac{P1b}{P_{Total}}\right) + \left(\frac{P2a}{P_{Total}} \times \frac{P2b}{P_{Total}}\right) \tag{24}$$

Following this, kappa coefficient is computed using:

$$\kappa = \frac{p_o - p_e}{1 - p_e} \quad 25$$

According to Landis and Koch [29], the value of κ can be interpreted in the following way as shown in table 3-3:

Table 3-3 *kappa* value interpretation [29]

κ	Strength of Agreement
< 0.00	Poor
0.00-0.20	Slight
0.21-0.40	Fair
0.41-0.60	Moderate
0.61-0.80	Substantial
0.81-1.00	Almost perfect

3.6.5 Receiver operator characteristic (ROC) curve and area under the ROC curve

Another common performance measure is the ROC curve [30]. ROC curves were first introduced in the 1940's and came along with the development of radar [31]. Ever since Spackman used these curves to evaluate and compare the performance of his machine learning algorithms in 1989, their use is spread widely [32]. The following description of ROC curves is based on Fawcett's article [32].

The ROC curve is generated by plotting sensitivity, also called the true positive rate (TPR), on the y-axis, against (1 – specificity), also called the false positive rate (FPR), on the x-axis [30, 32]. Equations for sensitivity and specificity can be found in equation 26 and 27, respectively. A diagonal line in the ROC space (y = x) reaching from (0,0) to (1,1) represents a classifier that randomly guesses the class belonging. A shift of the curve towards the upper left corner suggest that the algorithm detects some information from the given data that indicates the belonging to one of the two classes. A curve that lies below the diagonal performs worse than randomly guessing the class labels. The classifiers used in this research, produce a probability for each instance, called a score. The score indicates the likelihood of an instance belonging to a certain class. The curve is created by applying a threshold to the data and varying the threshold from - ∞ to + ∞. The threshold at + ∞ generates the point (0,0) and with lowering the threshold one value after the other is generated. Positive instances classified as positive are placed an increment up in positive y-direction and false positives,

negatives classified as positives, are placed one increment to the right in x-direction. This way, the ROC curve is stepwise created from (0,0) to (1,1).

For reasons of comparison, the area under the ROC curve (AUC) is commonly computed. This quantifies the ROC curve to one single value and allows for a fast and easy comparison of different algorithms. Due to the ROC graph's x- and y-limits of 0 and 1, the AUC value will always be between 0 and 1. An area of 0.5 represents the diagonal line mentioned earlier and corresponds to a randomly guessing algorithm. Thus, the area should always be greater than 0.5. A perfect classifier has an area of 1. AUC represents the probability that the algorithm ranks a randomly chosen instance from class 1 higher than a randomly chosen instance from class 2. This means that the more distinct the features of the classes are, the larger is AUC [33]. AUC indicates the confidence level in a prediction model; the higher AUC, the more confident is the model in assigning the correct class [34].

$$TPR = sensitivity = \frac{True\ positives}{True\ positive + False\ positivs} \qquad 26$$

$$1 - FPR = specificity = \frac{True\ negatives}{True\ negatives + False\ positivs} \qquad 27$$

3.6.6 Family-wise error rate /Bonferroni correction for multiple comparisons

For multiple comparisons of ERD/ERS features, as well as classifier outcomes, the respective *p*-values were used for evaluating the statistically significant features and classifier models respectively. In order to carry out multiple comparison corrections, the Bonferroni correction for *p*-values adjustment was followed using equation 28, from [35].

$$\alpha_{FW} = 1 - (1 - \alpha_{PC})^c, \qquad 28$$

where α_{FW} is the family wise error rate, α_{PC} is the specified per comparison error rate, and c is the number of comparisons performed, Bonferroni correction is given by Equation 29.

$$\frac{\alpha_{PC}}{c}, \qquad 29$$

where α_{PC} was kept to 0.05, with c the number of statistical analyses conducted on the data sample.

3.6.7 False discovery rate correction

The other approach used to compare the performance of multiple classifier models, is the false discovery rate (FDR) correction. As each feature vector is independent, we applied the Benjamini-Hochberg procedure to decrease the possibility of any false discovery rate [36]. For Table 3, equation 30, defines the FDR.

Table 3-4 Errors in multiple testing of *N* hypotheses [37]

Hypothesis	Non-significant discovery	Significant discovery	Total
True null	TN	FP	N_0
False null	FN	TP	$N - N_0$
Total declared	$DN = N - DP$	DP	N

FP and *FN* are number of false positives (Type I error) and false negatives (Type II error); *TP* and *TN* are number of correct declared significant and non-significant discoveries, and *DP* is number of rejected null hypotheses i.e. declared positives.

$$FDR = E\left(\frac{FP}{DP}\right) \qquad 30$$

This technique controls FDR at a threshold which is pre-specified, $fdr \leq q$, on an average. For this research study, the q level was designated to standard α level of 5% for the reason of comparison. To apply the procedure for multi-model testing correction with N models, the p-values are arranged in ascending order, $\{P(1) \leq P(2) \leq P(3) \ldots \leq P(N)\}$ corresponding to null hypotheses, $\{H_1, H_2, H_3, \ldots, H_N\}$. Following this, in a step-up manner, evaluate inequality given in equation 29, in reverse sequential order, beginning from the last p value $P(N)$,

$$P(i) \geq i\frac{q}{N} \qquad 31$$

The comparison is stopped when the above inequality is true. Finally, reject all the hypotheses $\{\mathrm{H_i}\}_{\mathrm{i=1..k}}$, for which $\mathrm{P(i)}$ is less than or equal to $\mathrm{P(k)}$ i.e., the models belonging to the rank $\mathrm{i} = 1..\mathrm{k}$ are significantly discriminant.

3.6.8 Mann-Whitney U test

In case of two classifier models, the statistical evaluation technique used to compare the classification results was the Mann-Whitney *U* test. Mann-Whitney *U* test also termed as the

Wilcoxon rank-sum test is a nonparametric test of the null hypothesis. The null hypothesis refers to the fact that it is equally likely that a randomly selected classification accuracy value from one algorithm will be less than or greater than a randomly selected classification accuracy value from the second algorithm.

Under the null hypothesis H_o, the resulting accuracies of populations from both the algorithms are equal. The alternative hypothesis H_1 is the contrary i.e. the accuracies are not equal. The probability of an observation from a population *A* exceeding an observation from population *B* is different (larger, or smaller) than the probability of an observation from *B* exceeding an observation from *A*.

$$P(A > B) \neq P(B > A) \qquad 32$$

3.7 Conclusions

In conclusion, it is clear that the evaluation criteria ensure reliability and better performance of the established BCI system, i.e. based on the truly observed performance of the classifier model and not by chance. For significant BP feature extraction, bootstrap method was employed, and for comparing results among references, family-wise error rate correction was used. In case of CSP features, kappa coefficient was used as performance measure of the classification algorithms. In addition to this, while classifying both features, the k-fold cross validation was deployed with each model. Finally the performance evaluation of each model was done using the FDR and Mann-Whitney *U* test.

3.8 References

1. Tariq, M., Z. Koreshi, and P. Trivailo. *Optimal control of an active prosthetic ankle*. in *Proceedings of the 3rd International Conference on Mechatronics and Robotics Engineering*. 2017. ACM.
2. Repovs, G. *Dealing with noise in EEG recording and data analysis*. in *Informatica Medica Slovenica*. 2010.
3. Schalk, G. and J. Mellinger, *A practical guide to brain–computer interfacing with BCI2000: General-purpose software for brain-computer interface research, data acquisition, stimulus presentation, and brain monitoring*. 2010: Springer Science & Business Media.
4. Jasper, H.H., *The ten-twenty electrode system of the International Federation.* Electroencephalogr. Clin. Neurophysiol., 1958. **10**: p. 370-375.
5. Nicolas-Alonso, L.F. and J. Gomez-Gil, *Brain computer interfaces, a review.* Sensors, 2012. **12**(2): p. 1211-1279.
6. Klem, G.H., et al., *The ten-twenty electrode system of the International Federation.* Electroencephalogr Clin Neurophysiol, 1999. **52**(3): p. 3-6.

7. Tariq, M., P.M. Trivailo, and M. Simic, *Motor imagery based EEG features visualization for BCI applications.* Procedia computer science, 2018. **126**: p. 1936-1944.
8. Delorme, A. and S. Makeig, *EEGLAB: an open source toolbox for analysis of single-trial EEG dynamics including independent component analysis.* Journal of neuroscience methods, 2004. **134**(1): p. 9-21.
9. Lisi, G., T. Noda, and J. Morimoto, *Decoding the ERD/ERS: influence of afferent input induced by a leg assistive robot.* Frontiers in systems neuroscience, 2014. **8**: p. 85.
10. Blankertz, B., et al., *Optimizing spatial filters for robust EEG single-trial analysis.* IEEE Signal processing magazine, 2008. **25**(1): p. 41-56.
11. Hyvärinen, A. and E. Oja, *Independent component analysis: algorithms and applications.* Neural networks, 2000. **13**(4-5): p. 411-430.
12. Ramoser, H., J. Muller-Gerking, and G. Pfurtscheller, *Optimal spatial filtering of single trial EEG during imagined hand movement.* IEEE transactions on rehabilitation engineering, 2000. **8**(4): p. 441-446.
13. Blankertz, B., et al., *The Berlin Brain-Computer Interface: Accurate performance from first-session in BCI-naive subjects.* IEEE Trans Biomed Eng, 2008. **55**(10): p. 2452-2462.
14. Makeig, S., *Auditory event-related dynamics of the EEG spectrum and effects of exposure to tones.* Electroencephalography and clinical neurophysiology, 1993. **86**(4): p. 283-293.
15. Graimann, B., et al., *Visualization of significant ERD/ERS patterns in multichannel EEG and ECoG data.* Clinical neurophysiology, 2002. **113**(1): p. 43-47.
16. Knösche, T.R. and M.C. Bastiaansen, *On the time resolution of event-related desynchronization: a simulation study.* Clinical neurophysiology, 2002. **113**(5): p. 754-763.
17. Graimann, B. and G. Pfurtscheller, *Quantification and visualization of event-related changes in oscillatory brain activity in the time–frequency domain.* Progress in brain research, 2006. **159**: p. 79-97.
18. Kalcher, J. and G. Pfurtscheller, *Discrimination between phase-locked and non-phase-locked event-related EEG activity.* Electroencephalography and clinical neurophysiology, 1995. **94**(5): p. 381-384.
19. Liu, Y.-H., et al., *Analysis of Electroencephalography Event-Related Desynchronisation and Synchronisation Induced by Lower-Limb Stepping Motor Imagery.* Journal of Medical and Biological Engineering, 2018: p. 1-16.
20. Ang, K.K., et al., *Filter bank common spatial pattern algorithm on BCI competition IV datasets 2a and 2b.* Frontiers in neuroscience, 2012. **6**: p. 39.
21. Alpaydin, E., *Introduction to Machine Learning, chapter 7*. 2004, The MIT Press.
22. Lotte, F., et al., *A review of classification algorithms for EEG-based brain–computer interfaces.* Journal of neural engineering, 2007. **4**(2): p. R1.
23. Duda, R.O., P.E. Hart, and D.G. Stork, *Pattern classification. 2nd.* Edition. New York, 2001. **55**.
24. Friedman, J.H., *On bias, variance, 0/1—loss, and the curse-of-dimensionality.* Data mining and knowledge discovery, 1997. **1**(1): p. 55-77.
25. Borisoff, J.F., et al., *Brain-computer interface design for asynchronous control applications: improvements to the LF-ASD asynchronous brain switch.* IEEE Transactions on Biomedical Engineering, 2004. **51**(6): p. 985-992.
26. Davison, A.C. and D.V. Hinkley, *Bootstrap methods and their application*. Vol. 1. 1997: Cambridge university press.
27. Kothe, C.A., *Lecture 4.4 Performance Evaluation. 2013, Calit2ube: YouTube.* 2013.
28. Pfurtscheller, G., et al., *Mu rhythm (de) synchronization and EEG single-trial classification of different motor imagery tasks.* NeuroImage, 2006. **31**(1): p. 153-159.
29. Landis, J.R. and G.G. Koch, *The measurement of observer agreement for categorical data.* biometrics, 1977: p. 159-174.
30. Hsu, W.-Y., *EEG-based motor imagery classification using neuro-fuzzy prediction and wavelet fractal features.* Journal of Neuroscience Methods, 2010. **189**(2): p. 295-302.

31. Streiner, D.L. and J. Cairney, *What's under the ROC? An introduction to receiver operating characteristics curves.* The Canadian Journal of Psychiatry, 2007. **52**(2): p. 121-128.
32. Fawcett, T., *An introduction to ROC analysis.* Pattern recognition letters, 2006. **27**(8): p. 861-874.
33. Hettiarachchi, I.T., T.T. Nguyen, and S. Nahavandi. *Motor imagery data classification for BCI application using wavelet packet feature extraction*. in *International Conference on Neural Information Processing*. 2014. Springer.
34. Chatterjee, R., et al. *Comparative Analysis of Feature Extraction Techniques in Motor Imagery EEG Signal Classification*. in *Proceedings of First International Conference on Smart System, Innovations and Computing*. 2018. Springer.
35. Tamhane, A. and D. Dunlop, *Statistics and data analysis: from elementary to intermediate.* 2000.
36. Benjamini, Y. and Y. Hochberg, *Controlling the false discovery rate: a practical and powerful approach to multiple testing.* Journal of the Royal statistical society: series B (Methodological), 1995. **57**(1): p. 289-300.
37. Singh, A.K. and I. Dan, *Exploring the false discovery rate in multichannel NIRS.* Neuroimage, 2006. **33**(2): p. 542-549.

Chapter 4

Comparison of event-related changes in oscillatory activity during different cognitive imaginary movements within same lower-limb

Chapter Overview

The spatial proximity of LL in the somatosensory cortex and its placement within the mesial wall halts its detection using EEG. This is particularly the case with ankle and knee joints. The aim of this chapter is to discriminate the left and right LL KMI and investigate the possibility to use two KMI tasks within the same limb. BP features in the *mu* (7-12 Hz) band were recorded from central electrode positions and inspected using the common average reference. This study exploits the distinct left knee and left foot imagery tasks, as a single cognitive entity, within the same left limb, and similar for the right LL. It could potentially increase the dimensionality of control signals in a BCI to restore the locomotion function in a LL assistive device for rehabilitation.

This study is published in ***Acta Polytechnica Hungarica.***

M. Tariq, P. M. Trivailo, Yutaka Shoji, and M. Simic. *Comparison of event-related changes in oscillatory activity during different cognitive imaginary movements within same lower-limb*. Acta Polytechnica Hungarica, 16(2) 77-92, 2019.

Comparison of Event-related Changes in Oscillatory Activity During Different Cognitive Imaginary Movements Within Same Lower-Limb

Madiha Tariq, Pavel M Trivailo, Yutaka Shoji and Milan Simic

School of Engineering, RMIT University
264 Plenty Road, Bundoora, VIC 3083, Australia
s3519022@student.rmit.edu.au, pavel.trivailo@rmit.edu.au,
s3278605@student.rmit.edu.au, milan.simic@rmit.edu.au

Abstract: The lower-limb representation area in the human sensorimotor cortex has all joints very closely located to each other. This makes the discrimination of cognitive states during different motor imagery tasks within the same limb, very challenging; particularly when using electroencephalography (EEG) signals, as they share close spatial representations. Following that more research is needed in this area, as successfully discriminating different imaginary movements within the same limb, in form of a single cognitive entity, could potentially increase the dimensionality of control signals in a brain-computer interface (BCI) system. This report presents our research outcomes in the discrimination of left foot-knee vs. right foot-knee movement imagery signals extracted from EEG. Each cognitive state task outcome was evaluated by the analysis of event-related desynchronization (ERD) and event-related synchronization (ERS). Results reflecting prominent ERD/ERS, to draw the difference between each cognitive task, are presented in the form of topographical scalp plots and average time course of percentage power ERD/ERS. Possibility of any contralateral dominance during each task was also investigated. We have compared the topographical distributions and based on the results we were able to distinguish between the activation of different cortical areas during foot and knee movement imagery tasks. Currently, there are no reports in the literature on discrimination of different tasks within the same lower-limb. Hence, an attempt towards getting a step closer to this has been done. Presented results could be the basis for control signals used in a cognitive infocommunication (CogInfoCom) system to restore locomotion function in a wearable lower-limb rehabilitation system, which can assist patients with spinal cord injury (SCI).

Keywords: Cognitive state; motor imagery; electroencephalography; brain-computer interface; event-related desynchronization; event-related synchronization

1 Introduction

Brain-computer interface (BCI) is an emerging technology that connects human brain to an output device, in order to communicate the cortical command signals to manipulate the actuator. These cortical signals are translated to device (e.g. computer) operatable commands [1]. The state-of-the art BCI is based on the idea of developing an artificial, muscle-free communication channel that acts as a natural communication channel between the brain and a machine [2, 3]. Applications of BCI systems are widespread and vary from the fields of neuroscience, rehabilitation, cognitive infocommunications (CogInfoCom) [4] to entertainment, and defence [5]. Neurorehabilitation is the research area, which caters audiences with neurodegenerative disorders, spinal cord injury (SCI), amyotrophic lateral sclerosis (ALS) [6, 7], or lower-limb amputation [8]. The applications include neurorobotics, e.g. BCI-controlled wearable/assistive robots for mobility restoration. Such devices can be useful for direct communication in inter-cognitive CogInfoCom applications [2, 9], and necessitates more research in this area.

In this study, the physiological signals used to detect natural cognitive capability of humans, are based on non-invasive modality, i.e. electroencephalography (EEG). We use this approach for its low cost and easy handling. When the human cognitive capability is combined with information and communication technologies (ICT), it results in an important aspect of CogInfoCom [10]. In order to connect high-level brain activity to infocommunication networks, BCI enables flow of rich information from the brain, and eventually heterogeneous cognitive entities into the ICT network [9, 10]. In this study, the source of information relevant to human cognitive states, include information on level of engagement during imagination of task and rest/idling, reflecting a *decrease* and *increase* in *mu* wave (8-12 Hz) respectively [11].

Investigations on the possibility to use BCI system for post-stroke rehabilitation have been carried out in order to reinstate upper and lower-limb functions [12]. However, applications of existing BCI systems, for the control of various devices, such as a robotic exoskeleton, are not straightforward. One potential factor is the low dimensional control of these systems, i.e., they can only identify limited number of cognitive tasks as unique control commands. The most frequently used cognitive state motor imagery tasks, in a BCI system, are left hand vs. right hand, and foot kinesthesis motor imageries [13]. Successful control of cursor movement in two dimensions, on a computer screen, based on left vs. right hand motor imagery, was done by deploying the *mu* (8-12 Hz) and *beta* (18-26 Hz) rhythm, followed by several training sessions [14]. The same BCI cursor control strategy was extended to three-dimensions, where in addition to left-right hand imagery, foot motor imagery was incorporated, as well [15].

Successful quantification of left vs. right hand and foot motor imagery have been reported, including studies on the discrimination of different upper limbs [16], but no literature exists on the decoding of different movements within the same 'lower limb'. Investigations on independent lower-limb motor imagery tasks have been reported recently [2, 17-19], however, those studies did not cover the same limb tasks. This is because of the well-established fact about 'mesial wall' location of lower-limb representation area on the sensorimotor cortex. That precludes its exploitation during different imagery tasks. In addition to that, each joint representation within the same limb has a very close spatial representation to each other [20], which makes it difficult to discriminate each movement with electroencephalographic (EEG) signals.

In our research, we included foot and knee kinaesthetic imagery tasks within the same limb, as cognitive states. Each state was further divided into left vs. right imagery tasks, in order to increase the possibility for discriminating each task; thereby increasing the dimensionality of the BCI control signal. Recorded EEG signals, against each task, were quantified by observing the event related changes associated to the task in oscillatory *mu* rhythm. The changes in oscillatory activity, with respect to an internally, or externally paced events, are time-locked, but not phase-locked, i.e. induced, known as event related desynchronization (ERD) or event related synchronization (ERS) [21, 22]. This study could be useful for the development of multi-dimensional control signals as a single cognitive entity in a BCI system for rehabilitation applications [9, 23]. Presented results are in accordance with an important aspect of CogInfoCom, i.e. the combination of the natural cognitive capability of human and ICT [24].

2 Methods

2.1 Experimental Protocol

This study was based on experiments performed on three healthy subjects with no history of neurological disorder, or any impairment. The age range was between 25-27 years, where all subjects participated on voluntary basis. None of the participants had any experience with BCI before. Ethics approval, for this research, was granted by the College Human Ethics Advisory Network (CHEAN) of RMIT University, Melbourne, Australia.

During the experiment every subject was directed to sit on a comfortable chair placed in front of a monitor screen (17'') at a length of approximately 1.5 m. The experimental protocol was based on the standard Graz protocol for synchronous BCI. Each trial began with a blank black screen that lasted for 30 seconds, in order to let the subject relax and get familiar with the environment. Following that, the

trial began with the presentation of a green fixation cross on screen for 3 seconds (used as reference period for processing of epochs). One second long audio beep stimulus, right before the visual cue display, was incorporated in the first trial only, to alert the subject about the beginning of the experiment, see Figure 1 (left). Next, the visual cues of 2 seconds length were displayed followed by a 5 seconds long blank screen to perform the related task (imagery), making a total of 10 seconds for each trial. The visual cues in each trial reflected either the left or right movement. The foot and knee session was carried out separately. Our experimental paradigm consisted of alternate sessions, i.e. the first session for left-right foot kinaesthetic motor imagery (KMI), next session for left-right knee KMI, third for foot KMI and finally knee KMI. The cue set for each session is shown in figure 2. This was introduced to avoid a state of confusion for the subject with several tasks in a single session.

A standard one session protocol is composed of 40 trials, including 20 trials for each tasks, i.e. left or right KMI. The visual cues in each trial were displayed in a random order so that no adaptation could occur. Each trial was followed by a random pause interval of 1.5 to 3.5 seconds, in which the subjects were asked to rest. The experiment was divided into 4 sessions, i.e. foot, knee, foot and knee KMI respectively. Figure 1 (left) presents the schematic of experimental protocol reflecting the timing of cues, where each trial is 10 seconds long. For each session the respective visual cue set is given in figure 2, where (a) depicts left and right foot movements (dorsiflexion for 1 second) and (b) depicts left and right knee movements (extension for 1 second) respectively.

Figure 1
Experimental protocol timing in seconds (left) and 10-20 electrode channel locations (right)

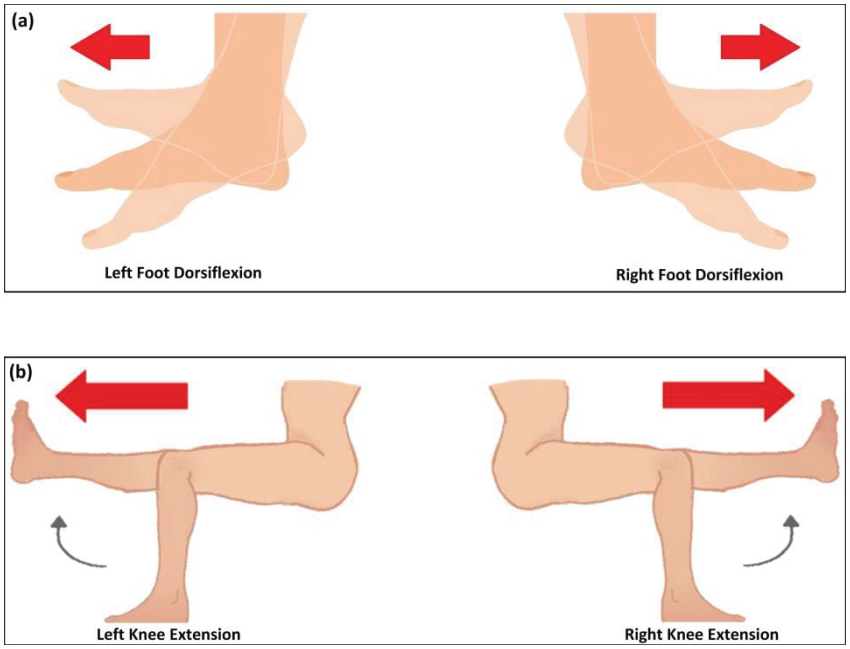

Figure 2
Visual cues in the experimental protocol, for (a) left - right foot dorsiflexion, and (b) left- right knee extension

2.2 EEG Recording

In order to record EEG activity, the EEG neurofeedback BrainMaster Discovery 24E amplifier (BrainMaster Technologies Inc., Bedford, USA) was utilised. The standard Graz synchronous BCI protocol was established using OpenViBE software (http://openvibe.inria.fr/downloads/) that also enabled the embedding of time stamps in each recorded trial. Overall experimental set up had the amplifier interfaced with the acquisition server of OpenViBE. To acquire brain signals from the motor cortex, the standard 10-20 Electro-cap was used [25]. The EEG system had 19 channels (10-20 sites), channel 20 (A2) was referenced to A1 (A2-A1) (Figure 1, right). Remaining channel including AUX1 and AUX2, provided for monitoring of other electrophysiological signals were not used. All channels were sampled using 256 Hz sampling frequency, with 24-bit resolution. The DC amplifier bandwidth was from 0.0 Hz to 100 Hz, followed by EEG channel bandwidth from 0.43 to 80 Hz.

The customized experimental protocol was designed using OpenViBE designer tool that comes along integrated feature boxes. The designer tool window is based on Lua script that was modified for generating customized scenario, Graz-

Stimulator box was used to allow for the onset of different visual cue timings. Figure 3 reflects the connection established between the BrainMaster Discovery 24E and OpenViBE together synchronized. Each session was recorded in the standard EDF and GDF file formats using writer boxes of designer tool in OpenViBE.

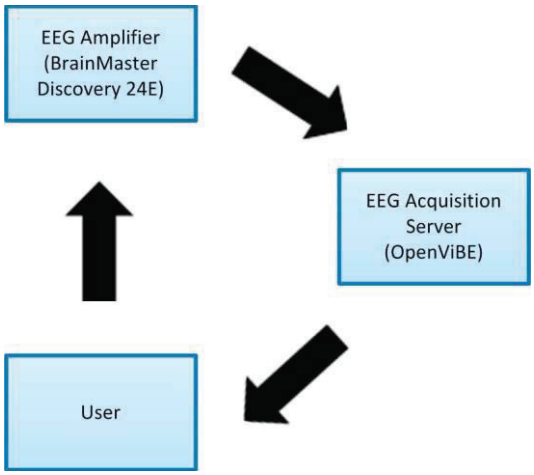

Figure 3

Established connection for real-time EEG data acquisition and incorporation of event time-stamps in the data stream

2.3 Signal Processing

In order to process and visualize the acquired data offline, the statistical EEGLAB package was used. During offline processing, the EEG data was converted to reference-free form by using the common average reference method. The data was pre-processed using FIR bandpass filter between 8-12 Hz, which was the required frequency bandwidth range for *mu* rhythm. Next, each epoch, i.e. trial of 10 seconds length was extracted, which included 3 seconds period prior to cue onset, to be used as reference period during analysis.

The epoched data was then filtered using spatial filter, i.e. the independent component analysis (ICA) for artifacts removal.

For each subject, spectral plots were generated that reflected the 2-class statistics, where each class was related to each task. Following this, the average time course ERD and ERS for *mu* rhythm (8-12 Hz) were plotted, where only statistically significant ERD/ERS were displayed. This was done using validation method to ensure statistically significant data, i.e. to allow assigning measures of accuracy (confidence interval) to sample estimates. We used the bootstrap statistical

significance method, with confidence interval of 95%. In this way the significant ERD-ERS features were selected. The central electrode areas C3, Cz, and C4 linked to sensorimotor cortex were used to analyse *mu* band with the most significant bandpower decrease, or increase, during each task.

The standard procedure for calculation of ERD/ERS patterns was adopted from [26]. After bandpass filtering of each trial, the samples were squared and subsequently averaged over trials and over sample points [27]. This directed to the resulting proportional power decrease (ERD), or power increase (ERS) compared to the reference interval, which was selected as the period of 3 seconds before the trigger onset of visual cues. In order to overcome masking of induced activities caused by the evoked potentials, the mean of the bandpass filtered data was subtracted from the data for each sample [28].

The ERD/ERS was calculated from EEGLAB [29, 30] integrated function event-related spectral perturbations (ERSP) based on wavelet decomposition. ERSP detects the event-related shifts in the power spectrum. It measures the mean event-related changes in the power spectrum at one data channel averaged over trials. P_j is the power or intertrial variance of the jth sample and R is the average power in the reference interval $[r_0, r_0+k]$. To convert ERSP to ERDS, equations 1 and 2 were used; ERSP was normalized to the reference interval [29]:

$$ERSP_j = 10\log\left(\frac{P_j}{R}\right) \tag{1}$$

$$ERDS_j = \left(10^{\frac{ERSP_j}{10}} - 1\right) \times 100 \tag{2}$$

3 Results

The results obtained from all three subjects, s1, s2 and s3 are presented in this section.

3.1 ERD/ERS Quantification

In order to quantify the significant cognitive bandpower changes of *mu* rhythm, each combination of lower-limb tasks was pre-processed and spatial filter was applied on the filtered data. Resulting signals were evaluated for each central electrode position directing towards the sensorimotor cortex, and the potential area where *mu* rhythm elicits. Table 1 shows the illustration of quantification approach.

Table 1
Unsupervised feature extraction-based approach

Tasks	Pre-processing	Spatial filter	Scalp location	Time-frequency feature extraction
LF vs. LK	Bandpass filtering, Epoching	ICA	C3	Wavelet (short-time DFT) transform
RF vs. RK			C4	
LF-LK vs. RF-RK			Cz	

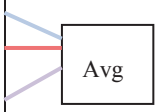

3.1.1 Spectral Topographical Plots

The cognitive state output, in the form of percentage power ERD and ERS spectral maps, for all participants, against the foot and knee tasks for each session respectively, were plotted between 8-12 Hz frequency of *mu* band. Each session comprised of left-right tasks of foot followed by knee, i.e. different movements within the same limb. Figure 4 represents the topographical scalp plots of each subject during left-right foot and left-right knee imagery respectively, for 8 to 12 Hz.

For s1, it was observed that during left foot, and left knee, imagery tasks, the foot as well as hand area *mu* rhythm (*mu* ERD) was enhanced in both cases. However, with left foot imagery the ERD was localized towards left hemisphere, C3, whereas the left knee imagery showed broad-banded ERD towards central area Cz and edged towards parietal region. The right foot and knee tasks, in the same limb somehow revealed similar output. However, with right foot imagery prominent *mu* ERD overlying the primary hand area was observed, where ERD was dominantly visible at electrode position C3 in addition to Cz. This pointed towards the possibility of contralateral spectral power dominance during right foot task. On the other hand, the right knee imagery depicted an enhancement in the *mu* ERD foot area representation edged towards parietal region.

The left foot imagery with s2 enhanced the ERD patterns at central electrode positions predominantly C3, similar to s1, as well as the premotor areas. This was not the case with left knee imagery task, which did not exhibit enhancement in power concentration. Following this, during the right foot imagery an overall increase in *mu* ERD power concentration was observed over the primary, supplementary and pre-motor areas with contralateral dominance. Interestingly a small increase in *mu* ERS spectral power was visible during the right knee imagery task, which was strictly localized towards the central and parietal regions. This directed towards no prominent ERD.

The resulting plots of s3, during left foot task, elicited power concentration in ERD focused towards the hand and foot area. However, the left knee imagery depicted a very clear focal enhancement in *mu* ERD foot area representation.

During the right foot task, a higher power concentration in *mu* ERD overlying the central cortical regions with a shift towards parietal area was visible. Similarly, the right knee task, elicited increased power ERD strictly in cortical foot area, at central region of the cortex. No contralateral power distribution was visible with subjects 2 and 3.

3.1.2 ERD/ERS Average Time Course in *mu* Rhythm

The resulting cognitive states, in form of ERD/ERS time course for *mu* rhythm with frequency range of 8-12 Hz at electrode positions C3, C4, and Cz are shown in Figure 5. The results elicited by s1 are presented.

In order to compute the specified time and frequency resolution, i.e. averaging over sample points, the EEGLAB integrated sinusoidal wavelet transform (short-time discrete fourier transform (DFT)) was used. A *t* percentile bootstrap statistic (percentile taken from baseline distribution, with a significance level of $\alpha = 0.05$, was applied to get significant ERD and ERS values [29]. The basic aim of bootstrap technique is to replace the unknown population distribution with a known empirical distribution and based on the empirical distribution estimator, determine the confidence interval, in this case 95% confidence [21].

Different movements within the same lower-limb elicit various percentage power ERD and ERS. Figure 5 reflects each combination of tasks for different joint positions, within the same lower-limb. The selection of central electrode position, for plotting each combination of tasks, within the same limb, was based on the probability to observe any contralateral dominance in the power concentration ERD. Therefore, C3 was selected for observing right imagery task characteristic ERD within the same limb. C4 was selected to detect left task characteristic ERD, Cz was chosen to observe left and right task ERD characteristics and their impact on the midline of the central lobe for each participant. The task combinations within the same lower-limb are given in Table 2.

Table 2

Task combinations within the same lower-limb

Electrode position	Mental task	Bandpower features
C3	Imagery right foot vs. right knee	ERDS average
C4	Imagery left foot vs. left knee	ERDS average
Cz	Imagery right foot-knee vs. left foot-knee	ERDS grand average

At C3 during right foot and knee imageries, ERD time course was obtained by taking average of power changes in *mu* rhythm across all trials with each subject. At the end of visual cue (shown by green window in Figure 5), the *mu* power attenuates for approximately 0.6 seconds, after onset of cue. Evident ERS was visible at approximately 3 seconds, which is referred to the period of task

performance. Since each of the foot dorsiflexion and knee extension task, were 1 second in length, the appearance of an ERS at 3 seconds correlates to the completion of task by the subject.

The left foot and knee imagery movements at electrode position C4 did not depict a very prominent ERD. However, at the beginning of cue onset at approximately 0.3 seconds a desynchronization of the foot area is visible followed by another dip at approximately 4 seconds (imagery interval). ERS was visible between 4 and 5 seconds towards the termination of the task performance interval.

Finally, at electrode position Cz, most dominant percentage power decrease, ERD was visible throughout the beginning of visual cue onset window followed by the task performance interval. These results are in accordance with the established results from the spectral power distribution maps. The presence of large centrally localized ERD patterns validates the notion of enhanced foot *mu* area representation elicited by Cz upon foot and knee imagery related tasks.

Clear results at Cz were due to the grand average taken for all four trials and sessions for each participant, which was not the case with C3 and C4, where the average of each trial and session for only two tasks was taken.

The grand-average amplitude of *mu* ERD for all subjects based on common average reference derivation at central electrode positions is shown in figure 6. The error bars represent the standard deviation. As depicted earlier from results, there was no significant inter-task difference within the same limb, observed at electrode positions C3, Cz and C4 ($P<0.05$, *t*-test). However, it is important to mention here that the bar graphs were only plotted for *mu* ERD and not ERS, to infer knowledge about its behavior output. Taking *beta* ERD/ERS features into account could add to the overall information during lower-limb tasks within the same limb.

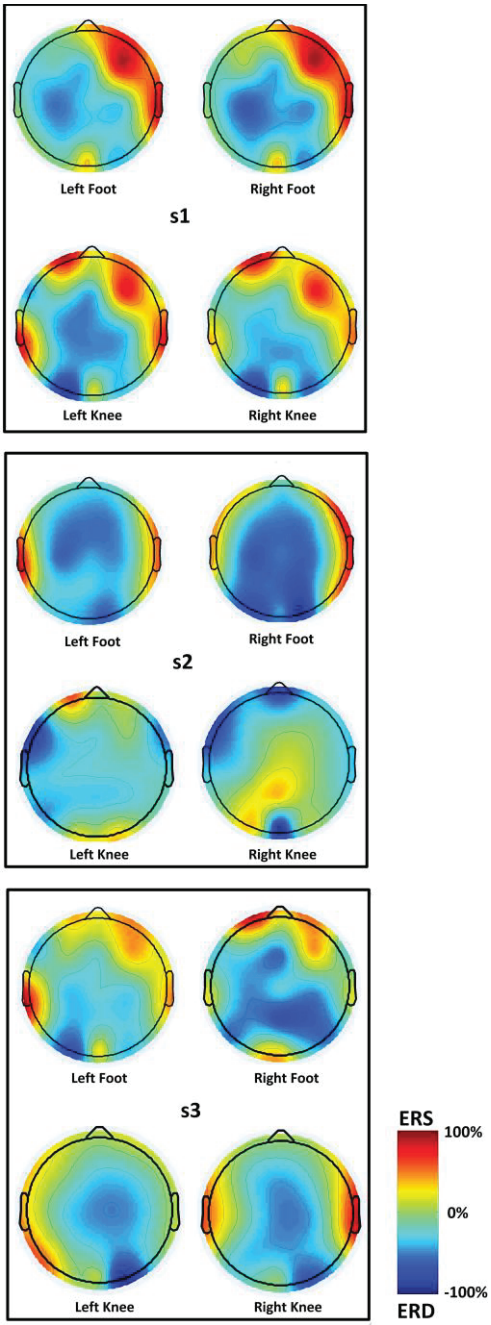

Figure 4
Topographical scalp maps of each subject during left-right foot and left-right knee imagery respectively between frequencies of 8-12 Hz

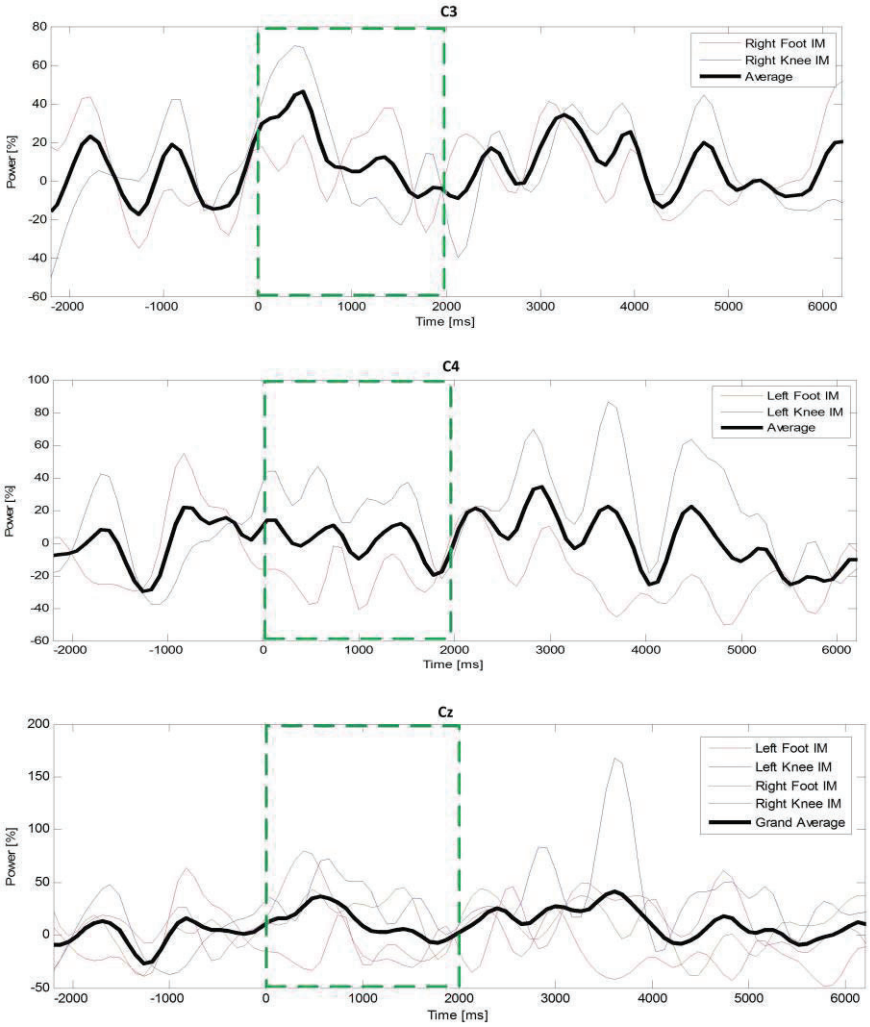

Figure 5

ERD and ERS time course for *mu* rhythm (8-12 Hz) of subject 3 at electrode position C3 for right foot and right knee imagery alongside their average, C4 for left foot and left knee imagery alongside their average, and Cz for left and right foot and knee imagery respectively alongside their average. The green window indicates visual cue presentation from 0 and 2 seconds

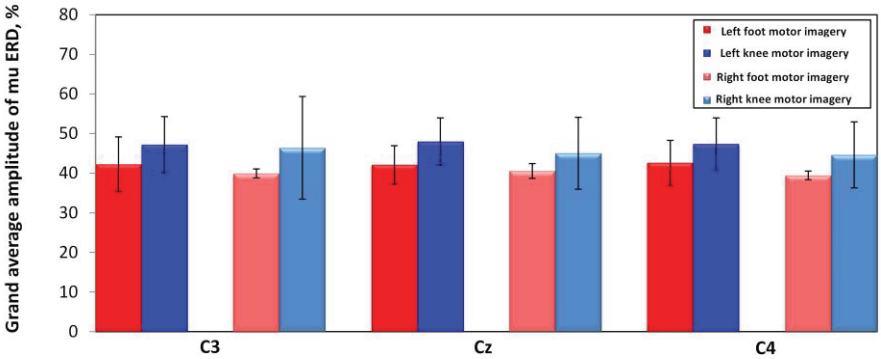

Figure 6
Average amplitude of *mu* ERD from all subjects based on common average reference derivation at central electrode positions. The red and blue bars indicate left foot and left knee motor imageries, respectively, and pale red and pale blue bars indicate right foot and right knee motor imageries, respectively. Error bars represent standard deviations

4 Discussion

We analysed the discrimination of cognitive states, as a result of imaginary left-right foot and knee motor tasks within the same limb. It was observed that an increase in power concentration of *mu* ERD overlying hand and foot area occured with majority of the subjects. Although the hand area in this study was not needed to perform a task, we therefore, consider it to be in an idling state. Generally, no explicit contralateral dominance was visible, except for s1 and s2, who both showed contralateral dominance during right foot imagery task at C3. As foot, the knee area representation is also situated in the mesial wall, which makes it difficult to elicit clear ERD patterns upon knee imagery tasks. However, with left and right knee discrimination tasks, in all subjects, centrally localized ERD patterns were mainly observed throughout. The focal *mu* rhythm was visible in cortical foot representation area with small activation of hand area with s1 only during left knee imagery.

For neurorobotics and human ICT applications, this can lead to the inference that kinaesthetic knee imagery blocks or desynchronizes foot area *mu* rhythm, at central electrode positions and shifts over supplementary, pre-motor areas and in some cases towards parietal region. Results suggest that the cortical knee representation area is situated near the foot sensorimotor areas. The other task in same lower-limb, i.e., foot motor imagery, not only activated hand and foot area *mu* ERD but also elicited contralateral dominance during right foot kinaesthetic imagery. The knee kinaesthetic imagery on the other hand does not provide enough evidence of contralateral dominance of the cognitive states upon left vs.

right imagery tasks. This was also validated by the average *mu* ERD bar graph, that reflected difference during left-right foot tasks but no significant difference during the knee tasks. More investigations in this area could be very useful for CogInfoCom based systems to highlight the activeness of specific brain regions indicating human level engagement in biofeedback-driven frameworks.

5 Conclusions and Future Work

This research broadened new horizons towards investigation of cognitive states as event-related changes in oscillatory activity of *mu* during foot and knee motor imageries within the same lower-limb. The results provide useful information on human level of engagement during imagination of task and rest, as reflected by *mu* rhythm activity. Despite a small lower-limb sensorimotor area representation in the homunculus, the foot and knee movement imagery elicited ERD patterns. Based on the spectral power plots, an increase in the mid-central ERD was observed overall with all the subjects. The kinaesthetic knee imagery triggered *mu* ERD, mainly in the cortical foot area representation, with small shift towards parietal lobe. No contralateral dominance of cortical areas was present in the case of left-right knee imagery tasks, unlike with foot tasks. Obtained results suggest that intra-subject cognitive-state variability exists during the reactivity of *mu* components. This makes it difficult to draw a clear difference between different lower-limb tasks within the same limb. However, clear results with one subject; indicate the possibility of discriminating different movements within the same lower-limb. Suggested protocol could be exploitable to increase the dimensionality of control signals, as a cognitive entity, in a BCI system. Involvement of more participants and classification of feature vector is the future aim of this investigation, to develop a multi-dimensional CogInfoCom tool for BCI controlled devices.

Acknowledgement

This work is supported by RMIT University through international post graduate research scholarship (IPRS).

References

[1] Wolpaw, J. R., et al., *Brain–computer interfaces for communication and control.* Clinical neurophysiology, 2002. **113**(6): pp. 767-791

[2] Tariq, M., et al. *Mu-beta rhythm ERD/ERS quantification for foot motor execution and imagery tasks in BCI applications*. in *Cognitive Infocommunications (CogInfoCom), 2017 8th IEEE International Conference on*. 2017, IEEE

[3] Henshaw, J., W. Liu, and D. M. Romano. *Improving SSVEP-BCI performance using pre-trial normalization methods*. in *Cognitive*

Infocommunications (CogInfoCom), 2017 8th IEEE International Conference on. 2017, IEEE

[4] Garcia, A. P., I. Schjølberg, and S. Gale. *EEG control of an industrial robot manipulator*. in *Cognitive Infocommunications (CogInfoCom), 2013 IEEE 4th International Conference on*. 2013, IEEE

[5] Katona, J., et al. *Speed control of Festo Robotino mobile robot using NeuroSky MindWave EEG headset based brain-computer interface*. in *Cognitive Infocommunications (CogInfoCom), 2016 7th IEEE International Conference on*. 2016, IEEE

[6] Vaughan, T. M., J. R. Wolpaw, and E. Donchin, *EEG-based communication: Prospects and problems.* IEEE transactions on rehabilitation engineering, 1996, **4**(4): pp. 425-430

[7] Millán, J. d. R., et al., *Combining brain–computer interfaces and assistive technologies: state-of-the-art and challenges.* Frontiers in neuroscience, 2010, **4**: p. 161

[8] Tariq, M., Z. Koreshi, and P. Trivailo. *Optimal Control of an Active Prosthetic Ankle*. in *Proceedings of the 3rd International Conference on Mechatronics and Robotics Engineering*. 201, ACM

[9] Baranyi, P. and A. Csapo, *Definition and synergies of cognitive infocommunications.* Acta Polytechnica Hungarica, 2012, **9**(1): pp. 67-83

[10] Baranyi, P., A. Csapo, and G. Sallai, *Cognitive Infocommunications (CogInfoCom)* 2015: Springer

[11] He, B., et al., *Noninvasive brain-computer interfaces based on sensorimotor rhythms.* Proceedings of the IEEE, 2015, **103**(6): pp. 907-925

[12] Ang, K. K. and C. Guan, *Brain-computer interface in stroke rehabilitation.* Journal of Computing Science and Engineering, 2013, **7**(2): pp. 139-146

[13] Pfurtscheller, G. and C. Neuper, *Motor imagery and direct brain-computer communication.* Proceedings of the IEEE, 2001, **89**(7): pp. 1123-1134

[14] Wolpaw, J. R. and D. J. McFarland, *Control of a two-dimensional movement signal by a noninvasive brain-computer interface in humans.* Proceedings of the National Academy of Sciences of the United States of America, 2004, **101**(51): pp. 17849-17854

[15] Royer, A. S., et al., *EEG control of a virtual helicopter in 3-dimensional space using intelligent control strategies.* IEEE Transactions on neural systems and rehabilitation engineering, 2010, **18**(6): pp. 581-589

[16] Yong, X. and C. Menon, *EEG classification of different imaginary movements within the same limb.* PloS one, 2015, **10**(4): p. e0121896

[17] Tariq, M., P. M. Trivailo, and M. Simic. *Detection of knee motor imagery by Mu ERD/ERS quantification for BCI based neurorehabilitation applications*. in *Control Conference (ASCC), 2017 11th Asian*. 2017, IEEE

[18] Tariq, M., P. M. Trivailo, and M. Simic, *Event-related changes detection in sensorimotor rhythm.* International Robotics & Automation Journal, 2018, **4**(2): pp. 119-120

[19] Pfurtscheller, G. and T. Solis-Escalante, *Could the beta rebound in the EEG be suitable to realize a "brain switch"?* Clinical Neurophysiology, 2009, **120**(1): pp. 24-29

[20] Plow, E. B., et al., *Within-limb somatotopy in primary motor cortex–revealed using fMRI.* Cortex, 2010, **46**(3): pp. 310-321

[21] Graimann, B., et al., *Visualization of significant ERD/ERS patterns in multichannel EEG and ECoG data.* Clinical Neurophysiology, 2002, **113**(1): pp. 43-47

[22] Pfurtscheller, G. and F. L. Da Silva, *Event-related EEG/MEG synchronization and desynchronization: basic principles.* Clinical neurophysiology, 1999, **110**(11): pp. 1842-1857

[23] Izsó, L. *The significance of cognitive infocommunications in developing assistive technologies for people with non-standard cognitive characteristics: CogInfoCom for people with non-standard cognitive characteristics*. in *Cognitive Infocommunications (CogInfoCom), 2015 6th IEEE International Conference on*. 2015, IEEE

[24] Baranyi, P., A. Csapo, and P. Varlaki. *An overview of research trends in CogInfoCom*. in *Intelligent Engineering Systems (INES), 2014 18th International Conference on*. 2014, IEEE

[25] Klem, G. H., et al., *The ten-twenty electrode system of the International Federation.* Electroencephalogr Clin Neurophysiol, 1999, **52**(3): pp. 3-6

[26] Kalcher, J. and G. Pfurtscheller, *Discrimination between phase-locked and non-phase-locked event-related EEG activity.* Electroencephalography and clinical neurophysiology, 1995, **94**(5): pp. 381-384

[27] Knösche, T. R. and M. C. Bastiaansen, *On the time resolution of event-related desynchronization: a simulation study.* Clinical Neurophysiology, 2002, **113**(5): pp. 754-763

[28] Graimann, B. and G. Pfurtscheller, *Quantification and visualization of event-related changes in oscillatory brain activity in the time–frequency domain.* Progress in brain research, 2006, **159**: pp. 79-97

[29] Delorme, A. and S. Makeig, *EEGLAB: an open source toolbox for analysis of single-trial EEG dynamics including independent component analysis.* Journal of neuroscience methods, 2004, **134**(1): pp. 9-21

[30] Delorme, A., et al., *EEGLAB, SIFT, NFT, BCILAB, and ERICA: new tools for advanced EEG processing.* Computational intelligence and neuroscience, 2011, **2011**: p. 10

Chapter 5

Mu-beta event-related (de)synchronization and EEG classification of left-right foot dorsiflexion kinaesthetic motor imagery for BCI

Chapter Overview

A study to differentiate between left and right foot KMI and the role of ML models in implementing this, is important to develop a better understanding of cortical excitability. The objective of the research reported in this chapter is, to investigate the cortical lateralization of ERD/ERS in the BP *mu* and *beta* bands, during left and right foot KMI, using EEG topographic and time-frequency maps. This was followed by the determination of classification accuracy of the two KMI tasks in a BCI paradigm. The study was conducted for two reference methods to record EEG, i.e. the common average and bipolar reference. Three ML models were deployed for statistical comparisons to evaluate the highest classification accuracy. Results confirmed the cortical lateralization of ERD/ERS and set forth the utilization of *mu* and *beta* as independent control features based on bilateral foot KMI in a BCI.

This study is currently under review in ***PLOS One***.

M. Tariq, P. M. Trivailo, M. Simic. *Mu-beta event-related (de)synchronization and EEG classification of left-right foot dorsiflexion kinaesthetic motor imagery for BCI.*

Mu-Beta event-related (de)synchronization and EEG classification of left-right foot dorsiflexion kinaesthetic motor imagery for BCI

Madiha Tariq, Pavel M. Trivailo, Milan Simic*

School of Engineering, RMIT University, Melbourne, VIC, Australia

*Corresponding author. Address: 264 Plenty Rd, Bundoora VIC 3083. Tel.: +61 3 9925 6223; fax: +61 0 992 56108. *E-mail address*: milan.simic@rmit.edu.au

ABSTRACT

The left and right foot representation area is located within the interhemispheric fissure of the sensorimotor cortex and share spatial proximity. This makes it difficult to visualize the cortical lateralization of event-related (de)synchronization (ERD/ERS) during left and right foot motor imageries. The aim of this study is to investigate the possibility of using ERD/ERS in the *mu*, low *beta*, and high *beta* bandwidth, during left-right foot dorsiflexion kinaesthetic motor imageries (KMI), as unilateral control commands for a brain-computer interface (BCI). EEG was recorded from nine healthy participants during cue-based left-right foot dorsiflexion KMI tasks. The features were analysed for common average and bipolar references. With each reference, *mu* and *beta* band-power features were analysed using time–frequency (TF) maps, scalp topographies, and average time course for ERD/ERS. The cortical lateralization of ERD/ERS was confirmed. Statistically significant features were classified using LDA, SVM, and KNN model, and evaluated using the area under ROC curves. Multiple comparisons to distinguish between classifier performances were done and false discovery rate (FDR) corrections were applied. An increase in high *beta* power following the end of KMI for both tasks was recorded, from right and left hemispheres, respectively, at the vertex. The single trial analysis and classification models resulted in high discrimination accuracies, i.e. maximum 83.4% for *beta* ERS, 79.1% for *beta* ERD, and 74.0% for *mu* ERD. With each model the features performed above the statistical chance level of 2-class discrimination for a BCI. Our findings indicate these features can evoke left-right differences in single EEG trials. This suggests that any BCI employing unilateral foot KMI can attain classification accuracy suitable for practical implementation. Given results stipulate the novel utilization of *mu* and *beta* as independent control features for discrimination of bilateral foot KMI in a BCI.

Keywords: event-related (de)synchronization (ERD/ERS), electroencephalography (EEG), *mu* ERD, *beta* ERD, *beta* ERS, brain–computer interface (BCI)

1. Introduction

People affected by neurological disorder, stroke, or spinal cord injury (SCI) necessitate a therapeutic goal of motor gait rehabilitation using assistive technologies [1, 2]. For lower-limb affectees, to re-gain the dorsiflexion of foot drop is vital [3-5]. The lost motor control functions could be emulated by inducing neuroplasticity using a brain-computer interface (BCI) system [6]. BCI provides an alternative neuropathway that translates human brain activities into commands for controlling external devices or prostheses [6, 7].

BCIs that use EEG features such as oscillatory/sensorimotor rhythm (SMR) are recorded over the somatic sensorimotor cortex. SMR are concentrated in the *alpha* (*mu*) (7-12 Hz), *beta* (13-35 Hz), and gamma (>36 Hz) frequency bands [8, 9]. BCIs have successfully deployed SMR to identify any changes related to the physical movement (motor execution, ME) or imagination of movement (motor imagery, MI) of any limb [10]. This is because an increase in the corticomotor excitability is involved during MI and ME of limb movement which is both muscle-specific and temporally modulated [11]. Both the execution and imagery tasks have been used in experiments, because the ME and MI implicate overlapping neural structures within the central nervous system [11]. However, from literature, MI tasks have been preferred over ME ones, to avoid any possibility of proprioceptive feedback. The MI is a covert cognitive process, where the user makes a kinaesthetic imagination of his/her own limb movement without any muscular intervention, also called kinaesthetic motor imagery (KMI) [1, 12].

Each limb movement elicits a unique pattern in the SMR *mu* and *beta* features [9]. These patterns are reflected in the form of either a power decrease termed event-related desynchronization (ERD) that correlate to movement preparation [13], or an increase in power termed event-related synchronization (ERS) associated to resting/idling state, or an inhibitory state [14, 15]. The cortical localization of ERD/ERS patterns is due to the somatotopic arrangement of the motor cortex. The upper limbs e.g. hand area representation is on the mantle of the cortex, followed by lateralization [16], that makes the spatial discrimination between left and right movement prominent compared to lower limbs. The right-left hand ME or KMI *mu* ERD correlate to the bilateral hand area (C3 and C4 electrode positions) of the sensorimotor cortex with evident contralateral dominance compared to ipsilateral side [17, 18]. These contralateral and ipsilateral differences in *mu* ERD have been classified by BCI to be used as control features for operating external devices [19-21].

On the contrary, right-left lower-limb ME or KMI tasks are not extensively deployed due to the close location of left-right lower-limbs' areas to each other. The foot motor area is situated deep within the interhemispheric fissure of the sensorimotor cortex that makes the left and right foot ME or KMI

difficult to be spatially discriminated since they produce nearly identical EEG patterns [16]. Therefore, we can find studies where general foot KMI-based BCIs deploy feet KMI as one feature without discriminating the left-right side [22, 23]. However, studies available on the left-right discrimination of foot KMI , proposed the *mu* ERD and *beta* ERS/rebound (post task completion), as possible EEG features for classification [7, 17, 24, 25]; where the ERD/ERS patterns generate at the vertex [24]. According to [18], if a BCI user exhibits a slight left–right difference, the differences could be enhanced, and improve the control accuracy of a BCI via visual feedback. Besides aforementioned features, the possibility to research *mu* ERS as a new feature for classification of left-right foot KMI task is less due to its limited frequency bandwidth, but *beta* ERD still has a significant margin to be explored due to its wider frequency range. Hashimoto et al. [17] proposed a bipolar referenced ERD–ERS lateralisation enhancement, resulting in a two-class (left vs. right foot) classification accuracy of 81.6% in synchronous mode for one out of nine subjects. However, this was not the case with the remaining eight subjects, with an average classification accuracy of 69.3% for all subjects. The low average classification accuracy yields the possibility to deploy other methodology designs for higher discrimination accuracy. Further analysis of ERD/ERS in the *mu* and *beta* frequencies could provide more informative feature vector.

The incorporation of machine learning algorithms in the bilateral left-right foot classification is limited to linear discriminant analysis (LDA) or to the support vector machine in case of unilateral foot KMI [17, 25]. Careful selection of a new algorithm based on the size of the feature vector and its dimensions is required. For BCI systems that employ low dimensional feature vectors, the KNN algorithm can prove to be efficient [26].

Present study investigated the possibility to exploit the spectral, spatial and temporal EEG features in the range of 7 to 35 Hz, i.e. *mu* ERD, *beta* ERD, and *beta* ERS (post movement). The aim was to propose a novel methodology for analysis and discrimination of unilateral foot KMI using the common average and bipolar references, and comparing the features resulting from each reference. We proposed three classification models i.e. LDA, SVM, and KNN, to assess their performance against the statistical chance level, followed by the evaluation of developed method and multiple comparison corrections. Such features could be useful in BCI applications where more than one output necessitate in a system. The study directs to the utilization of three independent control features that could be used within one BCI system.

2. Methods

2.1 Participants

This study involved nine healthy participants, aged between 21-28 years, taking part in the experiment voluntarily. All participants submitted a written consent, i.e. they signed a participant consent form to engage in the study. None of them had any history of neurological disorder. Participants had no prior BCI experience. For this research, the ethics committee granted the approval, i.e. the RMIT College Human Ethics Advisory Network (CHEAN) Melbourne, Australia.

Participants were directed to sit on a comfortable chair and watch a monitor screen (17'') placed in front of them, at a distance of approximately 1.5 m. In order to avoid the possibility of proprioceptive signals induced due to muscle movement, a flat wooden surface was placed underneath the feet of participants. This way, both legs were loosely fixed. That allowed the knees to flex at 60° from full extension position, and ankles at the neutral position. During the experiment, participants were asked to dorsiflex their foot approximately 25° for 1 second, in accordance with the nominal walking gait measurements [27].

2.2 Cortical activity recording

EEG signals were recorded using the neurofeedback BrainMaster Discovery 24E amplifier (BrainMaster Technologies Inc., Bedford, USA). EEG was referenced to the linked earlobes A1 and A2 and recorded from 19 scalp electrodes. In order to acquire signals from the motor cortex, an electrocap with electrodes (C3, C4, Cz, F3, F4, F7, F8, Fz, FP1, FP2, O1, O2, P3, P4, Pz, T3, T4, T5, T6) mounted in and positioned according to the international 10-20 system [28], was used, as shown in Fig 1(A). Monopolar EEG was amplified and band-pass filtered in the frequency range of 1-100 Hz. All channels were sampled at 256 Hz, quantised with 24-bit resolution. Ground electrode was positioned near the forehead of the participants. The experimental protocol was designed using OpenViBE designer tool that comes with integrated feature boxes [9, 29, 30].

After recording, EEG signals were processed. We converted the EEG signals into reference-free forms to analyse results from two different EEG derivations, i.e. common average and bipolar reference methods. The common average reference method used all electrodes as an identical reference electrode. Whereas for the bipolar method, the monopolar electrodes which were used for feature extraction, were limited to those near the vertex, i.e. voltage differences were transversely measured at two channels C3-Cz and Cz-C4, to emphasize the left-right cortical differences elicited in *mu*, low *beta*, and high *beta* for analysis.

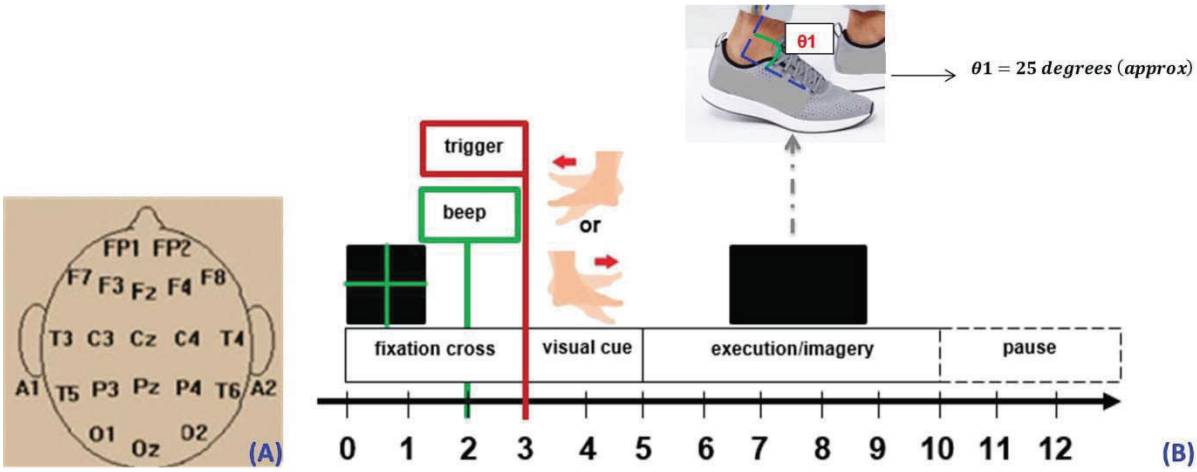

Fig 1. (A) EEG electrode/channel locations. (B) Experimental protocol for foot kinaesthetic motor imagery tasks, with cue timings expressed in seconds, during one trial.

2.3 Foot motor tasks

The experiment consisted of four cue-based sessions without feedback. Each session comprised of 40 trials, with 20 trials for left foot and 20 trials for right foot KMI in a random order. Before the four cue-based KMI sessions, a practice session was conducted, wherein participants performed a motor execution (ME) session of the same task in order to practice for measurement trials. During ME, participants were instructed to dorsiflex the foot approximately 25° maintained for 1 second (nominal walking gait) at each cue. Following practice, the KMI sessions were conducted.

Each trial began with the presentation of a green fixation cross on screen for 3 seconds, used as reference period for processing of epochs. One second long audio beep stimulus, precisely before the visual cue display, was incorporated in the first trial only. This was to alert the participant about the beginning of the experimental trial, see Fig 1(B). Next, the visual cue of 2 seconds length was displayed followed by a 5 seconds long blank screen to perform the related task (imagery), making a total of 10 seconds for each trial. This was followed by random pause intervals of 1.5-3.5 seconds at the end of the trials, to prevent fatigue. The visual cues in each trial reflected either the left or right foot dorsiflexion image with an arrow pointing in the respective direction. Both visual cues were displayed in a random order to avoid possibility of any adaptation.

2.4 Time-frequency analysis and topography of ERD/ERS

In this study, we analysed both the ERD and ERS for each SMR i.e. *mu* (7-12 Hz), low *beta* (13-24 Hz) and high *beta* (25-35 Hz) [31]. An internal or external paced event results in the generation of an ERD/ERS, which is not phase-locked to the event [32]. The decrease in percentage power or synchrony of the underlying neurons is termed ERD, while its increase is called ERS, with respect to a reference period [33]. We used an inter-trial variance (ITV) method [34] to calculate the values of

ERD/ERS. It is a frequency domain measure of exact or partial synchronization of activity at a specific latency and frequency, to a set of (experimental) events to which EEG data trials are time-locked [35]. This method compares EEG phases among trials and measures phase variance.

The EEG data was converted to reference-free form by using the common average reference method first and then the bipolar reference. Data was pre-processed using finite impulse response (FIR) bandpass filter (implemented in EEGLAB [35]) with a low-cut frequency of 7 Hz and high-cut frequency of 35 Hz for capturing *mu* and *beta* rhythms, as shown in Fig 2. These frequency bands contain most informative features about the limb movements for classification of feature vectors [36]. In addition to this, there is low possibility of any EMG contamination in those EEG frequency bands [37].

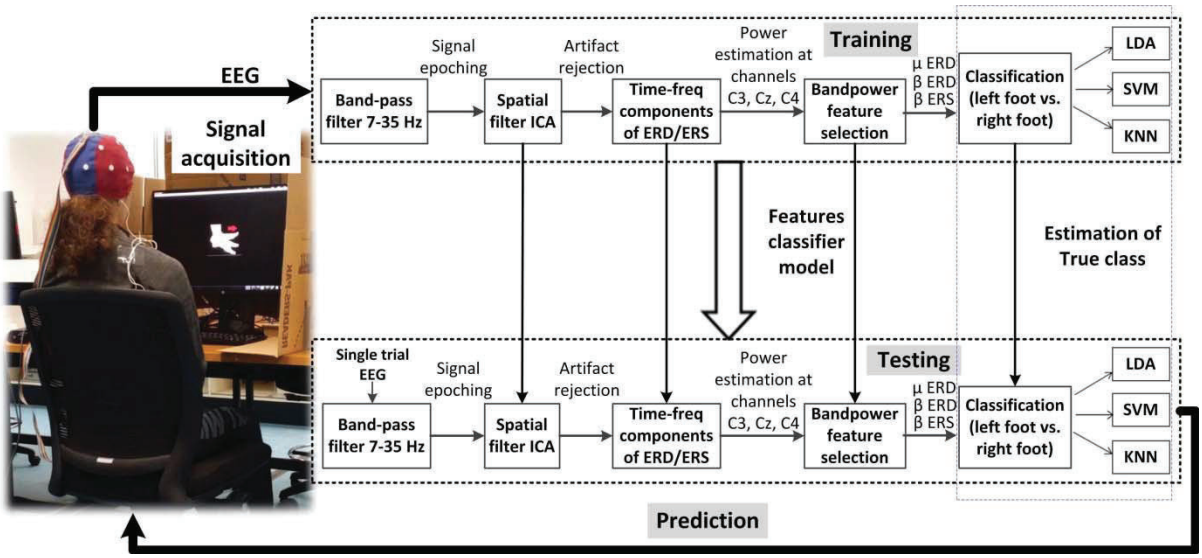

Fig 2. Band-power feature decoder with classifier training and testing in one-fold of the cross-validation.

Following this, epoching of the 40 trials (10 seconds) was done separately (class-wise), i.e. 20 left foot KMI and 20 right foot KMI epochs. Each extracted trial included the period of -3 to 0 seconds prior to the cue onset, used as reference period (baseline). The time window of cue for task performance was kept 5 seconds since dominant ERS occurs following movement offset. The processing of recorded data was based on single-trial EEG signals. Here the single-trial EEG refers to the EEG signals recorded during the KMI task (left vs. right) of one single trial. In order to remove any ocular artifact from the EEG signal, we employed the independent component analysis (ICA), as shown in Fig 2. It is proven from literature that spatial filters in single-trial analysis, improve the signal-to-noise ratio [38]. It decomposes EEG signal into separable localized sources of potentials [35]. The ICA transforms observed EEG signal (epoched data) as follows:

$$\boldsymbol{S_j} = \boldsymbol{W}\boldsymbol{E_j}, \tag{1}$$

where $\mathbf{E_j}$ is the observed single-trial EEG signal, $j = 1 \ldots n$, where *n* is the number of training trials. $\mathbf{W}$ is the un-mixing matrix and $\mathbf{S_j}$ is the single-trial signal, i.e. independent component [39]. From filtered data, we rejected artifacts (such as EMG contamination due to muscle movement) by using *'reject components by map'* (EEGLAB function).

To analyse the difference between left and right foot dorsiflexion in the spectral and temporal domains, the EEG power spectrum for left and right foot KMI was considered. Time-frequency (TF) features represent the subject-specific ERD/ERS patterns, from the independent component signal S. Based on the ITV method, the filtered average event-related potential (ERP) were subtracted from stimulus-locked single filtered EEG trials (class-wise), to overcome masking of induced activities. The samples were squared and sampled to estimate the power change in each frequency band, following method presented in [14, 40]. For every trial, a wavelet coefficient matrix was computed with 100 time samples and 3 separate frequency bins (7-12 Hz for *mu*, 13-24 Hz for low *beta* and 25-35 Hz for high *beta*) for the *i*-th component signal. In order to get spectral power, the resulting coefficients were squared and the $10\log_{10}$ transformation was computed to get resulting TF representation $\mathrm{c_i}$. The feature vector of the *j*-th trial v_j is obtained by the concatenation of the TF coefficients c_i that is computed from the *i*-th independent component signal inside S_j.

$$\boldsymbol{v}_j = \begin{bmatrix} \boldsymbol{c_1} \\ \boldsymbol{c_i} \\ . \\ . \\ . \\ \boldsymbol{c_s} \end{bmatrix}, \boldsymbol{c_i} = \left[c_{11}, \ldots, c_{f1}, c_{12}, \ldots, c_{f2}, \ldots, c_{1t}, \ldots, c_{ft}\right]^T \tag{2}$$

In Equation 2, v_j is the *j*-th feature vector, where $j = 1 \ldots n$, here n is the number of training trials, c_i is the TF coefficient vector of the *i*-th component, $i = 1 \ldots s$, where s is the number of independent components in S_j, the number of time samples is t and f is the number of frequency bins.

The significance of deviations from baseline power was evaluated using the bootstrap-t statistical method [41], with confidence interval of 95% ($p < 0.05$). In this method, a substitution for data distribution is created by selecting spectral estimates for each trial from the randomly selected latency windows in the assigned epoch baseline i.e. prior to the stimulus onset, followed by their averaging. After repeating this process many times (default: N=200) a substitute 'baseline' amplitude distribution was generated whose specified percentiles were then taken as significant thresholds i.e. significant ERD and ERS features. This was implemented by developing a MATLAB script. Significant ERD/ERS are shown as TF maps, as given in Fig 3.

2.5 Feature extraction

Based on literature, the most reactive channels associated to the motor imagery reflect in the central lobe [24]. A MATLAB script was used to extract *mu* and *beta* features from channels C3, Cz, and C4, associated to the sensorimotor cortex. It took into account the common average reference and bipolar references separately, for analysing the most significant band-power (BP) decrease, or increase, during each of the left and right KMI task. The power spectrum density of each EEG epoch, which was determined using TF analysis, was calculated. For BP calculations, let $x(t_0, t_f)$ be a single-trial EEG signal epoch within the time interval$(t_0 - t_f)$, where t_0 and t_f are the time points in seconds satisfying the condition for task performance duration i.e. $2 \leq t_0 < t_f \leq 7$. For a specific frequency band i.e. *mu*, low *beta*, or high *beta*, the percentage power change y for left or right KMI EEG epoch $x(t_0, t_f)$ is given as:

$$y(t_0, t_f) = \frac{BP_{MI}(t_0,t_f) - \overline{BP}_{baseline}(t_0,t_f)}{\overline{BP}_{baseline}(t_0,t_f)} \tag{3}$$

In Equation 3, $BP_{MI}(t_0, t_f)$ is the band-power of $x(t_0, t_f)$; and $\overline{BP}_{baseline}(t_0, t_f)$ is the mean band-power of the baseline prior to cue onset EEG epochs within the same time interval, given as:

$$\overline{BP}_{baseline}(t_0, t_f) = \frac{1}{N}\sum_{i=1}^{N} BP_{baseline}\,(t_0, t_f) \tag{4}$$

In Equation 4, $N = 20$, as twenty baseline EEG signals were taken as reference for twenty left epochs (KMI cues), similarly $N = 20$ for twenty right epochs with each participant.

2.5.1 Test-statistic and family-wise error rate correction for multiple comparisons of ERD and ERS

For statistic evaluation and comparison of features, two independent samples *t-test* were conducted on the two groups (left foot KMI and right foot KMI) of each feature for channels C3, Cz, and C4, across participants. Table 1 shows the actual test-statistic values for common average reference and bipolar reference driven features. These *p*-values were used for multiple comparisons, to direct towards the statistically significant features.

In order to carry out multiple comparison corrections, we used the Bonferroni correction for *p*-values adjustment from common average and bipolar references for each channel. Following scheme was followed:

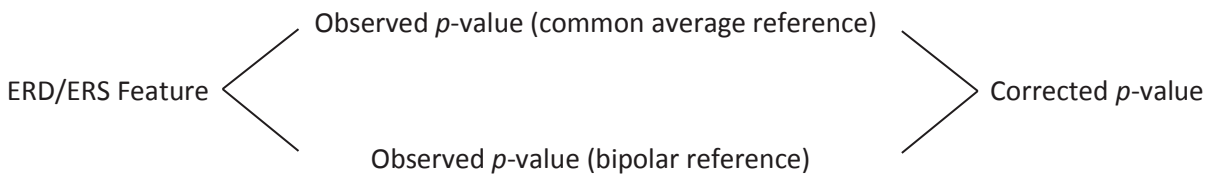

The observed *p*-values obtained from each reference were corrected for *mu* and *beta* ERD/ERS, respectively. Equation 5 is used to calculate the family-wise error rate [42].

$$\alpha_{FW} = 1 - (1 - \alpha_{PC})^{c}, \tag{5}$$

where α_{FW} is the family wise error rate, α_{PC} is the specified per comparison error rate, and c is the number of comparisons performed. Here, $\alpha_{PC} = 0.05$, with three statistical analyses conducted on the same sample of data, $c = 3$, the Bonferroni correction is given by Equation 6.

$$\frac{\alpha_{PC}}{c} \tag{6}$$

Any observed *p*-value less than the corrected *p*-value i.e., 0.017 is declared statistically significant, as seen in Table 1. With each feature, the comparisons were done for one channel from common average reference and two from bipolar channels, given as:

- C3, and C3-Cz, Cz-C4
- Cz, and C3-Cz, Cz-C4
- C4, and C3-Cz, Cz-C4

Table 1 reflects the statistical test results i.e. the degrees of freedom, *t*-values and adjusted *p*-values.

Following this, the 2-D topographic ERD/ERS (adjusted *p*-values) scalp maps were constructed for each participant, using the average ERD/ERS values in the most reactive frequency bands on all channels by using 'topoplot' (EEGLAB function).

Table 1: Test-statistic values of adjusted *p*-values with 95% confidence interval, by comparing left foot KMI vs. right foot KMI, for common average and bipolar references.

Feature	Source	Degrees of freedom, df	Common average reference (Left Vs. Right)						Bipolar reference (Left Vs. Right)			
			C3		Cz		C4		C3-Cz		Cz-C4	
			t	*p*	*t*	*p*	*t*	*p*	*t*	*p*	*t*	*P*
Mu ERD	Between feature groups	8	7.020	0.001	1.100	0.012	3.122	0.003	3.131	0.010	3.970	0.014
	Within feature groups	49										
Beta ERD	Between feature groups	8	5.415	0.004	1.176	0.013	1.846	0.002	1.243	0.016	2.757	0.013
	Within feature groups	189										
Beta ERS	Between feature groups	8	9.605	0.001	3.2739	0.015	6.413	0.015	7.069	0.006	14.206	0.003
	Within feature groups	189										

2.5.2 Individual peak latencies

With both references, the significant features with adjusted *p*-values were detected at a specific latency from cue-onset for each participant. They occur in the range of 7-12 Hz for *mu* ERD and between 13-35 Hz for *beta* ERD/ERS, as shown in Table 2. It reflects the individual peak latencies for left and right KMI task, in the respective frequency bands.

Table 2: Individual peak latencies from cue-onset for significant *mu* ERD, *beta* ERD, and *beta* ERS, using common average reference (CAR) and bipolar reference (BIP), across participants.

Participant	Mu ERD (7-12 Hz)				Beta ERD (13-35 Hz)				Beta ERS (13-35 Hz)			
	Latency from left- cue (s)		Latency from right- cue (s)		Latency from left- cue (s)		Latency from right- cue (s)		Latency from left- cue (s)		Latency from right- cue (s)	
	CAR	BIP	CAR	BIP	CAR	BIP	CAR	BIP	CAR	BIP	CAR	BIP
P1	2.62	2.75	2.80	2.90	1.90	1.80	1.82	2.00	4.20	4.65	4.50	4.50
P2	2.83	2.32	2.73	1.90	2.11	2.25	1.95	2.10	3.85	3.95	4.05	3.90
P3	1.80	2.10	2.22	2.10	1.62	2.15	1.78	1.95	2.80	2.75	3.15	3.05
P4	2.64	2.60	2.75	3.00	2.23	1.75	2.15	1.90	3.80	2.75	3.65	3.58
P5	2.70	2.65	2.42	2.55	1.75	1.88	2.17	1.65	2.65	2.88	2.60	2.58
P6	1.71	1.85	1.90	2.10	1.90	2.00	1.78	1.85	2.89	3.05	2.79	2.85
P7	2.00	2.10	2.15	2.60	1.81	1.74	1.77	1.75	3.52	3.65	3.55	3.80
P8	2.31	2.20	2.62	2.52	1.94	2.10	1.65	1.60	3.35	3.30	3.30	3.55
P9	2.45	2.15	2.20	2.52	1.60	1.70	2.15	2.25	3.55	3.78	3.60	3.58
Mean	2.34	2.30	2.42	2.47	1.87	1.93	1.91	1.89	3.40	3.42	3.50	3.58
S.D.	0.41	0.30	0.32	0.37	0.21	0.20	0.20	0.21	0.53	0.65	0.60	0.59

2.6 Evaluation of Foot kinaesthetic motor imagery classification

As this study is based on synchronous mode BCI, the classical LDA was used to measure the classification accuracy for discrimination of left and right foot KMI [43, 44]. However, in order to improve the classification accuracy, linear-SVM and KNN algorithms were employed in addition to LDA [26].

With each classifier model, cross validation was used to estimate the optimal parameters for a classifier and avoid overfitting the classifier to the training data [45]. The k-fold cross validation is used for estimating the true performance of machine learning models used in the study. We partitioned the training data set into k folds of equal size, then using $k-1$ part as a training set and checked the classification rate on the one remaining part (testing set). This is repeated for k times (folds). Finally the accuracy on each fold is estimated by calculating the average of k classification rates obtained for k testing sets [46]. Feature scaling (standardization) was performed on the training set that transferred over to the test set. With each model, the dataset was randomized thirty times and each time divided into five folds ($k = 5$). The training set for each participant

consisted of 190 trials, i.e. 95 trials for each KMI task. This means each test validation set consisted of 38 trials for each KMI task. Consequently, the weight vectors and classification accuracies of 5-folds were averaged. The mean and standard deviation of each classifier output was determined.

Linear SVM model used a linear kernel function [47]. The parameter C, which is the regularization parameter for controlling trade-off between attaining a low training and a low testing error, was verified for a range of values using MATLAB script. An optimal setting of $C = 10$ for the three models resulted in peak classification accuracies. In case of KNN, we used the weighted KNN method, and took into account $k = 10$, where k is the number of nearest neighbors, we wish to take vote from in the sample data [26]. The distance metric was Euclidean and the distance weight was squared inverse. In order to avoid overfitting, we assessed the training and validation error rate respectively, using different values of k and obtained the optimized result at $k = 10$ with each model and used it for prediction accuracy.

2.6.1 Area under receiver-operator characteristic curve

To evaluate the performance of the classifiers, the receiver operating characteristic (ROC) curves were utilized, as reported in [17]. When using the ROC curve as an evaluation tool, the area under curve (AUC) defines the performance of the detector. It indicates how much the model is capable of distinguishing between classes. In ROC, along the x-axis is the sensitivity, called true positive rate (TPR), given as:

$$TPR = \frac{TP}{TP+FN}, \tag{7}$$

where TP is the number of true positives and FN is the number of false negatives. Along the y-axis is 1-specificity, also termed the false positive rate (FPR), given as:

$$FPR = 1 - Specificity = \frac{FP}{TN+FP}, \tag{8}$$

where FP is the number of false positives and TN is the number of true negatives. Ideally, the area under the ROC, i.e. the AUC =1 indicates that there is 100% chance that the model will be able to distinguish between classes. For each model we calculated the TPR and FPR to obtain AUC-ROC in percentage across participants.

2.6.2 False discovery rate correction

In order to compare the performance of multiple classifier models, we used the false discovery rate (FDR) correction method. As each feature vector is independent, we applied the Benjamini-Hochberg procedure to decrease the possibility of any false discovery rate [48]. For Table 3, Equation 9, defines the FDR [49].

Table 3: Errors in multiple testing of *N* hypotheses

Hypothesis	Non-significant discovery	Significant discovery	Total
True null	TN	FP	N_0
False null	FN	TP	$N - N_0$
Total declared	$DN = N - DP$	DP	N

FP and *FN* reflect number of false positives (Type I error) and false negatives (Type II error); *TP* and *TN* denote numbers of correctly declared significant and non-significant discoveries. Here *DP* is the number of rejected null hypotheses (declared positives).

$$FDR = E\left(\frac{FP}{DP}\right) \tag{9}$$

This technique controls FDR at a pre-specified threshold, $fdr \leq q$, on an average. In this study, the q level was selected to standard α level of 5% for the purpose of comparison.

To apply the procedure for multi-model testing correction with N models, we arrange the p values in ascending order, $\{P(1) \leq P(2) \leq P(3) \ldots \leq P(N)\}$ corresponding to null hypotheses, $\{H_1, H_2, H_3, \ldots, H_N\}$. Following this, in a step-up manner, evaluate inequality given in Equation 10, in reverse sequential order, beginning from the last p value $P(N)$,

$$P(i) \geq i\frac{q}{N} \tag{10}$$

The comparison is stopped when the above inequality is true. Finally, reject all the hypotheses $\{H_i\}_{i=1..k}$, for which $P(i)$ is less than or equal to $P(k)$ i.e., the models belonging to the rank $i = 1..k$ are significantly discriminant.

3. Results

All participants followed the cues and performed the tasks successfully. There was no feedback regarding fatigue during the experiment.

3.1 Time-frequency map

The TF maps were individually analysed for each participant during the trial period of -3 to 7 seconds, i.e. 10 seconds. Figure 3 shows TF maps of the representative three participants (participant 1, 2, and 4). The common average reference and the most reactive two bipolar channels (C3-Cz and Cz-C4) were selected for comparison, as discussed in section 2.5.1. The TF map of each participant was used for selecting reactive bands of ERD/ERS and peak latency from cue-onset (Table 2). Each feature pattern can be observed from Fig 3 and latencies in Table 2 (for all participants). For common average reference, participant 1, reflected a strong *beta* ERS on average between 19-27 Hz

with peak latency from cue onset = 4.20-4.50 seconds ($p < 0.05$), during left and right KMI, respectively. Right KMI generated a concentrated *beta* ERS, compared to the left KMI. The bipolar method revealed a focused *beta* ERS at channel C3-Cz during left KMI i.e. no contralateral dominance. Contrary to this, channel Cz-C4 showed a prominent *beta* ERS during left KMI. For both references, *mu* ERD occurred at ≤ 12 Hz ($p < 0.05$) with participant 1. On average, the TF maps derived from both references demonstrated significant *beta* ERS for left and right KMI between 3.40-3.50 and 3.42-3.58 seconds, respectively. Similarly *mu* ERD was visible between 2.34-2.42 and 2.30-2.47 seconds respectively, and prominent *beta* ERD reflected between 1.87-1.91 and 1.93-1.89 seconds.

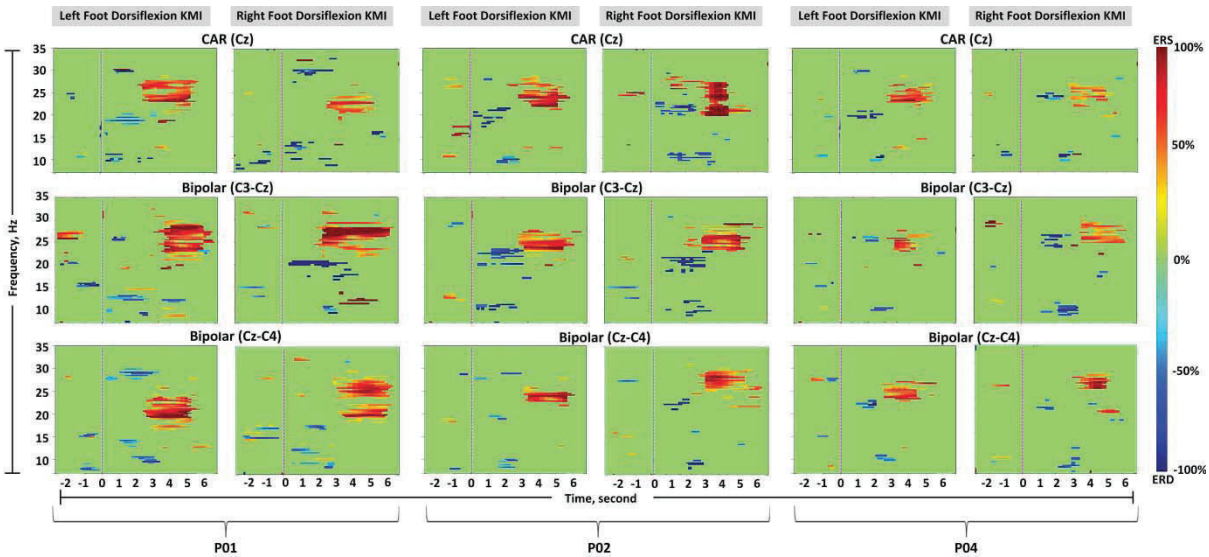

Fig 3. Time-frequency maps (participant 1, 2, and 4). Common average reference channel Cz, and two bipolar channels, C3-Cz and Cz-C4, are shown. The left columns show left foot dorsiflexion kinaesthetic motor imagery (KMI), and the right columns show right foot dorsiflexion KMI. Significant ($p < 0.05$) band-power changes are shown during the trial period of -3 to 7 s. The pink dotted line indicates the beginning of KMI.

Figure 4 reflects the grand-average amplitude of statistically significant *mu* ERD, *beta* ERD, and *beta* ERS for all nine participants. For both references, each left-right feature amplitude exhibited differences. While *mu* and *beta* ERD, showed lower amplitude over both common average and bipolar references, the maximum amplitude was visible in case of *beta* ERS. It was also observed that common average reference channel Cz showed little difference in amplitude between left and right foot KMI. The common average channel C3 elicited strong left-right differences over the contralateral side for all three features, followed by C4 with relatively less strong contralateral dominance. Bipolar channel Cz-C4 reflected prominent contralateral difference in *beta* ERS

discriminating the left-right foot KMI ($p < 0.05$, t-test). Maximum difference in amplitude between left and right KMI task is illustrated by green arrows in Fig 4.

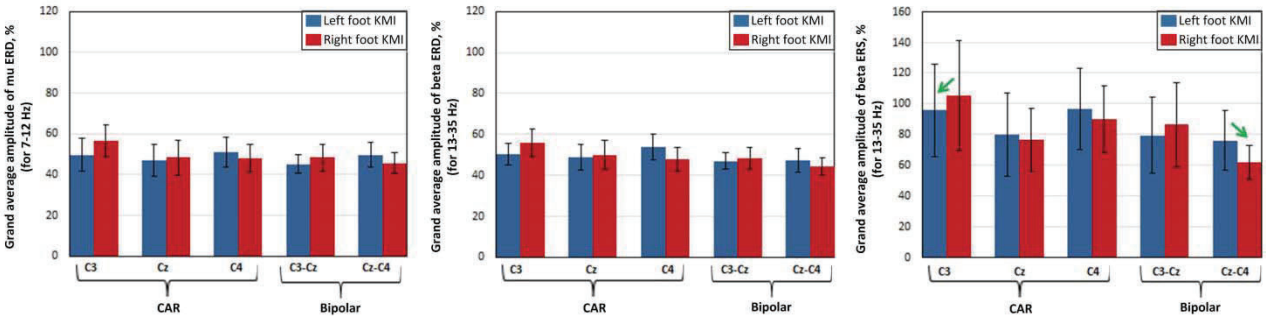

Fig 4. Average amplitude of significant *mu* ERD, *beta* ERD and *beta* ERS from all nine participants (N=9). The blue bars show average amplitude of each feature after left foot task whereas red bars represent right foot task. The error bars depict standard deviations. The significant values of adjusted *p* < 0.017 are plotted.

3.2 Average time course of ERD/ERS

Figure 5, represents the average time course of ERD/ERS for a representative participant (participant 2) with reference to the cue onset. The curves are based on most reactive ERD/ERS bands selected for each participant and peak latencies from cue onset, as reported in Table 2. The time-power curves of all participants reflected a strong peak in power amplitude at the end of the KMI period. The *mu* power attenuated with both common average and bipolar references, i.e. an ERD could be observed as soon as the visual cue was presented, with peak latency between 0-3 seconds, Fig 5. The low *beta* range also reflected an ERD from the beginning of the cue presentation window with a peak latency of 0.5-2.5 seconds. For high *beta*, a similar dip was observed during KMI period window i.e. approximately between 0-3.5 seconds, followed by a large spike i.e. an increase in power amplitude, ERS, on average of one second duration (post-imagery period).

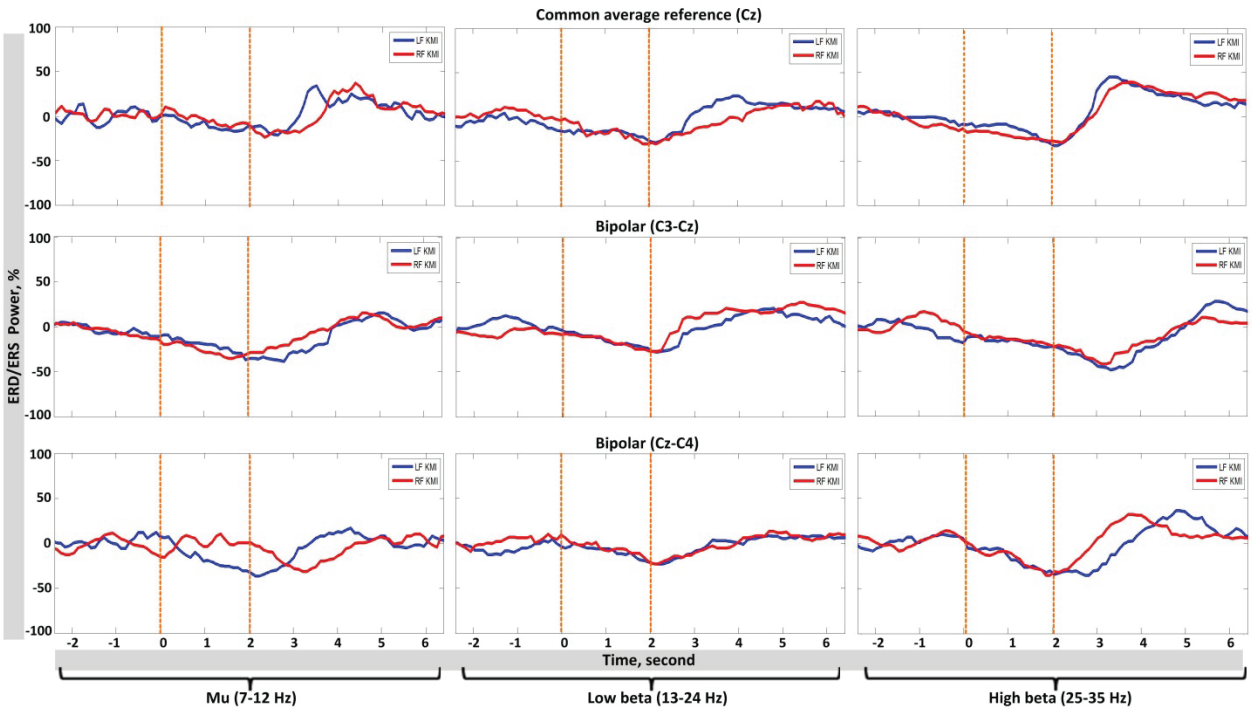

Fig 5. Average time course (participant 2) for ERD and ERS of common average reference channel Cz and two bipolar channels C3-Cz and Cz-C4 are shown. The left column reflects power changes in *mu* rhythm, mid column for *low beta* and right column for high *beta*.

3.3 EEG scalp topographies

The EEG scalp topographies of ERD/ERS from all participants with their incidence time and average specific reactive bands are displayed in Fig 6. We averaged the topographies over all nine participants. The common average reference method revealed that all three features were located across the vertex (Fig 6 top row). The *mu* ERD showed lateralized distribution during left and right foot KMI, whereas the *beta* ERS and ERD were localized centrally. Bipolar method (Fig 6 bottom row) demonstrated that *mu* ERD was contralaterally dominant during right foot KMI at Cz-C4, in agreement with results already obtained from Fig 3 and 4. Contrary to *mu* ERD, *beta* ERS revealed topographic scalp distribution with a contralateral dominance during left foot KMI at channel C3-Cz, whereas *beta* ERD remained centre-focused without lateralization. This is also in accordance with our established findings from previous sections.

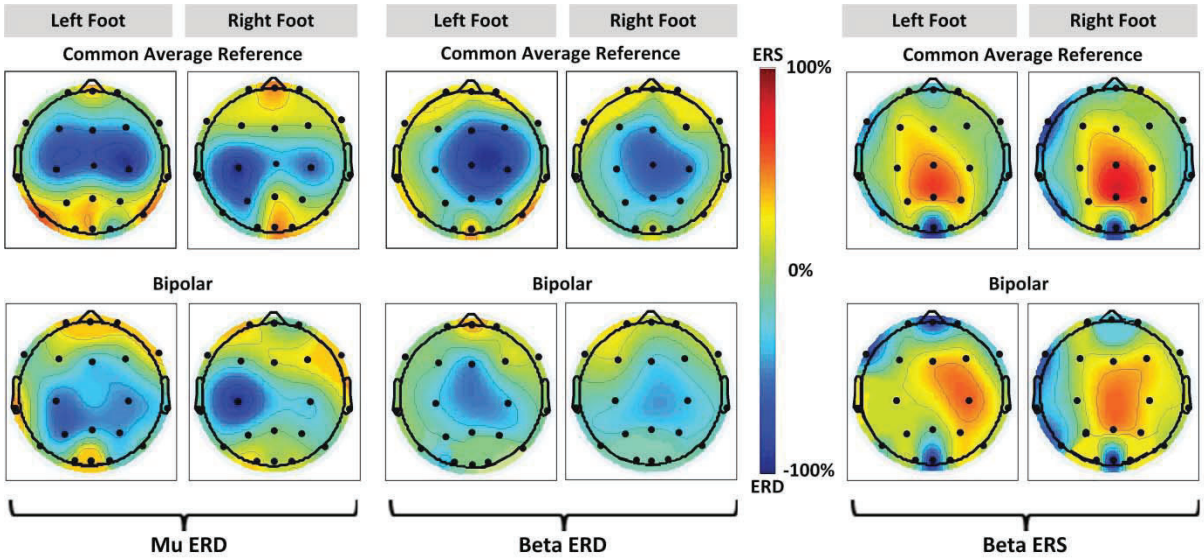

Fig 6. Average EEG topographies of ERD/ERS during foot KMI of all participants. Mu ERD is shown in the left column for left foot and right foot respectively, following this, *beta* ERD is in the mid column, and *beta* ERS is in the right column with distinguished ERS pattern. The top row illustrates ERD/ERS patterns for common average reference and the bottom for bipolar reference.

3.4 Classification accuracy

While in general, TF maps, average time-course for power, and scalp topographic analyses of the statistically significant EEG features revealed left-right KMI differences; there were instances (e.g. *beta* ERD amplitude graphs), where less differences exhibited. However, if a BCI user shows even a slight left-right difference, it is possible to enhance differences and improve the BCI control accuracy using machine learning techniques [50, 51]. Therefore, to enhance the left-right differences and confirm the cortical lateralization of features, selection of classification method is critical. Classification results for this research are derived from two linear i.e. LDA and SVM, and a non-linear model i.e. KNN.

Table 4 and 5 show the classification accuracy of all EEG features, resulting from three models, for common average and bipolar references, respectively. With first reference, the highest accuracy was achieved by participant 1, 83.4 %, for *beta* ERS during LDA classification. This was followed by SVM and KNN, i.e. 82.0% and 81.3% respectively. Maximum average accuracy with all models was observed for *beta* ERS compared to other features, given as KNN= 74.9% ± 5.20, LDA= 68.3% ± 6.72, and SVM= 67.2% ± 6.70. With bipolar reference, a similar trend was observed, i.e. participant 1 elicited highest classification accuracy of 80.4% for *beta* ERS using KNN. Similarly, average classification accuracies of *beta* ERS for all models was highest than the other features, i.e. KNN= 72.8% ± 3.64, LDA= 67.3% ± 4.70, and SVM= 65.7% ± 4.10.

Results also reveal that the average accuracy of all features are well above the statistical chance level of a 2-class discrimination BCI problem which is 57.5% ($p < 0.05$) or 60.0% ($p < 0.01$) for 80 trials, as described in [52].

In addition to classification accuracies, Table 4 and 5 also reflect the area under ROC curve (AUC) in percentage, of each participant. For ideal detection AUC should be 1. Beta ERS exhibited maximum AUC of 86.0% with KNN using common average reference, for participant 1. Similarly, with bipolar reference, it showed highest AUC of 85.0% with KNN model. Overall the average AUC was observed to be maximum for *beta* ERS using both references, i.e. KNN= 82.5% ± 2.55 and KNN= 82.0% ± 1.66, respectively. It can therefore be stated that *beta* ERS resulted in highest 2-class discrimination accuracy than other features, exceeding the chance level 60% at $p < 0.01$, with highest AUC. However, *mu* and *beta* ERD also performed above the chance level, of 2-class discrimination, as described earlier ($p < 0.05$ FDR adjusted). On average the KNN model outperformed LDA and SVM for all participants, as shown in Fig 7.

Table 4. The 5-fold cross-validation classification accuracy of left-right foot KMI using mu ERD, beta ERD, and beta ERS for common average reference

Parti-cipant	Mu ERD						Beta ERD						Beta ERS					
	LDA		SVM		KNN		LDA		SVM		KNN		LDA		SVM		KNN	
	Acc (%)	AUC (%)	Acc (%)	AUC (%)	Acc (%)	AUC (%)	Acc (%)	AUC (%)	Acc (%)	AUC (%)	Acc (%)	AUC (%)	Acc (%)	AUC (%)	Acc (%)	AUC (%)	Acc (%)	AUC (%)
P1	69.2**	80.0	67.0**	79.0	65.3**	74.0	75.4**	85.0	72.0**	85.0	79.1**	85.0	83.4**	85.0	82.0**	82.0	81.3**	86.0
P2	74.0**	82.0	68.3**	79.0	60.2**	69.0	67.2**	80.0	61.2**	69.0	70.2**	81.0	73.5**	82.0	71.1**	81.0	74.2**	82.0
P3	64.2**	75.0	57.9*	66.0	59.4*	69.0	65.3**	80.0	64.4**	72.0	69.1**	81.0	64.2**	79.0	63.1**	69.0	66.2**	78.0
P4	69.1**	80.0	62.2**	72.0	61.0**	69.0	63.2**	69.0	62.2**	72.0	67.0**	79.0	67.4**	80.0	65.4**	72.0	76.4**	84.0
P5	65.2**	74.0	62.6**	73.0	57.5*	65.0	64.1**	80.0	61.1**	71.0	65.3**	81.0	62.5**	72.0	63.5**	71.0	71.2**	81.0
P6	66.3**	71.0	61.0**	69.0	68.1**	78.0	64.3**	79.0	60.5**	69.0	69.1**	84.0	67.7**	80.0	67.1**	79.0	69.1**	80.0
P7	64.0**	74.0	57.8*	66.0	66.1**	75.0	63.0**	79.0	58.0*	69.0	66.2**	77.0	68.0**	80.0	65.3**	72.0	78.3**	83.0
P8	68.0**	79.0	61.0**	69.0	57.6*	65.0	61.1**	69.0	57.5*	66.0	69.0**	83.0	61.0**	69.0	58.0*	68.0	77.0**	84.0
P9	67.1**	79.0	62.3**	72.0	62.2**	69.0	60.1**	79.0	59.0*	69.0	68.1**	79.0	67.0**	80.0	69.2**	80.0	80.4**	85.0
Mean	67.4	77.1	62.2	71.6	61.9	70.3	64.9	77.7	61.5	71.3	69.2	81.1	68.3	78.5	67.2	74.8	74.9	82.5
S.D.	3.10	3.69	3.60	4.84	3.90	4.44	4.50	5.30	4.30	5.45	4.01	2.57	6.72	4.95	6.70	5.53	5.20	2.55

* Over chance level of 2-class discrimination, 57.50% ($p < 0.05$).

** Over chance level of 2-class discrimination, 60.00% ($p < 0.01$).

Table 5. The 5-fold cross-validation classification accuracy of left-right foot KMI using mu ERD, beta ERD, and beta ERS for Bipolar reference

Parti-cipant	Mu ERD						Beta ERD						Beta ERS					
	LDA		SVM		KNN		LDA		SVM		KNN		LDA		SVM		KNN	
	Acc (%)	AUC (%)	Acc (%)	AUC (%)	Acc (%)	AUC (%)	Acc (%)	AUC (%)	Acc (%)	AUC (%)	Acc (%)	AUC (%)	Acc (%)	AUC (%)	Acc (%)	AUC (%)	Acc (%)	AUC (%)
P1	72.3**	81.0	68.2**	79.0	70.3**	81.0	61.1**	69.0	61.0**	69.0	64.2**	79.0	72.2**	82.0	70.0**	80.0	80.4**	85.0
P2	70.1**	79.0	67.3**	79.0	64.5**	76.0	67.3**	79.0	60.2**	71.0	69.0**	80.0	69.4**	79.0	66.0**	79.0	73.0**	81.0
P3	65.1**	78.0	57.6*	66.0	59.0*	71.0	62.2**	69.0	60.1**	69.0	70.0**	81.0	63.4**	69.0	61.0**	69.0	72.1**	82.0
P4	73.0**	82.0	62.2**	71.0	65.1**	79.0	65.3**	75.0	61.1**	79.0	60.3**	74.0	71.1**	81.0	70.1**	80.0	71.1**	81.0
P5	66.2**	78.0	60.1**	70.0	59.2*	71.0	63.0**	69.0	59.3*	68.0	68.1**	80.0	64.4**	76.0	66.0**	79.0	69.2**	80.0
P6	63.1**	69.0	61.1**	69.0	68.0**	77.0	57.5*	67.0	57.7*	67.0	71.1**	81.0	62.4**	72.0	60.1**	71.0	76.0**	84.0
P7	70.2**	79.0	59.0*	69.0	66.3**	80.0	58.4*	67.0	60.0**	69.0	64.2**	78.0	61.3**	69.0	61.0**	69.0	70.1**	81.0

P8	69.4**	79.0	58.0*	69.0	61.1**	71.0	67.2**	79.0	60.3**	80.0	74.0**	83.0	67.4**	78.0	69.0**	80.0	74.0**	83.0
P9	71.0**	80.0	62.3**	71.0	64.1**	77.0	69.1**	80.0	60.1**	79.0	69.0**	80.0	74.1**	83.0	68.0**	79.0	69.2**	81.0
Mean	68.9	78.3	61.8	71.4	64.2	75.9	63.5	72.6	60.0	72.3	67.8	79.5	67.3	76.5	65.7	76.2	72.8	82.0
S.D.	3.40	3.74	3.80	4.53	3.90	3.98	4.10	5.52	1.02	5.36	4.10	2.50	4.70	5.41	4.10	4.96	3.64	1.66

* Over chance level of 2-class discrimination, 57.50% ($p < 0.05$).
** Over chance level of 2-class discrimination, 60.00% ($p < 0.01$).

4. Discussion

This study focused on the analysis of *mu* and *beta* ERD/ERS, following left and right foot dorsiflexion KMI. The analysis comprised of TF maps, time-power ERD/ERS, and EEG scalp topographies, for common average and bipolar references. In general, a decrease in *mu* band activity (ERD) during KMI, with a significant increase in high *beta* band following KMI (ERS), was observed. Low *beta* ERD was observed during KMI with little post-KMI rebound, which was in agreement with literature [17, 53, 54]. Beta ERS was localized at the vertex i.e. the foot area representation of the cortex. With common average reference, *beta* ERS showed a high power concentration, whereas with bipolar reference low power concentration followed by contralateral dominance were observed at channels C3-Cz and Cz-C4, Fig 6. Mu ERD was distributed bilaterally across the vertex, in case of both references. Beta ERD was focussed at the vertex with no prominent lateralization. In general, the common average reference method resulted in strong reflection of ERD/ERS, which is evident in scalp topographies, Fig 6 as well as grand average amplitude graphs, Fig 4. The bilateral *mu* ERD and *beta* ERS, could provide a basis for left-right discrimination of KMI tasks, contralateral to the side of movement.

4.1 Common average reference and bipolar method for discrimination of left-right *mu* ERD, *beta* ERD, and *beta* ERS

The common average reference method has been used as it is computationally simple and compliant to both on-chip and real-time applications. This spatial filter identifies small signal sources in very noisy recordings, with much higher signal-to-noise ratio than a Laplacian [55, 56]. It was used to detect intention of movement during imagination [57]. In contrast to a previous study on left-right difference of *beta* ERS, which did not observe any difference with common average reference [17], our study confirmed the difference for all three features, not only *beta* ERS. Mainly, the channels adjacent to the vertex i.e., C3 and C4 exhibited a contralateral dominance with reference to cue presentation. The selection of these channels was based on the studies confirming that foot KMI elicits ERD/ERS patterns in the sensorimotor cortex [10, 24]. The analyses indicated that unilateral foot KMI generated significant *mu* ERD ($p < 0.01$) and *beta* ERS ($p < 0.01$) in all participants with no BCI feedback training. Our results depict that foot KMI elicits broad-banded ERD (10.1 Hz ± 1) and narrow-banded ERS (24 Hz ± 0.8). Highest 2-class discrimination accuracy was achieved for *beta* ERS and *beta* ERD features with this reference.

However, the transverse bipolar method also demonstrated statistically significant left-right discrimination of foot KMI with all features, maximum with *beta* ERS. In contrast to Laplacian, it is a simple spatial filter, that derives the first spatial derivative, thus enhances the differences in voltage-gradient in a direction [56]. With multiple comparisons of left-right features between both reference channels, the family-wise error rate Bonferroni correction was performed.

With foot KMI, the broad band ERD indicated the involvement of supplementary motor area (SMA) in the preparation and performance of imagery tasks [33, 58]. In addition to this, the foot area enhancement was observed with narrower *beta* ERS. Therefore, it can be stated that the differences in ERD and ERS can be observed in *mu*, low *beta* and high *beta* frequency bands of sensorimotor cortex and SMA. However, for one BCI system with multiple users, the use of all three features, as individual control signal, could be tricky, as the decision boundary/threshold to discriminate between the features (frequency band) may vary.

4.2 Comparison of KNN with linear classifiers using false discovery rate correction

Figure 7 depicts the results from present study (FDR adjusted *p*-values of 0.05) with an average classification accuracy of ≥60% ($p < 0.01$) for all participants that deployed *mu* and *beta* ERD/ERS for discrimination between classes. It is evident for all three classifiers that *beta* ERS exceeded 80% accuracy for participant 1 (Table 4). These results clearly show an improved classification accuracy than a similar study [17], with the difference of BCI design. Our study involved artifacts rejection

using ICA and a KNN as classifier model that outperformed remaining models for *beta* ERD and ERS, Fig 7. These efficient results could be due to the low dimensional feature vectors deployed in the study for a BCI [26].

Significant ERD/ERS features associated with *mu* and *beta*, were evaluated using AUC-ROC for the binary classifier. However, since each classifier model is independent, we made multiple comparisons between models to evaluate the statistical significance of the models. Consequently, the FDR correction was applied, using the method of Benjamini-Hochberg, as described in section 2.6.2. The threshold for controlling FDR was selected to standard α level of 5% for the purpose of comparison, $q = 0.050$. Table 6 reflect the FDR corrections for LDA, SVM, and KNN models. It can be observed that all the comparisons resulted in the rejection of null hypotheses$\mathrm{H}_{0,}$ except for the last comparison, where the inequality in Equation 10 becomes true. This is due to the very close accuracies exhibited by KNN and SVM models, i.e. the performance efficiency of both classifiers has similar impact for *mu* ERD. These encouraging results suggest that the foot dorsiflexion KMI can potentially elicit left-right differences in EEG. Following this, the feedback training plays an effective role in enhancing the classification accuracy as suggested by [59]. Subsequently, our next aim would be to monitor the repetitive use of BCI training and its effects on classification accuracy.

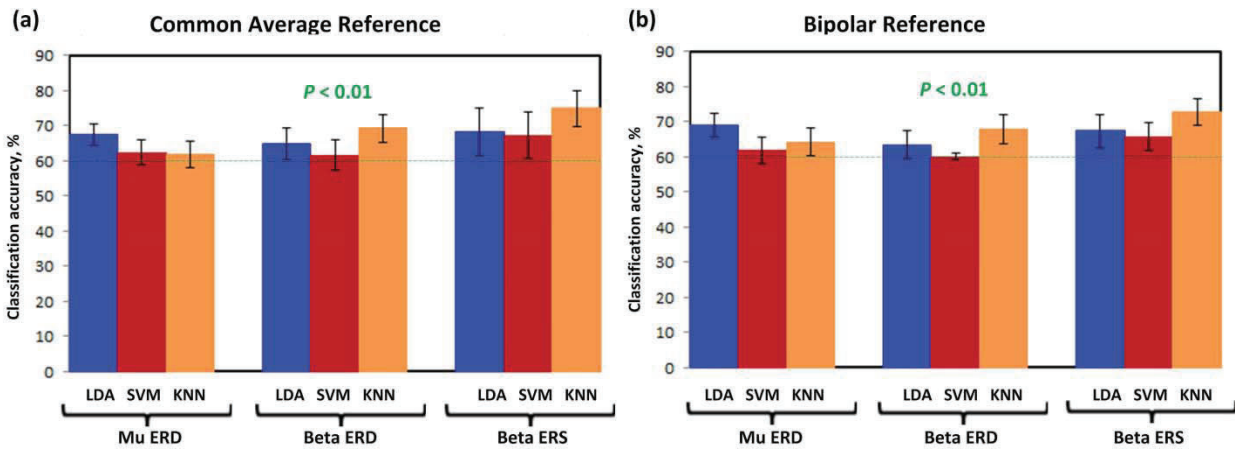

Fig 7. Classifiers performance accuracy in percentage, using (A) common average reference, and (B) bipolar reference. The error bars represent standard deviations.

Our next goal is to use the common spatial patterns (CSP) method for the same task i.e. discrimination of left-right foot KMI. In general, CSP has been used in BCI study for motor imagery (foot and hand/tongue) using only Laplacian derivation, not left and right foot KMI difference (e.g., [60]). However, our study reflected the enhancement of foot KMI differences using common average and bipolar references. The use of CSP features with the present study design, could improve the left-right differences of foot KMI and be used as independent control features.

Table 6. False discovery rate (FDR) corrections for LDA, SVM and KNN classifiers

			p-value	Linear setup	Adjusted-*p* $q = 0.050$	Rejected H_0
Mu ERD	Common average reference	LDA-SVM	*	*	0.003	1
		LDA-KNN	0.007	*	0.006	1
		KNN-SVM	0.435	*	0.008	1
	Bipolar reference	LDA-SVM	*	*	0.011	1
		LDA-KNN	0.004	*	0.014	1
		KNN-SVM	0.028	*	0.017	1
Beta ERD	Common average reference	LDA-SVM	*	0.002	0.019	1
		LDA-KNN	*	0.003	0.022	1
		KNN-SVM	*	0.004	0.025	1
	Bipolar reference	LDA-SVM	0.011	0.007	0.028	1
		LDA-KNN	0.020	0.007	0.031	1
		KNN-SVM	*	0.010	0.033	1
Beta ERS	Common average reference	LDA-SVM	0.046	0.011	0.036	1
		LDA-KNN	0.007	0.020	0.039	1
		KNN-SVM	0.003	0.028	0.042	1
	Bipolar reference	LDA-SVM	0.041	0.041	0.044	1
		LDA-KNN	0.010	0.046	0.048	1
		KNN-SVM	0.002	0.435	0.050	0

* denotes the *p*-value less than 0.001.

5. Conclusions

The aim of this research was to decode the bilateral foot motor imageries and obtain high classification accuracy in order to enhance the universality of lower-limb assistive BCI. The results of presented investigation show the lateralization of *mu* and *beta* features in association with left-right foot dorsiflexion KMI. We have demonstrated that the KNN model, with common average reference method, can improve ERD/ERS lateralization. Our method achieved highest accuracy level of 83.4% using EEG signals from channels at the vertex and its adjacent C3 and C4 positions. It is therefore concluded that *beta* ERS, in addition to *mu* ERD, and *beta* ERD can be used as independent control features for a synchronous BCI. These features could be deployed in a 2-class BCI as control commands for operating bionic foot or a foot neuroprosthesis.

Conflict of interest

None of the authors have potential conflicts of interest to be disclosed.

Competing interest

Authors declare no competing interests.

Acknowledgement

None.

References

1. Tariq, M., P.M. Trivailo, and M. Simic, *EEG-Based BCI Control Schemes for Lower-Limb Assistive-Robots.* Frontiers in Human Neuroscience, 2018. **12**(312).
2. Cervera, M.A., et al., *Brain-computer interfaces for post-stroke motor rehabilitation: a meta-analysis.* Annals of clinical and translational neurology, 2018. **5**(5): p. 651-663.
3. Tariq, M., et al. *Mu-beta rhythm ERD/ERS quantification for foot motor execution and imagery tasks in BCI applications*. in *2017 8th IEEE International Conference on Cognitive Infocommunications (CogInfoCom)*. 2017. IEEE.
4. Deng, W., et al., *Advances in Automation Technologies for Lower Extremity Neurorehabilitation: A Review and Future Challenges.* IEEE reviews in biomedical engineering, 2018. **11**: p. 289-305.
5. He, Y., et al., *Brain–machine interfaces for controlling lower-limb powered robotic systems.* Journal of neural engineering, 2018. **15**(2): p. 021004.
6. Lebedev, M.A. and M.A. Nicolelis, *Brain-machine interfaces: From basic science to neuroprostheses and neurorehabilitation.* Physiological reviews, 2017. **97**(2): p. 767-837.
7. Liu, Y.-H., et al., *Analysis of electroencephalography event-related desynchronisation and synchronisation induced by lower-limb stepping motor imagery.* Journal of Medical and Biological Engineering, 2019. **39**(1): p. 54-69.
8. Wolpaw, J. and E.W. Wolpaw, *Brain-computer interfaces: principles and practice*. 2012: OUP USA.
9. Tariq, M., et al., *Comparison of Event-related Changes in Oscillatory Activity During Different Cognitive Imaginary Movements Within Same Lower-Limb.* Acta Polytechnica Hungarica, 2019. **16**(2): p. 77-92.
10. Li, M.-A., et al., *Decoding of motor imagery EEG based on brain source estimation.* Neurocomputing, 2019. **339**: p. 182-193.
11. Stinear, C.M., et al., *Kinesthetic, but not visual, motor imagery modulates corticomotor excitability.* Experimental brain research, 2006. **168**(1-2): p. 157-164.
12. Mokienko, O., et al., *Increased motor cortex excitability during motor imagery in brain-computer interface trained subjects.* Frontiers in computational neuroscience, 2013. **7**: p. 168.
13. Hommelsen, M., et al., *Sensory Feedback Interferes with Mu Rhythm Based Detection of Motor Commands from Electroencephalographic Signals.* Frontiers in human neuroscience, 2017. **11**: p. 523.
14. Graimann, B. and G. Pfurtscheller, *Quantification and visualization of event-related changes in oscillatory brain activity in the time–frequency domain.* Progress in brain research, 2006. **159**: p. 79-97.
15. Kilavik, B.E., et al., *The ups and downs of beta oscillations in sensorimotor cortex.* Experimental neurology, 2013. **245**: p. 15-26.
16. Penfield, W. and E. Boldrey, *Somatic motor and sensory representation in the cerebral cortex of man as studied by electrical stimulation.* Brain, 1937. **60**(4): p. 389-443.
17. Hashimoto, Y. and J. Ushiba, *EEG-based classification of imaginary left and right foot movements using beta rebound.* Clinical neurophysiology, 2013. **124**(11): p. 2153-2160.
18. Neuper, C., M. Wörtz, and G. Pfurtscheller, *ERD/ERS patterns reflecting sensorimotor activation and deactivation.* Progress in brain research, 2006. **159**: p. 211-222.
19. Millán, J.d.R., et al., *Combining brain–computer interfaces and assistive technologies: state-of-the-art and challenges.* Frontiers in neuroscience, 2010. **4**: p. 161.

20. Daly, J.J. and J.R. Wolpaw, *Brain–computer interfaces in neurological rehabilitation.* The Lancet Neurology, 2008. **7**(11): p. 1032-1043.
21. Nam, C.S., et al., *Movement imagery-related lateralization of event-related (de) synchronization (ERD/ERS): motor-imagery duration effects.* Clinical Neurophysiology, 2011. **122**(3): p. 567-577.
22. Müller-Putz, G.R., et al., *Fast set-up asynchronous brain-switch based on detection of foot motor imagery in 1-channel EEG.* Medical & biological engineering & computing, 2010. **48**(3): p. 229-233.
23. Carlson, T. and J.d.R. Millan, *Brain-controlled wheelchairs: a robotic architecture.* IEEE Robotics & Automation Magazine, 2013. **20**(1): p. 65-73.
24. Pfurtscheller, G., et al., *Mu rhythm (de) synchronization and EEG single-trial classification of different motor imagery tasks.* NeuroImage, 2006. **31**(1): p. 153-159.
25. Pfurtscheller, G. and T. Solis-Escalante, *Could the beta rebound in the EEG be suitable to realize a "brain switch"?* Clinical Neurophysiology, 2009. **120**(1): p. 24-29.
26. Lotte, F., et al., *A review of classification algorithms for EEG-based brain–computer interfaces.* Journal of neural engineering, 2007. **4**(2): p. R1.
27. Tariq, M., Z. Koreshi, and P. Trivailo. *Optimal Control of an Active Prosthetic Ankle*. in *Proceedings of the 3rd International Conference on Mechatronics and Robotics Engineering*. 2017. ACM.
28. Klem, G.H., et al., *The ten-twenty electrode system of the International Federation.* Electroencephalogr Clin Neurophysiol, 1999. **52**(3): p. 3-6.
29. Renard, Y., et al., *Openvibe: An open-source software platform to design, test, and use brain–computer interfaces in real and virtual environments.* Presence: teleoperators and virtual environments, 2010. **19**(1): p. 35-53.
30. Tariq, M., P.M. Trivailo, and M. Simic, *Motor imagery based EEG features visualization for BCI applications.* Procedia computer science, 2018. **126**: p. 1936-1944.
31. Rangaswamy, M., et al., *Beta power in the EEG of alcoholics.* Biological psychiatry, 2002. **52**(8): p. 831-842.
32. Schomer, D.L. and F.L. Da Silva, *Niedermeyer's electroencephalography: basic principles, clinical applications, and related fields*. 2012: Lippincott Williams & Wilkins.
33. Pfurtscheller, G. and F.L. Da Silva, *Event-related EEG/MEG synchronization and desynchronization: basic principles.* Clinical neurophysiology, 1999. **110**(11): p. 1842-1857.
34. Kalcher, J. and G. Pfurtscheller, *Discrimination between phase-locked and non-phase-locked event-related EEG activity.* Electroencephalography and clinical neurophysiology, 1995. **94**(5): p. 381-384.
35. Delorme, A. and S. Makeig, *EEGLAB: an open source toolbox for analysis of single-trial EEG dynamics including independent component analysis.* Journal of neuroscience methods, 2004. **134**(1): p. 9-21.
36. Lisi, G., T. Noda, and J. Morimoto, *Decoding the ERD/ERS: influence of afferent input induced by a leg assistive robot.* Frontiers in systems neuroscience, 2014. **8**: p. 85.
37. Muthukumaraswamy, S., *High-frequency brain activity and muscle artifacts in MEG/EEG: a review and recommendations.* Frontiers in human neuroscience, 2013. **7**: p. 138.
38. Blankertz, B., et al., *Optimizing spatial filters for robust EEG single-trial analysis.* IEEE Signal processing magazine, 2008. **25**(1): p. 41-56.
39. Hyvärinen, A. and E. Oja, *Independent component analysis: algorithms and applications.* Neural networks, 2000. **13**(4-5): p. 411-430.
40. Graimann, B., et al., *Visualization of significant ERD/ERS patterns in multichannel EEG and ECoG data.* Clinical neurophysiology, 2002. **113**(1): p. 43-47.
41. Davison, A.C. and D.V. Hinkley, *Bootstrap methods and their application*. Vol. 1. 1997: Cambridge university press.

42. Tamhane, A. and D. Dunlop, *Statistics and data analysis: from elementary to intermediate.* 2000.
43. Pfurtscheller, G., et al., *Current trends in Graz brain-computer interface (BCI) research.* IEEE transactions on rehabilitation engineering, 2000. **8**(2): p. 216-219.
44. Lotte, F., et al., *A review of classification algorithms for EEG-based brain–computer interfaces: a 10 year update.* Journal of neural engineering, 2018. **15**(3): p. 031005.
45. Mitchell, T.M., *Machine learning*. 1997, McGraw hill.
46. Yong, X. and C. Menon, *EEG classification of different imaginary movements within the same limb.* PloS one, 2015. **10**(4): p. e0121896.
47. Garrett, D., et al., *Comparison of linear, nonlinear, and feature selection methods for EEG signal classification.* IEEE Transactions on neural systems and rehabilitation engineering, 2003. **11**(2): p. 141-144.
48. Benjamini, Y. and Y. Hochberg, *Controlling the false discovery rate: a practical and powerful approach to multiple testing.* Journal of the Royal statistical society: series B (Methodological), 1995. **57**(1): p. 289-300.
49. Singh, A.K. and I. Dan, *Exploring the false discovery rate in multichannel NIRS.* Neuroimage, 2006. **33**(2): p. 542-549.
50. Hashimoto, Y., et al., *Change in brain activity through virtual reality-based brain-machine communication in a chronic tetraplegic subject with muscular dystrophy.* BMC neuroscience, 2010. **11**(1): p. 117.
51. Pfurtscheller, G., et al., *EEG-based discrimination between imagination of right and left hand movement.* Electroencephalography and clinical Neurophysiology, 1997. **103**(6): p. 642-651.
52. Müller-Putz, G.R., et al., *Better than random? A closer look on BCI results.* International Journal of Bioelectromagnetism, 2008. **10**(1): p. 52-55.
53. Pfurtscheller, G., et al., *Beta rebound after different types of motor imagery in man.* Neuroscience letters, 2005. **378**(3): p. 156-159.
54. Jurkiewicz, M.T., et al., *Post-movement beta rebound is generated in motor cortex: evidence from neuromagnetic recordings.* Neuroimage, 2006. **32**(3): p. 1281-1289.
55. Ludwig, K.A., et al., *Using a common average reference to improve cortical neuron recordings from microelectrode arrays.* Journal of neurophysiology, 2009. **101**(3): p. 1679-1689.
56. Wolpaw, J.R., et al., *Brain–computer interfaces for communication and control.* Clinical neurophysiology, 2002. **113**(6): p. 767-791.
57. Syam, S.H.F., et al. *Comparing common average referencing to laplacian referencing in detecting imagination and intention of movement for brain computer interface*. in *MATEC Web of Conferences*. 2017.
58. Quinones-Hinojosa, A., *Schmidek and Sweet: Operative Neurosurgical Techniques 2-Volume Set: Indications, Methods and Results (Expert Consult-Online and Print)*. Vol. 2. 2012: Elsevier Health Sciences.
59. Orand, A., et al., *The comparison of motor learning performance with and without feedback.* Somatosensory & motor research, 2012. **29**(3): p. 103-110.
60. Ramoser, H., J. Muller-Gerking, and G. Pfurtscheller, *Optimal spatial filtering of single trial EEG during imagined hand movement.* IEEE transactions on rehabilitation engineering, 2000. **8**(4): p. 441-446.

Chapter 6

Classification of left and right foot kinaesthetic motor imagery using common spatial pattern

Chapter Overview

The confirmation of cortical lateralization of ERD/ERS, based on foot KMI, is presented in the previous chapter. Further investigations for the possibility to improve classification accuracy of the two foot KMI tasks, to be used in a BCI paradigm, has been presented in this chapter. CSP and filter-bank CSP (FBCSP) feature vectors were explored separately. The ML models, linear discriminant analysis and logistic regression, both deployed CSP and FBCSP feature vectors individually, resulting in four combinations of models. Resulting accuracies were statistically compared for each combination model. In context to band-power features, CSP features resulted in lower classification accuracy, but stood significantly above the statistical chance level of a 2-class BCI paradigm.

This study is accepted for publication in ***Biomedical Physics and Engineering Express***.

M. Tariq, P. M. Trivailo, and M. Simic. *Classification of left and right foot kinaesthetic motor imagery using common spatial pattern*.

Classification of left and right foot kinaesthetic motor imagery using common spatial pattern

Madiha Tariq, Pavel M. Trivailo, and Milan Simic*

School of Engineering, RMIT University, Melbourne, VIC, Australia

*Corresponding author. Address: 264 Plenty Rd, Bundoora VIC 3083, Australia.
Tel.: +61 3 9925 6223; fax: +61 3 9925 6108. *E-mail address*: milan.simic@rmit.edu.au

Abstract

Background and Objectives

Brain-computer interface systems typically deploy common spatial pattern (CSP) for feature extraction of *mu* and *beta* rhythms based on upper limbs kinaesthetic motor imageries (KMI). However, it has not been used to classify the left vs. right foot KMI, due to its location inside the mesial wall of the sensorimotor cortex, which makes it difficult to be detected. This study reports the novel classification of *mu* and *beta* EEG features, during left and right foot KMI cognitive task, using CSP, and the filter bank common spatial pattern (FBCSP) method, to optimize the subject-specific band selection. The study initially proposed CSP method, followed by the implementation of FBCSP for optimization of individual spatial patterns, wherein a set of CSP filters was learned, for each of the time/frequency filters in a supervised way. This was followed by the log-variance feature extraction and concatenation of all features (over all chosen spectral-filters). Subsequently, supervised machine learning was implemented, i.e. logistic regression (Logreg) and linear discriminant analysis (LDA), in order to compare the respective foot KMI classification rates. The training and testing data, used in the model, was validated using 10-fold cross validation. In this study four methodology paradigms were reported, i.e. CSP LDA, CSP Logreg, and FBCSP LDA, FBCSP Logreg. All the paradigms resulted in an average classification accuracy rate above the statistical chance level of 60.0% ($P < 0.01$). On average, FBCSP- LDA outperformed remaining paradigms with a kappa score of 0.41 and the area under ROC curve as 0.64. Similarly, this paradigm enabled discrimination between right and left foot KMI cognitive task at highest accuracy rate i.e. maximum 77.5% with kappa=0.55 (in single trial analysis). The proposed novel paradigms, using CSP and FBCSP, established a potential to exploit the left vs. right foot imagery classification, in a synchronous 2-class BCI for controlling robotic foot, or foot neuroprosthesis.

Keywords:

Common spatial pattern (CSP), filter bank common spatial pattern (FBCSP), kinaesthetic motor imagery (KMI), brain-computer interface (BCI), EEG, supervised machine learning.

1. Introduction

Brain-computer interface (BCI) is an augmented muscle-free communication channel between the human brain and output devices for assisting subjects with neuromotor disorders, spinal cord injuries (SCI) or amputated residual limbs [1-4]. It decodes a specific brain activity into computer command to control external device. Amongst the popularly used electroencephalography (EEG)-based brain activity is event-related (de)synchronization (ERD/ERS) localized in the sensorimotor cortex [5-9]. The ERD/ERS features can be quantified via band-power changes that occur during any kinaesthetic motor imagery (KMI) task performed by the subject, e.g. imagination of limb movement (left-right hand or foot) [5, 7]. Frequency bandwidths, that reflect imaginary activity in EEG, lie in the *mu* and *beta* oscillatory activity, i.e. between 7 to ~35 Hz.

In order to extract ERD/ERS EEG features for BCI, various methods have been introduced based on application requirements [1, 9-13]. According to [14], for a BCI that uses *mu* and *beta* rhythms, the selection of spatial filter can markedly affect its signal-to-noise ratio. The common spatial pattern (CSP) is one efficient method that has generally been used with oscillatory processes in the KMI feature extraction due to its simplicity, relatively high speed and robustness. However, literature reflects that this method has been used with either hand motor imagery (MI), e.g. left vs. right hand, or left-hand vs. rest, or hand vs. basic foot, or tongue movement imageries [15-18]. There was no evidence of left vs. right foot discrimination task. Less literature on discrimination of lower-limbs compared to upper limbs is due to the location of lower-limbs representation area near the "mantelkante" in the sensorimotor cortex [1, 7, 8]. It is located deep inside the mesial wall (within the interhemispheric fissure). In contrast to upper limbs, hip, knee, foot and toes share spatial proximity with each other that makes it difficult to detect them. This study therefore takes into account the left foot vs. right foot dorsiflexion KMI tasks for establishing the basis of a 2-class BCI (that could generate two independent commands) to control 2 degrees of freedom (DOF) robotic foot.

As CSP finds spatial filters, which maximize the variance of the (projected) signal from one class, and minimize it for the other class, it offers a natural approach to efficiently estimate the discriminant information about KMI [19]. Adaptive spatial filter uses the log-variance features over single non-adapted frequency range (that may have multiple peaks), and in the signal, neither temporal structure (variations) is captured, nor the interactions between frequency bands [20]. Successful application of CSP mainly relies on the filter band selection (a wide filter band lies in the 8-35 Hz for KMI classification). However, the most effective frequency band is typically subject-specific that can hardly be determined manually [16]. In order to fix the filter band selection problem, the approaches proposed include simultaneous optimization of spectral filters within the CSP [21-23]; and selection of significant CSP features from multiple frequency bands [24, 25]. Filter bank common spatial pattern (FBCSP) was introduced for the selection of optimal filter bands, through estimation of the mutual information among CSP features in several fixed filter bands [25]. Consequently, we

implemented the FBCSP as a further study, to optimize the subject-specific frequency band for CSP across participants.

The FBCSP is an extension of the CSP method. A set of CSP filters is learned for each of the several time/frequency filters, followed by the log-variance feature extraction, the concatenation of all features (over the chosen spectral filters), and finally machine learning. It could be very useful when oscillatory processes in different frequency bands (with different spatial topographies) e.g., *mu*, low *beta* and high *beta*, are jointly active. Their concerted reaction must be taken into account for the given prediction task [20]. In this study, since FBCSP's feature space dimensionality was larger than in CSP followed by complex interactions, a more complex classifier than linear discriminant analysis (LDA) was additionally deployed to learn the appropriate model. However, with more flexibility comes a risk of overfitting, i.e. a tradeoff, therefore we compared its performance with the standard CSP performance. Since complex (relevant) interactions between *mu* and *beta* bands are seemingly rarely observed, the selection of time and frequency regions was critical.

We have focused on the optimal selection of discriminative ERD/ERS features from multiple frequency bands of *mu* and *beta* and the effective imagery time window using two feature selection algorithms, CSP and FBCSP, designed in BCILAB (MATLAB toolbox and EEGLAB plugin) [20]. The selected features were concatenated, and two machine learning models, i.e. logistic regression model and LDA, were trained on the selected features, in order to classify the left and right foot KMI tasks. The single-trial classification accuracies used in the training and testing data were validated using 10-fold cross validations for session-to-session transfer with all participants. After testing FBCSP with Logreg and LDA, the resulting accuracy rates were compared to the rates obtained from basic CSP algorithm with Logreg and LDA. The classification performance of each algorithm was statistically evaluated using Cohen's kappa coefficient κ. With the highest average percentage accuracy of 70.28 ± 4.23, to discriminate between left and right foot KMI, FBCSP-LDA surpassed remaining algorithms, yielding a mean kappa value of 0.41 across all nine participants. This was followed by no experience of BCI protocol in advance, by any participant.

2. Materials and Methods:

2.1 Participants

This study involved nine healthy participants, with no history of neurological disorder, or any impairment, aged between 21-28 years, who voluntarily participated in the experiments. The participants had no BCI experience either. Ethics approval for the study was granted by the CHEAN (College Human Ethics Advisory Network) of RMIT University, Melbourne, Australia.

Participants were seated in a comfortable chair and were directed to watch a monitor (17'') from a distance of approximately 1.5 m. To avoid the possibility of any proprioceptive signals due to muscle movement, a flat wooden sheet was placed underneath the feet of participants. Hence both legs were

loosely fixed, with the knees flexed at 60° from full extension position, and ankles at neutral position. In the experiment, participants were directed to dorsiflex their foot approximately 25° for 1 second, analogous to the normal walking gait measurements [26].

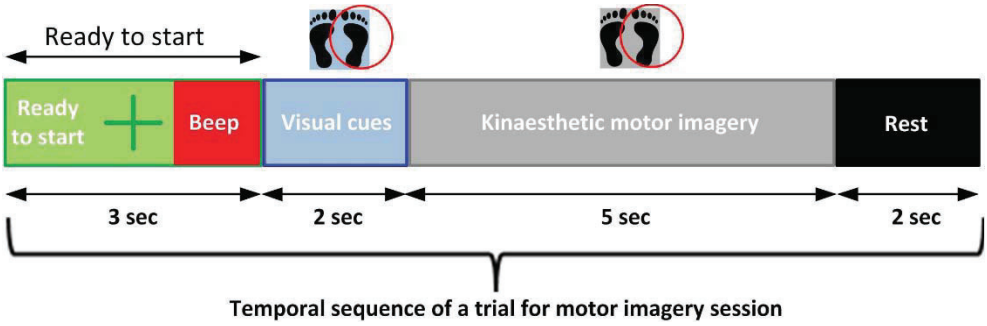

Figure 1 The temporal sequence of a trial for foot kinaesthetic motor imagery session followed in the experiment.

2.2 Cortical activity recording

The EEG signal was recorded from 19 scalp electrodes, using neurofeedback BrainMaster Discovery 24E amplifier (BrainMaster Technologies Inc., Bedford, USA); referenced to the linked earlobes A1 and A2 [9]. To acquire EEG signal from the motor cortex, an electrocap with mounted electrodes (C3, C4, Cz, F3, F4, F7, F8, Fz, FP1, FP2, O1, O2, P3, P4, Pz, T3, T4, T5, T6), positioned according to the international 10-20 system [27] was used. Monopolar EEG was amplified and bandpass filtered in the frequency range of 1-100 Hz. All channels were sampled at 256 Hz and quantised with 24-bit resolution with ground electrode located near the forehead of participants. Experimental protocol was designed using OpenViBE designer tool that comes with integrated feature boxes [28, 29].

2.3 Foot motor tasks

Four cue-based sessions were performed without feedback. Each session comprised of 40 trials, with 20 trials for left foot and 20 trials for right foot KMI in a random order. This led to 80 repetitions for each foot KMI task. Prior to the four cue-based KMI sessions, a motor-task practice session, without imagery, was conducted for the participants, in which they dorsiflexed each foot approximately 25° for 1 second (nominal walking gait) post cue. Following this, the KMI sessions were conducted.

In the experimental paradigm as shown in **Fig. 1**, each trial was initiated with presentation of a fixation cross on screen for 3 seconds, used as reference period for processing of epochs. An audio beep of one second, right before the visual cue display, was incorporated in the first trial only, to let the participant pay attention. The temporal sequence of 1 trial is given in **Fig. 1**. Next, the visual cues were displayed for 2 seconds, followed by the display of a blank screen (black), 5 seconds in length, for MI task performance. This made a total of 10 seconds for each trial. Following this, a random (pause) interval of 1.5-3.5 seconds at the end of each trial was incorporated, to prevent fatigue. The

visual cues in each trial reflected, either the right, or left foot dorsiflexion image with an arrow pointing in the respective direction. Both cues were displayed in a random order to avoid any adaptation. After recording, EEG signals were processed offline using MATLAB R2013b and BCILAB https://github.com/sccn/BCILAB .

2.4 Feature extraction using CSP and FBCSP

The filter bank common spatial pattern (FBCSP) has four stages involved in signal processing and machine learning, as illustrated in **Fig. 2**, adapted from [30]. First, a filter bank that decomposes EEG into multiple frequency pass bands using Chebyshev Type II filter is used. In this case a total of 3 bandpass filters are deployed, 8-12, 13-25, 28-32, covering ranges of *mu* and *beta* rhythms. Second stage involved spatial filtering using CSP algorithm. Third stage was the CSP feature selection, and finally the classification of these features based on the left vs. right foot KMI tasks. The CSP projection matrix for each filter band, discriminative CSP features, and classifier model are computed from the labelled training data (2-class KMI tasks). Parameters, computed from the training phase, are then used for the testing phase, and finally for the prediction of the single-trial KMI task.

We have initially deployed the common spatial pattern (CSP) method for 2-class discrimination of foot KMI tasks. Based on literature [19] it was demonstrated that, for improving the signal-to-noise ratio, spatial filters overall are useful in single-trial analyses. CSP algorithm transforms the observed EEG signal as:

$$\mathbf{S}_{b,j} = \mathbf{W}_b^T \mathbf{E}_{b,j} \tag{1}$$

where $\mathbf{E}_{b,j} \in \mathbb{R}^{s \times t}$ is the observed single-trial EEG signal from the *b*th bandpass filter (between 7-35 Hz) of the *j*th trial, $j = 1 \ldots n$, where *n* is the number of training trials.

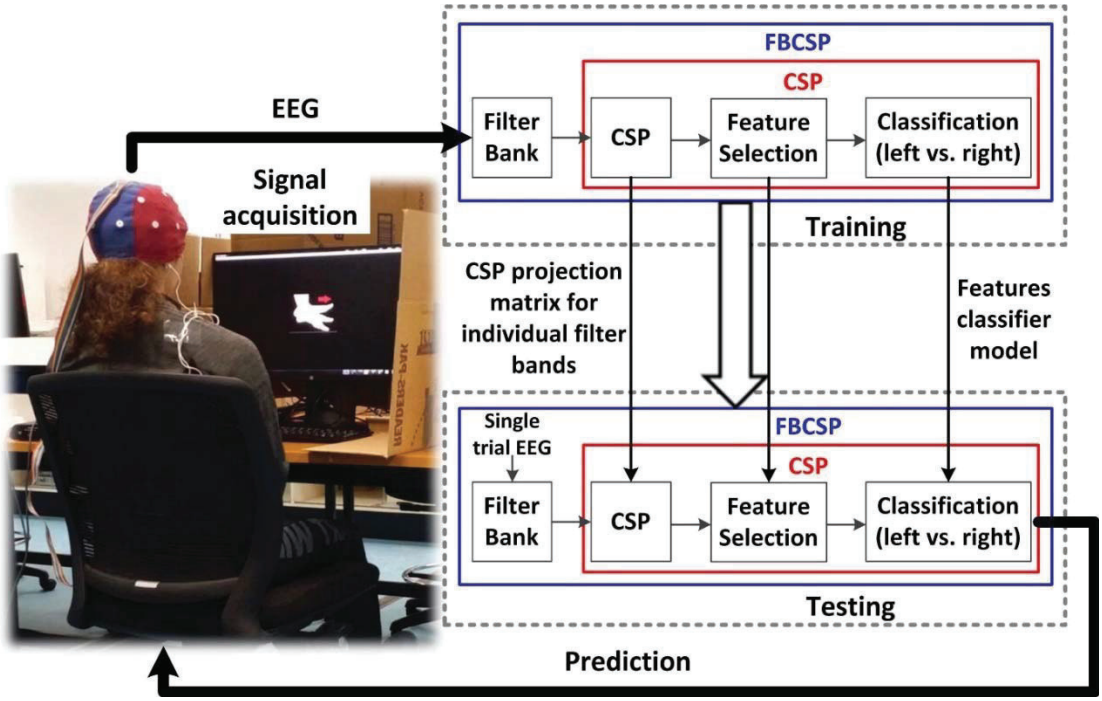

Figure 2 Experimental setup reflecting the methodology of common spatial pattern (CSP) and filter bank CSP (FBCSP) algorithms for training, testing and prediction.

$\mathbf{W}_b$ is the un-mixing matrix (CSP projection matrix) and $\mathbf{S}_{b,j}$ is the recovered single-trial sources after spatial filtering, and T denotes transpose operator. The CSP filter computes the un-mixing matrix $\mathbf{W}_b$ in order to yield features that have optimal variances for discriminating the classes of measured EEG signal [15, 19, 31], in this case two classes. This is achieved by resolving the eigenvalue decomposition problem.

$$\Sigma_{b,1}\mathbf{W}_b = (\Sigma_{b,1} + \Sigma_{b,2})\mathbf{W}_b\mathbf{D}_b \tag{2}$$

where $\Sigma_{b,1}$ and $\Sigma_{b,2}$ are the estimates of the covariance matrices of b-th bandpass filtered EEG signal based on two imagery tasks i.e. left and right foot movement. The diagonal matrix $\mathbf{D}_b$ consists of the eigenvalues of $\Sigma_{b,1}$, and the column vectors of $\mathbf{W}_b{}^{-1}$ are the filters for CSP projections. For best results, most suitable contrast is provided by filters with the highest and lowest eigenvalues. It is therefore common to retain e eigenvectors from both ends of the eigenvalue spectrum [19]. We used the MATLAB toolbox BCILAB https://github.com/sccn/BCILAB for algorithm implementation. Time window was kept [0 4], whereas for CSP algorithm we used the finite impulse response (FIR) filter for a frequency window of [7 8 32 35].

The CSP filter was applied for a left vs. baseline and right vs. baseline for each band, in the time segment starting after the cue presentation i.e. task performance duration of 5 seconds. Furthermore $e = 2$ eigenvectors from the top and from the bottom of the eigenvalue spectrum were retained. This

method was implemented on the pre-processed training dataset, that yielded the un-mixing matrix $\mathbf{W}_b \in \mathbb{R}^{s\times c}$ and source signals $\mathbf{S}_{b,j} \in \mathbb{R}^{s\times t}$, where $s = 2 \times e \times 3\ (frequency\ bands) \times 2(classes)$ is the number of sources i.e. the CSP projections, c is the number of channels, the number of time samples is t and $j = 1 \ldots n$, here n is the number of trials of training sets.

When the spatial filtered signal $\mathbf{S}_{b,j}$ from (1) uses $\mathbf{W}_b$ from (2), it maximizes the difference in variance of the two classes of bandpass filtered EEG signal. The *m* pairs of CSP features of *j*-th trial for *b*-th band-pass filtered EEG signal are given by:

$$\mathbf{v}_{b,j} = \log \frac{\mathrm{diag}\left(\bar{\mathbf{W}}_b^T \mathbf{E}_{b,j} \mathbf{E}_{b,j}^T \bar{\mathbf{W}}_b\right)}{\mathrm{tr}\left[\bar{\mathbf{W}}_b^T \mathbf{E}_{b,j} \mathbf{E}_{b,j}^T \bar{\mathbf{W}}_b\right]} \tag{3}$$

where $\mathbf{v}_{b,j} \in \mathbb{R}^{2m}$; $\bar{\mathbf{W}}_b$ signifies the first *m* and the last *m* columns of $\mathbf{W}_b$; $\mathrm{diag}(.)$ returns the diagonal elements of the square matrix; $\mathrm{tr}[.]$ returns the sum of diagonal elements in the square matrix [30].

Consequently, the FBCSP feature vector for the *j*-th trial is formulated as:

$$\mathbf{v}_j = \left[\mathbf{v}_{1,j}, \mathbf{v}_{2,j}, \mathbf{v}_{3,j}\right] \tag{4}$$

where $\mathbf{v}_j \in \mathbb{R}^{1\times(3*2m)}$, $j = 1,2, \ldots, n$; n represents the total number of trials in data.

The training data, that comprised extracted feature data, is given as (5) and the true class labels is denoted as (6), in order to make a difference from the testing and prediction data,

$$\bar{\mathbf{V}} = \begin{bmatrix} \bar{\mathbf{v}}_1 \\ \bar{\mathbf{v}}_2 \\ . \\ . \\ . \\ \bar{\mathbf{v}}_{n_t} \end{bmatrix} \tag{5}$$

$$\bar{\mathbf{y}} = \begin{bmatrix} \bar{\mathbf{y}}_1 \\ \bar{\mathbf{y}}_2 \\ . \\ . \\ . \\ \bar{\mathbf{y}}_{n_t} \end{bmatrix} \tag{6}$$

where $\bar{\mathbf{V}} \in \mathbb{R}^{n_t\times(3*2m)}$; $\bar{\mathbf{y}} \in \mathbb{R}^{n_t\times 1}$; and $\bar{\mathbf{v}}_j$; and $\bar{\mathbf{y}}_j$ are the feature vector and true class label respectively, from the *j*-th training trial, $j = 1,2, \ldots, n_t$; where n_t represents the total number of trials in training data [30].

2.5 Performance evaluation

This study uses the synchronous i.e. cue-based BCI protocol, therefore a traditional linear discriminant analysis (LDA) was used to measure classification accuracy, as recently reported [32] both for CSP and FBCSP features, respectively. However, in order to enhance the classification accuracy outcome of LDA, we deployed the logistic regression (Logreg), a supervised machine learning model for both features.

We deployed the cross validation method to estimate the optimal parameters for the classifiers and avoid overfitting classifiers to the training data [33]. The k-fold cross validation estimates the true performance of machine learning model. Classification with each model, for correctly discriminated trials, was performed with 10-fold cross-validation. For each participant data, we partitioned all motor imagery trials into $\mathrm{k} = 10$ folds of equal size, then using $\mathrm{k} - 1$ part as a training set and checking the classification rate on one remaining part (testing set) for prediction accuracy. This is repeated for k times (folds). Consequently, the weight vectors and accuracy on each fold is estimated by calculating the average k classification rates obtained for k testing sets [34]. Feature scaling (regularization) was performed on the training and test sets. The mean and standard deviation of each classifier output was determined. Our proposed methodology resulted in four combinations of models, i.e. CSP-LDA, CSP-Logreg, FBCSP-LDA, and FBCSP-Logreg.

For machine learning based studies, the performance measure of classification model is an essential task. We utilized the area under the receiver operator characteristic curve (AUC-ROC curve). The ROC curve is plotted with the true positive rate (TPR) against the false positive rate (FPR) at various threshold settings that illustrates the diagnostic ability of a binary classifier. It is a probability-curve and AUC signifies the degree of separability/distinguishing between classes [35]. In ROC, along x-axis lies the sensitivity, called true positive rate (TPR):

$$\mathrm{TPR} = \frac{\mathrm{TP}}{\mathrm{TP+FN}}, \tag{7}$$

where TP is the number of true positives and FN is the number of false negatives. Along y-axis lies 1-specificity, also termed the false positive rate (FPR):

$$\mathrm{FPR} = 1 - \mathrm{Specificity} = \frac{\mathrm{FP}}{\mathrm{TN+FP}}, \tag{8}$$

where FP is the number of false positives and TN is the number of true negatives. With a higher AUC, model is better at predicting 0s as 0s and 1s as 1s, i.e. distinguishing between left foot KMI and right foot KMI. Ideally, the AUC =1.

In addition to this, we statistically evaluated the performance of the classifiers, as a measure of distinctiveness between the two classes, by using Cohen's kappa coefficient κ [36, 37]. In our study of 2-class problem, the evaluation of the classifier is defined by its confusion matrix *H,* that describes the relationship between the true classes and observed output of the classifier. Given *H*, the classification accuracy ACC (overall agreement) is given as:

$$ACC = p_o = \frac{1}{N}\sum_i H_{ii} \tag{9}$$

The chance expected agreement is given as:

$$p_e = \frac{\sum_i n_{oi} n_{io}}{NN}, \tag{10}$$

where $N = \sum_i \sum_j H_{ij}$ is the number of samples, H_{ij} are the elements of confusion matrix H on the main diagonal, whereas n_{oi} and n_{io} are the sums of each column and row, respectively. Therefore, the estimate of kappa coefficient κ is given as:

$$\kappa = \frac{p_o - p_e}{1 - p_e}, \tag{11}$$

with the chance probability $p_e = \frac{1}{M}$ [38].

2.5.1 Test-statistic and family-wise error rate correction

In order to statistically evaluate and compare the outputs of proposed models, two independent samples *t*-test were conducted on the two groups of each feature (CSP and FBCSP), across participants. The *p*-values were used for comparisons, to direct towards the statistically significant features. Multiple comparison corrections were done using the Bonferroni correction, for *p*-values adjustment.

The observed *p*-values obtained from LDA and Logreg classifier models were corrected for CSP and FBCSP features, respectively as shown in the schematic below.

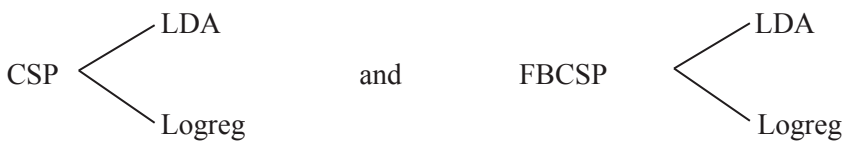

Results from LDA model were compared to Logreg model for CSP feature; similarly results from LDA were compared to those from Logreg for FBCSP. To calculate the family-wise error rate (12) is used, from [39].

$$\alpha_{FW} = 1 - (1 - \alpha_{PC})^c, \tag{12}$$

where α_{FW} is the family wise error rate, α_{PC} is the indicated per comparison error rate, and c is the number of comparisons performed. In this research, $\alpha_{PC} = 0.05$, with two statistical analyses conducted on the same sample of data, $c = 2$, the Bonferroni correction is given by (13).

$$\frac{\alpha_{PC}}{c} \tag{13}$$

Any observed *p*-value less than the corrected *p*-value of 0.025 is confirmed to be statistically significant.

3. Results

During the experimental trials, all participants successfully performed the tasks, as per instructions. There was no report from any participant about fatigue or anxiety during experiment.

3.1 Common spatial pattern scalp projections

As the anatomical properties of cortical folding between people are different [40, 41], the areas of maximum discrimination power for the ERD/ERS characteristic of foot movement and MI during experiment are not strictly located beneath electrode positions C3, Cz and C4 [17]. For this reason, the CSP method generates subject-specific spatial filters that are optimized for discrimination among the two experimental tasks. It spatially filters the raw EEG channels to smaller time-series, whose variances are optimized to discriminate the two classes, i.e. left foot KMI and right foot KMI.

For each participant a 3-pair set of CSP scalp projections were generated, however to save space, the **Fig. 3** illustrates a 3-pair set of CSP scalp projections generated for one participant, P01. Each CSP filter contains 2 patterns that illustrate how the signal projects to scalp through training data generated by FBCSP. During right and left foot KMI tasks, CSP pattern 1 reflects the time invariant EEG source distribution vectors i.e. the sensorimotor area activation around channel C3, this confirms the cortical lateralization of ERD/ERS. Similarly, the CSP pattern 3 elicits the contralateral dominance at channel C4, whereas, the pattern 2 is focused at the vertex (Cz). The CSP patterns 1 and 3 are concentrated in the contralateral hand area representation of the cortex. On the contrary CSP pattern 2 is centrally-focused around the vertex of sensorimotor cortex which is the foot area representation, as established by [5].

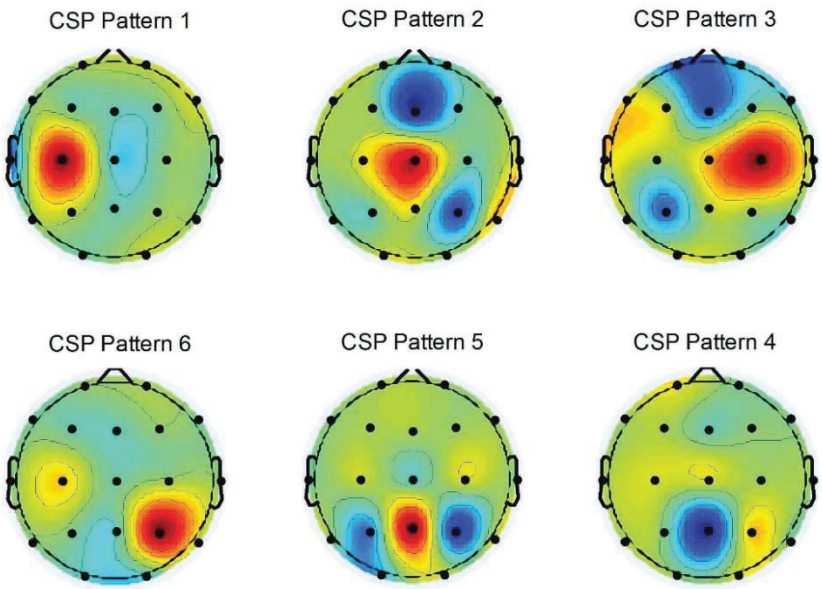

Figure 3 A set of common spatial patterns (CSPs) filters of participant P01, where CSPs are optimized for the discrimination of right and left foot kinaesthetic motor imageries with respect to reference period.

3.2 Classification accuracy and KMI task discrimination

While in general, the CSP scalp projections clearly revealed the discrimination of left-right foot imageries, there were cases where the projections did not exhibit strong left-right difference. Nevertheless, even if a slight left-right difference is shown by the BCI user, it is probable to enhance the difference and increase the control accuracy of BCI using machine learning [10].

Table 1, illustrates the misclassification rate (mcr) for nine participants using two feature vectors, and applying two different machine learning models on each feature vector individually. We began with the CSP features, in order to compare the results with FBCSP features. The CSP features were used for training and testing LDA model first. Following this, the Logreg was trained and tested. Both models resulted in prediction of misclassification rates (in percentage) for each participant. Similar approach was used for the FBCSP feature vector. In all four cases, models were cross-validated using 10-folds, for training and testing data. Majority of the participants performed above the statistical chance level of ≥ 60% for $p < 0.01$ with both classifiers. Remaining performances exceeded the chance level of ≥ 57.5% for $p < 0.05$. Participant, P01 performed the best amongst all with the lowest mcr in case of FBCSP-LDA = 22.50% and in case of CSP-Logreg = 25.00%. The average mcr for nine participants with CSP-LDA was 33.89 ± 3.56, with CSP-Logreg it was 36.94 ± 4.81, with FBCSP-LDA it was 29.72 ± 4.23, and with FBCSP-Logreg came out to be 35.83 ± 3.31. This implies that average classification accuracies of all models are clearly well above the chance level of a 2-class discrimination BCI problem which according to [42], should be 57.5% ($p < 0.05$) or 60.0% ($p < 0.01$) for a total of 80 trials.

Table 1 The 10-fold cross-validation performance of misclassification rate using CSP and FBCSP with linear discriminant analysis (LDA) and logistic regression (Logreg) classifiers.

Participant	CSP		FBCSP	
	LDA mcr (%)	Logreg mcr (%)	LDA mcr (%)	Logreg mcr (%)
P01	27.50**	25.00**	22.50**	30.00**
P02	32.50**	37.50**	25.00**	32.50**
P03	35.00**	40.00**	30.00**	35.00**
P04	37.50**	40.00**	27.50**	35.00**
P05	30.00**	37.50**	30.00**	40.00**
P06	32.50**	35.00**	30.00**	37.50**
P07	37.50**	37.50**	35.00**	40.00**
P08	35.00**	40.00*	32.50**	35.00*
P09	37.50*	40.00**	35.00**	37.50*
Average	33.89	36.94	29.72	35.83
S.D.	3.56	4.81	4.23	3.31

* Over chance level of 2-class discrimination, 57.50% ($p < 0.05$).
** Over chance level of 2-class discrimination, 60.00% ($p < 0.01$).

The area under ROC curve (AUC) for each participant is shown in **Fig. 4**, where x-axis denotes the FPR and y-axis denotes the TPR. The dark blue curve represents the CSP-Logreg output, green represents FBCSP-Logreg, yellow-chartreuse curve reflects CSP-LDA, and maroon curve represents FBCSP-LDA. In all graphs the grey line signifies the 50% chance level for the binary classifier. For ideal detection AUC should be 1. As discussed earlier, "the chance level of a 2-class discrimination BCI problem should be above or equal to 57.5% ($p < 0.05$) or 60.0% ($p < 0.01$)". In each case it is evident that the participants obtained the four respective AUCs above the chance level. From Table 2, it can be realized that participant P01 exhibited maximum AUC of 0.74 with CSP-Logreg, followed by AUC=0.73 with CSP-LDA. The maximum average AUC in case of CSP was with LDA, i.e. 0.62 ± 0.06, in case of FBCSP, it was with LDA as well, i.e. 0.64 ± 0.04.

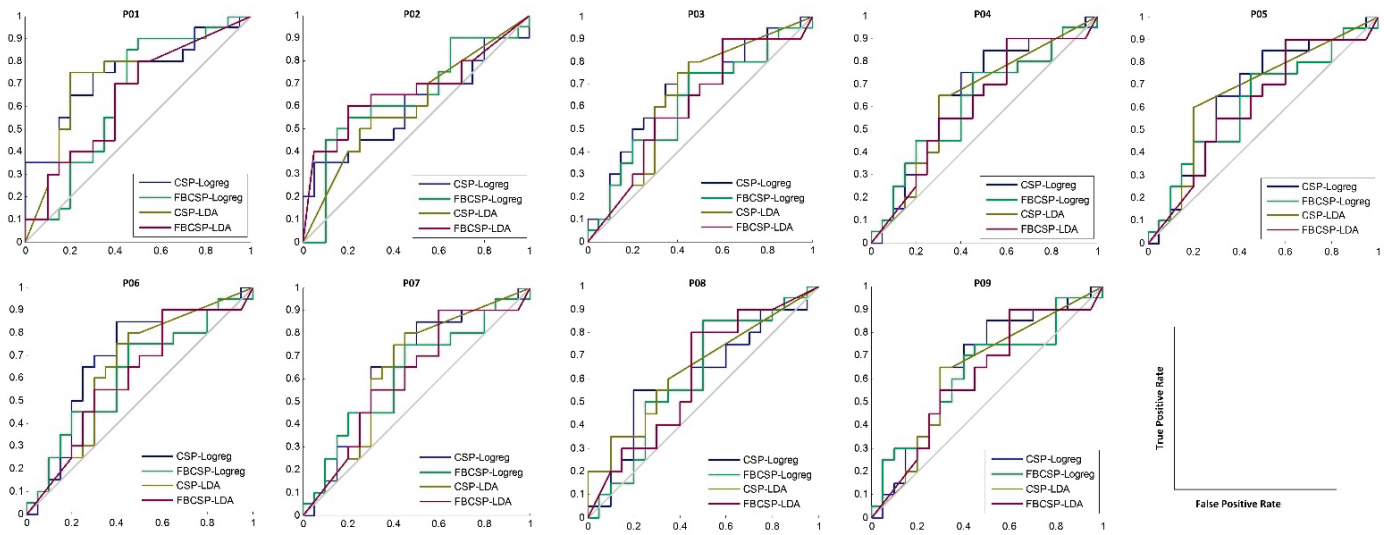

Figure 4 Receiver operator characteristics curves reflecting area under the curves for all participants.

FBCSP overall exhibited maximum average AUC amongst the four deployed models, although the average AUC difference amongst all the models was not much.

Table 2 also projects the kappa statistic scores. During study, it is observed that all kappa scores are above chance level ($\kappa = 0$). The average scores range between fair and moderate performance, based on the study from [43]. This implies that in the 0.21-0.40 range, the strength of agreement between the predicted and true class is fair, whereas between 0.41-0.60 it is moderate.

Importantly there is not much difference between average scores of CSP-Logreg and FBCSP-Logreg, given as 0.26, and 0.28, respectively. The maximum score was obtained for participant P01, using FBCSP-LDA i.e. 0.55. Similarly, FBCSP-LDA score surpassed remaining models with the maximum average score of 0.41 in discriminating between the two classes.

Table 2 The 10-fold cross-validation performance in terms of maximum kappa value and the Area under ROC Curve (AUC) using CSP and FBCSP with Linear discriminant analysis (LDA) and logistic regression (Logreg) models.

Participant	CSP				FBCSP			
	LDA		Logreg		LDA		Logreg	
	AUC	κ	AUC	κ	AUC	κ	AUC	κ
P01	0.73	0.45	0.74	0.50	0.70	0.55	0.65	0.40
P02	0.65	0.35	0.67	0.25	0.63	0.50	0.56	0.35
P03	0.65	0.30	0.61	0.20	0.61	0.40	0.61	0.30
P04	0.59	0.25	0.57	0.20	0.64	0.45	0.67	0.30
P05	0.61	0.40	0.62	0.25	0.67	0.40	0.64	0.20
P06	0.62	0.35	0.60	0.30	0.68	0.40	0.70	0.25
P07	0.60	0.25	0.59	0.25	0.61	0.30	0.55	0.20
P08	0.56	0.30	0.55	0.20	0.65	0.35	0.56	0.30
P09	0.55	0.25	0.57	0.20	0.56	0.30	0.55	0.25
Average	0.62	0.32	0.61	0.26	0.64	0.41	0.61	0.28
S.D.	0.06	0.07	0.06	0.10	0.04	0.09	0.06	0.07

We therefore can clearly state that FBCSP feature with LDA gave the best 2-class discrimination accuracy than the other feature models exceeding the chance level 60% at $p < 0.01$, with highest AUC and κ as shown in **Fig. 5**. On average LDA classifier outperformed Logreg with FBCSP, but in case of CSP feature vector, both models resulted in a close average accuracy with a difference of approximately 3%. From **Fig. 6**, individual participant performance can be viewed for each model; it can be observed that P01 exhibited minimum mcr comparatively.

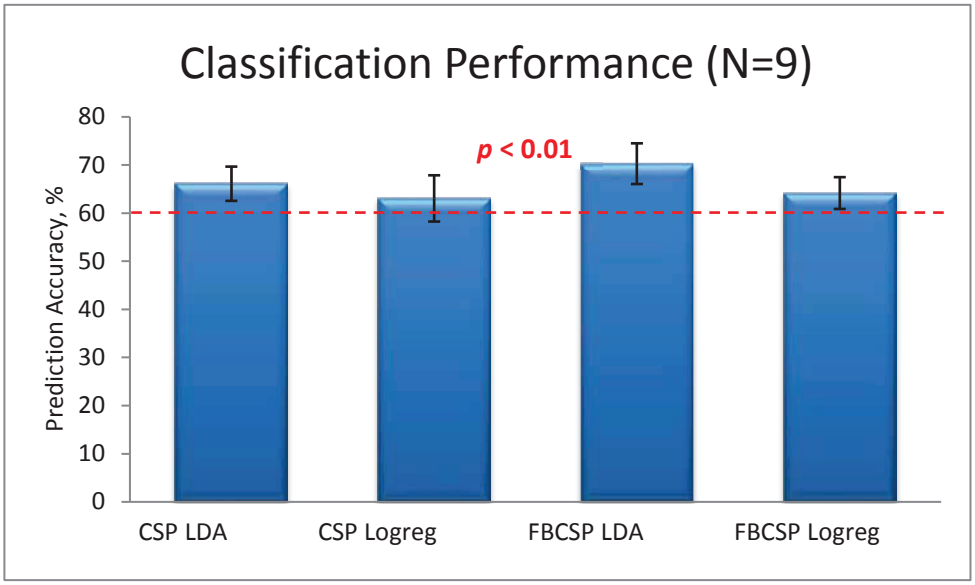

Figure 5 Average classification accuracies (in percentage) for each algorithm across participants, red dotted line shows average on and above chance level (p <0.01). The error bars represent standard deviations.

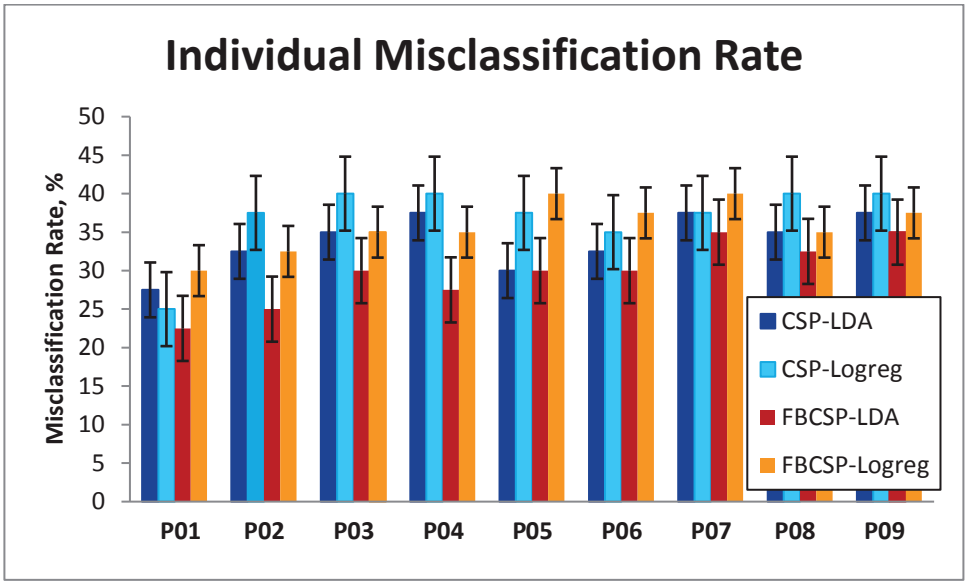

Figure 6 Resulting misclassification rate (in percentage) of CSP-LDA, CSP-Logreg, FBCSP-LDA, and FBCSP-Logreg algorithms for individual participant (N=9). The error bars represent standard deviations.

4. Discussion

In the research reported here, we have analysed *mu* and *beta* EEG features, using the CSP and FBCSP feature extraction methods, following machine learning to classify the left foot and right foot KMI. The proposed models deployed LDA and Logreg algorithms for discrimination of left and right foot KMI tasks. We used the CSP filter patterns for analysis of time invariant EEG source distribution vectors, that elicit upon visual cues i.e. cue-based synchronous BCI (Graz BCI protocol). Overall the

CSP patterns implicated the cortical lateralization of ERD/ERS during the left and right foot dorsiflexion KMI. The first pair of CSP pattern, exhibited a focal time invariant EEG source distribution (ERD/surround ERS) induced by KMI at channel Cz and C3 prominent over the contralateral side than the ipsilateral side [44]. Similarly, the third pair also reflected the time invariant EEG source distribution at C4 over the contralateral side than ipsilateral. In contrast to these, the second pair showed a centrally focal ERD/surround ERS at the vertex channel Cz. From [5], it is a well-established fact that "hand motor imagery activates neural networks in the cortical hand representation area which is manifested as blocking or desynchronization of the hand area *mu* rhythm (*mu* ERD)". Also less is known about the activation of the foot area in the sensorimotor cortex during foot KMI, because it is located in the mesial wall which makes it difficult to detect it [1]. However, in recent studies that used the foot KMI, on average a mid-central *mu* ERD followed by *beta* ERS has been reported in majority, and an enhancement in the hand area *mu* rhythm (*mu* ERS) [7, 9, 10]. Our results are in accordance with the recent developed studies that used the foot KMI. To our knowledge, this study provides the first example that exploits FBCSP feature vector for discrimination of left-right foot KMI. This could be exploited by an EEG-based BCI and serve as a contribution to the field.

4.1 FBCSP-LDA model

A previous study [10] underscored that the CSP method could be used in EEG-based classification of left and right foot MI. We therefore experimented with CSP method to improve the performance of our 2-class foot KMI. Initially classical LDA was deployed, that ensued in a classification accuracy of 66.11 ± 3.56 with a kappa score of 0.32, but for the improvement, Logreg algorithm was tested and that resulted in an accuracy of 63.06 ± 4.81 with kappa score of 0.26. This pointed to a difference of approximately 3% in the results of both models, as illustrated in **Fig. 5**. The average classification accuracy of both models resulted in above the chance level of 60.0% ($p < 0.01$) for 80 trials, as described by [42], with 10-fold cross validation. However, compared to the band-power method, the accuracy was low [10]. The study therefore took into account the FBCSP procedure to further improve results obtained by CSP method. FBCSP, in conjunction with LDA and Logreg, resulted in average accuracies of 70.28 ± 4.23 and 64.17 ± 3.31, respectively with average kappa scores of 0.41 and 0.28, respectively. This implied that the maximum 2-class accuracy for left-right foot KMI was with FBCSP-LDA, using 10-fold cross validation as shown in **Fig. 5**. For the same model, participant P01 scored the highest kappa of 0.55, following maximum classification accuracy of 77.5% among other participants, as reflected in **Fig. 6**.

With the proposed FBCSP model, the selection of time and frequency regions was critical, because there are complex interactions between *mu* and *beta* bands which are seemingly rarely observed. Therefore, the frequency regions are defined elaborately in FBCSP method that results in large space dimensionality. Since FBCSP's feature space dimensionality is larger than CSP's, there is a tradeoff between more flexibility and the risk of overfitting. We therefore compared the performance of

FBCSP with the standard CSP [16] and used the family-wise error rate. For multiple comparison corrections, the Bonferroni correction was deployed. Consequently, adjusted *p*-values are used in the study. According to [45], larger number of training trials and longer length of the experimental trial could prevent overfitting. Following this, it is overall observed that a tradeoff also exists between the classifier models and feature vector strategy, i.e. if FBCSP-LDA performs high, CSP-LDA performs lower, and similarly if FBCSP-Logreg performs better, CSP-Logreg elicited a lower performance.

Some closely related methods for EEG feature optimization and classification based on MI have recently been reported. Zhichao Jin, et al. [46] proposed a sparse Bayesian extreme learning machine (SBELM)-based algorithm to improve the classification performance of MI based BCI. The method "automatically controls the model complexity and excludes redundant hidden neurons by combining advantages of both ELM and sparse Bayesian learning". In another recent review [47], authors compared the traditional classification methods with deep learning techniques. With a comprehensive analysis they concluded that "deep learning not only enables to learn high-level features automatically from BCI signals, but also depends less on manual-crafted features and domain knowledge". For EEG-based BCI studies that deploy MI, discriminative models such as, multi-layer perceptron (MLP), recurrent neural networks (RNN), or convolutional neural networks (CNN), overall elicit highest classification accuracies in BCI applications.

Further useful methods include a sparse group representation model (SGRM) for increasing the efficiency of MI-based BCI, presented lately [48]. Using CSP features, a dictionary matrix is constructed with training samples from both the target and other subjects. The optimal representation of a test sample of the target subject is estimated as a linear combination of columns in the dictionary matrix, by exploiting within-group and group-wise sparse constraints. Consequently, classification is done by calculating the class-specific representation based on the significant training samples corresponding to the nonzero representation coefficients. This effectively reduces the required training samples from target subject because of auxiliary data available from other subjects. Using left vs. right hand MI, their study depicted a kappa score of 0.57 and 0.55 for two datasets respectively. Recently, a novel algorithm, temporally constrained sparse group spatial pattern (TSGSP) has been presented [49]. It concurrently optimizes filter bands and time-windows within CSP in order to enhance EEG based MI classification. Their classification results were 88.5%, 83.3%, and 84.3%, for 4-class MI left hand, right hand, feet, tongue, for 2-class MI left vs. right hand, and for 4-class MI left hand, right hand, foot, tongue, respectively.

4.2 Band-power feature for classification

The band power or time-frequency method has successfully been used in numerous (offline) BCI studies based on MI [5, 7, 9, 10, 50]. This study is based on foot KMI. We therefore followed the same experimental paradigm as in the earlier studies [7, 9, 10, 13], i.e. with no prior feedback training. Contradictory to [10], the CSP method did not improve the performance of the left-right foot

KMI BCI system, however the FBCSP-LDA model improved the average performance for nine participants. Although both CSP and FBCSP resulted in classification accuracies above the statistical chance level of 60.00% ($p < 0.01$), it was less than the maximum accuracy of 81.6% in single trial analysis [10], i.e. a maximum accuracy of 77.5% was attained in our case. However, the average accuracy of band power method using LDA was 69.3% ± 6.1 [10], whereas our study resulted in improved accuracy of 70.28 ± 4.23. The maximum average kappa statistic for this study is in the 0.41<0.60 range i.e. the strength of agreement between classes is moderate [43]. Participant P01 outperformed with a kappa statistic of 0.55 which is also in the moderate range. The strength of agreement between classes needs to be more substantial, which is not in case of CSP-Logreg and FBCSP-Logreg method. This was followed by no practice (no feedback training) of BCI in advance, that could mark a difference in results [51]. As suggested by [45], larger number of training trials could also prevent overfitting and improve results.

Based on our experimental outcomes, we would suggest an alteration in the experimental protocol, i.e. it could be modified by the inclusion of feedback training, since training without feedback might be inclusive of irrelevant imageries. In future we aim at increasing the practice sessions as well. Furthermore, the suggested methodology procedures from our study could potentially be deployed by BCI systems run by multiple users, as its decoding technique could allow for the selection of optimal feature bands suitable for multiple users. The FBCSP could be exploited in combination with neural networks to investigate for an enhancement in the classification accuracy of foot KMI.

5. Conclusions

In this study, we proposed the novel approach to incorporate CSP and FBCSP in conjunction with LDA and Logreg model for the selection of significant filter bands, to improve the left-right foot KMI classification accuracy. FBCSP feature with LDA resulted in highest discrimination accuracy than the other feature models exceeding the chance level 60% at $p < 0.01$ with 10-fold cross validation and the highest κ statistic. These results encourage the classification of left-right foot KMI and can be exploited as control commands in a bionic foot-BCI operation or a foot neuroprosthesis. The left-right foot KMI discrimination results are encouraging in view of the covert anatomical representation area of foot in the human sensorimotor cortex compared to that of the hand. We next aim to monitor the repetitive use of neurofeedback training and its effects on classification accuracy.

Conflict of interest

None of the authors have potential conflicts of interest to be disclosed.

Competing interest

Authors declare no competing interests.

Acknowledgement

None.

References

1. Tariq, M., P. Trivailo, and M. Simic, *EEG-Based BCI Control Schemes for Lower-Limb Assistive-Robots.* Frontiers in human neuroscience, 2018. **12**: p. 312.
2. He, Y., et al., *Brain–machine interfaces for controlling lower-limb powered robotic systems.* Journal of neural engineering, 2018. **15**(2): p. 021004.
3. Lebedev, M.A. and M.A. Nicolelis, *Brain-machine interfaces: from basic science to neuroprostheses and neurorehabilitation.* Physiological reviews, 2017. **97**(2): p. 767-837.
4. Cervera, M.A., et al., *Brain-computer interfaces for post-stroke motor rehabilitation: a meta-analysis.* Annals of clinical and translational neurology, 2018. **5**(5): p. 651-663.
5. Pfurtscheller, G., et al., *Mu rhythm (de) synchronization and EEG single-trial classification of different motor imagery tasks.* NeuroImage, 2006. **31**(1): p. 153-159.
6. Tariq, M., P. Trivailo, and M. Simic, *Event-related changes detection in sensorimotor rhythm.* Int. Rob. Autom. J, 2018. **4**: p. 119-120.
7. Tariq, M., et al. *Mu-beta rhythm ERD/ERS quantification for foot motor execution and imagery tasks in BCI applications*. in *2017 8th IEEE International Conference on Cognitive Infocommunications (CogInfoCom)*. 2017. IEEE.
8. Tariq, M., P.M. Trivailo, and M. Simic. *Detection of knee motor imagery by Mu ERD/ERS quantification for BCI based neurorehabilitation applications*. in *2017 11th Asian Control Conference (ASCC)*. 2017. IEEE.
9. Tariq, M., et al., *Comparison of Event-related Changes in Oscillatory Activity During Different Cognitive Imaginary Movements Within Same Lower-Limb.* Acta Polytechnica Hungarica, 2019. **16**(2): p. 77-92.
10. Hashimoto, Y. and J. Ushiba, *EEG-based classification of imaginary left and right foot movements using beta rebound.* Clinical neurophysiology, 2013. **124**(11): p. 2153-2160.
11. Pfurtscheller, G. and T. Solis-Escalante, *Could the beta rebound in the EEG be suitable to realize a "brain switch"?* Clinical Neurophysiology, 2009. **120**(1): p. 24-29.
12. Lisi, G., T. Noda, and J. Morimoto, *Decoding the ERD/ERS: influence of afferent input induced by a leg assistive robot.* Frontiers in systems neuroscience, 2014. **8**: p. 85.
13. Neuper, C. and G. Pfurtscheller, *Post-movement synchronization of beta rhythms in the EEG over the cortical foot area in man.* Neuroscience letters, 1996. **216**(1): p. 17-20.
14. McFarland, D.J., et al., *Spatial filter selection for EEG-based communication.* Electroencephalography and clinical Neurophysiology, 1997. **103**(3): p. 386-394.
15. Ramoser, H., J. Muller-Gerking, and G. Pfurtscheller, *Optimal spatial filtering of single trial EEG during imagined hand movement.* IEEE transactions on rehabilitation engineering, 2000. **8**(4): p. 441-446.
16. Zhang, Y., et al., *Optimizing spatial patterns with sparse filter bands for motor-imagery based brain–computer interface.* Journal of neuroscience methods, 2015. **255**: p. 85-91.
17. Rozado, D., A. Duenser, and B. Howell, *Improving the performance of an EEG-based motor imagery brain computer interface using task evoked changes in pupil diameter.* PloS one, 2015. **10**(3): p. e0121262.
18. Xygonakis, I., et al., *Decoding Motor Imagery through Common Spatial Pattern Filters at the EEG Source Space.* Computational intelligence and neuroscience, 2018. **2018**.
19. Blankertz, B., et al., *Optimizing spatial filters for robust EEG single-trial analysis.* IEEE Signal processing magazine, 2008. **25**(1): p. 41-56.
20. Kothe, C.A. and S. Makeig, *BCILAB: a platform for brain–computer interface development.* Journal of neural engineering, 2013. **10**(5): p. 056014.

21. Higashi, H. and T. Tanaka, *Simultaneous design of FIR filter banks and spatial patterns for EEG signal classification.* IEEE transactions on biomedical engineering, 2013. **60**(4): p. 1100-1110.
22. Dornhege, G., et al., *Combined optimization of spatial and temporal filters for improving brain-computer interfacing.* IEEE transactions on biomedical engineering, 2006. **53**(11): p. 2274-2281.
23. Lemm, S., et al., *Spatio-spectral filters for improving the classification of single trial EEG.* IEEE transactions on biomedical engineering, 2005. **52**(9): p. 1541-1548.
24. Thomas, K.P., et al., *A new discriminative common spatial pattern method for motor imagery brain–computer interfaces.* IEEE Transactions on Biomedical Engineering, 2009. **56**(11): p. 2730-2733.
25. Ang, K.K., et al. *Filter bank common spatial pattern (FBCSP) in brain-computer interface*. in *2008 IEEE International Joint Conference on Neural Networks (IEEE World Congress on Computational Intelligence)*. 2008. IEEE.
26. Tariq, M., Z. Koreshi, and P. Trivailo. *Optimal control of an active prosthetic ankle*. in *Proceedings of the 3rd International Conference on Mechatronics and Robotics Engineering*. 2017. ACM.
27. Klem, G.H., et al., *The ten-twenty electrode system of the International Federation.* Electroencephalogr Clin Neurophysiol, 1999. **52**(3): p. 3-6.
28. Renard, Y., et al., *Openvibe: An open-source software platform to design, test, and use brain–computer interfaces in real and virtual environments.* Presence: teleoperators and virtual environments, 2010. **19**(1): p. 35-53.
29. Tariq, M., P.M. Trivailo, and M. Simic, *Motor imagery based EEG features visualization for BCI applications.* Procedia computer science, 2018. **126**: p. 1936-1944.
30. Ang, K.K., et al., *Filter bank common spatial pattern algorithm on BCI competition IV datasets 2a and 2b.* Frontiers in neuroscience, 2012. **6**: p. 39.
31. Blankertz, B., et al., *The Berlin Brain-Computer Interface: Accurate performance from first-session in BCI-naive subjects.* IEEE transactions on biomedical engineering, 2008. **55**(10): p. 2452-2462.
32. Lotte, F., et al., *A review of classification algorithms for EEG-based brain–computer interfaces: a 10 year update.* Journal of neural engineering, 2018. **15**(3): p. 031005.
33. Mitchell, T.M., *Machine learning*. 1997, McGraw hill.
34. Yong, X. and C. Menon, *EEG classification of different imaginary movements within the same limb.* PloS one, 2015. **10**(4): p. e0121896.
35. Tharwat, A., *Classification assessment methods.* Applied Computing and Informatics, 2018.
36. Kraemer, H.C., *Kappa coefficient.* Wiley StatsRef: Statistics Reference Online, 2014: p. 1-4.
37. Lotte, F., et al., *A review of classification algorithms for EEG-based brain–computer interfaces.* Journal of neural engineering, 2007. **4**(2): p. R1.
38. Cohen, J., *A coefficient of agreement for nominal scales.* Educational and psychological measurement, 1960. **20**(1): p. 37-46.
39. Tamhane, A. and D. Dunlop, *Statistics and data analysis: from elementary to intermediate.* 2000.
40. DeFelipe, J., *The evolution of the brain, the human nature of cortical circuits, and intellectual creativity.* Frontiers in neuroanatomy, 2011. **5**: p. 29.
41. Mueller, S., et al., *Individual variability in functional connectivity architecture of the human brain.* Neuron, 2013. **77**(3): p. 586-595.
42. Müller-Putz, G., et al., *Better than random: a closer look on BCI results.* International Journal of Bioelectromagnetism, 2008. **10**(ARTICLE): p. 52-55.
43. Landis, J.R. and G.G. Koch, *The measurement of observer agreement for categorical data.* biometrics, 1977: p. 159-174.

44. Neuper, C., M. Wörtz, and G. Pfurtscheller, *ERD/ERS patterns reflecting sensorimotor activation and deactivation.* Progress in brain research, 2006. **159**: p. 211-222.
45. Huang, G., et al., *Model based generalization analysis of common spatial pattern in brain computer interfaces.* Cognitive neurodynamics, 2010. **4**(3): p. 217-223.
46. Jin, Z., et al., *EEG classification using sparse Bayesian extreme learning machine for brain–computer interface.* Neural Computing and Applications, 2018: p. 1-9.
47. Zhang, X., et al., *A Survey on Deep Learning based Brain Computer Interface: Recent Advances and New Frontiers.* arXiv preprint arXiv:1905.04149, 2019.
48. Jiao, Y., et al., *Sparse group representation model for motor imagery EEG classification.* IEEE journal of biomedical and health informatics, 2018. **23**(2): p. 631-641.
49. Zhang, Y., et al., *Temporally constrained sparse group spatial patterns for motor imagery BCI.* IEEE transactions on cybernetics, 2018. **49**(9): p. 3322-3332.
50. Liu, Y.-H., et al., *Analysis of electroencephalography event-related desynchronisation and synchronisation induced by lower-limb stepping motor imagery.* Journal of Medical and Biological Engineering, 2019. **39**(1): p. 54-69.
51. Orand, A., et al., *The comparison of motor learning performance with and without feedback.* Somatosensory & motor research, 2012. **29**(3): p. 103-110.

Chapter 7

Analysis and classification of EEG event-related (de)synchronization induced by left-right knee motor imagery for BCI applications

Chapter Overview

In addition to foot KMI, the knee KMI is inevitable in context to LL as one entity. Recent literature reveal limited studies on exploiting the left and right foot KMI as input to a BCI, and does not reflect the adoption of knee KMI as a separate cognitive task. This chapter proposes a novel cognitive task deployable in a BCI. The effect of cortical lateralization of ERD/ERS upon left and right foot KMI have been discussed in chapter 5 and 6. The aim of this chapter is to analyse the effect of cortical lateralization of ERD/ERS and measure the intensity of *beta* ERS at the end of imagination and *mu* ERD during imagination of left and right knee using the common average reference. The ML KNN model depicts classification accuracies adequate for practical implementation, i.e. 81.04% for a participant and confirms the cortical lateralization of ERD/ERS. No new area in the sensorimotor cortex was activated, except for the foot area. This provides the basis of utilization of left and right knee KMI as cognitive inputs that could be exploited as two unilateral commands for navigation control in a BCI-controlled bionic knee. Results infer the possibility to deploy the novel knee KMI as a cognitive task in a BCI paradigm.

Abstract

This research is based on the investigation of deploying left and right knee kinaesthetic motor imagery (KMI) in a synchronous BCI, and to evaluate the possibility of cortical lateralization of event-related (de)synchronization (ERD/ERS). There is no comprehensive study in literature that shows the utilization of knee KMI in a BCI, as the lower-limbs (LL) share a close spatial proximity in the sensorimotor cortex of human. This study explicitly analysed the *beta* ERS and *mu* ERD features, whose frequency bandwidth is in the range of 7-35 Hz, using the time-frequency maps, and scalp topographies. The feature vector was then classified, for 2-class classification, using machine learning models (ML). Linear SVM and weighted KNN were used, followed by the 5-fold cross validation. Each ML model was evaluated for significant outputs through area under receiver-operator characteristics (AUC-ROC) curve. Subsequently, for comparison and estimation of truly observed (statistically significant) classification accuracies from both models, the Mann-Whitney U-test was deployed. Resulting precisions reflected a maximum accuracy of 81.04% and an AUC of 0.84, with one participant, that provides a platform for further evaluation of *beta* and *mu* ERD/ERS features, to be used as individual control signals in a BCI. It could be used as control signals for actuating a LL, or knee BCI.

7.1 Introduction

Dysfunction of lower-limb(s) (LL) can halt human walking gait. This could possibly be due to the neuromotor disorder, such as spinal cord injury (SCI), or cognitive impairment, or LL amputation such as transfemoral or transtibial amputation [1]. In each of the aforementioned causes, the generation of input signal from its source i.e. brain, to compensate for the halt in a seamless manner is inevitable. Electroencephalography (EEG) is one of the most popular non-invasive modality to record electrical activity from the motor cortex (brain) in context to the control of limbs movement [2]. EEG is one of the electrophysiological signals used as input in a non-invasive brain-computer interface (BCI). The BCI is a state-of-the-art communication channel that connects the brain to an external (robotic) device for control purposes [3-6]. Non-invasive BCIs could either be dependent or independent. Visually evoked potentials are dependent BCIs, for they depend on the muscular control of gaze direction [7]. On the other hand, slow cortical potentials (SCP), P300 event-related potentials (ERPs), and oscillatory rhythms (*mu* and *beta* rhythms) are independent BCIs [3, 7]. When

deploying oscillatory rhythms in a BCI, they could either serve as input to a synchronous, or asynchronous BCI; where synchronous BCI is cue-based and asynchronous BCI is self-paced, i.e. independent of cue onset [8]. The synchronous BCI requires a cue followed by an imagination of the cue, usually limb motor activity [9].

In context to LL, literature reflects few studies that focus on the discrimination of left and right foot motor imageries. However, investigation on motor imagery of the knee extension deployed as a distinct cognitive task has not been reported. Research reported in this chapter is based on the band-power (BP) features analysis in the *mu* and *beta* rhythms, elicited upon and after left and right knee kinaesthetic motor imagery (KMI), respectively. KMI is a stealthy cognitive process which is based on the imagination of the subject's own limb movement, without any muscular intervention [10]. With oscillatory rhythms, these cognitive tasks arise in the *mu* (8-12 Hz) and *beta* (13-35 Hz) rhythms.

Consequent to the KMI task performance, BP features are elicited in the sensorimotor cortex. Patterns that characterise an imagined limb movement in the BP features are defined as event-related desynchronization (ERD) and event-related synchronization (ERS) [11]. The decrease or blocking response is referred to as ERD, whereas an increase in amplitude is referred to as ERS [12-14]. However, as the left and right LL areas in the sensorimotor cortex share close spatial proximity compared to upper limbs [15-17], it becomes difficult to discriminate between them. This is an impending reason for less literature on LL imagery tasks in BCI. Henceforth, no study on the classification of left-right knee extension KMI for subjects with lost knee function or any evidence of cortical lateralization is available [18-21].

Following the methodology paradigm of BP features from left and right foot KMI, this study exploits the *mu* ERD and *beta* ERS (post task completion) as possible EEG features for classification [12, 19, 22-24], using the common average reference. The ERD/ERS patterns corresponding to the limb movements generate in the vertex of the cortex [12]. Subsequent to the signal pre-processing and feature extraction, machine learning (ML) was instigated on the selected feature vectors. The study deployed two ML models for the 2-class classification problem based on the size and dimensions of the feature vector. Linear support vector machine (SVM) and weighted k-nearest neighbors (KNN) algorithms were taken into account [25]. KNN can prove to be efficient for BCIs that employ low dimensional feature vectors [26]. Two ML models were considered to estimate the best classification accuracy for discriminating between left and right knee KMI tasks. The *k*-fold cross validation was applied

for the single-trial classification accuracies. For statistical evaluation of ML models, the area under the receiver operator characteristic curve, (AUC-ROC) curve was used. In order to draw a comparison between the performances of ML paradigms the Mann-Whitney *U* test also termed Wilcoxon rank-sum test [27, 28] was employed, which ensured that the accuracies occurred by true observation and not by chance.

Overall, the classification of both features resulted in an accuracy above the statistical chance level of 60.0% ($p < 0.01$) for 80 trials [29], in case of SVM and KNN model respectively. Beta ERS post task, produced maximum individual accuracy of 81.04% and AUC of 0.84 for participant 5 using KNN model, similarly, the maximum average accuracy of *mu* ERD was obtained using KNN for all participants, 74.59 ± 5.1% and AUC = 0.64. This study did not include BCI practice in advance by any participant. These results are encouraging for the proposed novel cognitive task of knee KMI. It confirms the cortical lateralization of ERD/ERS during left right knee tasks, and provides basis for establishing a 2-class BCI to control a bionic knee using left-right knee KMI.

7.2 Methods

The methodology followed for this study is already explained in Chapter 3, section 3.2, 3.3, 3.4.1, 3.4.2, 3.5.2, 3.5.3, 3.6.1, 3.6.2, 3.6.5, and 3.6.8, respectively.

7.3 Results

This research is based on experiments carried out on five participants, who volunteered for the study. None of the participant gave feedback concerning fatigue during the experiments. All participants followed the synchronous BCI protocol, i.e. visual cues and executed the KMI tasks successfully.

7.3.1 Time-frequency map

The time-frequency (TF) maps resulting from BP feature vector are displayed in figure 7.1. For each participant the TF maps were individually analysed, to determine the peak latencies from cue-onset for significant/most reactive *mu* ERD and *beta* ERS features. The common average reference channel Cz was selected, as it accounts for the unilateral limb activity in the sensorimotor motor [12, 23, 30, 31]. Figure 7.1 represents all significant ERS in red, ERD in blue, whereas no change is represented in green colour. The time window is shown for one trial, from -3 to 7 seconds. Pink dotted line reflects the beginning of visual cue. During left and right knee KMI, significant *mu* ERD ($P < 0.05$) starts eliciting at the end of cue-onset

and extends till beginning of task performance session approximately 4 seconds, with an average peak latency of 2.5 seconds from cue-onset. The frequency range of its occurrence is approximately from 7 Hz to $\leq$ 13 Hz. At the end of KMI, strong *beta* ERS exhibited on average between 27 Hz to 32 Hz with average peak latency from cue onset = 4.24 seconds, ($P < 0.05$). In all five participants, prominent *mu* and *beta* features were observed. Table 7.1 depicts the individual peak latencies of participants from cue-onset as shown in figure 7.1, for selection of statistically significant ERD/ERS features in the reactive 7-35 Hz bands.

Figure 7.2 shows the grand-average amplitude of *mu* ERD and beta ERS, for all five participants at central channels C3, C4, and the vertex Cz. Statistically significant features were evaluated using Bootstrap-t statistical method ($P < 0.05$) as explained in chapter 3, section 3.4.1 and 3.6.1. Both EEG feature amplitudes exhibited left-right differences. Beta ERS reflected strong left-right amplitude difference at channel C4, followed by C3 and Cz, respectively. Similarly, for *mu* ERD, channel C4 exhibited maximum left-right amplitude difference, compared to C3 and Cz. In case of both features, contralateral dominance is visible at channels C3 and C4. However, little difference was observed in the left-right KMI amplitude at channel Cz.

Table 7.1 Individual peak latencies from cue-onset for significant *mu* ERD and *beta* ERS.

Participant	Mu ERD (7-12 Hz)		Beta ERS (13-35 Hz)	
	Latency from left- cue (s)	Latency from right- cue (s)	Latency from left- cue (s)	Latency from right- cue (s)
P1	1.92	3.05	3.95	4.20
P2	1.75	1.75	3.80	3.50
P3	2.65	2.20	3.20	4.50
P4	2.32	3.15	4.80	5.00
P5	2.50	3.25	4.50	4.90
Mean	2.23	2.68	4.05	4.42
S.D.	0.38	0.67	0.62	0.61

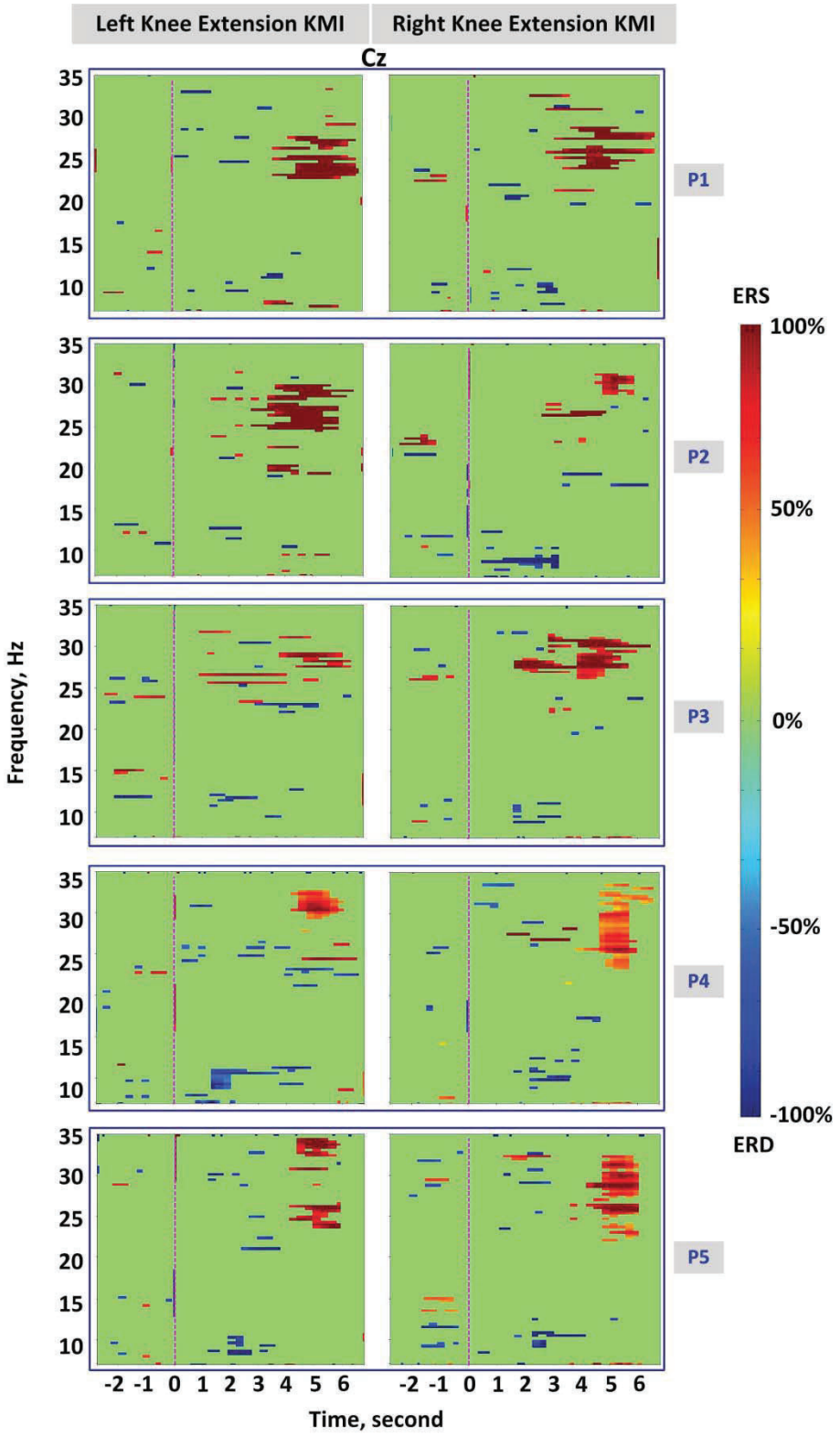

Figure 7.1 Time-frequency maps reflecting ERD/ERS of all participants. Left column shows left knee extension kinaesthetic motor imagery (KMI), and right column shows right knee extension KMI. Significant ($P < 0.05$) band-power changes are shown during the trial period of -3 to 7 s. The pink dotted line indicates the beginning of the visual cue.

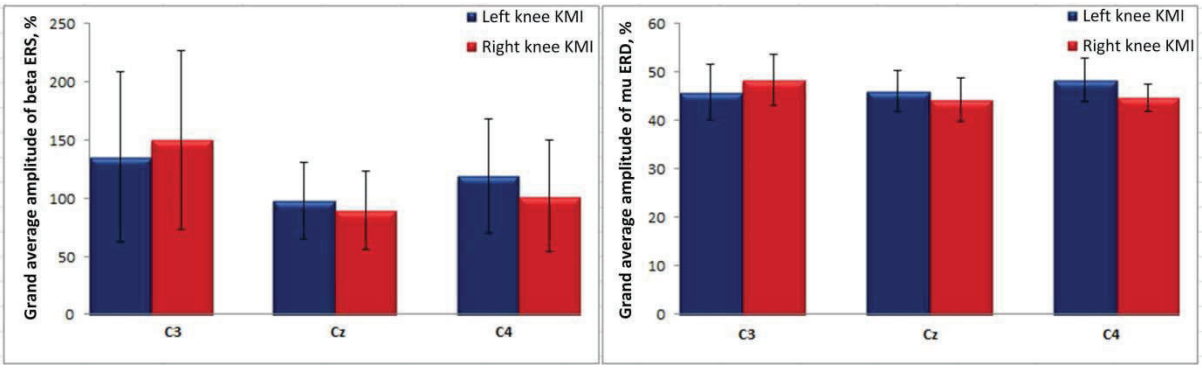

Figure 7.2 Average amplitude of *beta* ERS and *mu* ERD from five participants (N=5). Blue bars show average amplitude of respective feature after left knee task, and red bars represent right knee task. Error bars depicts the standard deviations.

7.3.2 EEG topographies

EEG topographies of *mu* ERD and *beta* ERS from participant-specific reactive bands and the time of occurrence are displayed to show the distribution on the scalp, as shown in figure 7.3. The topographies were averaged for all five participants and top view of the scalp is shown in figure 7.3. It can be seen that *mu* ERD features are located across the vertex. During right knee KMI task, *mu* ERD is prominent at channel C3, which confirms the contralateral dominance and in agreement with results obtained from section 7.3.1. During left KMI, both channels C3 and C4 reflect a *mu* ERD, i.e. lateralized distribution with no unilateral dominance. Beta, on the contrary elicits ERS which is localized centrally at the vertex, with no left-right discrimination, in accordance with the established findings from figure 7.2 and [12, 22, 23]. During left knee KMI, a strong ERS can be viewed at channel Cz, whereas during right task, less strong ERS is localized at Cz (the vertex).

7.3.3 Classification accuracy

The *mu* and *beta* feature vectors resulting from previous sections, were next classified to confirm the possibility of discriminating left and right knee KMI tasks for using them as unilateral control commands. For classification, ML models were used. Initially the classical linear SVM model was deployed, however, to improve the classification accuracy, weighted KNN model with 10 nearest neighbors, was also used [25, 32]. Each model's performance after data standardization was evaluated using k-fold cross validation method for training and testing phases [33, 34], for $k = 5$.

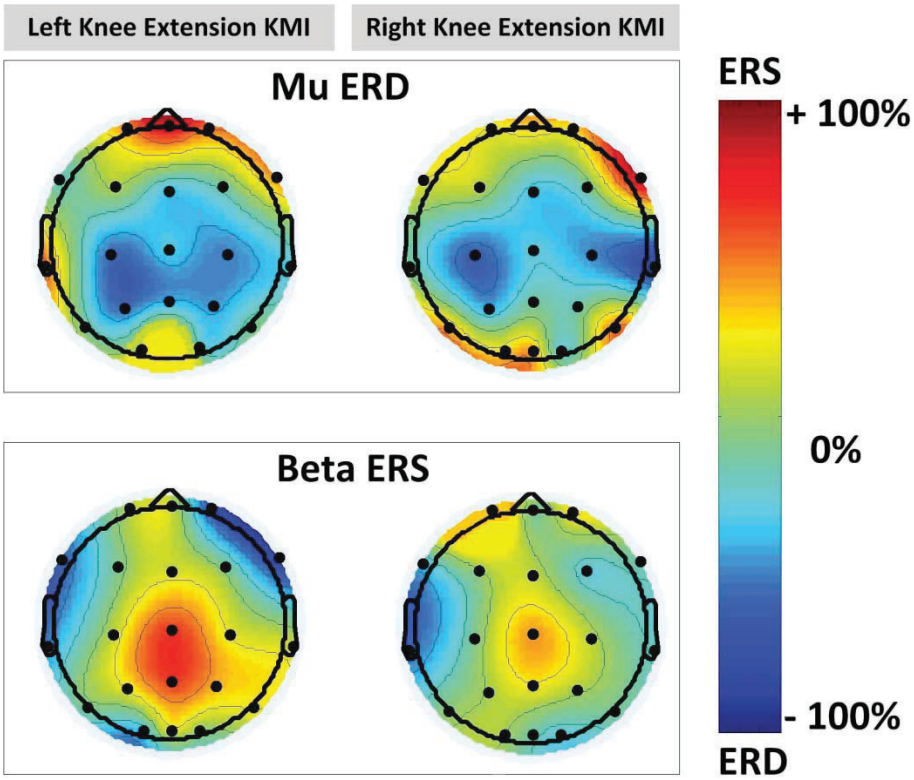

Figure 7.3 Average EEG topographies of ERD/ERS during knee KMI of all participants. Beta ERS is shown in the top row for left and right knee respectively, and *mu* ERD is in the bottom row.

Table 7.2 gives the average binary classification accuracies and standard deviations of *beta* ERS and *mu* ERD using SVM and KNN ML models, respectively to discriminate between left and right knee KMI tasks. For *beta* ERS, participant 5 showed the highest accuracy percentage of 81.04% using KNN model, compared to SVM which is 67.47% elicited by participant 2. The average accuracy of *beta* ERS is 71.88% ± 7.5 using KNN model, followed by 63.13% ± 3.3 with SVM model. For *mu* ERD, the participant 5 again exhibited maximum classification accuracy of 80.00% using KNN, and maximum accuracy of 74.40% using SVM. The average accuracy of *mu* ERD using KNN is 74.59% ± 5.1 and 68.09% ± 4.6 using SVM model. Results reveal that on average each feature's accuracy, for SVM and KNN model, is above the statistical chance level of 60.0% ($P < 0.01$). For a 2-class BCI discrimination problem, the statistical chance level should be greater than, or equal to 57.5% ($P < 0.05$) or 60.0% ($P < 0.01$) for 80 trials, as given in [29].

It can clearly be stated that overall, the KNN model outperformed SVM in case of both features. Figure 7.4 reflects the average of each classifier model for *beta* ERS and *mu* ERD. Both ML models resulted in average classification accuracy above the statistical chance level

of 60.0% ($P < 0.01$). The maximum average accuracy was obtained with *mu* ERD with a difference of 2.71% from *beta* ERS. However, individual maximum accuracy for discriminating between left and right knee KMI task was achieved with *beta* ERS.

Table 7.2 The 5-fold cross-validation classification accuracy and AUC-ROC values of left-right knee KMI using beta ERS and mu ERD

Participant	Beta ERS				Mu ERD			
	SVM (%)	AUC-ROC	KNN (%)	AUC-ROC	SVM (%)	AUC-ROC	KNN (%)	AUC-ROC
P1	65.82	0.70	61.19	0.57	64.08	0.63	74.68	0.61
P2	67.47	0.60	68.71	0.72	65.14	0.61	75.67	0.63
P3	61.14	0.52	75.61	0.79	65.37	0.58	66.17	0.54
P4	60.42	0.64	72.85	0.80	71.46	0.71	76.45	0.62
P5	60.81	0.56	81.04	0.84	74.40	0.83	80.00	0.79
Mean	63.13	0.60	71.88	0.75	68.09	0.67	74.59	0.64
S.D.	3.3	0.07	7.5	0.11	4.6	0.10	5.1	0.09

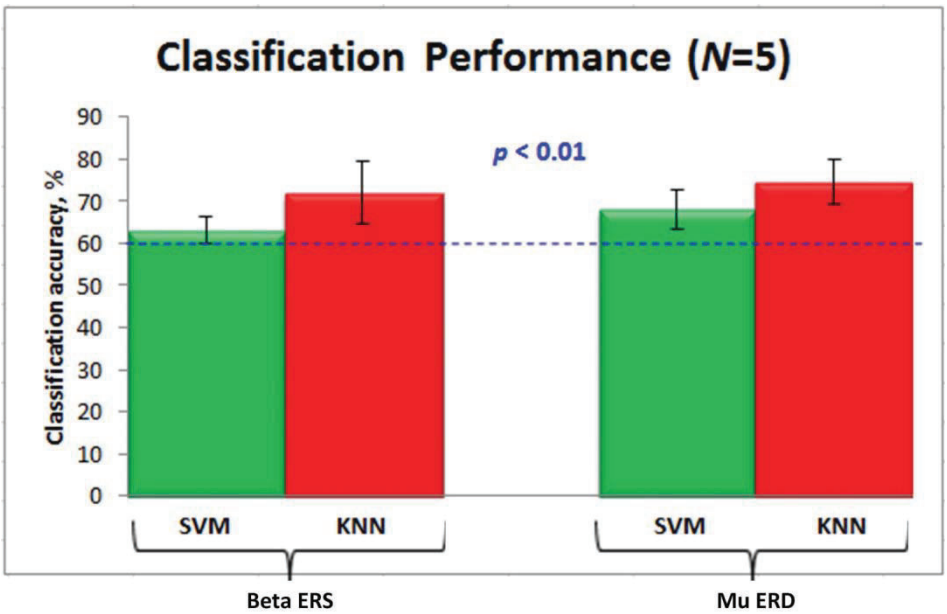

Figure 7.4 Average classifier models performance in percentage, using common average reference. The error bars represent standard deviations.

Figure 7.5 depicts the individual prediction accuracies for discriminating between left and right knee KMI tasks for $n = 5$, where n is the total number of participants. It can be observed that participant 5 exhibited highest prediction accuracy for *beta* ERS followed by *mu* ERD feature with KNN model. Participants 3, 4, and 5 performed lowest for *beta* ERS

using SVM model. This indicates a tradeoff exists between the model performances, i.e. it can be deduced that when KNN outperforms, SVM performs the least.

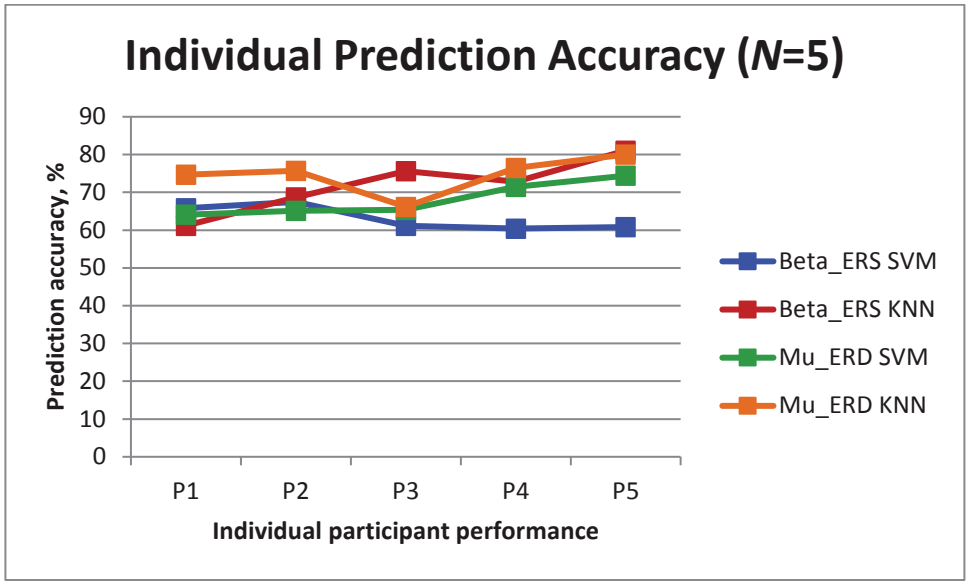

Figure 7.5 Individual participant prediction accuracies in percentage for N=5.

In addition to classification accuracy, table 7.2 also shows the normalized AUC-ROC curve values of each participant for SVM and KNN models. The ROC curve is deployed as an evaluation tool, and the AUC determines the performance of the detector, i.e. truly observed classification and not by chance. In case of ideal detection, as described in Chapter 3, section 3.6.5, the true positive rate (TPR) should be 100%, and the false positive rate (FPR) should be 0%, whereas the AUC should be 100% [35]. From table 7.2, it can be seen that participant 5 elicited highest AUC-ROC of 0.84 for *beta* ERS feature using KNN, and a maximum AUC-ROC = 0.83 for *mu* ERD, using SVM. Ideally AUC-ROC = 1, after normalization. With *beta* ERS feature, the maximum average AUC was 0.75 ± 0.11 using KNN, and with *mu* ERD, the highest average AUC was 0.67 ± 0.10 using SVM. However, with KNN, *mu* feature showed a closer AUC value of 0.64 ± 0.09 using KNN, with a difference of 3% only. The average AUC values are satisfying for both features, in context to [23, 28, 35]. It can therefore be stated that *beta* ERS reflected the best AUC value for 2-class discrimination BCI that enables its utilization as a control command in a BCI operation.

Figure 7.6 displays the AUC-ROC plots with maximum values for both features using their corresponding ML model. Along the x-axis is the FPR, and along the y-axis is the TPR, where both axes are normalized. The plots displayed in figure 7.6 are from participant 5's AUC-ROC values. The left graphs represent AUC-ROC curves plotted against class 1, i.e.

left knee KMI and the right column against class 2, i.e. right knee KMI task, respectively. The top row shows AUC-ROC of *beta* ERS and the bottom row exhibits that of *mu* ERD. For carrying out the statistical comparison of SVM and KNN classifier models, the Mann-Whitney *U* test was used; details are presented in Discussion section 7.4.2.

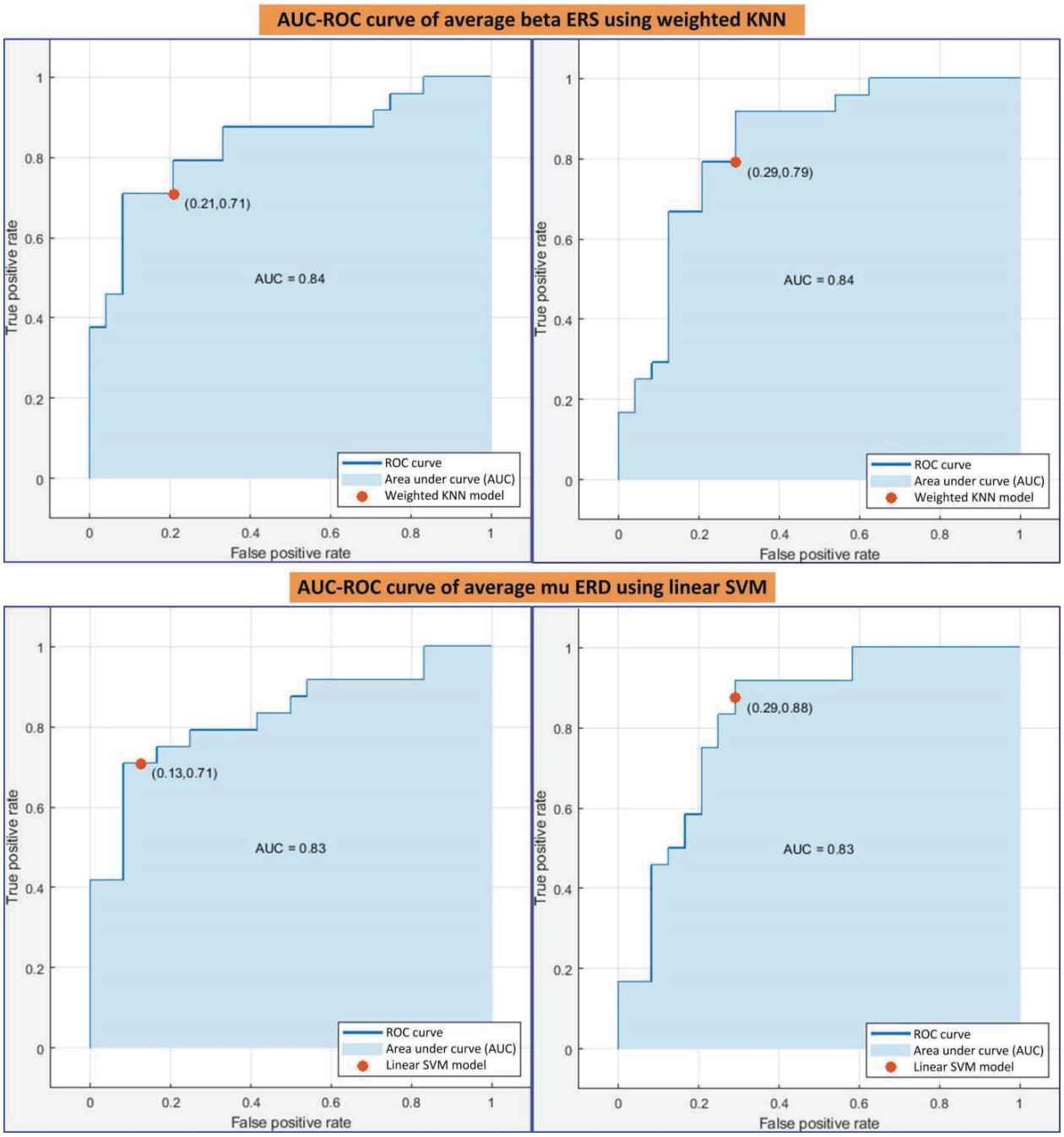

Figure 7.6 AUC-ROC plots with maximum AUC values for *beta* ERS using KNN model and *mu* ERD using SVM model, during classification of left vs. right knee KMI.

7.4 Discussion

This research study analysed and classified EEG features elicited upon novel cognitive KMI task of left and right knee. As the study is novel, for the beginning, less number of participants were involved; the future directions include deployment of more participants for further analysis on large population. The analysis of *beta* ERS and *mu* ERD was done based on EEG topography and TF maps using common average reference method. Significant *beta* ERS were observed at the end of the left, or right knee imagery, which was consistent with studies on LL i.e. left-right foot imagery [23, 24, 36]. This implies that knee and foot areas are closely located to each other in the somatosensory cortex, which is in context to the established finding [15]. The distribution of *beta* ERS was localized at the vertex during both left and right KMI tasks, as displayed in the EEG scalp topography. However, *mu* ERD was distributed on contralateral sides that made the left-right differences evident. This work offers the first example of analysing left-right differences in *beta* ERS and *mu* ERD based on unilateral knee KMI in EEG.

7.4.1 Detection of left vs. right ERD/ERS features using bipolar method

Studies on left-right difference using LL motor imagery commonly deployed the bipolar, Laplacian, or common average reference methods [11, 12, 18, 19, 22, 23]. Majority of these studies followed the foot motor imagery. An initial study related to this chapter, in Appendix A, on the analysis of *mu* ERD/ERS based on knee KMI, used the common average reference method to extract BP ERD/ERS features from *mu* rhythm. Consequently, as a continuation to it, this chapter is elaborated and covers a wider range of analyses including another feature, as well as, more participants. The reference technique for recording and evaluating EEG features therefore remains the same i.e. the common average reference method. This reference is computationally simple and compliant to both on-chip and real-time applications, therefore was the first choice. It identifies small signal sources in noisy recordings, with a higher signal-to-noise ratio compared to Laplacian filter [7, 37]. It has successfully been used to detect the intention of motion during imagery [38]. Current study confirmed the left-right difference in both *mu* and *beta* ERD/ERS features using common average reference, supported by ML models results, that exceed the 2-class chance level of 60% ($P < 0.01$).

From previous studies on left-right discrimination using foot imagery, the bipolar reference has been successfully deployed for analysis of EEG features [22, 23]. This provides a source of analysing the BP features, from this study, using bipolar method. The use of this method

could possibly increase the classification accuracy for knee KMI based BCI studies. In addition to this, given results from this study are not based on experiments including neurofeedback training. This factor could add value to the resulting classification accuracies of both features.

7.4.2 Performance comparison of KNN and SVM using Mann-Whitney *U* test

To statistically compare the performance of the proposed linear SVM and weighted KNN ML models, Mann-Whitney *U* test, also termed Wilcoxon rank-sum test, was used. It is a nonparametric test of the null hypothesis H_0. For each feature the P-value was separately calculated. This resulted in the acceptance, or rejection, of the null hypothesis, i.e. 0 or 1, respectively. Table 7.3 shows the individual P-values for each feature and their respective hypothesis values. It is clear that with both features, the null hypothesis was rejected, that validates the classification of EEG features. This proves that the resulting classification accuracy, from both models, truly occurred and not by any random chance.

Table 7.3 Mann-Whitney *U* test for SVM and KNN machine learning models

SVM vs. KNN	*P*-value	H_0
Mu ERD	0.0317	1
Beta ERS	0.0317	1

Results show that knee KMI elicits broad-banded ERD (observed in both *mu* and *beta* rhythms) and narrow-banded ERS (post task). An enhancement in the foot area of the cortex was observed with concentrated *beta* ERS, which indicates no enhancement in a new area of the cortex and confirms the spatial proximity of LL [19]. ERD/ERS differences, can be observed in the *mu* and high *beta* frequency bands.

The next goal is to deploy the common spatial pattern feature vector for the proposed left vs. right knee KMI cognitive task. Chapter 8 is based on findings from analysis of CSP and filter bank CSP (FBCSP) features.

7.5 Conclusion

In conclusion, this study revealed the cortical lateralization of ERD/ERS in association with the proposed novel knee imagery cognitive tasks. This indicates that they can be deployed as separate unilateral control commands in a BCI. In synchronous mode, these results achieved the same level of accuracy as that of hand and foot motor imagery-based BCI, using EEG

signals recorded via three channels on the vertex. The influence of neurofeedback training on the classification accuracy is required to be investigated further.

Acknowledgement

None.

References

1. Tariq, M., Z. Koreshi, and P. Trivailo. *Optimal control of an active prosthetic ankle.* in *Proceedings of the 3rd International Conference on Mechatronics and Robotics Engineering*. 2017. ACM.
2. Schalk, G. and J. Mellinger, *A practical guide to brain–computer interfacing with BCI2000: General-purpose software for brain-computer interface research, data acquisition, stimulus presentation, and brain monitoring*. 2010: Springer Science & Business Media.
3. Tariq, M., P.M. Trivailo, and M. Simic, *EEG-Based BCI Control Schemes for Lower-Limb Assistive-Robots.* Frontiers in Human Neuroscience, 2018. **12**.
4. Lebedev, M.A. and M.A. Nicolelis, *Brain-machine interfaces: From basic science to neuroprostheses and neurorehabilitation.* Physiological reviews, 2017. **97**(2): p. 767-837.
5. Deng, W., et al., *Advances in Automation Technologies for Lower Extremity Neurorehabilitation: A Review and Future Challenges.* IEEE reviews in biomedical engineering, 2018. **11**: p. 289-305.
6. Cervera, M.A., et al., *Brain-computer interfaces for post-stroke motor rehabilitation: a meta-analysis.* Annals of clinical and translational neurology, 2018. **5**(5): p. 651-663.
7. Wolpaw, J.R., et al., *Brain–computer interfaces for communication and control.* Clinical neurophysiology, 2002. **113**(6): p. 767-791.
8. Pfurtscheller, G., C. Neuper, and N. Birbaumer, *14 Human Brain–Computer Interface.* 2005.
9. Pfurtscheller, G., et al., *Graz-BCI: state of the art and clinical applications.* IEEE Transactions on neural systems and rehabilitation engineering, 2003. **11**(2): p. 1-4.
10. Mokienko, O., et al., *Increased motor cortex excitability during motor imagery in brain-computer interface trained subjects.* Frontiers in computational neuroscience, 2013. **7**: p. 168.
11. Tariq, M., et al. *Mu-beta rhythm ERD/ERS quantification for foot motor execution and imagery tasks in BCI applications*. in *2017 8th IEEE International Conference on Cognitive Infocommunications (CogInfoCom)*. 2017. IEEE.
12. Pfurtscheller, G., et al., *Mu rhythm (de) synchronization and EEG single-trial classification of different motor imagery tasks.* NeuroImage, 2006. **31**(1): p. 153-159.
13. Pfurtscheller, G. and F.L. Da Silva, *Event-related EEG/MEG synchronization and desynchronization: basic principles.* Clinical neurophysiology, 1999. **110**(11): p. 1842-1857.
14. Hommelsen, M., et al., *Sensory feedback interferes with Mu rhythm based detection of motor commands from electroencephalographic signals.* Frontiers in human neuroscience, 2017. **11**: p. 523.

15. Penfield, W. and E. Boldrey, *Somatic motor and sensory representation in the cerebral cortex of man as studied by electrical stimulation.* Brain, 1937. **60**(4): p. 389-443.
16. Wolpaw, J. and E.W. Wolpaw, *Brain-computer interfaces: principles and practice*. 2012: OUP USA.
17. Millán, J.d.R., et al., *Combining brain–computer interfaces and assistive technologies: state-of-the-art and challenges.* Frontiers in neuroscience, 2010. **4**: p. 161.
18. Tariq, M., P.M. Trivailo, and M. Simic. *Detection of knee motor imagery by Mu ERD/ERS quantification for BCI based neurorehabilitation applications*. in *2017 11th Asian Control Conference (ASCC)*. 2017. IEEE.
19. Tariq, M., et al., *Comparison of Event-related Changes in Oscillatory Activity During Different Cognitive Imaginary Movements Within Same Lower-Limb.* Acta Polytechnica Hungarica, 2019. **16**(2): p. 77-92.
20. Kilicarslan, A., et al. *High accuracy decoding of user intentions using EEG to control a lower-body exoskeleton*. in *2013 35th Annual International Conference of the IEEE Engineering in Medicine and Biology Society (EMBC)*. 2013. IEEE.
21. Contreras-Vidal, J.L. and R.G. Grossman. *NeuroRex: A clinical neural interface roadmap for EEG-based brain machine interfaces to a lower body robotic exoskeleton*. in *2013 35th Annual International Conference of the IEEE Engineering in Medicine and Biology Society (EMBC)*. 2013. IEEE.
22. Liu, Y.-H., et al., *Analysis of electroencephalography event-related desynchronisation and synchronisation induced by lower-limb stepping motor imagery.* Journal of Medical and Biological Engineering, 2019. **39**(1): p. 54-69.
23. Hashimoto, Y. and J. Ushiba, *EEG-based classification of imaginary left and right foot movements using beta rebound.* Clinical neurophysiology, 2013. **124**(11): p. 2153-2160.
24. Pfurtscheller, G. and T. Solis-Escalante, *Could the beta rebound in the EEG be suitable to realize a "brain switch"?* Clinical Neurophysiology, 2009. **120**(1): p. 24-29.
25. Lotte, F., et al., *A review of classification algorithms for EEG-based brain–computer interfaces: a 10 year update.* Journal of neural engineering, 2018. **15**(3): p. 031005.
26. Lotte, F., et al., *A review of classification algorithms for EEG-based brain–computer interfaces.* Journal of neural engineering, 2007. **4**(2): p. R1.
27. Wilcoxon, F., S. Katti, and R.A. Wilcox, *Critical values and probability levels for the Wilcoxon rank sum test and the Wilcoxon signed rank test.* Selected tables in mathematical statistics, 1970. **1**: p. 171-259.
28. Demšar, J., *Statistical comparisons of classifiers over multiple data sets.* Journal of Machine learning research, 2006. **7**(Jan): p. 1-30.
29. Müller-Putz, G., et al., *Better than random: a closer look on BCI results.* International Journal of Bioelectromagnetism, 2008. **10**(ARTICLE): p. 52-55.
30. Klem, G.H., et al., *The ten-twenty electrode system of the International Federation.* Electroencephalogr Clin Neurophysiol, 1999. **52**(3): p. 3-6.
31. Li, M.-A., et al., *Decoding of motor imagery EEG based on brain source estimation.* Neurocomputing, 2019. **339**: p. 182-193.
32. Pfurtscheller, G., et al., *EEG-based discrimination between imagination of right and left hand movement.* Electroencephalography and clinical Neurophysiology, 1997. **103**(6): p. 642-651.
33. Tharwat, A., *Classification assessment methods.* Applied Computing and Informatics, 2018.

34. Rodriguez, J.D., A. Perez, and J.A. Lozano, *Sensitivity analysis of k-fold cross validation in prediction error estimation.* IEEE transactions on pattern analysis and machine intelligence, 2009. **32**(3): p. 569-575.
35. Fawcett, T., *An introduction to ROC analysis.* Pattern recognition letters, 2006. **27**(8): p. 861-874.
36. Pfurtscheller, G., et al., *Beta rebound after different types of motor imagery in man.* Neuroscience letters, 2005. **378**(3): p. 156-159.
37. Ludwig, K.A., et al., *Using a common average reference to improve cortical neuron recordings from microelectrode arrays.* Journal of neurophysiology, 2009. **101**(3): p. 1679-1689.
38. Syam, S.H.F., et al. *Comparing common average referencing to laplacian referencing in detecting imagination and intention of movement for brain computer interface.* in *MATEC Web of Conferences*. 2017.

Chapter 8

Classification of left and right knee extension motor imagery using common spatial pattern for BCI applications

Chapter Overview

The possibility of deploying novel knee KMI, for confirming the cortical lateralization of ERD/ERS, using BP feature vector in a BCI paradigm, is presented in detail in the previous chapter. This chapter further investigates and quantifies the ERD/ERS features in the *mu* and *beta* frequency band of 7-35 Hz, using CSP and FBCSP feature vectors, to be used as independent unilateral control commands in a 2 degree of freedom BCI paradigm. In order to distinguish between left and right knee KMI tasks, two ML models are employed for determining the highest classification accuracy and were statistically compared. Results successfully differentiated between both knee tasks, and confirmed the cortical lateralization. However, the classification accuracy from this study was lower than the previous study, but above the statistical chance level of 2-class imagery based-BCI. This infers that BP features and proposed ML models work better than the CSP feature and ML model, as shown in this chapter.

This study has been published in ***International Journal of Knowledge-Based and Intelligent Engineering Systems: Procedia Computer Science***.

M. Tariq, P. M. Trivailo, M. Simic. *Classification of left and right knee extension motor imagery using common spatial pattern for BCI applications.* International Journal of Knowledge-Based and Intelligent Engineering Systems: Procedia Computer Science, 159, 2598-2606, 2019.

Available online at www.sciencedirect.com

ScienceDirect

Procedia Computer Science 00 (2019) 000–000

Procedia Computer Science

www.elsevier.com/locate/procedia

23rd International Conference on Knowledge-Based and Intelligent Information & Engineering Systems

Classification of left and right knee extension motor imagery using common spatial pattern for BCI applications

Madiha Tariq*, Pavel M. Trivailo, Milan Simic

School of Engineering, RMIT University, Bundoora Plenty Road, Victoria 3083, Australia

Abstract

Research on the deployment of various cognitive tasks in the experimental paradigm of a human brain-computer interface (BCI) is on-going in particular upper-limb tasks. Less has been investigated on the lower-limbs, due to its somatotopic arrangement in the sensorimotor cortex compared to that of upper limbs. Hip, knee, foot and toes share spatial proximity with each other. We therefore investigated the possibility to deploy the left vs. right knee extension kinaesthetic motor imagery (KMI) as a cognitive task in a BCI for the control of lower-limbs, primarily for people with neurodegenerative disorders, spinal cord injury or lower-limb amputation. The method involved feature extraction using common spatial pattern (CSP), and filter bank common spatial pattern (FBCSP) algorithm for the optimization of individual spatial patterns. This was followed by supervised machine learning using logistic regression (Logreg) and linear discriminant analysis (LDA) for classification of tasks. The paradigms resulted in four combinations/methods for discriminating between left and right knee tasks. The FBCSP-Logreg outperformed remaining paradigms with a maximum accuracy of 70.00% ± 2.85 and kappa=0.40. The results elicit the possibility to deploy left vs. right knee extension KMI in a 2-class BCI for controlling robotic/prosthetic knee.

Keywords: brain-computer interface (BCI); common spatial pattern (CSP); filter bank common spatial pattern (FBCSP); kinaesthetic motor imagery (KMI)

* Corresponding author. Tel.: +61 421 136 356; fax: +0-000-000-0000 .
E-mail address: madiha.tariq@rmit.edu.au

1. Introduction

Brain-Computer Interface (BCI) is an emerging research field that establishes a real-time bidirectional connection between the human brain and a computer/output device. It serves as a communication tool for patients with neuromotor disorder, spinal cord injuries, or amputation [1, 2]. Amongst its diverse applications, neurorehabilitation to deliver sensory feedback and brain controlled biomedical devices, are most popular. Gait rehabilitation is the therapeutic aim for enhancement of motor control functions by actuating neuroplasticity [3]. This can be discerned by distinguishing brain signals corresponding to the movement imagination of the affected limb and translating it into an output command [4]. Subsequently the user can re-establish the lost motor control by getting feedback on the output command affecting his/her brain activity [3, 5].

The kinesthetic motor imagery (KMI) is a covert cognitive process based on the imagination of user's own limb movement without muscular intervention [6]. These cognitive tasks ensue in the mu (8-12 Hz) and beta (13-35 Hz) oscillatory rhythms. Patterns that reflect an imagined limb movement are characterized by event-related desynchronization (ERD) and event-related synchronization (ERS) and are localized in the sensorimotor cortex. A decrease, or blocking response is referred to ERD, while an enhancement in amplitude is ERS. However, due to the somatotopic organization of the motor cortex [7], the left and right lower-limb areas are closely located to each other compared to upper limbs e.g., hands [8]. This is a potential reason for less reported literature on lower-limb imagery tasks in BCI. To our knowledge there is no study on classification of left-right knee extension KMI for people with lost knee function. With merely one study on feature extraction as recently presented in [3], this study is therefore novel.

With common spatial pattern (CSP) algorithm being commonly used in feature extraction process of motor imagery based BCIs, it has been observed that none of the reported studies deployed knee extension as a KMI task. Most studies were based on upper limb imageries, e.g. left hand vs. right hand [9]. This study is a contribution to discrimination of left vs. right knee KMI using CSP in order to provide two unilateral control commands to a BCI system. The CSP is a relatively simple algorithm with high processing speed. It finds spatial filters that maximize the variance of (projected) signal from one class (left knee KMI) and minimize it for the other class (right knee KMI), and vice versa to get maximum discrimination evidence [10]. As motor imageries reflect in the mu-beta range, this implies that a broad frequency range of 8 to 35 Hz is expected to be considered. Therefore, the filter band selection is a very crucial step for producing effective results. However according to [11], the most effective frequency band is subject-specific which can barely be determined manually. Our study therefore incorporates the filter bank common spatial pattern (FBCSP) algorithm as an enhancement in the study across participants. The FBCSP is an extension of CSP method for the selection of optimal filter-bands. It estimates the mutual information among CSP features present in several fixed filter-bands [12, 13]. It is very useful for oscillatory processes occurring in different frequency bands (having different spatial topographies) [14], for instance mu and beta can jointly be active during task.

Following signal pre-processing and feature extraction, machine learning was implemented on the selected feature vectors. The study deployed two classification algorithms classical linear discriminant analysis (LDA) and the supervised logistic regression (Logreg). This resulted in four different combinations of proposed methodology paradigms, i.e. CSP-LDA, CSP-Logreg, FBCSP-LDA, and FBCSP-Logreg. It was done to draw a comparison between the paradigms and be able to configure the best features that resulted in maximum discrimination accuracy between the left and right knee KMI tasks.

We used the 5 x 5-fold cross validations for the single-trial classification accuracies resulting from the training and testing phases with all participants. For statistical evaluation of classification performance, we used the Cohen's kappa coefficient κ. Results reflected that FBCSP-Logreg outperformed the remaining paradigms with highest accuracy percentage of 66.0 ± 2.85 with a mean kappa of 0.32. In addition to kappa scores, the area under the receiver operator characteristic curve, (AUC-ROC) curve was also included in the study as a measure of statistical evaluation. Following similar pattern FBCSP-Logreg produced highest average AUC-ROC of 65% for all participants. This study was not inclusive of BCI practice in advance by participants. These results are encouraging and provide a basis for establishing a 2-class BCI based on knee KMI for controlling a robotic knee system or knee neuroprosthesis.

2. Methodology

2.1. Experimental paradigm and EEG recording

Based on the required BCI application, study involves left/right knee extension KMI tasks. Since this investigation was not conducted before, we engaged five participants in an initial phase. All participants were healthy, aged between 21-28 years, with no medical history, and no experience of BCI beforehand. They took part in the experiment voluntarily. Ethical consent to conduct experiment was granted by the CHEAN (College Human Ethics Advisory Network), RMIT University, Melbourne, Australia.

Experimental setup comprised of a comfortable seat facing monitor screen (17”), placed at about 1.5 m distance from the participants. They were asked to sit and pay attention to visual cues presented on the monitor. To ensure that no proprioception artefact (caused by muscles) occurs in the feedback, we placed a flat wooden sheet, as a stable platform under participant feet. This way the legs were loosely fixed and allowed the knees to flex at 60° from full extension during rest position. Participants were instructed to perform kinaesthetic imagination of full knee extension following cue presentation. This task corresponds to the normal human walking gait.

For recording electrical activity from the scalp, we deployed non-invasive electroencephalography (EEG) modality. Signals were recorded using the 19 channel electrocap (C3, C4, Cz, F3, F4, F7, F8, Fz, FP1, FP2, O1, O2, P3, P4, Pz, T3, T4, T5, T6) positioned in the international 10-20 system [15], referenced to the linked earlobes A1 and A2 [16] interfaced with neurofeedback BrainMaster Discovery 24E amplifier (BrainMaster Technologies Inc., Bedford, USA. All channels were sampled at 256 Hz and digitized with 24-bit resolution. Ground electrode was located near the forehead position. Our study is based on synchronous (cue paced) BCI, therefore the temporal sequence of visual cues was designed using Graz BCI protocol, a feature of OpenViBE® that comes along integrated feature boxes [17, 18].

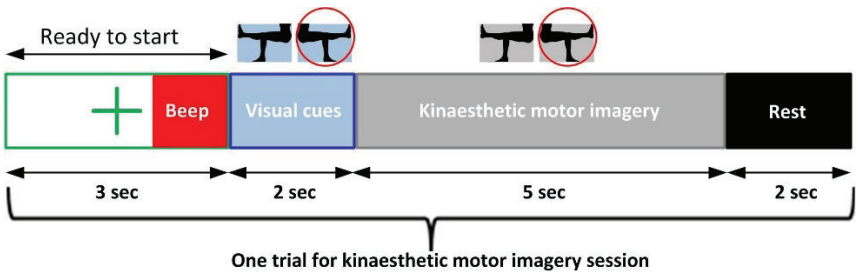

Fig. 1. Temporal sequence of one trial of knee kinaesthetic motor imagery followed in the experiment.

The temporal sequence of one trial is shown in Fig. 1. It begins with a 3 seconds long fixation cross, which is used as reference period for processing of epochs. During the last second of fixation cross, an audio beep of 1 second is incorporated for the first trial only, to alert the participant. This was followed by left or right knee extension visual cue, for 2 seconds (displayed randomly). Next, a blank screen appeared for 5 seconds for the kinaesthetic imagery of task. The total length of each trial was 10 seconds. At the end, a pause interval of 1.5-3.5 seconds (randomly selected) was used, to avoid fatigue. Recorded signals were processed using BCILAB https://github.com/sccn/BCILAB.

The experiment included four sessions without feedback, with each session encompassing 40 trials; 20 trials for left knee and 20 trials for right knee KMI. This resulted in 80 trials of each knee task.

2.2. Common spatial pattern and filter bank common spatial pattern for feature extraction

From recorded EEG signal the feature extraction for classifying left vs. right knee KMI was carried out using the common spatial pattern (CSP) method. It is effective in constructing optimal spatial filters for the discrimination of 2-class KMI EEG data in a BCI [10]. For effective results we specified the frequency for band-pass filtering as 7-35

Hz, the time interval of the signal taken relative to the cue (3 seconds prior to cue), and 3 subsets of CSP filters were used. However, the performance of CSP algorithm is subject-specific due to individual characteristics of brain; therefore, it can be enhanced using individual parameters [19]. We therefore exploited the filter bank common spatial pattern (FBCSP) that was first introduced by [12]. Feature vectors resulting from CSP and FBCSP were individually used for machine learning.

The four stages of FBCSP that are followed in this study were adapted from [13]. as shown in Fig. 2. It comprises of a filter bank that fragments the EEG signal into three frequency pass bands, 7-12, 13-25, and 28-32 Hz using Chebyshev Type II filter. Those frequency pass bands cover the mu and beta oscillatory rhythms. In the second stage, spatial filtering is done using CSP algorithm. It is reported by [20], that the CSP algorithm is very effective in calculating spatial filters for the detection of ERD/ERS. CSP transforms the observed signal as shown:

$$\mathbf{S}_{\mathrm{j}} = \mathbf{W}\mathbf{E}_{\mathbf{j}}, \tag{1}$$

where $\mathrm{E_j}$ is the observed single-trial EEG signal from pass band (7- 35 Hz) of j-th trial, $\mathrm{j} = 1 \ldots \mathrm{n}$, where n is the number of training trials. $\mathbf{W} \in \mathbb{R}^{\mathrm{s}\times\mathrm{c}}$ is the un-mixing matrix and $\mathbf{S_j} \in \mathbb{R}^{\mathrm{s}\times\mathrm{t}}$ is the recovered single-trial source after spatial filtering, where $s = 2 \times e \times 3\ (frequency\ bands) \times 2(classes)$ is the number of sources i.e. the CSP projections, c is number of channels, and the number of time samples is t. Filter computes the un-mixing matrix $\mathbf{W}$ to yield features with optimal variances for discriminating the two classes of measured EEG [9, 19]. This is realized by determining the eigenvalue decomposition problem.

$$\sum_1 \mathrm{W} = (\Sigma_1 + \Sigma_2)\mathrm{WD}, \tag{2}$$

where Σ_1 and Σ_2 are the estimates of the covariance matrices of EEG signal based on two imagery tasks i.e. left and right knee extension. Diagonal matrix D comprises of the eigenvalues of Σ_1, whereas the column vectors of W^{-1} are the filters for CSP projections. For producing best results, the suitable most contrast is delivered by filters with the highest and lowest eigenvalues. Hence it is common to retain e eigenvectors via both ends of the eigenvalue spectrum [10], in this case, $e = 2$. The CSP filter was individually applied for right vs. baseline and left vs. baseline for each band, during the task performance time segment, i.e. the time starting after the cue presentation of 5 seconds. We selected a time window of [0 4].

Third stage is the CSP feature selection, where the difference in variance of the two classes of pass band EEG is maximized, using $\mathbf{W}$ from (2) and substituting in the spatial filtered signal $\mathbf{S}_j$ from (1). The m pairs of CSP features of j-th trial for pass band EEG are given by:

$$\mathbf{v}_j = \log \frac{\mathrm{diag}\left(\bar{\mathbf{W}}^T \mathbf{E}_j \mathbf{E}_j^T \bar{\mathbf{W}}\right)}{\mathrm{tr}\left[\bar{\mathbf{W}}^T \mathbf{E}_j \mathbf{E}_j^T \bar{\mathbf{W}}\right]} \tag{3}$$

where $\mathrm{v_j} \in \mathbb{R}^{2\mathrm{m}}$; $\bar{\mathbf{W}}$ indicate the first m and last m columns of $\mathbf{W}$; diag(.) returns diagonal elements of the square matrix. Sum of the diagonal elements in the square matrix is returned by tr[.] [13]. The FBCSP feature vector for j-th trial is subsequently formulated as:

$$\mathrm{v_j} = \left[\mathrm{v}_{1,\mathrm{j}}, \mathrm{v}_{2,\mathrm{j}}, \ldots, \mathrm{v}_{9,\mathrm{j}}\right], \tag{4}$$

where $\mathrm{v_i} \in \mathbb{R}^{1\times(3*2\mathrm{m})}$, $\mathrm{j} = 1,2, \ldots, \mathrm{n}$; n is the total number of trials in the data.

Finally, the classification of these features elicited upon left and right knee KMI tasks is performed. The classifier model is computed from the labelled training data (2-class KMI). Parameters that are computed from the training phase are employed for the testing phase, consequently for predicting the single-trial knee KMI task. We deployed the classical LDA and Logreg to measure the classification accuracy [21] and draw a comparison between classifier performances. For implementation of the above defined algorithm, we used the MATLAB (R2013b) toolbox BCILAB https://github.com/sccn/BCILAB.

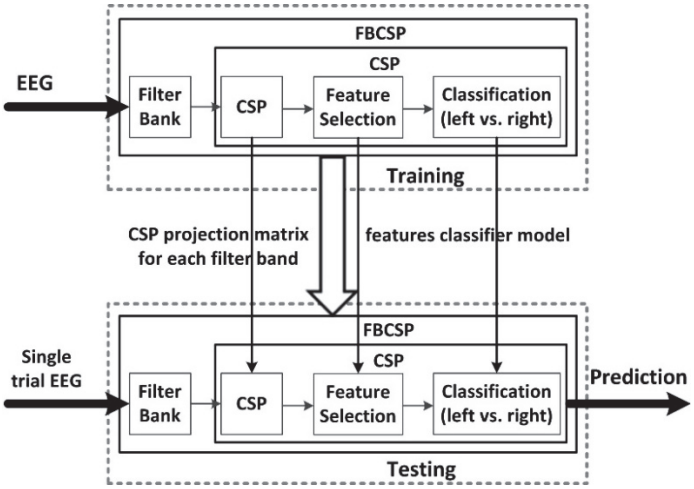

Fig. 2. Paradigm of common spatial pattern (CSP) and filter bank CSP (FBCSP) algorithms for training, testing and prediction phases, adapted from [13].

2.3. Classifier evaluation

Proposed methodology resulted in four paradigms, i.e. CSP-LDA, CSP-Logreg, FBCSP-LDA, and FBCSP-Logreg. In each case the classification was done with a 5x5 fold cross-validation. The trials were partitioned into five equal sub-datasets. Classifiers were individually trained on four of the sub-datasets and tested the model for accurate discrimination of trials from the remaining sub-dataset (validation). This resulted in individual prediction accuracies. Weight vectors and classification accuracies were averaged from 5-folds. We determined the mean and standard deviation of each classifier, as well as, individual participant performance, as shown in Fig. 3.

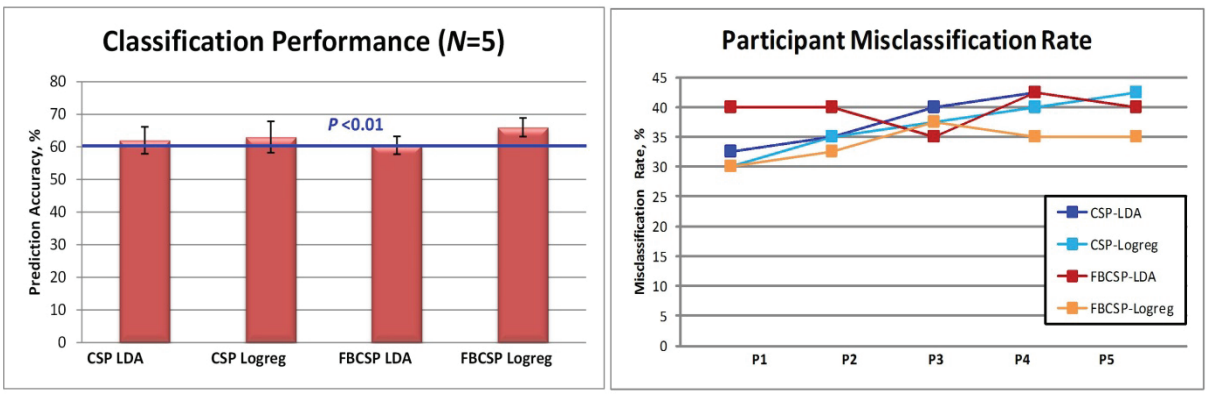

(a) (b)

Fig. 3. (a) Classification accuracies in percentage across participants where blue line shows average on and above chance level ($p<0.01$). (b) Individual misclassification rate in percentage (for N=5) of CSP-LDA, CSP-Logreg, FBCSP-LDA, and FBCSP-Logreg algorithms.

Since our study is based on machine learning, we took into account the AUC-ROC curve, as a performance measure of the classifiers. ROC is a probability-curve plotted between the true positive rate (TPR) (y-axis) and the false positive rate (FPR) (x-axis) at various threshold values to diagnose the ability of binary classifier. The AUC reflect the degree of separability between 2-classes [22], i.e. left and right knee tasks. Higher the AUC in the range 0 to 1, the better the prediction range between none to perfect.

Another important evaluation criterion for assessing the performance of the classifiers is the coefficient κ [23]. For the 2-class problem, the classifier evaluation is defined by its confusion matrix H, which defines the correlation between the true classes and observed output of the classifier. The estimate of kappa coefficient κ is given by:

$$\kappa = \frac{p_o - p_e}{1 - p_e}, \tag{5}$$

where p_o is the overall observed agreement, and p_e is the chance expected agreement for N number of samples. For more detailed explanation refer to [24].

3. Results

Sensorimotor rhythms underlie in the central cortical areas located at channels C3, Cz, and C4 [25]. However, due to intra-humans varying anatomical properties of cortical folding, the areas discriminating ERD/ERS power characteristic against knee imagery are not exactly located underneath channels C3, Cz, and C4 during the experiment.

The CSP method produces subject-specific spatial filters which are optimized for discriminating right vs. left knee tasks. BCILAB spatially filters raw EEG channels into smaller time-series. Their variances are optimized to distinguish between the two classes. We developed a 3-pair set of CSP scalp projections for each participant. Figure 4 demonstrates the 3-pair set of CSP scalp projections for participant P01. During right and left knee imageries, CSP pattern 1 shows the ERD/ERS activation of electrode positions C3 and C4, that is the hand representation area in the cortex [26]. In contrast, CSP pattern 3 elicits the mid central ERS at the vertex, Cz, enhancing the foot area beta ERS. Pattern 2 reflects a contralateral dominance enhancing mu ERD and beta ERS at channels Cz and C4 respectively.

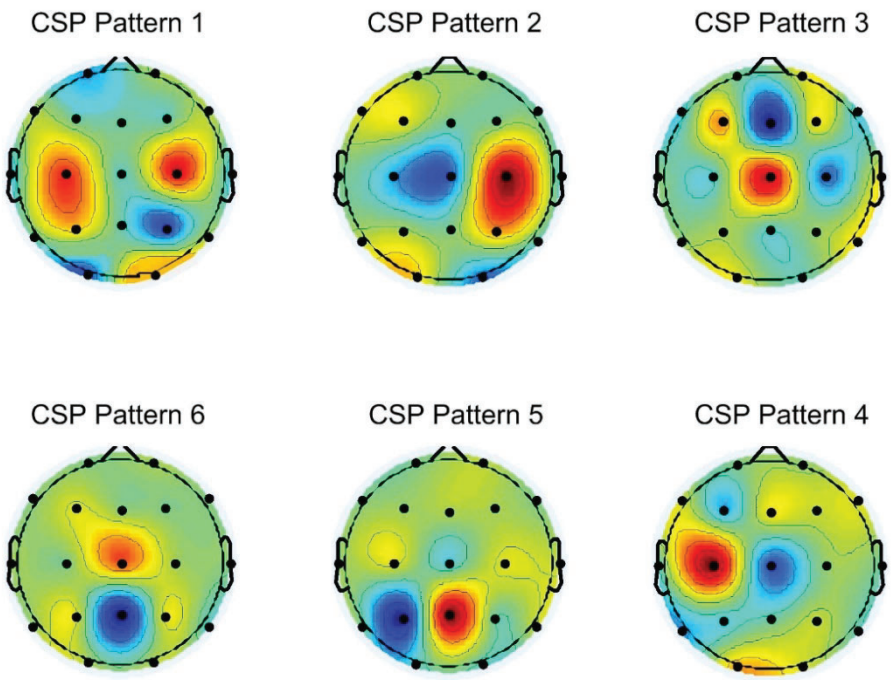

Fig. 4. A set of common spatial patterns (CSPs) filters of participant P01. The CSPs are optimized for the discrimination of right and left knee kinaesthetic motor imageries from the reference period.

The misclassification rate (mcr) elicited by each participant is reported in Table 1, with a 5-fold cross validation. For each combination of methods, accuracies are calculated in percentage and the respective average and standard deviations are reported. For CSP feature extraction method, Logreg showed lower mcr of 37.00% ±4.81, whereas with LDA reflected the mcr was not much different i.e. 38.00% ± 4.12. The FBCSP method with Logreg performed better than with LDA, as it produced a mcr of 34.00% ± 2.85, with LDA mcr was highest i.e. 39.50% ± 2.74. Overall the average classification accuracy with all four paradigms was above the chance level of 60.00% for $p < 0.01$ for 2-class BCI (with 80 trials), as explained by [27]. In only 3 cases participant 4 and 5 performed above the chance level of 57.50% for $p < 0.05$. FBCSP-Logreg outperformed the remaining paradigms, where P01 performed the best with classification accuracy of 70.00% ± 2.85, as shown in Fig. 3.

Table 1. Misclassification rate using CSP and FBCSP with linear discriminant analysis (LDA) and logistic regression (Logreg) classifiers with 5x5-fold of cross-validation.

Participant	CSP		FBCSP	
	LDA mcr (%)	Logreg mcr (%)	LDA mcr (%)	Logreg mcr (%)
P1	32.50**	30.00**	40.00**	30.00**
P2	35.00**	35.00**	40.00**	32.50**
P3	40.00**	37.50**	35.00**	37.50**
P4	42.50*	40.00**	42.50*	35.00**
P5	40.00**	42.50*	40.00**	35.00**
Average	38.00	37.00	39.50	34.00
S.D.	4.12	4.81	2.74	2.85

* Over chance level of 2-class discrimination, 57.50% ($p < 0.05$).

** Over chance level of 2-class discrimination, 60.00% ($p < 0.01$).

Figure 5 illustrates the AUC-ROC curves, along the x-axis is FPR and along y-axis lays the TPR. In all plots, the diagonal grey line represents 50% chance level for the binary classifier. Ideally AUC should be 1 (exact 90° angle) for 100% accuracy. In each case, the participants produced an AUC-ROC above chance level, with P01 performing with a maximum AUC in case of FBCSP-Logreg, as shown in Table 2. The colour legend for each curve is given as, blue: CSP-Logreg, green: FBCSP Logreg, yellow-chartreuse: CSP-LDA, and maroon: FBCSP-LDA.

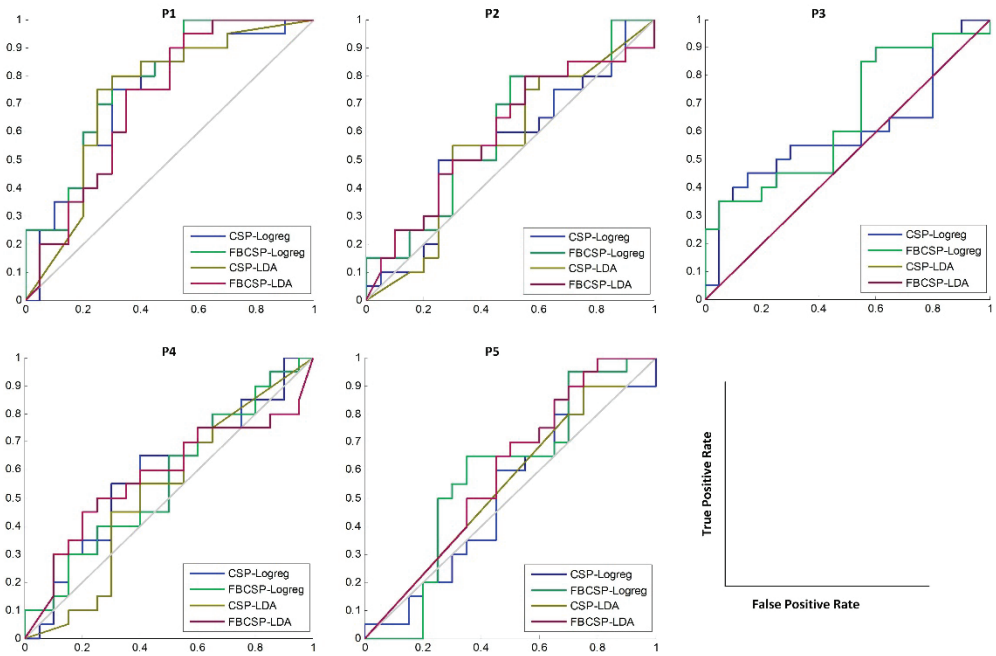

Fig. 5. Receiver operator characteristics curves depicting area under the curves for all participants.

Table 2. Area under (ROC) curve (AUC) and kappa scores using CSP and FBCSP with linear discriminant analysis (LDA) and logistic regression (Logreg) classifiers.

Participant	CSP				FBCSP			
	LDA		Logreg		LDA		Logreg	
	AUC	κ	AUC	κ	AUC	κ	AUC	κ
P1	0.73	0.35	0.73	0.40	0.71	0.20	0.78	0.40
P2	0.69	0.30	0.75	0.30	0.55	0.20	0.62	0.35
P3	0.56	0.20	0.58	0.25	0.59	0.30	0.61	0.25
P4	0.55	0.15	0.59	0.20	0.58	0.15	0.60	0.30
P5	0.57	0.20	0.55	0.15	0.60	0.20	0.62	0.30
Average	0.62	0.24	0.64	0.26	0.61	0.21	0.65	0.32

Table 2 also highlight the kappa scores with each paradigm. The maximum kappa was scored by P01 with FBCSP-Logreg and CSP-Logreg. Overall the maximum kappa was obtained with FBCSP-Logreg with an average score of 0.32. According to [28], the strength of agreement between predicted and true class for 0.21-0.40 is fair. Thus, for the maximum obtained score, the strength of agreement is fair.

4. Discussion and conclusion

This study presents a novel finding on knee kinaesthetic motor imagery employed as cognitive task for a 2-class BCI. We proposed 4 methodology paradigms for analyzing and discriminating the left vs. right knee KMI feature vectors, i.e. CSP-LDA, CSP-Logreg, FBCSP-LDA, and FBCSP-Logreg. Each of the proposed paradigms demonstrated classification accuracy above the chance level of a 2-class BCI, i.e. 60.00% ($p < 0.01$) with a 5-fold cross validation for training and testing phases. The CSP pair patterns exhibited an enhancement in the hand and foot area *mu* and *beta* rhythm. This implicates that the knee KMI does not enhance a new area in the cortex, possibly due to the location of knee representation area in the mesial wall of the cortex. The results, however, are overall encouraging as the average kappa score for each paradigm lies in the fair range of agreement between predicted and true class, with maximum score of 0.40. Generally, FBCSP-Logreg produced a maximum individual classification accuracy rate of 70% and an average accuracy rate of 64%. These results are encouraging and provide the basis to exploit left vs. right knee KMI to be used as individual control signals in a 2-class BCI for operating a knee neuroprosthesis, or robotic knee for lower-limb amputees. We aim at engaging more participants and provide feedback training for the future investigation.

References

[1] Tariq, M., P. Trivailo, and M. Simic, EEG-Based BCI Control Schemes for Lower-Limb Assistive-Robots. Frontiers in human neuroscience, 2018. 12: p. 312.

[2] Lebedev, M.A. and M.A. Nicolelis, Brain-machine interfaces: From basic science to neuroprostheses and neurorehabilitation. Physiological reviews, 2017. 97(2): p. 767-837.

[3] Tariq, M., P.M. Trivailo, and M. Simic. Detection of knee motor imagery by Mu ERD/ERS quantification for BCI based neurorehabilitation applications. in 2017 11th Asian Control Conference (ASCC). 2017. IEEE.

[4] Wolpaw, J. and E.W. Wolpaw, Brain-computer interfaces: principles and practice. 2012: OUP USA.

[5] Tariq, M., et al. Mu-beta rhythm ERD/ERS quantification for foot motor execution and imagery tasks in BCI applications. in 2017 8th IEEE International Conference on Cognitive Infocommunications (CogInfoCom). 2017. IEEE.

[6] Mokienko, O., et al., Increased motor cortex excitability during motor imagery in brain-computer interface trained subjects. Frontiers in computational neuroscience, 2013. 7: p. 168.

[7] Penfield, W. and E. Boldrey, Somatic motor and sensory representation in the cerebral cortex of man as studied by electrical stimulation. Brain, 1937. 60(4): p. 389-443.

[8] Hashimoto, Y. and J. Ushiba, EEG-based classification of imaginary left and right foot movements using beta rebound. Clinical neurophysiology, 2013. 124(11): p. 2153-2160.

[9] Ramoser, H., J. Muller-Gerking, and G. Pfurtscheller, Optimal spatial filtering of single trial EEG during imagined hand movement. IEEE transactions on rehabilitation engineering, 2000. 8(4): p. 441-446.

[10] Blankertz, B., et al., Optimizing spatial filters for robust EEG single-trial analysis. IEEE Signal processing magazine, 2007. 25(1): p. 41-56.

[11] Zhang, Y., et al., Optimizing spatial patterns with sparse filter bands for motor-imagery based brain–computer interface. Journal of neuroscience methods, 2015. 255: p. 85-91.

[12] Ang, K.K., et al. Filter bank common spatial pattern (FBCSP) in brain-computer interface. in 2008 IEEE International Joint Conference on Neural Networks (IEEE World Congress on Computational Intelligence). 2008. IEEE.
[13] Ang, K.K., et al., Filter bank common spatial pattern algorithm on BCI competition IV datasets 2a and 2b. Frontiers in neuroscience, 2012. 6: p. 39.
[14] Kothe, C.A. and S. Makeig, BCILAB: a platform for brain–computer interface development. Journal of neural engineering, 2013. 10(5): p. 056014.
[15] Klem, G.H., et al., The ten-twenty electrode system of the International Federation. Electroencephalogr Clin Neurophysiol, 1999. 52(3): p. 3-6.
[16] Tariq, M., et al., Comparison of Event-related Changes in Oscillatory Activity During Different Cognitive Imaginary Movements Within Same Lower-Limb. Acta Polytechnica Hungarica, 2019. 16(2): p. 77-92.
[17] Renard, Y., et al., Openvibe: An open-source software platform to design, test, and use brain–computer interfaces in real and virtual environments. Presence: teleoperators and virtual environments, 2010. 19(1): p. 35-53.
[18] Tariq, M., P.M. Trivailo, and M. Simic, Motor imagery based EEG features visualization for BCI applications. Procedia computer science, 2018. 126: p. 1936-1944.
[19] Blankertz, B., et al., The Berlin Brain-Computer Interface: Accurate performance from first-session in BCI-naive subjects. IEEE transactions on biomedical engineering, 2008. 55(10): p. 2452-2462.
[20] Pfurtscheller, G. and F.L. Da Silva, Event-related EEG/MEG synchronization and desynchronization: basic principles. Clinical neurophysiology, 1999. 110(11): p. 1842-1857.
[21] Lotte, F., et al., A review of classification algorithms for EEG-based brain–computer interfaces: a 10 year update. Journal of neural engineering, 2018. 15(3): p. 031005.
[22] Tharwat, A., Classification assessment methods. Applied Computing and Informatics, 2018.
[23] Kraemer, H.C., Kappa coefficient. Wiley StatsRef: Statistics Reference Online, 2014: p. 1-4.
[24] Cohen, J., A coefficient of agreement for nominal scales. Educational and psychological measurement, 1960. 20(1): p. 37-46.
[25] Tariq, M., P.M. Trivailo, and M. Simic, Event-related changes detection in sensorimotor rhythm. International Robotics & Automation Journal, 2018. 4(2): p. 119-120.
[26] Pfurtscheller, G., et al., Mu rhythm (de) synchronization and EEG single-trial classification of different motor imagery tasks. NeuroImage, 2006. 31(1): p. 153-159.
[27] Müller-Putz, G., et al., Better than random: a closer look on BCI results. International Journal of Bioelectromagnetism, 2008. 10(ARTICLE): p. 52-55.
[28] Landis, J.R. and G.G. Koch, The measurement of observer agreement for categorical data. biometrics, 1977: p. 159-174.

Chapter 9

Conclusions and future work

Chapter Overview

The goal of this chapter is to summarise general conclusions on the feature extraction and classification of left-right foot, and left-right knee KMI, and how the current work's findings can be helpful to develop a LL KMI based real-time BCI. Finally, recommendations for future work are presented.

9.1 Conclusions

Research on seamless control of LL assistive devices for navigation, or gait assistance, has emerged as a promising area in the field of rehabilitation. For people with lost motor, e.g. SCI or amputation, but intact sensory control, the origination of control signals from the source, i.e. electrophysiological signals, is indispensable for control of assistive devices. With established literature, it is well known that motion intentions primarily arise in the cortical areas of brain. When opting for portable non-invasive modality to record motion intentions, EEG is most suitable. EEG signals applicable in independent BCIs that have successfully been used with assistive technology, are the oscillatory rhythms/SMR and ERP. ERP paradigm accounts for a large hardware setup to provide stimulus to the user, during operation of the assistive device. In contrast, the oscillatory rhythms do not necessitate large hardware setup for stimulating cortical activity; instead it relies on the motor imagery produced synchronously, or asynchronously by the user. This motor imagery, or KMI, is produced after rigorous training trials. Commonly deployed cognitive tasks include limb motor tasks, yet there is no consensus on standardised methods, or selection of cognitive tasks, during performance in a BCI paradigm. Selection of cognitive tasks, to produce detectable feature vector, that correlate to the user's intent, is one key factor to improve the performance of a BCI.

Motor imageries associated to limbs predominantly remain with the upper-limbs, due to the anatomical placement of LL representation areas in the sensorimotor cortex. The contralateral hemispheres of the cortex share close spatial proximity and are placed inside the interhemispheric fissure of the sensorimotor cortex. These two factors account for difficulty in the detection of EEG features elicited upon imagination of LL. Therefore, a deep understanding and investigation of the ERD/ERS in frequency band of *mu* and *beta* oscillatory rhythms, during left and right LL KMI in humans, is an important area for research. Solution to these issues is important for the development of robust controllers in asynchronous BCI paradigms, to control LL assistive devices seamlessly. However, it is a challenging area in which different research groups have conflicting opinions, whether the cortical lateralization of LL using EEG features is possible, for practical implementation, in a BCI paradigm, or not. Focus of the present study was to investigate the cortical lateralization of ERD/ERS, based on KMI of foot dorsiflexion and knee extension individually, using BP and CSP feature vector. The study deployed synchronous BCI paradigm, to ensure that the users elicit oscillatory rhythms upon motor imagery of LL for the possibility of practically implementing a control system in a BCI. Results obtained from

these studies have been discussed in detail and reported in Chapters 4 to 8. This chapter underscores the main conclusions that are drawn from the research.

Since cortical EEG signals are non-stationary, that offers arduous challenges, from data analysis viewpoint. It is characterized by trial-to-trial and participant-to-participant variability followed by, the low signal-to-noise ratio, which is not favourable. Cortical signals are high-dimensional with relatively few samples that are available for fitting models to the data. Due to these factors, machine learning (ML) methods were included into the tool of choice for online analysis of single-trial EEG data. In comparison to this, the classical neurophysiological analysis methods use averaging methods for e.g. taking grand averages over trials, participants, and sessions, to discard various sources of variability. Therefore, the selection of suitable ML model is another challenging area, for the accurate and statistically true detection of the class of KMI.

To increase the dimensionality of control signals, in a BCI paradigm, for restoration of locomotion function in LL assistive devices, an analysis of BP features, based on foot and knee KMI within the same LL was done in Chapter 4. Conclusions from this study are as follows:

1. Despite a small LL sensorimotor area representation in the homunculus, the foot and knee KMI elicited event-related changes respectively, in the *mu* (7-12 Hz) band within the same limb. Based on the spectral power plots, an increase in the mid-central ERD was observed with all the participants. Mu ERD was mainly observed in the cortical foot area representation, with small shift towards parietal lobe.
2. In contrast to foot, the left-right knee KMI tasks did not exhibit prominent contralateral dominance of ERD, except for one participant. This could possibly be due to less number of participants and the spatial proximity of left-right LL and its placement in the interhemispheric fissure of the mesial wall in the sensorimotor cortex. Results suggested that intra-subject cognitive-state variability exists during the reactivity of *mu* components. This makes it difficult to draw a clear difference between both LL tasks within the same limb. However, clear results with one participant; indicate the possibility of discriminating different movements within the same LL.

While ERD successfully exhibited in the *mu* band, analysis of *beta* ERD/ERS in the BP feature with more participants was important for investigation. The next study was based on

the possibility to deploy the *mu* ERD and *beta* ERD/ERS features, as independent control features in a BCI paradigm, based on foot KMI. It was discussed in Chapter 5. The analysis was done for common average and bipolar reference methods respectively. In order to evaluate this possibility, implementation of suitable ML model was essential. The key conclusions from this study are as follows:

1. Confirmation of cortical lateralization of ERD/ERS during left and right foot KMI was done in the *mu* (7-12 Hz), low *beta* (13-24 Hz) and high *beta* (25-35 Hz) frequency bandwidths. This was obtained from the three channels at the vertex i.e. C3, Cz, and C4 using common average and bipolar reference methods.
2. The k-nearest neighbors (KNN) model outperformed LDA and SVM models with the highest classification accuracy of 83.4% ± 6.72 with an AUC-ROC of 0.85, using common average reference in comparison with bipolar reference. Results from this study produced an enhancement in the *beta* ERS classification accuracy in comparison to another similar study from literature that used different methodology.
3. The trade-off between attaining a low training and a low testing error during classification was controlled with the optimal regularization parameter from a range of values, for all three ML models, using the *k*-fold cross validation.
4. Classification accuracies of the three features, *mu* ERD, *beta* ERD, and *beta* ERS, based on left-right foot KMI, suggest the possibility of using them in a single BCI paradigm with 6 degrees of freedom (DOF) commands; or as unilateral control features in a synchronous 2-class BCI for operating bionic or neuro-prosthetic foot.

BP feature vector was employed for classification of left and right foot KMI using two references for comparison, followed by three ML models, to confirm the cortical lateralization. The next goal was to improve the classification accuracy by adopting common spatial pattern (CSP) feature vector and analysing it for LDA and logistic regression (Logreg) ML models, respectively. In addition to CSP, the study encompasses filter-bank CSP (FBCSP) for optimization of individual spatial patterns of participants. The low-cut and high-cut frequency bands of optimal filters were 8-12 Hz, 13-25 Hz, and 28-32 Hz that encompass the *mu* and *beta* range. Results from this have been reported in Chapter 6. The key conclusions from this study are as follows:

1. Bilateral foot KMI resulted in the discrimination of left and right foot tasks using the CSP and FBCSP feature vectors. Since FBCSP's feature space dimensionality is

larger than that of CSP, with more flexibility, a risk of overfitting is associated, i.e. a tradeoff between overfitting and estimation of optimal parameters. This necessitated a comparison of FBCSP feature with the standard CSP.

2. The selection of time and frequency regions is critical, as the complex (relevant) interactions between *mu* and *beta* bands are seemingly rarely observed. It could be very useful when oscillatory processes in different frequency bands (with different spatial topographies) e.g., *mu*, low *beta* and high *beta*, are jointly active. Their concerted reaction must be taken into account for the given prediction task.
3. The FBCSP with LDA model resulted in highest classification accuracy of 77.5% ± 4.23 compared to other models with an AUC-ROC of 0.70. The CSP and FBCSP features with Logreg performed above the statistical chance level of 60% ($P < 0.01$) as per a 2-class BCI problem. However, the highest classification accuracy of this study could not exceed the single trial analysis classification accuracy from the previous study (Chapter 5).
4. The maximum kappa score was 0.55 and the maximum average kappa statistic was also in the 0.41<0.60 range, i.e. the strength of agreement between classes was moderate. A 10-fold cross validation method was used to estimate the optimal parameters for the classifiers and avoid overfitting classifiers to the training data. It predicted the true performance of ML models. Given results stipulate the utilization of *mu* and *beta* as independent control features for discrimination of bilateral foot KMI in a BCI.

After detailed analysis of left and right foot KMI, the next direction was to implement similar strategies as those inferred in Chapters 5 and 6 respectively, to the left and right knee KMI. Chapter 7 and 8 exploit the knee KMI using BP and CSP feature vectors respectively, in order to predict the cortical lateralization of ERD/ERS in the mu and beta (7-35 Hz) frequency bandwidth followed by the excitability of new cortical regions. Since the knee KMI has never been exploited before, these studies are novel, therefore, as a pilot study, only five participants were involved in the experiments. Conclusions from Chapter 7 and 8 are given as:

1. Using BP features, the left and right knee KMI showed cortical lateralization at the three vertex channels i.e., C3, Cz, and C4, using common average reference method, as concluded in Chapter 5 for better performance. The maximum classification accuracy was 81.04% ± 7.5 and AUC-ROC = 0.84, using KNN classifier model for

beta ERS feature in comparison to SVM model. However, the maximum overall average accuracy was obtained in case of *mu* ERD, 74.59% ± 5.1, again with KNN. These results are very encouraging in view of the covert anatomical representation area of left and right knee, in the human sensorimotor cortex, compared to that of upper limbs/hands. Following this, all proposed ML models performed above the statistical chance level of 60% ($P < 0.01$) as per a 2-class BCI problem.

2. With CSP and FBCSP feature vectors, the left-right knee discrimination was also successful, where all classifier models resulted in accuracy ≥ 60% ($P < 0.01$). The maximum accuracy was achieved with FBCSP-Logreg model of 70.00% ± 2.85, a kappa statistic of 0.40, and an AUC-ROC of 0.78 in comparison to LDA model. Albeit the strength of agreement between the two classes is fairly good but not substantial. Therefore, engagement of more participants could ensure better understanding and visualization of deploying the CSP and FBCSP feature vectors in a BCI based on knee KMI.
3. No excitability of a new area in the sensorimotor cortex was detected, for knee KMI tasks. ERD/ERS was only observed in the vicinity of the vertex and in the foot area representation of the cortex.
4. The results from ERD/ERS in the BP feature vector however provide the basis for utilization of left and right knee KMI as cognitive inputs that could be exploited as two unilateral commands for navigation control in a BCI-controlled bionic knee. Results from Chapter 7 infer the possibility to deploy the novel knee KMI as a cognitive task in a BCI paradigm.

9.2 Suggestions for future studies

The inferences drawn out of this study have been acquired from somewhat less number of participants, due to constraints of time and resources. Engagement of more participants for further studies is required to extend the contribution of this thesis for establishing a better understanding of the area. Some suggestions and recommendations for future research to expand our knowledge of the various EEG pre-processing and feature extraction methods, and classification algorithms, as well as the real-time implementation of the analysed cognitive tasks addressed in this thesis, are outlined in this section. Recommendations to study these factors are given as follows:

1. Testing of the proposed methods in all four studies on a larger population could endorse and emphasize on the drawn conclusions from the studies presented in this thesis. This should particularly be in the case of left-right knee KMI, as the suggested cognitive task is novel and the study conducted was pilot. With left-right foot KMI, albeit the number of participants was nine, which is good enough to draw a conclusion as per references. The involvement of more participants could ensure the viability of utilizing two independent control commands based on left-right foot KMI in real-time BCI. This could also be imperative in case of commercialization of the results for real-time BCI applications.
2. In all four studies presented in this thesis, the number of training trials was kept to a standard of 80 trials, per class per session (with total of 160 trials per session). It would be interesting to know the effects of larger number of training trials and longer length of the experimental trial on the prevention of overfitting, i.e. possibility of a tradeoff between number of training trials and overfitting.
3. The feedback training plays an effective role in enhancing the classification accuracy of a motor imagery based BCI paradigm. In the four conducted studies from this thesis, none of them involved neurofeedback training during practicing of the experimental synchronous BCI protocol. Therefore, further studies with more time allocated to the BCI neurofeedback training for participants are required, to determine its effects on the classification accuracy.
4. Further studies are required to discriminate between four independent cognitive tasks, i.e. left foot, left knee, right foot, and right knee, within the same limb, that could increase the dimensionality of control signals, as a cognitive entity in a BCI paradigm. This could help develop a 4 DOF cognitive tool to actuate four aspects of an assistive device in a single BCI controller. Although one aspect of this study attempted to improve the classification accuracy of left-right foot KMI, further experimentation with more non-linear ML models is needed. For instance, neural-networks could be used to improve the knowledge about discrimination of foot KMI tasks, and its effects on the cortical lateralization of ERD/ERS and latency reduction in the real-time BCI.
5. Since the primary aim of the four studies was to visualize the possibility of deploying left-right foot and left-right knee KMI in a real-time BCI, all methods and analyses revolved around the attempt to attain maximum classification accuracy, satisfying the test-statistics. The future aim directs towards testing the developed methodologies and ML models from the four studies in real-time, i.e. implement

designed methods on a real-time BCI paradigm and interface it with LL assistive hardware. This could be instigated by using lab-streaming layer (LSL) which allows synchronization of the streaming data across devices. Alternatively, EEG signals could be transferred to the BCI operator via communication protocol that further directs them to the actuator, for instance, Transmission Control Protocol/Internet Protocol (TCP/IP), a suite of communication protocols used to interconnect network devices on the internet, or a private network.

6. Integration of electromyography (EMG) sensors with EEG in the experimental setup for monitoring the muscle activity during performance of imagery tasks could indicate the prevalence of accidental EMG activity. The EMG sensors could be fixed on the left and right tibialis anterior muscles over the muscle belly. Effects of recorded EMG activity on the lateralized brain activity could be checked.
7. Wireless EEG for portable assistance (BCI assistive device) is necessary because ideally the independent BCI based on oscillatory rhythm works asynchronously, for instance portable exoskeleton, orthosis, prosthesis, or wheelchair for gait assistance necessitates a wireless portable controller. Synchronous BCI paradigms that result in sufficient classification accuracy for real-time BCI could be used as a practice for asynchronous BCI, in order to improve the data transfer rate from BCI controller to output device. Further, since in a cue-based synchronous BCI controller, the decision time is relatively slow for real-time applications, such as walking, where a seamless execution of command from the assistive-device is essential, the self-paced asynchronous BCI is the solution. An asynchronous BCI fully paced by user intent, could result in a seamless walking gait with assistive device, be less tiring, and could provide a source of comfort to the user.

Appendices

Appendix A.

Other published articles and articles in press.

Appendix B.

Ethics approval.

Appendix A.

Event-related changes detection in sensorimotor rhythm

Chapter Overview

The aim of this study is to investigate the sensorimotor rhythms (SMR) that exhibit upon left and right leg imagery for locomotion task. From SMR, the *mu* rhythm was observed for possibility of any contralateral dominance in the topographic maps. The experiments were based on motor execution (ME) and motor imagery (MI) tasks to validate the notion that for the same task, the MI should excite same cortical areas as those during ME. The notion was validated, however, there was no significant cortical lateralization observed.

This work has been published in ***International Robotics & Automation Journal.***

M. Tariq, P. M. Trivailo, M. Simic. *Event-related changes detection in sensorimotor rhythm*. International Robotics & Automation Journal, 4(2) 119-120, 2018.

MedCrave
Step into the World of Research
International Robotics & Automation Journal

Research Article

Open Access

Event-related changes detection in sensorimotor rhythm

Abstract

Brain activities initiate motion in the human body. In our research we try to detect brain electrical activities and generate control signals for robotic devices like prosthetic legs. Human legs are associated with a small representation area in the sensorimotor (SMR) cortex, which is located deep inside the inter hemispheric fissure. It is difficult to observe any electroencephalographic activity related to the legs. Detection of sensorimotor signals, based on leg imagery, could potentially be useful in medical applications, i.e. for systems that are using brain-computer interface for lower limbs assistance. We investigate reactivity of sensorimotor rhythm i.e., mu rhythm, as a result of given tasks, such as, motor execution (ME) and motor imagery (MI) of the leg. Resulting SMR was analyzed, for each task state and evaluated in terms of event-related de synchronization and event-related synchronization patterns. Higher power concentration was observed in the foot representation and peripheral areas, during both ME and MI tasks. No contralateral dominance was detected during left or right discrimination tasks. Results provide a foundation for leg imagery based, interfacing and control signals creation. This could be used for locomotion functions' restoration in a lower limb wearable rehabilitation system. Spinal cord injury patients could, also, be potential users of this type of biomechanical systems.

Keywords: electroencephalography, brain-computer interface, motor execution, motor imagery, event-related desynchronization, event-related synchronization

Volume 4 Issue 2 - 2018

Madiha Tariq, Pavel M Trivailo, Milan Simic
School of Engineering, RMIT University, Australia

Correspondence: Milan Simic, School of Engineering, RMIT University, Australia, Tel +61 3 992 56223, Fax +61 3 992 56108, Email milan.simic@rmit.edu.au

Received: February 01, 2018 | **Published:** March 28, 2018

Abbreviations: EEG, Electroencephalography; BCI, brain-computer interface; ME, motor execution; MI, motor imagery; ERD, event-related desynchronization; ERS, event-related synchronization, SMR, sensorimotor rhythms

Introduction

Human walking gait is disrupted by the spinal cord injury (SCI) or amputation.[1] Gait rehabilitation involves improvement of the motor control functions by the activation of neuro-plasticity. It can be achieved by deciphering and translation of brain signals that correspond to the execution, or action imagery, of the affected limb, into output commands. BCI could be used to build new communication channel between the brain and output devices. EEG features, generated against motor execution or imagery tasks, comprise of sensorimotor rhythms generated in the primary and sensory motor cortex. SMR are usually concentrated in the *mu* (8-11Hz) or *beta* (12-32Hz) frequency bands.[2] SMR changes against each task are unique and can be exploited using feature extraction and classifications. This report highlights the changes in *mu* rhythm against the ME and MI of leg movement. The *mu* rhythm changes are quantified in terms of event-related desynchronization and event-related synchronization. ERD is associated with the proportional power decrease in concentration, while ERS with the proportional power increase in the signal. SMR ERD is linked with MI, as well as, with actual movement.[3] Studies on tasks related to lower limbs are presented here.[4,5] Investigations are required of SMR on leg tasks, both for ME and MI, to be used as control signals in BCI applications. The limbs somatotopy, in the sensory and motor cortices, enables cortical localization of ERD patterns. Lower limbs area representation is located deep within the interhemispheric fissure of the sensorimotor cortex, which makes it hard to detect ERD patterns.[6]

Materials and methods

Study involved three healthy participants, 25-27 years old. Ethics approval was granted by the University ethics committee. Experiments were based on the Graz BCI protocol for ME/MI tasks and consisted of 6 runs, 3 for each task. Standard 10-20 Electro-cap was used to acquire brain signals from the motor cortex. EEG system includes 20 channels sampled at 256Hz with 24-bit resolution. Statistical EEGLAB package (http://www.sccn.ucsd.edu/eeglab/) was used to process and analyse data. Acquired signals were band pass filtered between 8 to 11Hz which is the required frequency bandwidth range of *mu* rhythm followed by epoching of the trials (10seconds in length). Extracted and analyzed trials included period of 3seconds prior to cue onset used as reference period. This was followed by artifact removal method, the independent component analysis (ICA).[7] Quantification of *mu* ERD/ERS patterns was done following method proposed by Kalcher et al.[8] Proportional power decrease or increase, compared to the reference interval, is usually in the period of several seconds before the event onset. A 3 second interval, prior to visual cue onset, was selected as reference.

Results and discussion

Experiments involved execution and imagination of left and right legs movements. Topographical scalp maps of participant 1 during imagery and execution of left leg movement are presented in Figure 1. Color bar indicates the spectral power concentration over the scalp for all channels in the *mu* frequency range. Power spectral density is represented in logarithmic scale. For participant 1 it was observed that a high spectral power concentration was in the central regions. The left leg ME enhanced the *mu* rhythm concentrated in the foot area representation. This was visible at both 8 and 11Hz frequencies.

Similarly with MI task, the ERD was centrally localized and edged towards right parietal region, which could be an indication of contralateral dominance at 8 and 11Hz frequencies. However, this was not the case with remaining participants. After experiments with all participants, we have collected large amount of data that we analyze and try to decipher.

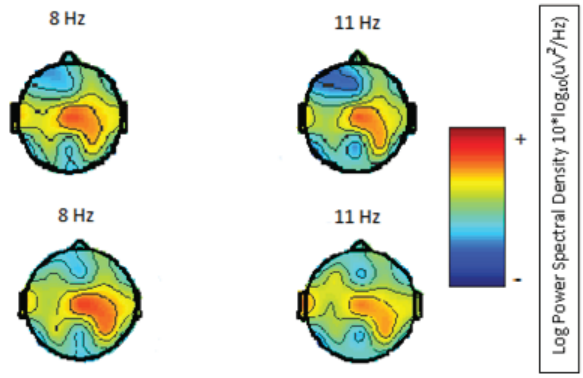

Figure 1 Participant 1 topographical scalp maps during left leg ME and MI sessions, at 8Hz and 11Hz.

Conclusion

The ME and MI signals elicited against leg movement tasks can prove to be potential control signals in the BCI application for assistive technologies, useful for SCI patients or amputees with intact brain functions. The spectral topographic plot suggested the central cortical areas to be high in power concentration during leg imagery and execution tasks. Motor execution tasks activate same cortical areas as imagery tasks. In all cases, at the beginning of the visual cue onset a desynchronization in the leg *mu* area was visible followed by a dominant ERS at the end of the trial. These results are in coherence with the established results from the spectral power distribution maps. Further study is needed for a comprehensive mapping of our thoughts to robotics control signals, but obtained results are promising.

Acknowledgements

None.

Conflict of interest

The author declares there is no conflict of interest.

References

1. Tariq M, Koreshi Z, Trivailo P. Optimal control of an active prosthetic ankle. In Proceedings of the 3rd International Conference on Mechatronics and Robotics Engineering; 2017 Feb 8-12; Paris, France. ACM; 2017. p. 113–118.
2. Wolpaw J, EW Wolpaw. Brain-computer interfaces: principles and practice. *Bio Medical Engineering Online*; 2012;1–424.
3. Jasper H, Penfield W. Electrocorticograms in man: effect of voluntary movement upon the electrical activity of the precentral gyrus. *European Archives of Psychiatry and Clinical Neuroscience*. 1949;183(1-2):163–174.
4. Boord P, Craig A, Tran Y, et al. Discrimination of left and right leg motor imagery for brain–computer interfaces. *Med Biol Eng Comput*. 2010;48(4):343–350.
5. Lisi G, Noda T, Morimoto J. Decoding the ERD/ERS: influence of afferent input induced by a leg assistive robot. *Front Syst Neurosci*. 2014;8:85.
6. Hashimoto Y, Ushiba J. EEG-based classification of imaginary left and right foot movements using beta rebound. *Clin Neurophysiol*. 2013;124(11):2153–2160.
7. Barlaam F, Descoins M, Bertrand O, et al. Time–frequency and ERP analyses of EEG to characterize anticipatory postural adjustments in a bimanual load-lifting task. *Front Hum Neurosci*. 2011;5:163.
8. Kalcher J, Pfurtscheller G. Discrimination between phaselocked and non-phase-locked event-related EEG activity. *Electroencephalogr Clin Neurophysiol*. 1995;94(5):381–384.

Citation: Tariq M, Trivailo PM, Simic M. Event-related changes detection in sensorimotor rhythm. *Int Rob Auto J.* 2018;4(2):119–120. DOI: 10.15406/iratj.2018.04.00105

Motor imagery based EEG features visualization for BCI applications

Chapter Overview

The use of EEG-based BCIs in medical and non-medical applications has augmented the quality of life. For medical applications, the availability of real-time data processing platforms for BCI to control robotic devices is limited to few. This study assesses the possibility to analyse and visualize EEG *mu* and *beta* features using the OpenViBE acquisition platform in offline mode, albeit it's real-time processing capability. Aim was to discover the tools/options available for processing the data in offline mode. Using OpenViBE, EEG signals were acquired, pre-processed, and features were extracted for quantification of event-related (de)synchronization (ERD/ERS) by developing scenarios using the designer toolbox. Since the experimental study involved foot kinaesthetic motor imagery (KMI), the acquired data was recorded using the standard built-in Graz BCI protocol. Results showed that OpenViBE is a streaming tool that supports processing and analysis of EEG online, contrary to visualization of data in global mode. It is one potential tool for real-time control of assistive technologies using BCI paradigm.

This work has been published in ***International Journal of Knowledge-Based and Intelligent Engineering Systems: Procedia Computer Science.***

M. Tariq, P.M. Trivailo, and M. Simic. *Motor imagery based EEG features visualization for BCI applications*. International Journal of Knowledge-Based and Intelligent Engineering Systems: Procedia Computer Science 126, 1936-1944, 2018.

Available online at www.sciencedirect.com

ScienceDirect

Procedia Computer Science 126 (2018) 1936–1944

Procedia Computer Science

www.elsevier.com/locate/procedia

22nd International Conference on Knowledge-Based and Intelligent Information & Engineering Systems

Motor imagery based EEG features visualization for BCI applications

Madiha Tariq*, Pavel M. Trivailo, Milan Simic

School of Engineering, RMIT university Bundoora Plenty Road, 3083 Victoria Australia

Abstract

Over recent years, electroencephalography's (EEG) use in the state-of-the-art brain-computer interface (BCI) technology has broadened to augment the quality of life, both with medical and non-medical applications. For medical applications, the availability of real-time data for processing, which could be used as command signals to control robotic devices, is limited to specific platforms. This paper focuses on the possibility to analyse and visualize EEG signal features using OpenViBE acquisition platform in offline mode apart from its default real-time processing capability, and the options available for processing of data in offline mode. We employed OpenViBE platform to acquire EEG signals, pre-process it and extract features for a BCI system. For testing purposes, we analysed and tried to visualize EEG data offline, by developing scenarios, using method for quantification of event-related (de)synchronization ERD/ERS patterns, as well as, built in signal processing algorithms available in OpenViBE-designer toolbox. Acquired data was based on deployment of standard Graz BCI experimental protocol, used for foot kinaesthetic motor imagery (KMI). Results clearly reflect that the platform OpenViBE is a streaming tool that encourages processing and analysis of EEG data online, contrary to analysis, or visualization of data in offline, or global mode. For offline analysis and visualization of data, other relevant platforms are discussed. In online execution of BCI, OpenViBE is a potential tool for the control of wearable lower-limb devices, robotic vehicles and rehabilitation equipment. Other applications include remote control of mechatronic devices, or driving of passenger cars by human thoughts.

Keywords: EEG; BCI; OpenViBE; kinaesthetic motor imagery (KMI)

* Corresponding author. Tel.: +61 421 136 356; fax: +0-000-000-0000 .
E-mail address: madiha.tariq@rmit.edu.au

10.1016/j.procs.2018.08.057

1. Introduction

In recent years, new attributes to human computer interaction have revolutionized various fields of application, e.g. medicine, entertainment, etc. Predominantly, these technologies are of the key interest to researchers in the areas of health and rehabilitation, e.g. upper or lower-limb wearable robot control such as prosthetic, exoskeleton, or orthosis devices [1]. The state of the art brain-computer interface (BCI) has enabled real-time monitoring of the brain activities, and allows the brain signals to control external devices, like neuroprosthesis, without the involvement of any muscular activity [2-5]. It also functions as a bridge to bring sensory input into the brain, bypassing damages sight, listening or sensing abilities. A BCI system commonly deploys input signals that are elicited upon execution of motor imagery tasks, i.e. kinaesthetic imagination of a limb movement; these could be hand, foot or tongue movements.

The application areas of BCI range from wheelchair control to security system [6]. BCI has been used to control vehicles in 3D environment recently, as already presented in [7-15]. Various types of BCI system applications are shown in Fig. 1. In the near future, we hope to see a new revolutionary application of the BCI control of human limbs, in the cases when patients have spinal cord injuries. Driving a virtual car in a simulated and in realistic city using EEG is already presented [12]. System is based on P300 wave signal acquisition, which is analysed, recognised and converted into control commands. Virtual car is controlled in 3D environment. The P300 is an event related potential associated to brain activities in decision making. Vehicle control, in a car racing game, which is based on EEG signals that correspond to the driver's right hand, left hand and both hands imaginary movements is also investigated and reported here [10].

In order to analyse and visualize acquired EEG signals, the approach could be offline, or online. Offline analysis enables better understanding of brain functions and building the knowledge based on acquired data, it provides options of various processing tools needed to analyse data and visualize it graphically (in form of plots or graphs). However, it does not allow real-time execution of commands that could be used to control output devices in real-time. On the contrary, online processing is suitable for real-time control of output devices; however, the limitations lie with the data analysis and realization of actions. Online processing of EEG data is apt for experts in the field who can visualize the quality of data. To analyse or process data, various tools are available, both for online and offline mode, and both open source and non-open source, such as, OpenViBE, BioSig, BCI2000, BCI++, MATLAB toolboxes EEGLAB, BCILAB (plug-in of EEGLAB) [16-20]. OpenViBE is open source software, popular and easy to access. It provides a platform for designing, testing and using the BCI in real-time and in virtual-time environments [21].

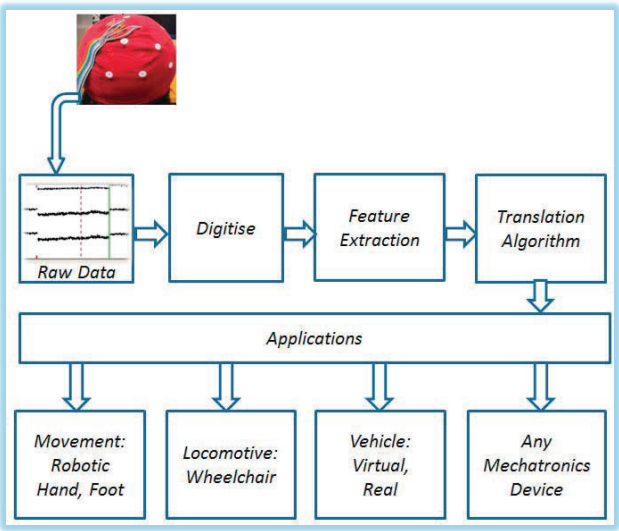

Fig. 1. BCI system's structure for various applications

The OpenViBE platform comprises of a set of software modules dedicated to: Data Acquisition, Data Pre-processing, Data Processing, and Cortical Data Visualization. It also includes the module for interaction with virtual reality (VR) displays. OpenViBE is designed based on the concept of a box, i.e. a fundamental component controlling a fraction of the whole processing pipeline. This enables to develop reusable components, decreases development time and allows for quick extend of functionalities. The platform enables users to add new software modules based on their customized needs [21].

This paper focuses on the testing of OpenViBE platform for the possibility to analyse KMI-based EEG signals in offline or global mode and visualize resulting features in form of output plots. For materializing this, we formulated our band power feature method in the designer window of OpenViBE. To select features of interest, from the recorded *mu* (8-11 Hz) and *beta* (12-30 Hz) rhythms, event-related desynchronization (ERD) and event-related synchronization (ERS) were quantified using standard methods [22, 23]. This paper will provide readers an insight of the possibilities to use OpenViBE for visualization of data in offline mode.

2. Methods

2.1. Experimental paradigm and data collection

We started our investigation by concentrating on the BCI controlled robotic foot movement i.e. one of the rehabilitation applications, as shown in Fig.1. This was based on the detection and decoding of EEG signals that could be used for the control of a robotic foot. Once reliable signal detection and decoding via pre-processing and feature extraction methods is achieved, the next step simply requires conversion, or translation of the feature vector that could be applied to any application. We should highlight here that robotic foots or hands, as well as locomotive equipment, vehicles, or mechatronics devices are intelligent systems. Following that, there is no need for detailed, step by step control of the applications. This approach simplifies the requirements of BCI system, which could use different data acquisition (DAQ) systems. We have concentrated on electrophysiological signals, EEG, as input signals, since it is based on non-invasive methods to record brain activity, and provides reliable output.

The study involved the evaluation of raw EEG data collected from four healthy participants, with no history of neurological disorder and no BCI experience. All were aged between 24-27 years. Ethics approval was granted by the College of Human Ethics Advisory Network (CHEAN) Committee of RMIT University, Melbourne, Australia. EEG neurofeedback (24-channel) BrainMaster Discovery 24E was used to record EEG signals from the brain. The experiment was based on performance of foot kinesthetic motor imagery. In order to set experimental protocol, the Graz motor imagery BCI stimulator box was used from OpenViBE acquisition platform, as shown in Fig. 2. Each trial consisted of a 3 sec reference period for the processing of epochs. An audio beep of 1 sec was incorporated in the beginning of the trial to alert the subject, see Table 1. Each trial was in total 10 sec long. That included 2 sec for cues display and 5 sec for performing motor imagery task, i.e. left or right foot movement. In total, one run consisted of 40 trials, including 20 for left foot and 20 for right foot, displayed randomly to overcome any adaptation. As the task involved kinesthetic motor imagery (KMI), therefore the *mu* and *beta* rhythms were analyzed [2, 3].

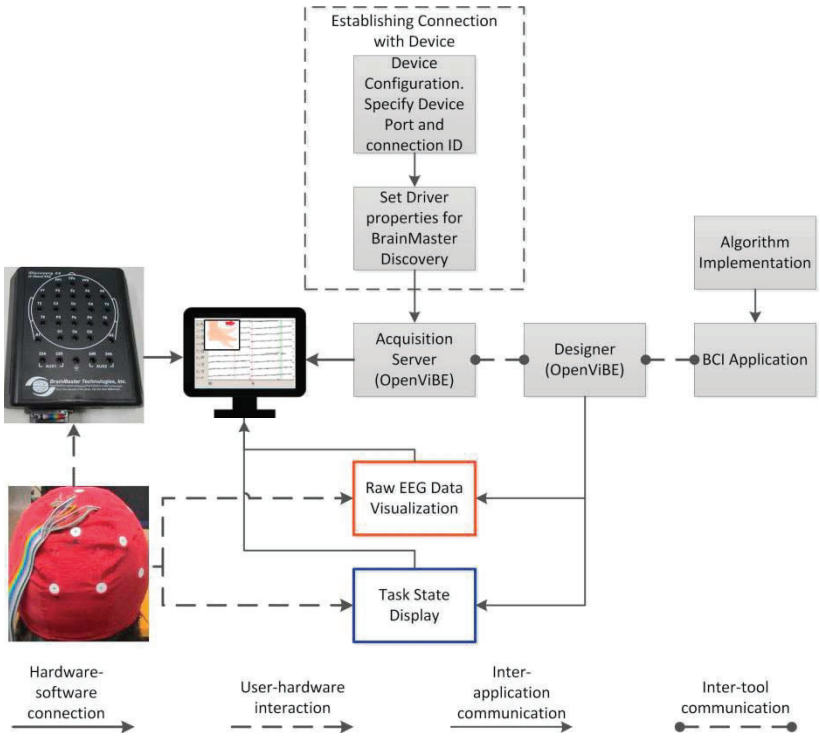

Fig. 2. Established hardware-software connection between Discovery 24E amplifier and OpenViBE acquisition software (adapted from [2, 3])

Table 1. Motor imagery protocol for each cue in OpenViBE

Cues	Visuals	Action
Fixation cross		Prepare for experiment to start
Audio beep		Get alert to start
Visual cue		
Performance task		Imagine Moving Foot Left or Right
Rest	Relax	Relax or rest

2.2. Data processing using OpenViBE

Using the designer tool of OpenViBE, we created a scenario by incorporating modules from the tool panel, see Fig 3. The ERD/ERS quantification was based on method suggested by [22, 23].

$$y_{ij} = \left(s_{ij} - \bar{s}_j\right)^2;\ A_j = \frac{1}{N-1}\sum_{i=1}^{N} y_{ij} \tag{1}$$

$$R = \frac{1}{k}\sum_{r_0}^{r_0+k} A_j \tag{2}$$

In equation 1, s_{ij} is the j-th sample of the i-th trial of the bandpass filtered data, $\bar{s}_j$ is the mean of the j-th sample averaged over all bandpass filtered trials, and A_j is the power of the j-th sample. In equation 2, R is the average power in the reference interval $[r_0, r_0 + k]$.

In order to quantify ERD and ERS patterns from oscillatory rhythms, the channel selector box was used to specify channels C3, Cz, and C4, i.e. effective electrode positions from the primary motor cortex, for analysis of *mu* and *beta* rhythms. Each of the *mu* and *beta* rhythms were bandpass filtered using 5th order Butterworth filter with low cut frequency of 8 Hz and high cut frequency of 11 Hz for *mu*, and a low cut frequency of 12 Hz and high cut frequency of 30 Hz for *beta*. This was done using the temporal filter box. Next, simulation based epoching was done for each rhythm against each task, i.e. left foot and right foot KMI. Following that, simple Digital Signal Processing (DSP) block was used to square each signal respectively. For each trial (20 for left and 20 for right foot KMI) epoch averaging was done. Averaging over sample points was done using time based epoching feature box.

However, calculating the ERD/ERS using equation 3:

$$ERD_j = \frac{A_j - R}{R} \times 100\% \tag{3}$$

was not possible, as the whole data epoch was not accessible at the same time. Following that, the mean of one epoch could not be subtracted from equation 1. Because only small chunks of the signal were available on time, averaging over sample points resulted in a shorter output signal. Therefore data needed to be loaded into another platform for further processing.

Alternate approach was the utilization of spectral analysis box based on Fast Fourier Transform (FFT), however in that case, pre-processing of data was only possible using a combination of temporal filtering and time based epoching in contrast to stimulation based epoching. In that case, selection of independent epochs related to left and right event markers was not possible and data would have been treated as a complete trial without segmentation displaying the real-time power spectrum for each chunk of data being analysed.

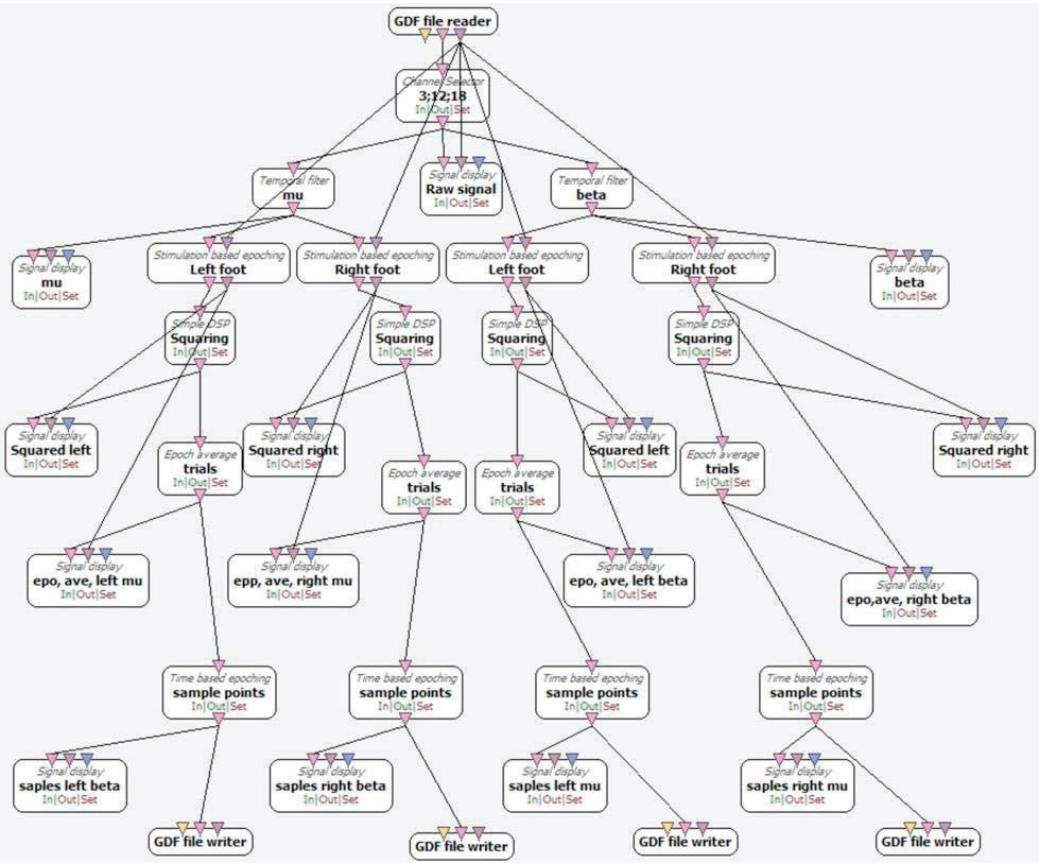

Fig. 3. Schematic organisation of boxes used to pre-process acquired data using OpenViBE designer

3. Results

Fundamental procedures to calculate ERD/ERS for analysis of data in one step could not be implemented using OpenViBE platform due to availability of data in small chunks at a time, as already explained. Resulting plots could only be achieved for run time, nor overall analysis. Following equation 1, for signals elicited from foot representation area, i.e. electrode position C3, Cz, and C4, the run-time resulting epochs for filtered *mu* and *beta* rhythm are shown in figure 4. Figure 5 and 6 reflect the run-time squared signal epochs followed by averaged epoched signals over trials for *mu* and *beta* frequency range, respectively. While epoching the signal based on stimulation for distinguishing between left vs. right task cue, it was observed that stimulation marker did not match the time that was set during experimental protocol, as after epoching the stream does not remain continuous anymore.

Since the proposed study was based on extraction of band power features as suggested in equation 3, alternate sensorimotor features (of interest), elicited upon KMI, such as common spatial patterns (CSP) or time-frequency features, could be used. In OpenViBE designer toolbox there are options as, spectral analysis to display the power spectrum in real-time, and CSP method.

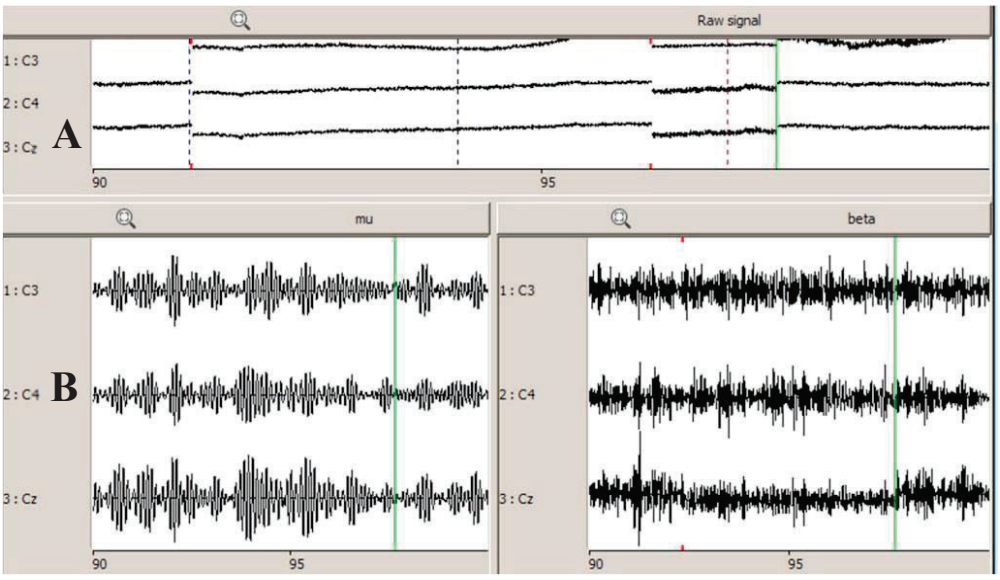

Fig. 4. Chunk of signal in run-time of OpenViBE designer at electrode positions C3, C4 and Cz (green pointer indicates run-time of each epoch). (A) acquired raw signal display with stimulations; (B) pre-processing part signal display following temporal filtering in the *mu* frequency range between 8Hz to 11 Hz and the *beta* frequency range 12Hz to 30 Hz with stimulations

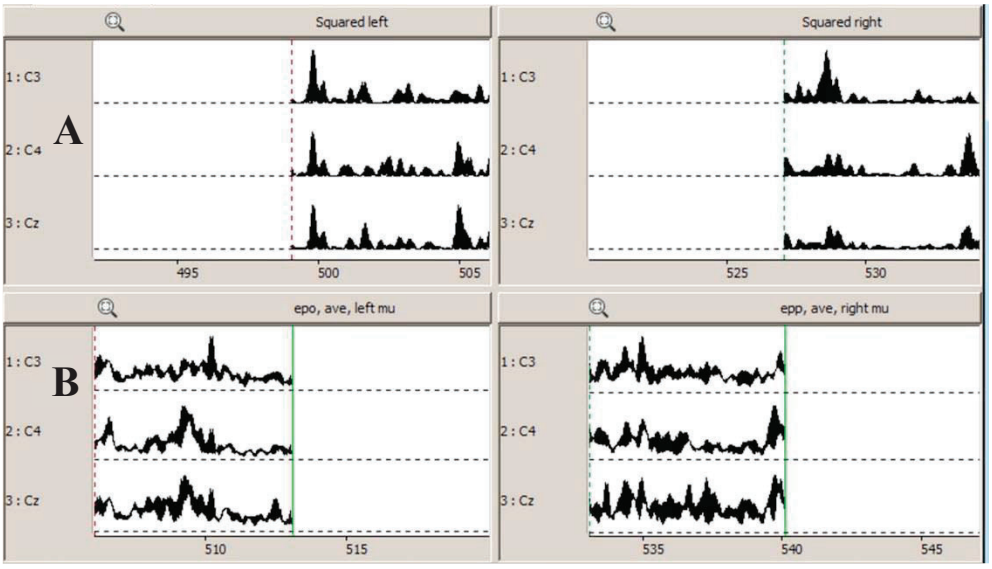

Fig. 5. Epoched signal in run-time of OpenViBE designer at electrode positions C3, C4 and Cz (green pointer indicates run-time of each epoch). (A) pre-processing part signal display following squaring (simple DSP block) of left and right epoch, respectively in mu range; (B) processing part signal display following averaging over trials of epoched data in the *mu* frequency range

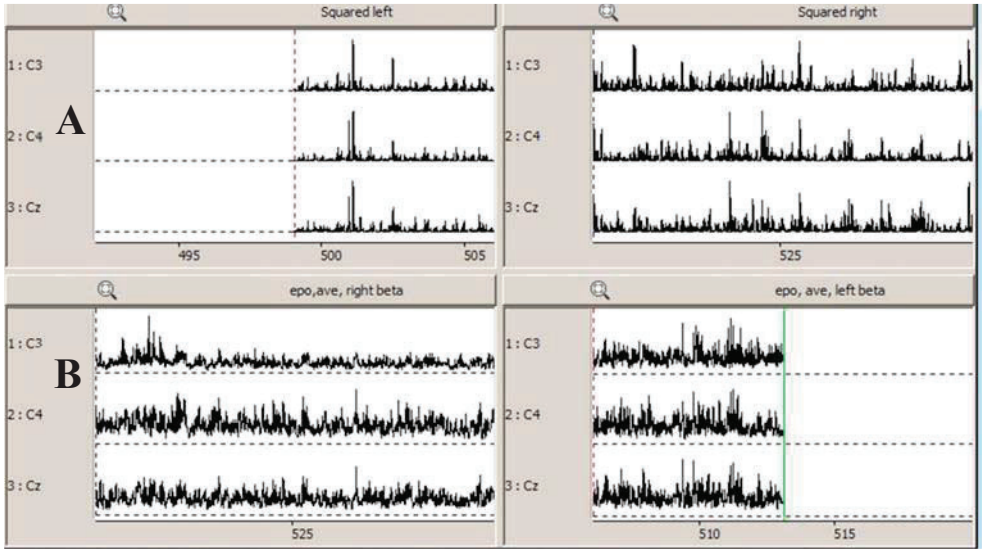

Fig. 6. Epoched signal in run-time of OpenViBE designer at electrode positions C3, C4 and Cz (green pointer indicates run-time of each epoch). (A) pre-processing part signal display following squaring (simple DSP block) of left and right epoch, respectively in mu range; (B) processing part signal display following averaging over trials of epoched data in the *mu* frequency range.

4. Discussion and Conclusion

For different applications, such as controlling various local output devices in the real-time, based on BCI, or online control of mechatronic devices, both in real and virtual environments, OpenViBE is probably one of the most viable platform. However, it is not suitable for analysing command signals offline, nor it allows for visualization in form of plots or graphical outputs that could be saved for later use. OpenViBE is originally designed as a streaming tool for 'online' BCI experiments. Its operating philosophy is built on the logic of boxes processing small chunks of streamed signal at a time. It is contrary to MATLAB plugins, such as BCILAB, EEGLAB, or R/scipy etc. that provide access to analysis of data offline, where all the data (or epoch) is available at once in the form of big matrices or tensors. Although that one very large epoch can be formed in OpenViBE with available tool boxes to do the required analysis using a buffer box, clearly the platform is not designed for analysis or exploration of data offline. For analysis and visualization of data offline or in global sense, the data needs to be exported to a classical statistical package, as mentioned above. OpenViBE is best suitable for real-time control of output devices or systems driven by cortical signals in real or virtual environments.

Results from our research presented here suggest that OpenViBE could, potentially be a tool for the control of robotic foot controlled via KMI signals in real-time. The same imaginary actions could be used to control passenger cars through acceleration and brake pedals control, with the right foot and steering with the left foot. It is certain that such vehicles should include high level of automations, known as function specific, as defined in [24], i.e. applications like GPS navigation, collision avoidance, electronic stability control, emergency braking, parking assistance and others. These vehicles are not completely autonomous; therefore the driver could still have a sense of control, using his/her thoughts. Investigation on BCI control of various other applications that include all kind of virtual and real vehicles and mechatronic systems are subject to associated research projects.

The future prospects of this project involve the actuation of robotic foot model via KMI using OpenViBE. Smart robotic foot investigation and model design are subjects of an associated project conducted concurrently to our EEG BCI project. Model design, reliable data acquisition and decoding, using BCI methods, are the key steps in all these

novel and exciting applications.

References

[1] Tariq, M., Z. Koreshi, and P. Trivailo. *Optimal Control of an Active Prosthetic Ankle*. in *Proceedings of the 3rd International Conference on Mechatronics and Robotics Engineering*. 2017. ACM.

[2] Tariq, M., et al. *Mu-beta rhythm ERD/ERS quantification for foot motor execution and imagery tasks in BCI applications*. in *Cognitive Infocommunications (CogInfoCom), 2017 8th IEEE International Conference on*. 2017. IEEE.

[3] Tariq, M., P.M. Trivailo, and M. Simic. *Detection of knee motor imagery by Mu ERD/ERS quantification for BCI based neurorehabilitation applications*. in *Control Conference (ASCC), 2017 11th Asian*. 2017. IEEE.

[4] Lee, F., et al. *A comparative analysis of multi-class EEG classification for brain computer interface*. in *Proceedings of the 10th Computer Vision Winter Workshop*. 2005.

[5] Tariq, M., P.M. Trivailo, and M. Simic, *Event-related changes detection in sensorimotor rhythm.* International Robotics & Automation Journal, 2018. **4**(2): p. 119-120.

[6] Shende, P.M. and V.S. Jabade. *Literature review of brain computer interface (BCI) using Electroencephalogram signal*. in *2015 International Conference on Pervasive Computing (ICPC)*. 2015.

[7] González-Mendoza, A., et al. *Brain Computer Interface based on SSVEP for controlling a remote control car*. in *2015 International Conference on Electronics, Communications and Computers (CONIELECOMP)*. 2015.

[8] Hongtao, W., L. Ting, and H. Zhenfeng. *Remote control of an electrical car with SSVEP-Based BCI.* in *2010 IEEE International Conference on Information Theory and Information Security*. 2010.

[9] Huh, W.-G. and S.-B. Cho. *Optimal partial filters of EEG signals for shared control of vehicle*. in *Soft Computing and Pattern Recognition (SoCPaR), 2015 7th International Conference of*. 2015. IEEE.

[10] Kim, D. and S.B. Cho. *A brain-computer interface for shared vehicle control on TORCS car racing game*. in *2014 10th International Conference on Natural Computation (ICNC)*. 2014.

[11] Kreilinger, A., H. Hiebel, and G.R. Müller-Putz, *Single Versus Multiple Events Error Potential Detection in a BCI-Controlled Car Game With Continuous and Discrete Feedback.* IEEE Transactions on Biomedical Engineering, 2016. **63**(3): p. 519-529.

[12] Pan, X., et al. *Enjoy driving from thought in a virtual city*. in *2017 36th Chinese Control Conference (CCC)*. 2017.

[13] QingKai, L., et al. *Remote Control System of an Electric Car Based on the Alpha Wave in EEG*. in *2006 6th World Congress on Intelligent Control and Automation*. 2006.

[14] Venuto, D.D., V.F. Annese, and G. Mezzina. *An embedded system remotely driving mechanical devices by P300 brain activity*. in *Design, Automation & Test in Europe Conference & Exhibition (DATE), 2017*. 2017.

[15] Wu, G., Z. Xie, and X. Wang. *Development of a mind-controlled Android racing game using a brain computer interface (BCI)*. in *2014 4th IEEE International Conference on Information Science and Technology*. 2014.

[16] Dornhege, G., *Toward brain-computer interfacing*. 2007: MIT press.

[17] Mellinger, J. and G. Schalk, *BCI2000: a general-purpose software platform for BCI research.* Towards brain-computer interfacing, 2007.

[18] Maggi, L., et al., *BCI++: an object-oriented BCI prototyping framework*. 2008: Citeseer.

[19] Delorme, A. and S. Makeig, *EEGLAB: an open source toolbox for analysis of single-trial EEG dynamics including independent component analysis.* Journal of neuroscience methods, 2004. **134**(1): p. 9-21.

[20] Delorme, A., et al., *EEGLAB, SIFT, NFT, BCILAB, and ERICA: new tools for advanced EEG processing.* Computational intelligence and neuroscience, 2011. **2011**: p. 10.

[21] Renard, Y., et al., *Openvibe: An open-source software platform to design, test, and use brain–computer interfaces in real and virtual environments.* Presence: teleoperators and virtual environments, 2010. **19**(1): p. 35-53.

[22] Graimann, B., et al., *Visualization of significant ERD/ERS patterns in multichannel EEG and ECoG data.* Clinical Neurophysiology, 2002. **113**(1): p. 43-47.

[23] Graimann, B. and G. Pfurtscheller, *Quantification and visualization of event-related changes in oscillatory brain activity in the time–frequency domain.* Progress in brain research, 2006. **159**: p. 79-97.

[24] Elbanhawi, M., M. Simic, and R. Jazar, *In the Passenger Seat: Investigating Ride Comfort Measures in Autonomous Cars.* IEEE Intelligent Transportation Systems Magazine, 2015. **7**(3): p. 4-17.

Mu-beta rhythm ERD/ERS quantification for foot motor execution and imagery tasks in BCI applications

Chapter Overview

The goal of this research study is the quantification and investigation of the sensorimotor *mu* and *beta* ERD and ERS, based on left-right foot motor execution (ME) and motor imagery (MI) tasks, for inter and intra-user variability. The analysis was carried out for EEG signals recorded from central cortical channels C3, Cz, and C4 using the common average reference method. As the foot ME and MI reflect user's physical and imagination state of foot movement respectively, their accurate translation is one of the basic challenge for application as control signals in BCI to restore motor function. Initial results enabled a good platform for left-right foot ME/MI discrimination based BCI applications.

This work has been published in ***8th IEEE International Conference on Cognitive Infocommunications.***

M. Tariq, L. Uhlenberg, P.M. Trivailo, K.S. Munir, and M. Simic. *Mu-Beta Rhythm ERD/ERS Quantification for Foot Motor Execution and Imagery Tasks in BCI Applications*. 8th IEEE International Conference on Cognitive Infocommunications (CogInfoCom), 2017, pp. 091-096. IEEE, 2017, Debrecen, Hungary.

Mu-Beta Rhythm ERD/ERS Quantification for Foot Motor Execution and Imagery Tasks in BCI Applications

Madiha Tariq*, Lena Uhlenberg, Pavel Trivailo, Khurram S Munir, and Milan Simic
School of Engineering
RMIT University
Melbourne, Australia
*s3519022@student.rmit.edu.au

***Abstract*—Viable usage of Brain-Computer Interface (BCI) in real-time applications significantly relies on the pre-processing techniques applied on the detected electroencephalography (EEG) signals. In EEG, sensorimotor (SMR)/oscillatory signals, such as *mu* and *beta* rhythm based BCIs, can be used to restore motor function by neuro-plasticity applied to re-establish normal brain function. This study is based on the evaluation of the foot motor execution (ME) and motor imagery (MI), in order to design a BCI neurorehabilitation system. Because foot ME and MI reflect the user's physical and imagination state of foot movement respectively, in order to be used as control signals, their appropriate translation is the basic challenge. This paper mainly focuses on the quantification and investigation of *mu-beta* event-related desynchronization (ERD) and event-related synchronization (ERS), for inter and intra-subject variability, making use of the available design tools in open-source platforms such as the OpenViBE software. Results show that the frequency of the most reactive components for *mu* was 8.8±0.5 Hz and 21.3±0.4 Hz for *beta*. Interestingly a contralateral dominance was visible at electrode position C3 during right foot ME/MI tasks. The results have enabled the implementation of a good platform for left-right foot ME/MI discrimination based BCI applications.**

Keywords—Brain-Computer Interface (BCI); electroencephalography (EEG); neuro-plasticity; event-related desynchronization (ERD); event-related synchronization (ERS); Graz-BCI protocol

I. Introduction

Neurodegeneration, spinal cord injury (SCI) or stroke causing paralysis can affect the lower limbs (LL) of a human body in addition to amputation, ending up in gait impairment. The primary therapeutic goal of such people is the rehabilitation of gait, or development of assistive technologies [1] for people with non-standard cognitive characteristics [2] to re-gain the dorsiflexion of foot drop. The rehabilitation of gait intents to ameliorate the motor control functions by inducing neuro-plasticity. This could be achieved by detecting and translating particular brain features, which correspond to the ME or MI of the affected limb, such as foot, into an output control command. A feedback on this output command can be sent to the user that in turn can affect the brain activity of the user, and re-establish the motor control. One apt tool that could be employed to turn this problem into real-time application is the BCI technology.

BCIs based on particular EEG features used to decipher user intent are of different types; one being the SMR/oscillatory rhythms. SMR generate in the somatic sensorimotor areas and are concentrated in the alpha, or mu (8-12 Hz) and beta (12-32 Hz) frequency bands, but also include gamma (35-200 Hz) frequency bands [3]. SMR have been deployed by researchers in order to identify any changes in them relating to any ME or MI task. Such changes in rhythms are detected based on feature extraction and classification. The execution, or imagination of body part movements, e.g. foot, creates a unique pattern in the SMR.

These patterns in the SMR are reflected in form of, a power decrease called ERD, or a power increase called ERS, in the EEG signal. Each of the ERD/ERS is associated to an internal or external event. An ERD pattern exhibits an actual or imagined movement of a limb, characterized by localized cortical topography and frequency specificity. On the contrary the ERS relates to the rest, or relaxation period [4, 5].

ERD patterns are useful in determining the correlation of brain activity during the task with actual performance, or as an estimator of brain activity related to an event. This can be achieved by quantifying the ERD/ERS patterns using tools such as topographic, or time-frequency maps. Topographic maps represent the spatial distribution of ERD/ERS for a specific frequency, where they can be studied as a function of space. The time-frequency maps are used to detect the transient event-related spectral perturbation (ERSP) or event-related shifts in the power spectrum and inter-trial coherence (ITC) events in the signal. Amongst the available tools for data evaluation, EEGLAB, a MATLAB toolbox for processing EEG signals was used in this study.

The cortical localization of ERD patterns is due to the somatotopic arrangement of the sensory and motor cortices. This arrangement has the hand area representation on the mantle of the cortex, followed by lateralizion the reason why ERD patterns of the left and right hand can be easily discriminated spatially in EEG. Whereas the foot's motor area

978-1-5386-1264-4/17/$31.00 ©2017 IEEE

is deep within the interhemispheric fissure of the cortex which makes it difficult to detect ERD patterns through EEG [6].

Although there is literature about the detection of lower limbs (LL) tasks [7], the detection of distinct left and right foot tasks for applications as brain controlled robotic foot is limited. This study therefore focuses on the quantification of ERD/ERS patterns for foot ME-MI tasks in order to expand the limited knowledge about the discrimination of left-right foot tasks to be used as a CogInfo Communication [8] tool for neurorehabilitation in controlling BCI based robot applications [9] for LL.

II. Materials and Methods

A. Subjects and Experimental Paradigm

Three female subjects with no BCI experience and no history of any neurological disorder (age range 22-32 years) voluntary participated in this study. Ethics approval was granted by the CHEAN (College Human Ethics Advisory Network) of RMIT University, Melbourne, Australia.

Each subject was instructed to sit comfortably in front of a monitor screen (17'') at a distance of about 1.5 m from the screen. At the beginning of each run a blank screen was presented for 30 seconds. This period was used as baseline and the participant was asked to relax and become ready for experiment. After the baseline measurement, each trial started with the presentation of a fixation cross for 3 seconds followed by 2 seconds of visual cue display and 5 seconds of performing the task (execution/ imagery), making a total of 10 seconds for one trial. The visual cues reflected right and left foot dorsiflexion-plantarflexion. Subjects were asked to dorsiflex and planterflex their foot only once during each task performance period in each trial. Visual cues were displayed in random order to ensure no adaptation took place. Each trial was followed by a random pause interval between 1.5 seconds to 3.5 seconds where the subject was asked to relax/rest. Each session/run consisted of 40 trials, ensuring a total of 20 trials for each task. Furthermore, the experiment was divided into 4 sessions/runs, 2 for motor execution (ME) and 2 for motor imagery (MI) tasks. A schematic overview of protocol timing can be seen in *Fig. 1*, left. For the first trial only an audio stimulus (beep) of 1 second before the visual cue display was incorporated to alert the subject that the experiment was about to begin.

B. Data Acquisition

For data acquisition the 24 channel EEG neurofeedback BrainMaster Discovery 24E amplifier (BrainMaster Technologies Inc., Bedford, USA) was interfaced with the acquisition server of the open source software OpenViBE (http://openvibe.inria.fr/downloads/). An electrode cap (10-20 Electro-cap) with incorporated 20 electrodes was placed over the scalp of different brain areas following the international 10–20 [10]. Channels were referenced to linked earlobes (LE) derived from the electrodes A1 and A2 (see *Fig. 1*, right). Data was sampled with 256 Hz on all channels, with a resolution of 24-bit and amplifier bandwidth from 0 Hz to 100 Hz and EEG channel bandwidth of 0.43 to 80 Hz.

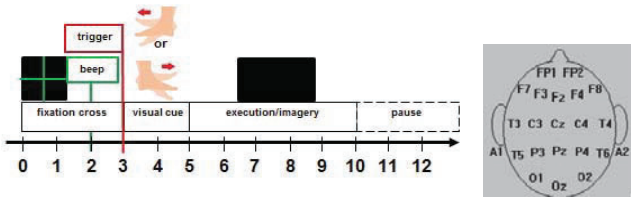

Fig. 1. Experimental protocol reflecting timing of cue including 'beep', for the first trial only, at the beginning of each session (left) and electrode channel locations (right)

Experimental protocol was set using the OpenViBE designer tool with its integrated feature boxes presented in *Fig. 2*. To allow for different onset visual cue timing, the default settings and the .lua script inside the Graz-Stimulator box were modified. Synchronization of the BrainMaster Discovery software with OpenViBE was achieved by setting the acquisition server properties and connecting the modules appropriately ensuring establishment of data connection via TCP/IP connection as shown in *Fig. 3*. To gather and visualize all the cues in recorded EEG data different trigger points were sent as stimulations, in real time, to the visual cue display box inside the OpenViBE designer via TCP/IP protocol. All data was saved using the edf and gdf writer boxes to store signals and stimulations together in .edf and .gdf file format, respectively.

C. Data Processing

As OpenViBE is a streaming tool for online/real-time BCI experiments and not for data analysis and data exploration, the classical statistical free package EEGLAB (http://www.sccn.ucsd.edu/eeglab/) was used for offline processing of the acquired data.

To get topographic maps of the scalp, EEG segments (trials) of 10 seconds' length with 3 seconds prior to cue onset were extracted and analysed. Data was band pass filtered between 5 Hz and 40 Hz. Artefact removal was carried out using independent component analysis (ICA) [11] alongside visual inspection (and other artefact rejection) tools integrated in EEGLAB toolbox.

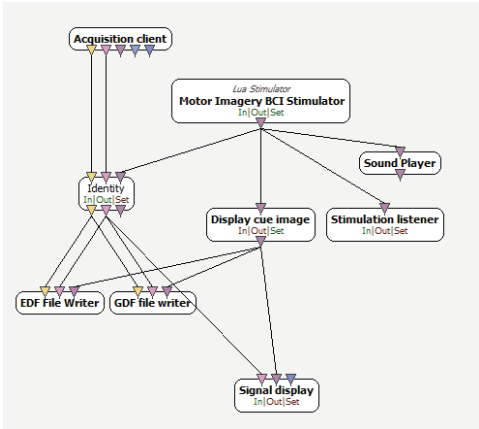

Fig. 2. OpenViBE Designer graphical user interface. Schematic overview of boxes used for experimental protocol

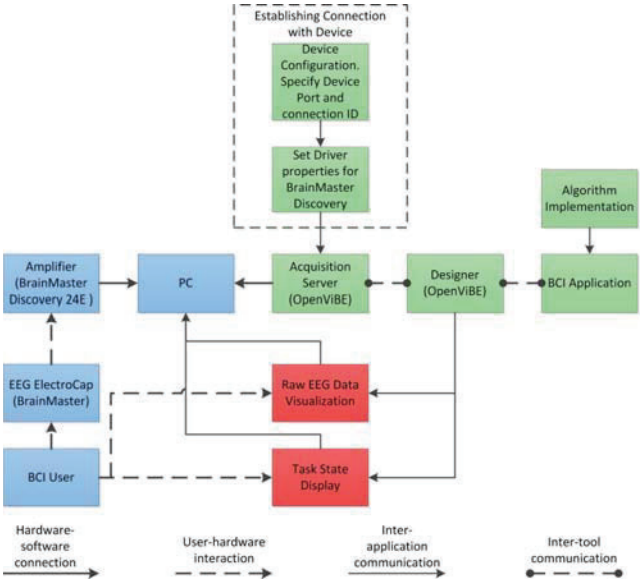

Fig. 3. Flow diagram of the established hardware-software connection between BrainMaster and OpenViBE with the user

Time-frequency maps were obtained with frequency range of 5 to 40 Hz with a step of 1 Hz. They were then used for selecting mu and beta bands with the most significant band power decrease or increase during the ME and MI tasks at the central electrode positions C3, Cz, and C4.

ERD/ERS quantification was conducted following the methods proposed by [12]. The ERD/ERS is defined as the proportional power decrease (ERD) or power increase (ERS) relative to the reference interval, that is usually several seconds before the event onset [4]. For this study the interval containing 3 seconds prior to visual cue onset was selected. Samples were squared and labelled as y_{ij} after subtracting the mean of the band pass filtered data for each sample to overcome masking of induced activities by the evoked potentials (Equation 1). Furthermore, samples were averaged over trials and over sample points (Equation 2-4) [4, 13].

$$y_{ij} = (x_{ij} - \bar{x}_j)^2 \tag{1}$$

$$P_j = \frac{1}{N-1}\sum_{i=1}^{N} y_{ij} \tag{2}$$

$$R = \frac{1}{k+1}\sum_{r_0}^{r_0+k} P_j \tag{3}$$

$$ERDS_j = \frac{P_j - R}{R} * 100\% \tag{4}$$

where N is the total number of trials, x_{ij} is the jth sample of the ith trial of the bandpass filtered data, and $\bar{x}_j$ is the mean of the jth sample averaged over all bandpass filtered trials. P_j is the power or inter-trial variance of the jth sample and R is the average power in the reference interval (r_0, r_0+k) [5].

III. Results

As subject 3 (S3) could not participate in all training sessions, she did not show any significant output results, therefore only the results of subject 1 (S1) and subject 2 (S2) have been reported. *Fig. 4* and *Fig. 5* show the topographical scalp maps of S1 and S2, left and right foot ME and MI tasks. The color bar indicates the spectral power concentration over the scalp for all channels

A. Topographical Scalp Maps

Motor execution task:

S1: At the mu frequency range, corresponding to frequencies between 8-11 Hz, during right foot ME a high power concentration was reflected near the center lobe or mid central mu ERD which is the activation of the foot representation area. At frequencies between 16-30Hz, corresponding to beta rhythm, a shift towards the central region occurred. Especially the right side was more active at electrode position C4 than the left side at electrode position C3. This contralateral power distribution was however only dominant for left foot movement, shown in *Fig. 4*. At the central electrode position Cz the power concentration was decreased during higher frequencies. S2: At the mu frequency range the power is concentrated over the frontal and central region probably because of the proprioceptive induced due to movement of the foot (ME task). For the beta frequency range this trend was again visible in the frontal area followed by an interesting enhancement in the hand area beta rhythm representation power decrease (beta ERS). Furthermore, the central region showed a decrease in spectral power with increasing frequency. Left foot ME resulted in lower a power concentration than right foot motor execution.

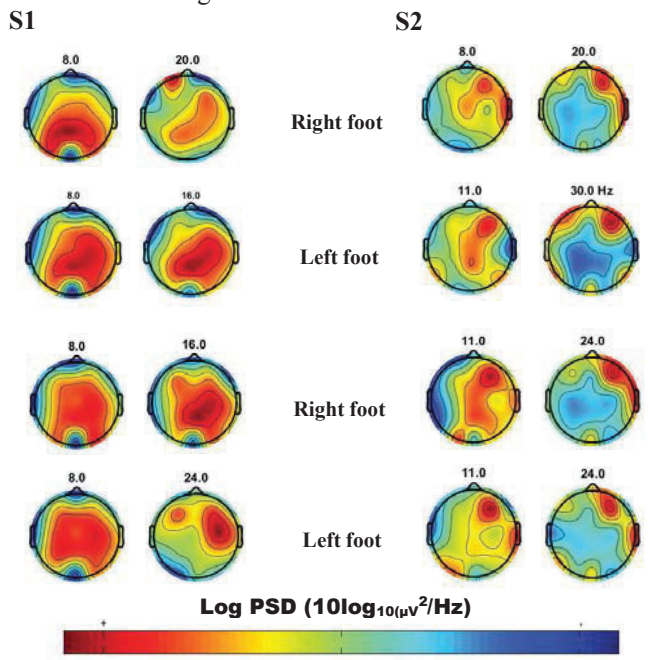

Fig. 4. *Topographical scalp maps showing mean power spectral distribution for right-left foot ME (top rows) and MI (bottom rows) for all channels*

Motor imagery task:

S1: At the mu frequency range, spectral power was concentrated in the central region. The left foot MI interestingly enhanced the hand area mu rhythm (mu ERD). At the beta frequency range a shift from the central region occurred. C4 and F4 showed higher power concentration during left foot imagery and at frequencies higher than 24 Hz. S2: At the mu frequency range the power is concentrated over the frontal and central region with increased power values for the right side of the cortex for both right and left foot MI. For the beta frequency range there was a decrease in power concentration in the central region, followed by an enhancement in the hand area beta rhythm (beta ERS) representation visible for lateralization of ERS i.e. right foot MI enhanced left side beta ERS. But this trend was not followed in the case of left foot MI, *Fig. 4*.

In general ME and MI scalp maps showed relatively same power distribution pattern for intra subject. In contrast, prominent inter subject differences were obtained regarding decreased spectral power at higher frequencies at the central region.

B. Time Frequency Maps

Fig. 5 show the time-frequency maps of the most reactive ERD/ERS at electrode positions C3 and Cz for S2 during left and right foot motor tasks obtained from EEGLAB. Because only most reactive ERD/ERS have been reported, we did not include C4 as it did not reflect prominent ERD/ERS patterns. Only significant values (α=0.05) are displayed in color: red indicates ERD and blue indicates ERS. Non- significant values are displayed in green. The colour bar indicates the ERSP in decibel.

The right foot ME (*Fig. 5 (a)*) resulted in a significant ERD at electrode position C3 during the end of visual cue display at second 2 between 8-35 Hz for a period till execution of task ends. Similarly for Cz ERD was visible from the beginning of visual cue between low mu 8 Hz and beta 22 Hz frequency till the subject finished performing the task at second 4-5. An ERS at the end of the execution period over approximately whole frequency range (8-30 Hz) was evident at Cz but little ERS was seen at position C3 after task completion. The ERS was visible from aprroximately 4 seconds because the subject only performed the task once (dorsiflexion-planterflexion of foot) which is no longer than 1.5 to 2 seconds. It is therefore justified that ERD gets visible right from the beginning when the subject prepares for the presentation of visual cue till performance of task is done, followed by an ERS (blue) reflecting a relaxation period. In *Fig. 5 (b)* the left foot ME resulted in a significant ERD at electode position C3 right from start of visual cue display at approxmiately all frequencies between 8-40 Hz. ERS was not very significant and occurred near the completion of the task at 3.5 seconds. At position Cz ERD was prominent starting from visual cue onset at frequencies between 5-25 Hz and a dominant ERS was visible at near 5 seconds upon finishing of task and relaxing from 24 to 37 Hz. *Fig. 5 (c)* reflected the time frequency maps during the right foot MI task at position C3 and Cz. At C3 a very dominant ERD pattern was visible from 8 to 32 Hz during the cue onset till execution of task. Prominent ERS occurred at 4 till 5.5 seconds indicating the ending of task and initialization of rest. The map at electrode position Cz for the right foot MI didn't show a clear ERD pattern. It rather reflected scattered ERD powers in low mu and high beta ranges followed by a dominant ERS occuring during the imagery task between 9 to 20 Hz.

In general, not all electrode positions depicted explicitly clear ERD/ERS patterns; however in few conditions the electrodes reflected good results.

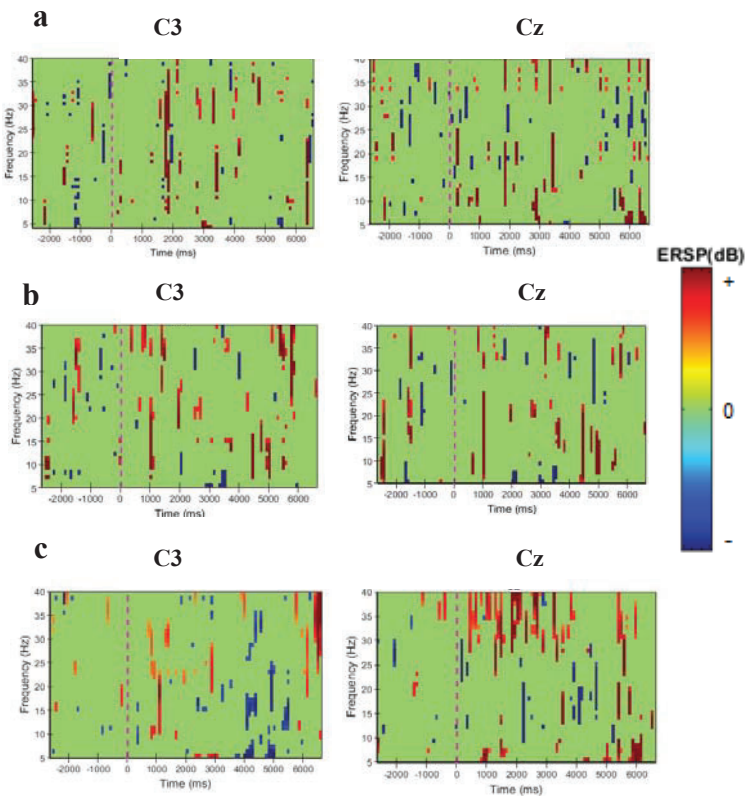

Fig. 5. Time-frequency maps displaying significant ERD (red) and ERS (blue) for subject S2 for electrode position C3 and Cz (a) right foot ME, (b) left foot ME, and (c) right foot MI

C. ERD/ERS Quantification

Table 1 presents results of band power changes (ERD and ERS) of the most reactive mu and beta components in Hz for the electrode positions C3, Cz and C4 for the two ME (left foot, right foot) and two MI (left foot, right foot) tasks. For the mu frequency range, most reactive components ranged between 8 and 11 Hz for the ME/MI tasks. For the beta frequency range, most reactive components ranged between 12 to 29 Hz for the ME/MI tasks. Both mu and beta reactive frequency components were found at all central electrode positions.

The maximum ERD occurred at electrode position corresponding to Cz for left foot ME/MI in beta frequency range. For the right foot ME/MI maximum ERD was witnessed at position C3 in beta frequency range. Whereas maximum ERS for left foot ME/MI was visible at electrode

position Cz corresponding to beta frequency range. For the right foot ME/MI the maximum ERS was visible at electrode position C3 in beta frequency range. Hence it can be clearly extracted that for the left foot ME/MI tasks ERD and ERS are maximum at electrode position Cz, which correlate to the already established findings reported in the literature [14]. For the right foot ME/MI the maximum ERD and ERS occur at electrode position C3 reflecting a contralateral dominance.

IV. Discussion

In general both the ERD and ERS were visible for S1 and S2 as shown in *Fig. 6* to *Fig. 8*. *Fig. 6* shows an exemplary ERD/ERS time curve at 8 Hz mu rhythm for S1 performing left foot ME at electrode position C3. An ERD is prominent around 300 milliseconds after the visual cue display. About 1 second after the subject stopped executing an ERS can be seen at second 5.7.

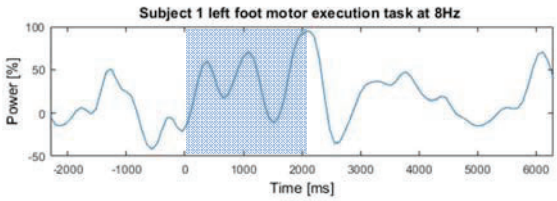

Fig. 6. ERD/ERS time curve obtained from left foot ME task for S1 at electrode position C3 for 8 Hz mu rhythm. Shaded area indicates cue display

Fig. 7 shows an exemplary ERD/ERS time curve at 14 Hz beta rhythm for S1 performing right foot MI at electrode position Cz. An ERD starts shortly before the end of visual cue display and continues until 800ms after the cue. An ERS is prominent around second 3-4 and at the end of the trial at second 6.

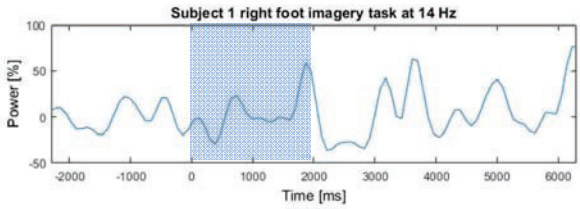

Fig. 7. ERD/ERS time curve obtained from right foot MI task for S1 at electrode position Cz for 14 Hz beta rhythm

Fig. 8 shows the exemplary ERD/ERS time curve at electrode position C3 averaged over two runs for S2 at 9 Hz. Averaging was conducted over two runs of ME and two runs of MI for the left foot. A prominent ERS at the end of the trial was obtained. A small ERD was obtained starting around 400 milliseconds after the cue display.

Based on the results it can be drawn that left and right foot discrimination task based BCI is valid both for ME as well as MI. Both subjects showed a percentage power increase and decrease for ERD and ERS respectively. This enables the implementation of a brain controlled bionic foot which is an interdisciplinary research area of socio-technical neurorehabilitation systems and addresses research questions in the field of intelligent robots and rehabilitation systems, and cognitive modeling of user adaptability. These questions are in accordance to some of the research areas addressed by CogInfoCom [15] as the augmented social intelligence, cognitive info-communication channels and industrial engineering aided by CogInfoCom.

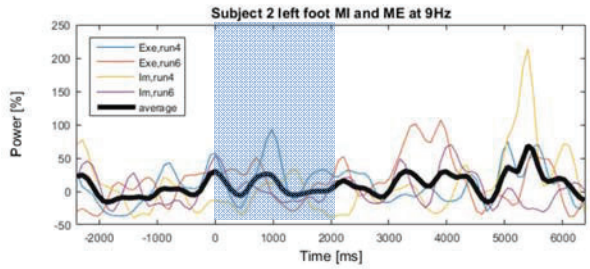

Fig. 8. ERD/ERS time curve obtained from left foot averaged over 2 runs for ME and MI task for S2 at electrode position C3 for 9 Hz mu rhythm

V. Conclusions

According to literature the MI/ME at electrode position Cz should enhance the foot area mu or beta rhythm respectively. However due to lack of literature available about the left and right foot tasks discrimination this study was based on distinguishing the left and right foot ME and MI tasks. Following that several results could be concluded. Our results overall suggest that, a BCI based on left and right foot ME/MI discrimination can be developed, despite the location of foot's motor area representation which is deep within the interhemispheric fissure of the cortex. The topographic maps reflected an interesting enhancement in the hand area high beta rhythm (beta ERS) representation during the individual left and right foot ME tasks. And a similar pattern was observed during low mu ERD and high beta ERS rhythms for right and left foot MI tasks individually followed by a contralateral dominance of the cortex for ERS patterns at position C3 during right foot MI task. The mean percentage of most reactive bands for ERD were not as high as expected, because of limited training sessions and less participants involved in the study. The main contribution of the conducted research, presented here, is the introduction and the trial of the new BCI concept for enabling the control of a robotic foot. In the future we aim to proceed this work by incorporating more subjects and classifying the left and right foot tasks for both ME and MI sessions to be used as a CogInfo Communication tool establishing a platform for neurorehabilitation in controlling BCI based robot applications for LL.

Acknowledgment

We would like to acknowledge Mr.Yutaka Shoji from Electrical and Biomedical, School of Engineering RMIT for helping us with the OpenViBE experimental protocol settings.

TABLE 1(A) *MU* AND (B) *BETA* FREQUENCY BAND POWER CHANGES FOR MOST REACTIVE ERD -ERS FOR ME AND MI TASKS CALCULATED WITH BOOTSTRAP (α=0.05)

(a)	Left foot										Right foot								
	C3			Cz			C4				C3			Cz			C4		
ME	Hz	% (ERD)	% (ERS)	Hz	% (ERD)	% (ERS)	Hz	% (ERD)	% (ERS)	ME	Hz	% (ERD)	% (ERS)	Hz	% (ERD)	% (ERS)	Hz	% (ERD)	% (ERS)
S1	8	-41	50	10	-25	30	8	-31	62		11	-41	52	10	-39	52	11	-38	49
S2	9	-37	52	9	-37	49	8	-33	54		9	-35	47	9	-43	32	8	-28	63
MI										MI									
S1	9	-49	90	8	-50	51	10	-57	65		11	-47	74	11	-50	80	10	-60	52
S2	9	-39	76	9	-45	41	9	-42	42		9	-32	117	9	-33	103	9	-36	82
Mean	8.8	-41.5	67	9	-39.3	42.8	8.8	-40.8	55.8		10	-38.8	72.5	9.8	-41.3	66.8	9.5	-40.5	61.5
SD	0.5	5.3	19.4	0.8	10.9	9.5	0.9	11.8	10.3		1.2	6.7	31.9	0.9	7.1	31.1	1.3	13.7	14.9

(b)	Left foot										Right foot								
	C3			Cz			C4				C3			Cz			C4		
ME	Hz	% (ERD)	% (ERS)	Hz	% (ERD)	% (ERS)	Hz	% (ERD)	% (ERS)	ME	Hz	% (ERD)	% (ERS)	Hz	% (ERD)	% (ERS)	Hz	% (ERD)	% (ERS)
S1	27	-44	75	29	-42	127	25	-53	39		14	-47	66	22	-48	68	12	-44	60
S2	17	-48	54	26	-57	70	22	-44	72		14	-57	72	28	-44	60	20	-48	79
MI										MI									
S1	26	-52	109	14	-56	83	21	-51	83		17	-60	78	20	-31	71	15	-43	61
S2	15	-40	86	28	-42	88	17	-41	98		24	-43	80	24	-41	71	24	-39	76
Mean	21.3	-46	81	24.3	-49.3	92	21.3	-47.3	73		17.3	-51.8	74	23.5	-41	67.5	17.8	-43.5	69
SD	6.8	5.2	22.9	6.9	8.4	24.5	3.4	5.7	25		4.7	8	6.3	3.4	7.3	5.2	5.3	3.7	9.9

REFERENCES

[1] Tariq, M., Z. Koreshi, and P. Trivailo. *Optimal Control of an Active Prosthetic Ankle*. in *Proceedings of the 3rd International Conference on Mechatronics and Robotics Engineering*. 2017. ACM.

[2] Izsó, L. *The significance of cognitive infocommunications in developing assistive technologies for people with non-standard cognitive characteristics: CogInfoCom for people with non-standard cognitive characteristics*. in *Cognitive Infocommunications (CogInfoCom), 2015 6th IEEE International Conference on*. 2015. IEEE.

[3] Wolpaw, J. and E.W. Wolpaw, *Brain-computer interfaces: principles and practice*. 2012: OUP USA.

[4] Graimann, B., et al., *Visualization of significant ERD/ERS patterns in multichannel EEG and ECoG data.* Clinical Neurophysiology, 2002. **113**(1): p. 43-47.

[5] Graimann, B. and G. Pfurtscheller, *Quantification and visualization of event-related changes in oscillatory brain activity in the time–frequency domain.* Progress in brain research, 2006. **159**: p. 79-97.

[6] Carrere, L. and C. Tabernig. *Detection of Foot Motor Imagery Using the Coefficient of Determination for Neurorehabilitation Based on BCI Technology*. in *VI Latin American Congress on Biomedical Engineering CLAIB 2014, Paraná, Argentina 29, 30 & 31 October 2014*. 2015. Springer.

[7] Hashimoto, Y. and J. Ushiba, *EEG-based classification of imaginary left and right foot movements using beta rebound.* Clinical neurophysiology, 2013. **124**(11): p. 2153-2160.

[8] Baranyi, P., A. Csapo, and G. Sallai, *Cognitive Infocommunications (CogInfoCom)*. 2015: Springer.

[9] Katona, J., et al. *Speed control of Festo Robotino mobile robot using NeuroSky MindWave EEG headset based brain-computer interface*. in *Cognitive Infocommunications (CogInfoCom), 2016 7th IEEE International Conference on*. 2016. IEEE.

[10] Klem, G.H., et al., *The ten-twenty electrode system of the International Federation.* Electroencephalogr Clin Neurophysiol, 1999. **52**(3): p. 3-6.

[11] Barlaam, F., et al., *Time–Frequency and ERP Analyses of EEG to Characterize Anticipatory Postural Adjustments in a Bimanual Load-Lifting Task.* Frontiers in human neuroscience, 2011. **5**: p. 163.

[12] Kalcher, J. and G. Pfurtscheller, *Discrimination between phase-locked and non-phase-locked event-related EEG activity.* Electroencephalography and clinical neurophysiology, 1995. **94**(5): p. 381-384.

[13] Knösche, T.R. and M.C. Bastiaansen, *On the time resolution of event-related desynchronization: a simulation study.* Clinical neurophysiology, 2002. **113**(5): p. 754-763.

[14] Pfurtscheller, G., et al., *Mu rhythm (de) synchronization and EEG single-trial classification of different motor imagery tasks.* NeuroImage, 2006. **31**(1): p. 153-159.

[15] Baranyi, P., A. Csapo, and P. Varlaki. *An overview of research trends in coginfocom*. in *Intelligent Engineering Systems (INES), 2014 18th International Conference on*. 2014. IEEE.

Detection of knee motor imagery by mu ERD/ERS quantification for BCI based neurorehabilitation applications

Chapter Overview

Cognitive/mental tasks affiliated to lower-limbs (LL) in BCI paradigms mainly use foot movements. However, when designing assistive technologies for gait assistance or locomotion rehabilitation, other joints such as the knee, needs to be taken into account. This study presents a novel LL motor cognitive task, i.e. left-right knee motor imagery (MI). Quantification of event-related desynchronization (ERD) and synchronization (ERS) is performed for both motor execution (ME) and MI tasks in the *mu* frequency range, to ensure the correlation between ME and MI that enhance same cortical areas. Analysis was based on EEG signals recorded from the vertex and adjacent channels C3, Cz, and C4 using the common average reference method. Preliminary results depicted a contralateral dominance of *mu* ERD that provides the possibility to use the left-right knee tasks for BCI rehabilitation applications.

This work has been published in ***11th IEEE Asian Control Conference.***

M. Tariq, P.M. Trivailo, and M. Simic. *Detection of Knee Motor Imagery by Mu ERD/ERS Quantification for BCI Based Neurorehabilitation Applications*. 11th Asian Control Conference (ASCC), 2017, pp. 2215-2219. IEEE, 2017, Gold Coast, Australia.

2017 11th Asian Control Conference (ASCC)
Gold Coast Convention Centre, Australia
December 17-20, 2017

Detection of Knee Motor Imagery by Mu ERD/ERS Quantification for BCI Based Neurorehabilitation Applications

Madiha Tariq, Pavel M.Trivailo, and Milan Simic

Abstract—**This study underscores the reactivity of sensorimotor rhythms (SMR) in EEG such as mu rhythm in connection with the imagination and voluntary movement of left and right knee extension with able-bodied subjects using the standard Graz brain-computer interface (BCI) paradigm. As the knee motor execution (ME) and motor imagery (MI) reflect the user's voluntary physical and imagination state of knee extension respectively, they have been analyzed in order to be used as control signals to restore motor function with neuro-plasticity for BCI applications. This reactivity has been evaluated using the quantification of event-related desynchronization (ERD) and event-related synchronization (ERS) patterns. Investigations on the cortical lateralization of ERD/ERS during the left and right knee MI and ME for the extension task was done. During left and right knee MI, the foot area mu rhythm was desynchronized in all subjects, whereas no enhancement of the hand area mu rhythm was observed during any task. The frequency of the most reactive components for mu rhythm was 8.8±0.5 Hz. Interestingly a contralateral dominance was visible at a central electrode position, during left knee extension MI task. This lead to the establishment of an understanding of the left-right knee MI and its associated cognitive behavior.**

I. Introduction

One of the constituent building blocks of human activity is his/her walking gait. The walking gait can be affected by any lower limbs (LL) disorder including knee, ankle and foot [1]. The usual cause of disorder could be the spinal cord injury (SCI), stroke, amputation or neurodegeneration disorder. The rehabilitation of gait is the therapeutic aim in order to enhance the motor control functions by inducing neuro-plasticity. This could be realized by the identification and translation of brain signals which correspond to the respective imagination or voluntary movement of the affected limb, such as knee, into an output command [2]. Consequently the user can get a feedback on this output command that can affect his/her brain activity, and re-establish the lost motor control. To transform this logic into real-time application, the state of the art BCI technology could be a potential tool used as the mode of interface between human brain and computer based on EEG.

For lost knee function little is reported explicitly about the knee MI and ME tasks that lead us to the investigation and research of this study. Early clinical studies show that SMR ERD is associated with motor imagery as well as actual movement [3]. In general BCIs are based on particular EEG features that encode cortical activity in association to user intent for a particular task, e.g. the knee, create a unique pattern in the SMR. The mu rhythm being one of the SMR generates in the somatic sensorimotor areas and is concentrated in 8-12 Hz frequency band [2]. Mu rhythm has been exploited by researchers to identify any variation, such as a power decrease called ERD or a power increase called ERS relating to any MI task. However, evaluation of knee imagery and its effectiveness on mu rhythm lacks comprehensive details which keeps it open for investigation and research [4, 5].

The ERD/ERS pattern is related to internal or external event. The ERD pattern reflects an imagined or voluntary movement of a limb characterized by frequency specificity and localized cortical topography. An ERS in contrast is linked to relaxation period or idling [6, 7]. ERD pattern can be a source estimator of brain activity associated to an event. To quantify ERD/ERS patterns the topographic maps were used, that show the spatial distribution of ERD/ERS for a specific frequency, alongside the time-frequency maps, that detect the transient event-related spectral perturbation (ERSP) or shifts in the power spectrum and inter-trial coherence (ITC) events in the signal [8].

The somatotopic arrangement of the sensory and motor cortices results in the cortical localization of ERD patterns. Unlike the hand area representation, the knee motor area representation is situated deep within the cortex's interhemispheric fissure which challenges the detection of ERD patterns [9]. This study therefore aims at developing an understanding on the cortical lateralization of knee area representation (discrimination of left and right knee tasks) followed by its effects on the foot and hand area representation of the cortex for neurorehabilitation applications based on BCI.

II. Methodology

A. Experimental Design

Three healthy subjects (2 females and 1 male) with no history of neurological disorder, or any impairment, aged between 25-35 years, voluntary participated in this study. The participants had no BCI experience either. For this study an ethics approval was granted by the CHEAN (College Human Ethics Advisory Network) of RMIT University, Melbourne, Australia.

The subjects were directed to sit on a comfortable seat in front of a monitor screen (17'') keeping a distance of about 1.5 m. The experimental paradigm was based on the standard Graz BCI protocol. Each run initiated with a blank screen

Madiha Tariq is with the School of Engineering, RMIT University, Melbourne, Australia (e-mail: madiha.tariq@rmit.edu.au).
Pavel M.Trivaio, is with the School of Engineering, RMIT University, Melbourne, Australia (e-mail: pavel.trivailo@rmit.edu.au).
Milan Simic is with the School of Engineering, RMIT University, Melbourne, Australia (e-mail: milan.simic@rmit.edu.au).

that lasted for 30 seconds, called the baseline. During baseline period, the participant was asked to relax and get ready for the experiment. Baseline was followed by the initiation of each trial. The trial began with the presentation of a fixation cross on screen for 3 seconds (used as reference) followed by 2 seconds of visual cue display and 5 seconds of related task performance (imagery or execution), making 10 seconds in total for one trial. The visual cues reflected the left and right knee extension. Subjects were instructed to extend their knee only once during each task performance period. To ensure no adaptation is taking place the visual cues were displayed in a random order. Each trial was followed by a random pause interval of 1.5 to 3.5 seconds during which subjects were asked to relax. Each session/run consisted of 40 trials, with a total of 20 trials for each task. The experiment was divided into 5 sessions/runs, 1 for ME and 4 for MI task respectively. Fig. 1 (left) presents the schematic overview of protocol timing for the experiment. An audio stimulus, as an 1 second beep, right before the visual cue display, was incorporated in the first trial only, to alert the subject that the experiment was about to begin.

B. Data Acquisition

EEG neurofeedback BrainMaster Discovery 24E amplifier (BrainMaster Technologies Inc., Bedford, USA) was used in the experiment; it was interfaced with the acquisition server of OpenViBE software (http://openvibe.inria.fr/downloads/). The standard 10-20 Electro-cap was used to acquire brain signals from the motor cortex [10]. And system's 19 channels were referenced to linked earlobes (LE) derived from the electrodes A1, A2 and a ground (Fig. 1, right). Remaining channels provided for monitoring other electrophysiological signals were not used. All channels were sampled using 256 Hz sampling frequency, with a 24-bit resolution. Amplifier bandwidth was from 0 to 100 Hz and EEG channel bandwidth was from 0.43 to 80 Hz.

Fig. 1 Knee extension task experimental protocol showing timing of cue with 'beep', assigned to the first trial in the beginning of each run (left) and electrode channel locations (right)

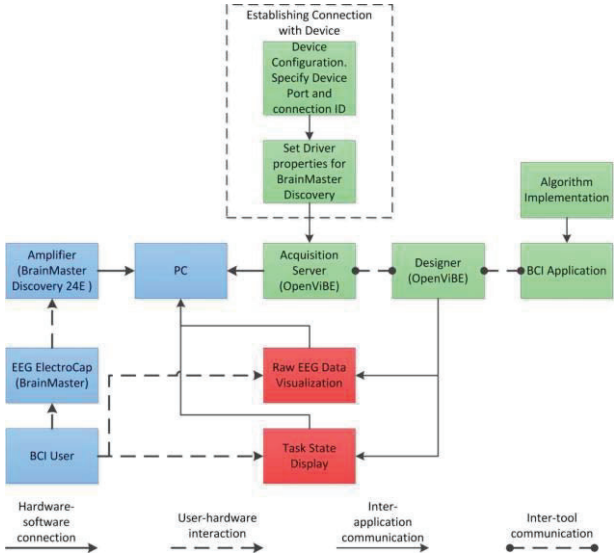

Fig. 2 Flow diagram of the established hardware-software connection between BrainMaster amplifier and OpenViBE acquisition software

In order to set the experimental protocol, the OpenViBE designer tool that comes along integrated feature boxes was used. Inside OpenViBE designer window the .lua script and the default settings were customized for using the Graz-Stimulator box to allow for the onset of different visual cue timings. The BrainMaster Discovery and OpenViBE software were synchronized by setting the acquisition server properties of OpenViBE and connecting the required modules as presented in Fig. 2. The recordings were made using the edf and gdf writer boxes of OpenViBE that lead to the storage of both signals and the corresponding stimulations, respectively.

C. Signal Processing

For the data processing and analysis, the statistical EEGLAB package (http://www.sccn.ucsd.edu/eeglab/) was used. The EEG signals were bandpass filtered for the required frequency bandwidth range of mu rhythm followed by epoching of the trials (10 seconds in length). The trials extracted and analyzed included the period of 3 seconds prior to cue onset used as reference period.

The independent component analysis (ICA) was performed for the artifact removal [11]. ICA component rejection was done using EEGLAB toolbox.

Resulting topographic maps of the scalp were plotted and analyzed followed by plotting of time-frequency maps for required bandwidth (8-30 Hz) with a step of 1 Hz. The mu band with the most significant band power decrease, or increase, during the knee MI and ME tasks at the central electrode positions C3, Cz, and C4 were recorded and investigated.

For quantifying the ERD/ERS patterns from obtained signal, method proposed by [12] was followed. The ERD/ERS is the proportional power decrease, or power increase, respectively compared to the reference interval, which is usually the period of several seconds before the event onset [6]. In this study the 3 seconds interval prior to visual cue onset was selected as reference. The samples were squared after subtracting the mean of the band pass filtered

data, for each sample, to overcome masking of induced activities by the evoked potentials. This was followed by the averaging of samples over trials and over sample points as in (1) [6, 13]. Given P_j is the power or inter-trial variance of the j-th sample and R is the average power in the reference interval (r_0, r_0+k) [7].

$$ERDS_j = \frac{P_j - R}{R} * 100\% \quad (1)$$

III. Results

This section presents the results acquired from participant subjects S1, S2 and S3.

A. Channel Spectra Topographical maps

The resulting topographical scalp maps against the left and right MI and ME of knee extension task for subject 1 (S1), subject 2 (S2) and subject 3 (S3) have been reported in this section in Fig. 3. In Fig. 3, the color bar indicates the spectral power concentration over the scalp for all channels.

Knee extension MI:

Results for S1 and S3 reflected a high spectral power concentration broadly spread over the central and frontal regions. The left knee MI exhibited a contralateral mu ERD for the right hand area and enhanced the mu ERD for foot area representation. However, this contralateral dominance was not visible in case of the right knee MI task for both S1 and S3; instead a decrease in power concentration levels was observed in S1 followed by frontal region activation. For S2 on the other hand a dominant spectral power concentration was visible strictly in the central region. During left knee MI the foot area representation mu ERD was evident. Similarly for the right knee MI mu ERD for foot area were observed for S2 and S3 followed by an increase in power concentration compared to the left knee task. However S2 did not show any hand area mu ERD or ERS for the knee MI task.

Knee extension ME:

For knee ME the results were unexpectedly different for all subjects, resulting in intra subject variability. This could potentially be due to the proprioceptive feedback due to the voluntary task movement. For S1 and S3 an increase in spectral power concentration was evident over the central, as well as, areas near the parietal lobe. During the left knee ME, the mu ERD was visible at the central cortex, accompanied by an ERD of the 8-12 Hz visual alpha rhythm recorded over the parieto-occipital (visual) cortex. For S1 the right knee ME did not exhibit any significant ERD/ERS pattern however, the visible pattern was concentric over foot area. The results of S2 were contrary to those of S1 and S3 for left knee extension, although the spectral power was centered in the middle of the cortex. Its concentration was lower for the left knee ME. For the right knee ME, both S2 and S3 reflected a high concentration of the spectral power, which was observed in the central region, including areas of the parietal cortex. For both the left and right knee ME tasks mu ERD for foot area was noted. No signs of ERD/ERS were present in the hand area during knee ME task for any subject.

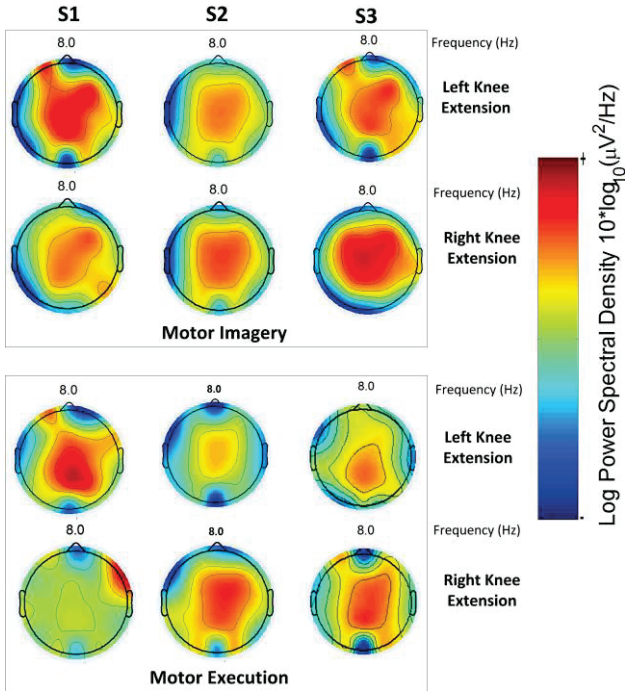

Fig. 3 Topographical scalp maps showing mean power spectral distribution for left-right knee extension imagery and execution for 24 channels at 8 Hz

B. Time-frequency Maps

Results of the time-frequency maps for subject S1 are discussed in this section. Fig. 4 presents the time-frequency maps of the most reactive ERD/ERS patterns at electrode positions C3, Cz and C4 against the left and right knee extension imagery task obtained from EEGLAB. Only significant values (α=0.05) are displayed in color: red indicates ERD and blue indicates ERS. Non- significant values are displayed in green. The colour bar indicates the ERSP in decibel.

For the knee extension imagery, the subject was directed to imagine extending the knee one time right after the onset visual cue finishes. It was expected to observe a dominant ERD during the performance of the task, however unexpectedly the subject exhibited dominant ERD right from the moment the onset cue was presented. These results support the concept based on literature that ERD starts over the relevant motor area several seconds prior to movement i.e. during the task preparation [2].

During left knee extension imagery, a dominant ERD at all three electrode positions C3, Cz and C4 is evident. It begins at the end of visual cue display at around second 2 and ends at around 5 to 6 seconds for the period till the task ends. To be precise more concentration is reflected in the 2.5 to 5 seconds duration which validates the real-time observance as the subject took around 2 seconds to finish the knee extension task. This dominance was visible for all frequencies between 8-30 Hz. During the presentation of fixation cross and the beginning of visual cue ERS has been observed specifically at electrode position Cz and more explicitly at position C4.

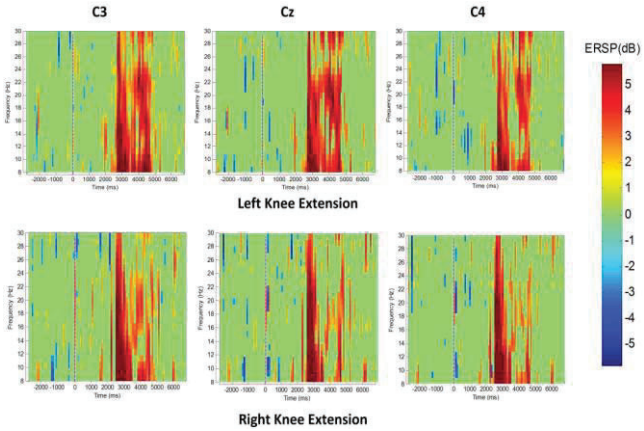

Fig. 4 Time-frequency maps displaying significant (de)synchronization (ERD in red and ERS in blue) patterns of subject S1 for electrode position C3, Cz and C4 against imagery tasks of left knee extension (top) and right knee extension (bottom) respectively

Results for the right knee extension somehow offered same trend throughout the electrode positions C3, Cz and C4. Like in case of left knee imagery, for this task the prominent ERD were observed starting at the position where the visual cue end, and last till the end of execution session. However the span for ERD, in this case, was prolonged to 6 seconds. ERS was not very dominant, since it lasted from -1 to around 1 seconds, i.e. for a small period before and after onset visual cue presentation.

C. *ERD/ERS Quantification*

The results of the most reactive mu components band power changes (ERD and ERS) at central electrode positions C3, Cz and C4 for the left and right knee extension MI and ME tasks have been reported in Table 1. The most reactive components ranged between 8 and 12 Hz.

For left knee MI/ME the highest value of ERD occurred at electrode position C4 that supports the contralateral dominance of mu hand area. During the right knee MI/ME most dominant ERD was observed at position Cz which correlate to the established findings about the mu ERD foot area enhancement reported in [14]. The highest values of ERS for both tasks during MI/ME were detected at electrode position Cz.

IV. Discussion

The ERD and ERS in general were noticeable for all subjects during knee imagery and execution tasks. The time-power outputs against only right knee MI (at 8 Hz) for subject S2 at electrode position C3, Cz and C4 are depicted in Fig. 5 as exemplary ERD/ERS time curves. In Fig. 5 the duration of onset visual cue has been highlighted by a blue rectangular window for a clear understanding. The time curve for C3 illustrates a prominent ERD at around 3,000 milliseconds after the end period of visual cue display. After around 0.5 seconds of ERD a prominent ERS is visible at around 3,500 milliseconds. For Cz a dominant ERD is visible during cue display at around 1,500 milliseconds. The ERS was dominant at around 3,500 milliseconds as in case of C3. The time curve for C4 showed a similar trend, as in case of Cz i.e. during cue onset ERD was observed at around 1,700 milliseconds followed by a relatively prominent ERS at around 3,500 milliseconds.

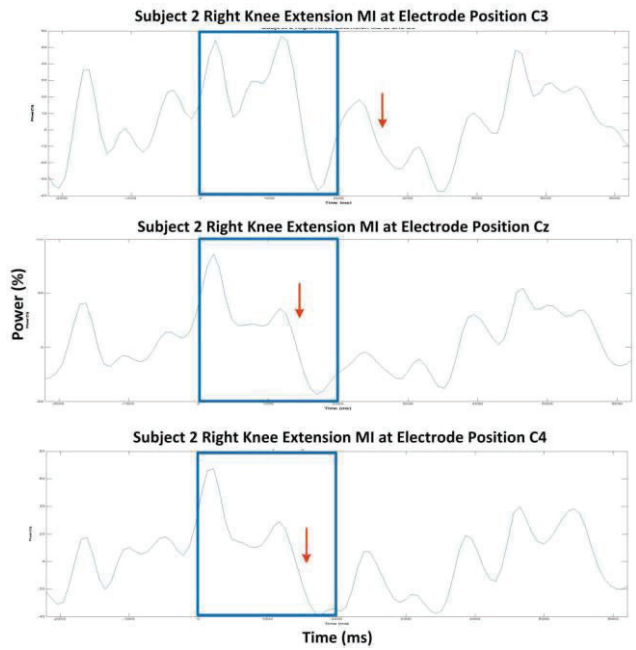

Fig. 5 (de)synchronization (ERD/ERS) time curve obtained from right knee extension imagery of subject S2 at electrode positions C3, Cz and C4 respectively (red arrow indicates most prominent ERD pattern), the blue rectangular window depicts onset visual cue period

V. Conclusions

This study was based on the detection of knee MI from mu rhythm and analyzing its effects on related cortical areas of brain. The resulting mu ERD-ERS presented satisfactory results to enable an understanding of the knee imagery behavior despite a small knee area representation on the cortical homunculus. The topographical scalp maps reflected an evident mu ERD foot area representation for all subjects during both MI and ME tasks. Though contralateral dominance during left knee imagery, for subjects 1 and 3, was observed, that could suggest the knee MI has potential to elicit left-right discrimination in EEG, it was not the case with right knee imagery. Furthermore no ERS or ERD enhancement for hand area was visible in any subject. The results suggest that a BCI, using the unilateral knee imagery, could be used to control a knee neuroprosthesis. We aim at advancing this research work by including more participants and classifying the left and right knee tasks. The key contribution of this study is the introduction and the testing of the new BCI concept. This study offers a potential platform for initiation of knee MI based BCIs for neurorehabilitation application.

TABLE I. TABLE FOR MU RHYTHM AND BAND POWER CHANGES OF THE MOST REACTIVE BANDS DISPLAYING ERD-ERS FOR KNEE EXTENSION MI AND ME TASKS CALCULATED WITH EEGLAB BOOTSTRAP (α=0.05)

	Left knee								
	C3			**Cz**			**C4**		
MI	Hz	% (ERD)	% (ERS)	Hz	% (ERD)	% (ERS)	Hz	% (ERD)	% (ERS)
S1	9	-40	54	9	-39	62	12	-43	63
S2	12	-42	53	12	-38	63	12	-39	56
S3	9	-39	51	11	-40	62	11	-41	60
ME									
S1	8	-42	56	10	-38	60	10	-46	60
S2	11	-36	63	12	-42	59	8	-43	49
S2	12	-40	61	12	-37	61	10	-47	60
Mean	10.2	-40	56.3	11	-39	61.2	11	-43	58
SD	1.7	2.2	4.7	1.3	1.8	1.5	1.5	3	5
	Right knee								
	C3			**Cz**			**C4**		
MI	Hz	% (ERD)	% (ERS)	Hz	% (ERD)	% (ERS)	Hz	% (ERD)	% (ERS)
S1	11	-38	56	10	-44	52	10	-38	61
S2	12	-43	57	8	-39	54	12	-42	57
S3	11	-42	54	9	-42	52	10	-39	61
ME									
S1	12	-44	62	12	-52	82	10	-40	63
S2	9	-38	54	10	-37	53	9	-37	52
S3	9	-39	58	12	-49	56	10	-41	59
Mean	10.7	-40.7	56.8	10.2	-43.8	58.2	10.2	-40	59
SD	1.4	2.7	3	1.6	5.8	11.8	1	1.9	4

REFERENCES

1. Tariq, M., Z. Koreshi, and P. Trivailo. *Optimal Control of an Active Prosthetic Ankle*. in *Proceedings of the 3rd International Conference on Mechatronics and Robotics Engineering*. 2017. ACM.
2. Wolpaw, J. and E.W. Wolpaw, *Brain-computer interfaces: principles and practice*. 2012: OUP USA.
3. Jasper, H. and W. Penfield, *Electrocorticograms in man: effect of voluntary movement upon the electrical activity of the precentral gyrus.* European Archives of Psychiatry and Clinical Neuroscience, 1949. **183**(1): p. 163-174.
4. Boord, P., et al., *Discrimination of left and right leg motor imagery for brain–computer interfaces.* Medical & biological engineering & computing, 2010. **48**(4): p. 343-350.
5. Lisi, G., T. Noda, and J. Morimoto, *Decoding the ERD/ERS: influence of afferent input induced by a leg assistive robot.* Frontiers in systems neuroscience, 2014. **8**.
6. Graimann, B., et al., *Visualization of significant ERD/ERS patterns in multichannel EEG and ECoG data.* Clinical Neurophysiology, 2002. **113**(1): p. 43-47.
7. Graimann, B. and G. Pfurtscheller, *Quantification and visualization of event-related changes in oscillatory brain activity in the time–frequency domain.* Progress in brain research, 2006. **159**: p. 79-97.
8. Delorme, A. and S. Makeig, *EEGLAB: an open source toolbox for analysis of single-trial EEG dynamics including independent component analysis.* Journal of neuroscience methods, 2004. **134**(1): p. 9-21.
9. Hashimoto, Y. and J. Ushiba, *EEG-based classification of imaginary left and right foot movements using beta rebound.* Clinical neurophysiology, 2013. **124**(11): p. 2153-2160.
10. Klem, G.H., et al., *The ten-twenty electrode system of the International Federation.* Electroencephalogr Clin Neurophysiol, 1999. **52**(3): p. 3-6.
11. Barlaam, F., et al., *Time–Frequency and ERP Analyses of EEG to Characterize Anticipatory Postural Adjustments in a Bimanual Load-Lifting Task.* Frontiers in human neuroscience, 2011. **5**: p. 163.
12. Kalcher, J. and G. Pfurtscheller, *Discrimination between phase-locked and non-phase-locked event-related EEG activity.* Electroencephalography and clinical neurophysiology, 1995. **94**(5): p. 381-384.
13. Knösche, T.R. and M.C. Bastiaansen, *On the time resolution of event-related desynchronization: a simulation study.* Clinical neurophysiology, 2002. **113**(5): p. 754-763.
14. Pfurtscheller, G., et al., *Mu rhythm (de) synchronization and EEG single-trial classification of different motor imagery tasks.* NeuroImage, 2006. **31**(1): p. 153-159.

RMIT University

Science Engineering and Health

College Human Ethics Advisory Network (CHEAN)

Plenty Road
Bundoora VIC 3083

PO Box 71
Bundoora VIC 3083
Australia

Tel. +61 3 9925 4620
Fax +61 3 9925 6506
www.rmit.edu.au

26 August 2016

Professor Pavel Trivailo
School of Engineering
RMIT Unviersity

Dear Professor Trivailo

ASEHAPP 21-16 Brain-computer interface controlled bionic ankle-foot model: EEG-based BCI

Thank you for submitting your amended application for review.

I am pleased to inform you that the CHEAN has approved your application for a period of **3 Years** from the date of this letter to **26 August 2019** and your research may now proceed.

The CHEAN would like to remind you that:

All data should be stored on University Network systems. These systems provide high levels of manageable security and data integrity, can provide secure remote access, are backed up on a regular basis and can provide Disaster Recover processes should a large scale incident occur. The use of portable devices such as CDs and memory sticks is valid for archiving; data transport where necessary and for some works in progress. The authoritative copy of all current data should reside on appropriate network systems; and the Principal Investigator is responsible for the retention and storage of the original data pertaining to the project for a minimum period of five years.

Please Note: Annual reports are due on the anniversary of the commencement date for all research projects that have been approved by the CHEAN. Ongoing approval is conditional upon the submission of annual reports failure to provide an annual report may result in Ethics approval being withdrawn.

Final reports are due within six months of the project expiring or as soon as possible after your research project has concluded.

The annual/final reports forms can be found at:
www.rmit.edu.au/staff/research/human-research-ethics

Yours faithfully,

Associate Professor Barbara Polus
Chair, Science Engineering & Health
College Human Ethics Advisory Network

Cc Student Investigator/s: Madiha Tariq, School of Engineering

College Human Ethics Advisory Network (CHEAN)
College of Science, Engineering and Health

Email: seh-human-ethics@rmit.edu.au
Phone: [61 3] 9925 4620
Building 91, Level 2, City Campus/Building 215, Level 2, Bundoora West Campus

27 September 2017

Professor Pavel Trivailo
School of Engineering
RMIT University

Dear Professor Trivailo

ASEHAPP 21-16 Brain-computer interface controlled bionic ankle-foot model: EEG-based BCI

Thank you for requesting an amendment to your Human Research Ethics project titled: **Brain-computer interface controlled bionic ankle-foot model: EEG-based BCI**, which was originally approved by Science Engineering and Health CHEAN in 2016 for a period of **3 years**.

I am pleased to inform you that the CHEAN has **approved** your amendment as outlined in your request.

The CHEAN notes and thanks you for providing all documentation that incorporates these amendments. This documentation will be appended to your file for future reference and your research may now continue.

The committee would like to remind you that:

All data should be stored on University Network systems. These systems provide high levels of manageable security and data integrity, can provide secure remote access, are backed up on a regular basis and can provide Disaster Recover processes should a large scale incident occur. The use of portable devices such as CDs and memory sticks is valid for archiving; data transport where necessary and for some works in progress; The authoritative copy of all current data should reside on appropriate network systems; and the Principal Investigator is responsible for the retention and storage of the original data pertaining to the project for a minimum period of five years.

Please Note: Annual reports are due on the anniversary of the commencement date for all research projects that have been approved by the CHEAN. Ongoing approval is conditional upon the submission of annual reports failure to provide an annual report may result in Ethics approval being withdrawn.

Final reports are due within six months of the project expiring or as soon as possible after your research project has concluded.

The annual/final reports forms can be found at:
www.rmit.edu.au/staff/research/human-research-ethics

Yours faithfully,

Associate Professor Barbara Polus
Chair, Science Engineering & Health
College Human Ethics Advisory Network

Cc Student Investigator/s: Madiha Tariq, School of Engineering